

A Temporal Analysis of Host Chromatin Changes and Transcriptional Responses Induced by Latent Kaposi's Sarcoma-associated Herpesvirus Infection

Dissertation

zur Erlangung des Doktorgrades (Dr. rer. nat.)

an der Fakultät für Mathematik, Informatik und Naturwissenschaften

Fachbereich Biologie
der Universität Hamburg

vorgelegt von

Jacqueline Fröhlich

Hamburg, Dezember 2020

The experimental work depicted in this thesis has been carried out at the Heinrich-Pette Institute, Leibniz Institute for Experimental Virology in Hamburg, Germany in the research department Virus Genomics under the supervision of Prof. Dr. Adam Grundhoff.

Reviewer:

Prof. Dr. Adam Grundhoff

Prof. Dr. Stefan Hoth

Date of the thesis defense: Friday, 19th of March 2021

In dedication to my family

Abstract

The human γ -herpesvirus Kaposi's sarcoma-associated herpesvirus (KSHV) is associated with several cancers, including Kaposi Sarcoma, a tumor of endothelial origin as well as the two B cell malignancies Primary Effusion Lymphoma and Multicentric Castleman's Disease. Like other herpesviruses, KSHV can establish a latent state of infection, which allows life-long persistence in its host. Previous studies revealed that latent KSHV infection does not only lead to the acquisition of epigenetic modifications on the viral genome but might also induce re-localization of epigenetic host factors. Additionally, there is evidence from more recent data that KSHV infected cells undergo epigenetic changes at distinct host loci which might play a role during tumorigenesis. However, a detailed and, more importantly, a temporal genome wide analysis of host epigenetic changes upon KSHV infection in a relevant *in vitro* system is still missing.

Thus, the aim of this study was to investigate KSHV-induced epigenetic short- and long-term consequences with the help of an efficient latent infection system in endothelial cells. ChIP-seq, MeDIP-seq and RNA-seq were performed to monitor histone modification and DNA methylation changes, as well as associated alterations of transcription patterns at various time points post infection.

Despite the moderate transcriptomic deregulation observed during KSHV infection, a distinct interferon response signature persisted for several weeks in strictly latent cultures. Single cell RNA-seq furthermore suggests that these signatures originated from a small subset of cells, which show no evidence of lytic reactivation. While interferon regulated genes were not affected by histone modification changes due to a potential epigenetic pre-activation, several other regions were identified that undergo significant epigenetic remodeling. Remodeling was observed for activating as well as repressive histone modifications, with the most evident changes occurring at the level of acetylated histone H3 lysine 27 (H3K27ac), which is a mark for active genes as well as enhancer regions. Multiple altered regions mapped to genes which exhibited mild but detectable transcriptional deregulation. However, remodeled regions were also detected which are not directly linked to differentially expressed genes, indicating a potential predisposition which might only lead to phenotypic manifestation upon the presence of additional stimuli. Comparison of KSHV infected and cleared cells allowed for the investigation of such predisposed regions. A subset of histone modification changes remained stable in the cleared population although the transcriptional profile

of these cells was almost completely reconstituted to the initial uninfected state. Challenging these cells with different stimuli, like KSHV re-infection led to a more pronounced transcriptional response of at least some of the predisposed regions. Based on these findings, we suspect that KSHV actively modulates epigenetic pathways, which might affect the viral life cycle, but also lead to alterations of the host epigenome. Beside KSHV dependent chromatin changes, a subset of deregulated regions might become independent of the infection as indicated by stable changes in KSHV cleared cells. As it is thought that virus-mediated tumorigenesis is a long-term consequence of latent infection, these distinct epigenetic states, potentially together with other stimuli, may promote KSHV mediated tumorigenesis.

Zusammenfassung

Das γ -Herpesvirus Kaposi Sarkom-assoziiertes Herpesvirus (KSHV) ist ein humanpathogenes Virus, welches mit der Entstehung zahlreicher Tumore assoziiert ist. Dazu zählt zum einen das Kaposi Sarkom, ein Tumor endothelialen Ursprungs, sowie die beiden B Zell Tumore Primäres Effusionslymphom und die multizentrische Castleman Erkrankung. Wie auch andere Herpesviren kann KSHV einen latenten Infektionsstatus einnehmen, der es ihm erlaubt lebenslang im Wirt zu persistieren. Während dieses latenten Lebenszyklus erhält das virale Genom nicht nur epigenetische Modifikationen, um große Teile seines Genoms transkriptionell still zu legen. KSHV scheint auch in der Lage zu sein, epigenetische Faktoren gezielt zu manipulieren, um den Aufbau der epigenetischen Modifikationen auf dem viralen Genom zu fördern. Neuere Erkenntnisse deuten ebenfalls darauf hin, dass KSHV infizierte Zellen epigenetische Veränderungen in spezifischen Wirtsregionen aufweisen, die eine Rolle bei der Virus-induzierten Tumorentstehung spielen könnten. Allerdings wurde bezüglich dieser veränderten Regionen bisher keine detaillierte und zeitlich aufgelöste Genom-weite Studie in einem relevanten *in vitro* System durchgeführt.

Das Ziel dieser Arbeit war es deshalb, ein latentes KSHV Infektionssystem in Endothelzellen zu etablieren, womit die Analyse von KSHV induzierten Kurz- und Langzeitfolgen auf dem Wirtsepigenom ermöglicht wurde. ChIP-seq, MeDIP-seq und RNA-seq wurden durchgeführt, um Veränderungen von Histonmodifikationen und DNA-Methylierung zu detektieren und diese auch mit transkriptionellen Mustern zu korrelieren.

Obwohl lediglich geringe transkriptionelle Veränderungen während einer KSHV Infektion festgestellt wurden, war dennoch eine deutliche Interferon Antwort in latent infizierten Zellen erkennbar, die sich über einen unerwartet langen Zeitraum erstreckte. Mithilfe von Einzel-Zell Sequenzierung konnte darüber hinaus gezeigt werden, dass lediglich einzelne Zellen für diese späte Immunantwort verantwortlich sind, die allerdings keinerlei Zeichen einer lytischen Reaktivierung von KSHV aufwiesen. Während für Interferon-induzierte Gene kaum Veränderungen auf Histonmodifikationsebene festgestellt werden konnten, womöglich aufgrund eines epigenetisch prä-aktivierten Zustands, wurden zahlreiche andere Regionen mit differentiellen epigenetischen Mustern identifiziert. Veränderungen konnten sowohl für aktivierende also auch für reprimierende Modifikationen detektiert werden, jedoch

zeigten sich die am auffälligsten veränderten Regionen fast immer auf der Ebene von H3K27ac, eine Modifikation, die charakteristisch für Enhancer-Bereiche ist. Während zahlreiche dieser differentiellen Bereiche auch leichte, aber detektierbare Veränderungen bezüglich der Transkription aufwiesen, gab es auch einige Regionen, die nicht direkt mit einer transkriptionellen Antwort einhergingen. Deshalb wurde vermutet, dass solche Regionen einer Prädisposition unterzogen werden, die lediglich durch einen sekundären Stimulus zu einer phänotypischen Ausprägung führt. Um diese Hypothese zu untersuchen wurden KSHV infizierte Zellen mit einer parallel kultivierten Population verglichen, die eine Infektion erfolgreich überwinden konnte. Dies ermöglichte die Identifizierung von stabilen Veränderungen, die selbst nach einer abgeklungenen Infektion noch erhalten blieben und das obwohl auf transkriptioneller Ebene eine komplette Rekonstitution des initialen, nicht infizierten Zustands auftrat. Wurden diese Zellen mit unterschiedlichen Stimuli induziert, wie zum Beispiel einer Re-Infektion mit KSHV, konnte zumindest für einen Teil der Gene eine deutlich stärkere transkriptionelle Antwort im Vergleich zu den Kontrollzellen festgestellt werden.

Diese Daten deuten darauf hin, dass KSHV aktiv epigenetische Faktoren manipuliert, was zum einen den viralen Lebenszyklus beeinflusst, jedoch auch zu epigenetischen Veränderungen der Wirtszelle führt. Die Untersuchung der Zellen mit abgeklungener KSHV Infektion lassen die Vermutung zu, dass es neben KSHV abhängigen Veränderungen auch einen Anteil an deregulierten Regionen gibt, die Infektions-unabhängig werden. Beide Veränderungen könnten bei der KSHV abhängigen Tumorentstehung eine wichtige Rolle einnehmen, da dieser Prozess als Konsequenz einer latenten Langzeit-Infektion verstanden wird.

Table of contents

1	Introduction	1
1.1	<i>Human herpesviruses</i>	1
1.2	<i>Kaposi's sarcoma associated herpesvirus</i>	3
1.2.1	Particle structure and early steps of infection	3
1.2.2	The type I interferon response	5
1.2.3	Genome organization	7
1.2.4	Biphasic lifecycle	8
1.2.4.1	Latent infection	9
1.2.4.2	Lytic reactivation	11
1.2.5	Cell tropism	13
1.2.6	KSHV induced tumorigenesis	14
1.3	<i>KSHV associated malignancies</i>	15
1.3.1	Seroprevalence and epidemiology	15
1.3.2	Primary Effusion Lymphoma	16
1.3.3	Multicentric Castleman's Disease	17
1.3.4	Kaposi's sarcoma	18
1.4	<i>Epigenetic Modifications</i>	19
1.4.1	DNA methylation	19
1.4.2	Histone modifications	22
1.4.3	KSHV and the interplay with host epigenetic pathways	25
2	Aim of the study	28
3	Material and Methods	29
3.1	<i>Material</i>	29
3.1.1	Chemicals, commercial systems and expendable materials	29
3.1.2	Instruments and equipment	29
3.1.3	Software and online resources	29
3.1.4	Constructs	30
3.1.5	Oligonucleotides	30
3.1.6	Antibodies	31
3.2	<i>Methods of prokaryotic cell culture</i>	32
3.2.1	Bacteria	32
3.2.2	Media and culture of bacteria	32
3.2.3	Preparation of chemically competent <i>E. coli</i>	33
3.2.4	Preparation of electro-competent <i>E. coli</i>	34
3.2.5	Transformation of chemically competent <i>E. coli</i>	34
3.2.6	Transformation of electro-competent <i>E. coli</i>	34
3.3	<i>Methods of eukaryotic cell culture and cell biology</i>	35
3.3.1	Culture of eukaryotic cell lines	35
3.3.2	Long-term storage and initiation of cell cultures	36
3.3.3	Transient transfection	37
3.3.4	Production of lentiviral particles	37
3.3.5	Transduction of cells with lentiviral particles	38
3.3.6	Preparation of infectious KSHV stocks	39
3.3.7	Preparation of infectious Bac16 stocks	39
3.3.8	<i>De novo</i> KSHV infection	40
3.3.9	Cell proliferation assay	40
3.4	<i>DNA techniques</i>	41
3.4.1	Isolation of plasmid and bacmid DNA from bacteria	41
3.4.2	Extraction of genomic DNA from eukaryotic cells	42
3.4.3	Digestion of plasmid and bacmid DNA with restriction enzymes	43
3.4.4	Agarose gel electrophoresis	43
3.4.5	Purification of DNA fragments and plasmid DNA from gels	44
3.4.6	Ligation of DNA fragments	44

3.4.7	Gibson assembly	44
3.4.8	Amplification of DNA by Polymerase Chain Reaction (PCR)	45
3.4.9	Quantitative Real-time PCR.....	46
3.4.10	Determination of nucleic acid concentrations	47
3.4.11	Sanger-sequencing of DNA and sequence analysis	47
3.5	<i>RNA techniques</i>	47
3.5.1	Extraction of total RNA from eukaryotic cells.....	47
3.5.2	cDNA synthesis from total RNA.....	48
3.6	<i>Microscopy-related methods</i>	49
3.6.1	Tube formation assay.....	49
3.6.2	Immunofluorescence analysis	49
3.7	<i>FACS analysis</i>	50
3.7.1	Titration of infectious (lenti-)viral particles	50
3.7.2	Staining of intracellular molecules	50
3.7.3	Annexin V apoptosis assay.....	51
3.8	<i>Native Chromatin Immunoprecipitation (nChIP)</i>	51
3.9	<i>Methylated DNA Immunoprecipitation (MeDIP)</i>	54
3.10	<i>High-Throughput sequencing</i>	56
3.10.1	RNA-sequencing	56
3.10.2	Single-Cell RNA-sequencing	56
3.10.3	ChIP-sequencing	57
3.10.4	MeDIP-sequencing	57
3.11	<i>Bioinformatic analysis</i>	58
3.11.1	Analysis of RNA-sequencing	58
3.11.2	Analysis of ChIP-sequencing.....	58
3.11.3	Analysis of MeDIP-sequencing.....	58
3.11.4	Coverage Plots of viral genomes.....	59
3.12	<i>Statistical analyses</i>	59
4	Results	60
4.1	<i>Latent KSHV infection model in endothelial cells</i>	60
4.1.1	Experimental design to investigate transient and stable consequences of a KSHV infection	60
4.1.2	TIME cells are latently infected with KSHV	62
4.2	<i>Transient and stable transcriptional alterations upon latent KSHV infection</i>	64
4.2.1	Prolonged type I interferon response in KSHV infected cells	64
4.2.2	Comparison of prolonged and <i>de novo</i> type I interferon responses	67
4.2.3	Single cells express high levels of interferon regulated genes	71
4.3	<i>Host DNA methylation patterns in KSHV infected cells</i>	75
4.3.1	Quality control of methylated DNA immunoprecipitation sequencing	75
4.3.2	KSHV infection does not induce global DNA methylation changes	78
4.4	<i>Host chromatin changes upon KSHV infection</i>	81
4.4.1	Quality control of native chromatin immunoprecipitation sequencing	81
4.4.2	KSHV infection induces abundant epigenetic alterations on the host chromatin level ...	83
4.5	<i>Identification of KSHV induced stable epigenetic changes</i>	88
4.5.1	Loss of KSHV reconstitutes the initial transcriptomic profile.....	88
4.5.2	A subset of KSHV-induced epigenetic changes remains stable after clearance	91
4.6	<i>Epigenetic predisposition alters the outcome of specific cellular pathways upon stimulation</i>	94
4.6.1	Cells are not altered in their capability to induce apoptosis.....	94
4.6.2	Increased angiogenic potential in infected and cleared subsets	95
4.6.3	Re-Infection with KSHV leads to more pronounced transcriptional responses in a subset of predisposed regions	97

5	Discussion	102
5.1	<i>KSHV and the type I interferon response</i>	102
5.1.1	Sporadic interferon signatures in strictly latent infected cells	102
5.1.2	Unresponsiveness of cleared cells to a second infection	104
5.2	<i>KSHV induced epigenetic changes</i>	106
5.2.1	Host DNA methylation changes	106
5.2.2	A subset of stable histone modification changes stays even after cleared infection	108
5.2.3	Putative epigenetic pre-activation of interferon responsive genes	110
5.2.4	Stable histone modification changes might affect enhancers.....	111
5.3	<i>KSHV mediated tumorigenesis and the role of epigenetics</i>	113
5.4	<i>Conclusion and Outlook</i>	116
6	References	119
7	Supplementary Material	137
8	Indices	142
8.1	<i>Figures</i>	142
8.2	<i>Tables</i>	143
9	Publications, Oral Presentations, and Awards	146
10	Acknowledgements	147
11	Bestätigung der Korrektheit der englischen Sprache	149
12	Eidesstattliche Versicherung	150

1 Introduction

1.1 Human herpesviruses

The family of herpesviruses is comprised of more than 100 members which have been discovered in a wide range of vertebrates but also in at least one invertebrate like oyster (Farley et al. 1972). The high species specificity observed in nature highlights that herpesviruses have evolved with their host over a long period of time (McGeoch et al., 1995). This makes them not only well adapted to their host but also very complex. One aspect of complexity involves their dsDNA genome with a size that ranges from around 125 to 240 kb, thereby providing the capacity for a huge variety of genes (Dolan et al., 2004; Russo et al., 1996). Another layer of complexity can be added with regard to the virus' lifecycle which can be divided into two parts. During latency only a small subset of the viral genome is actively transcribed rendering the virus a quiescent state, which enables its lifelong persistence within the host (Dittmer et al., 1998; Staskus et al., 1997). However, this latency state is also reversible upon environmental or physiological stimuli leading to the expression of the entire viral gene set in a temporal cascade (Davis et al. 2001; Ye et al. 2011). This results in the lytic replication and finally in production of viral progeny allowing the virus not only to disseminate within the host but also to cause *de novo* infection.

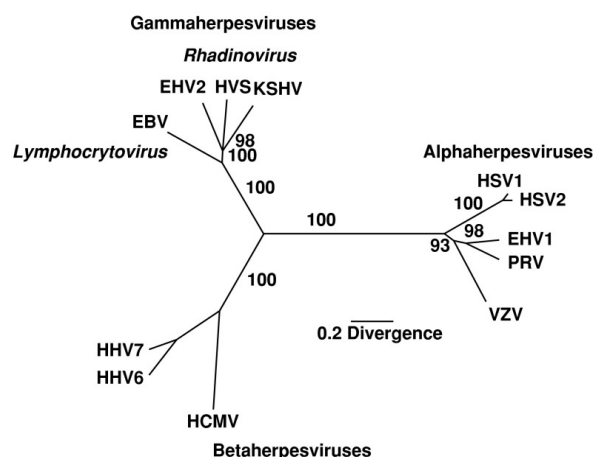


Figure 1: Phylogenetic tree of the herpesvirus family: Phylogenetic tree for a subset of herpesviruses was generated based on the comparison of aligned amino acid sequences for the major capsid protein gene. Depicted are predominantly the human herpesviruses with their closest relatives from the animal field. The branch lengths are proportional to the divergence (Moore et al., 1996).

Based on comparisons of amino acid sequences of conserved viral genes herpesviruses can be classified into three subfamilies called α -, β -, and γ -

herpesviruses (Figure 1). Furthermore, different herpesviruses have evolved distinct latency mechanisms to maintain their genome in the host cell.

α -herpesviruses like HSV-1 reside predominantly in non-dividing cells like sensory neurons in the peripheral dorsal root ganglia or in the trigeminal ganglia in order to persist within the host. Among the β - herpesviruses multiple latency strategies exist, including the integration of the HHV-6 genome into host telomere regions (Arbuckle et al., 2010). Lastly, γ -herpesviruses evolved a tethering mechanism which enables the association of the viral genome to host chromatin. This, in turn, leads to one round of licensed viral DNA replication with the help of the host replication machinery and finally results in the proper segregation of viral DNA to daughter cells during mitosis (Ballestas et al., 1999).

While most of the α - and β -herpesviruses directly undergo lytic replication in cell culture systems, γ -herpesviruses predominantly enter the latent state. The fact, that this latency state can also be reversed by certain chemicals make γ -herpesviruses a good model system to study the viral lifecycle (Miller et al., 1997). Studying γ -herpesviruses is additionally of interest as they are highly associated with cancer in their host and therefore are referred to as tumor viruses. While infections mostly proceed with mild or even no symptoms, in rare cases infected cells can give rise to tumors if the host immune system is impaired. Prominent examples for tumor viruses are Epstein-Barr virus (EBV) and Kaposi's Sarcoma associated Herpesvirus (KSHV). These two viruses are lymphotropic as are many of the other members of the γ -herpesviruses and so there is an association with predominantly lymphoproliferative diseases in B and/or T cells. EBV as a member of the genus lymphocryptoviruses is highly associated with Burkitt's Lymphoma but it can also lead to cancers of epithelial origin like nasopharyngeal carcinomas. KSHV can be assigned to the second genus of γ -herpesviruses, termed rhadinoviruses, and it is linked to Primary Effusion Lymphoma (PEL) and Multicentric Castleman's Disease (Cesarman et al., 1995; Soulier et al., 1995). Kaposi's sarcoma as a tumor of endothelial origin can also be assigned to KSHV (Chang et al., 1994; Whitby et al., 1995). Although substantial work has been carried out to understand the γ -herpesvirus lifecycle and the association to certain cancers there is still the urgent need for an *in vitro* transformation model especially for KSHV. This would enable the study of essential steps during virus-mediated tumorigenesis and unravel the underlying molecular mechanisms with the aim to design improved or new treatment options.

1.2 Kaposi's sarcoma associated herpesvirus

1.2.1 Particle structure and early steps of infection

Since its discovery in 1994 by representational difference analysis in Acquired Immunodeficiency Syndrome (AIDS) patients suffering from Kaposi's sarcoma (KS), Human Herpesvirus 8 (HHV-8) also known as Kaposi's sarcoma-associated Herpesvirus (KSHV) has been investigated intensively (Chang et al., 1994). While the virus was rapidly classified to the herpesvirus family according to comparative sequence analysis, the investigation of the virion structure proved difficult due to inefficient isolation methods. With the establishment of KSHV positive B cell lines, like BCBL-1, and the ability to induce lytic replication of the virus it became finally possible to isolate viral particles and to study structural aspects.

The linear double-stranded DNA genome of KSHV, free of nucleosomes or other DNA binding proteins, is surrounded by a highly structured, icosahedral capsid (Renne et al. 1996; Wu et al. 2000). The capsid is composed of hexameric and pentameric substructures called capsomers, containing the Major Capsid Protein (MCP, encoded by ORF25). The structures linking these capsomers are heterotrimeric complexes, consisting of one molecule of ORF62 and two molecules of ORF26 (Nealon et al., 2001; Trus et al., 2001; Wu et al., 2000). The fourth protein encoded by ORF65 is located at the surface of the capsid and, in contrast to the other capsid proteins, does not show significant sequence homology to its relatives from other subfamilies (Nealon et al., 2001; Sathish & Yuan, 2010). Finally, ORF17.5 as a scaffolding protein is also associated with the capsid and plays an important role during virus assembly (Unal et al. 1997; Deng et al. 2008). The capsid itself is embedded into a proteinaceous tegument layer, containing capsid-associated proteins, loosely associated proteins as well as viral RNAs (Zhu et al. 2005; Dai et al. 2014; Bechtel, Grundhoff, and Ganem 2005). The whole particle, consisting of the viral DNA, the capsid, and the tegument, is surrounded by a host derived lipid bilayer called envelope. Within the envelope several viral glycoproteins are embedded fulfilling crucial functions concerning viral entry into the host cell. All together these described structures form the KSHV virion, depicted in Figure 2A and 2B, with a size of around 120-150 nm (Said et al., 1997). In order to infect cells, KSHV encodes a variety of glycoproteins that are embedded into the virion envelope. These glycoproteins enable interaction with host surface receptors which marks the first step of a KSHV infection (Figure 2C).

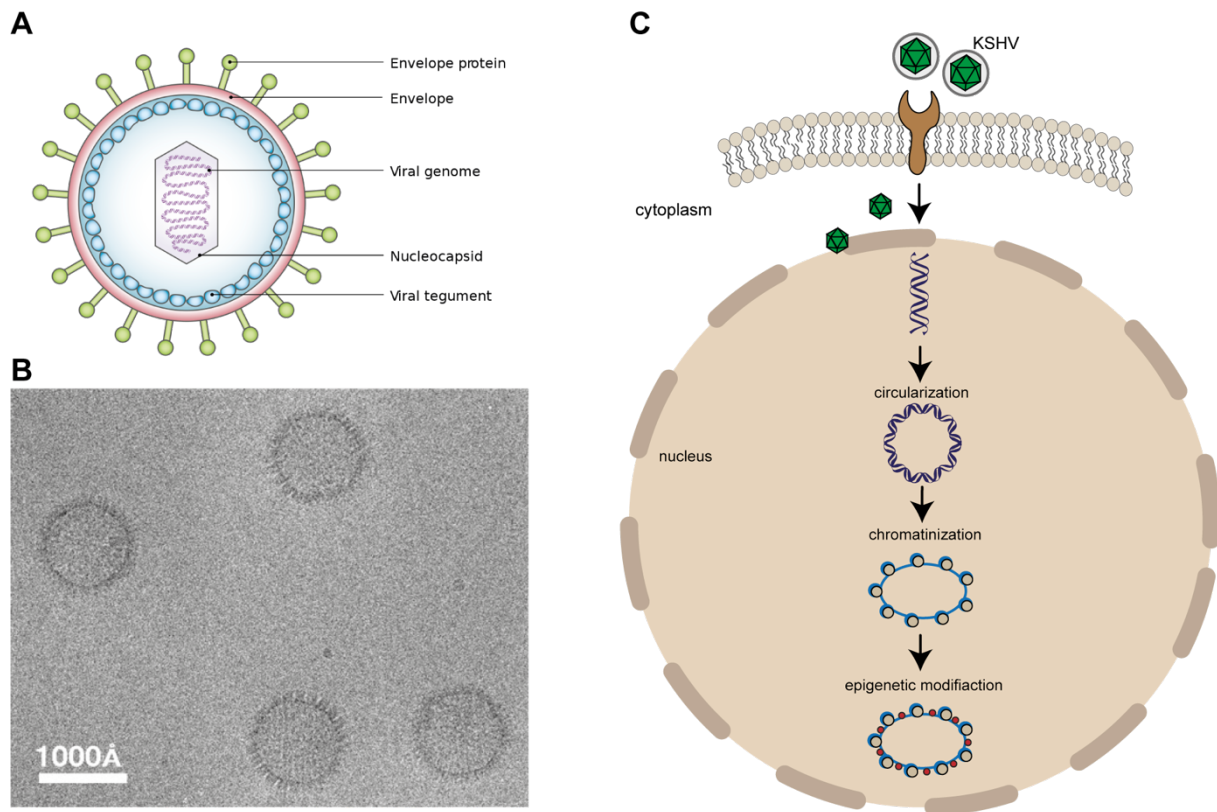


Figure 2: KSHV virion and early steps of infection: (A) Schematic overview of a herpesvirus virion. The linear dsDNA genome of KSHV is surrounded by the nucleocapsid. This structure is further embedded into the tegument, a layer composed of several viral proteins but also viral RNAs. Finally, the virion is protected by a host-derived lipid bilayer, termed envelop. Within this envelope several glycoproteins are embedded, allowing initial virus-host interactions. (B) Cryo-electron micrograph of KSHV capsids, scale bar 1000Å (modified from (Trus et al., 2001)). (C) Early steps of a KSHV infection. The KSHV glycoproteins interact with cell surface receptors which allows entry into the host cell via endocytosis. The virus is transported across the cytoplasm via the host microtubule network and finally reaching the nucleus. There, the viral DNA is injected through the nuclear pore. Within the nucleus, the viral DNA is circularized and chromatinized, leading to the decoration of the viral genome with epigenetic modifications (modified from (Lieberman, 2013)).

Among these proteins, gB encoded by ORF8 and the heterodimer of gH (ORF22) and gL (ORF47) are the most studied glycoproteins. The viral entry process starts with a non-specific interaction of viral glycoproteins and heparan sulfate proteoglycans on the cell surface. Especially gB, gH/gL, and K8.1A were identified as crucial proteins for this initial attachment process (Akula et al., 2001; Birkmann et al., 2001; Hahn et al., 2009). This first interaction brings the viral glycoproteins in close proximity to specific cell surface receptors, that are used by the virus to get internalized into the host cell. Several studies showed, that KSHV uses predominantly integrins and ephrin receptors, which are expressed on a wide variety of cell types. Akula et al. identified the cellular integrin $\alpha_3\beta_1$ (CD49) as an important receptor used by the viral glycoprotein gB (Akula et al., 2002). $\alpha_v\beta_3$ and $\alpha_v\beta_5$ receptors were added as additional interaction partners of gB (Garrigues et al., 2008; Veetil et al., 2008). Among the ephrin receptors, EphA2 was found to interact with the viral heterodimer of gH/gL thereby facilitating

internalization of the KSHV virion into endothelial cells (Hahn et al. 2012). Simultaneously, xCT and DC-SIGN were identified as entry receptors for KSHV with the latter being more specific for dendritic cells, macrophages, and activated B cells (Kaleeba and Berger 2006; Rappocciolo et al. 2006; 2008). Although KSHV uses variable, partly cell type specific glycoprotein/receptor interactions for the attachment to the cells, all of these interactions seem to result in endocytosis as the default pathway for the internalization of the KSHV virion (Akula et al., 2003). After internalization KSHV is located in low pH compartments which is thought to be an important step for further transport. The virion envelope subsequently fuses with the endocytic vesicle membrane which allows the release of the capsid into the cytoplasm. However, the exact mechanism of this fusion event and the involved viral and host proteins are still not investigated sufficiently. Within the cytoplasm, the KSHV capsid is further transported via host microtubules towards the nucleus (Naranatt et al., 2005). The viral capsid then disassembles, and the linear dsDNA enters the nucleus through the nuclear pore. Within the nucleus, circularization of the viral DNA represents one of the first steps to protect the genome against degradation. The mechanism of KSHV circularization is still not completely understood, but it is thought that it involves DNA end processing, homologous recombination, and ligation. In this context the terminal repeat region of the virus, consisting of multiple copies of 801 bp DNA elements, seems to play a crucial role (reviewed in Lieberman 2013). Regarding host factors, it was shown that IFI16 and proteins of the DNA damage response (DDR) are early nuclear interaction partners of the KSHV genome (Kerur et al., 2011; Roy et al., 2016; Singh et al., 2014). These factors might not only play a role during the circularization but might also be involved in a variety of further mechanisms like antiviral defense or the chromatinization of the viral genome, another crucial step within the nucleus. Chromatinization, the compaction of DNA with histone proteins, is a prerequisite for the decoration of the viral genome with epigenetic modifications. These modifications have a strong impact on viral gene expression and play a crucial role for the latency establishment of KSHV (Günther & Grundhoff, 2010; Toth et al., 2010).

1.2.2 The type I interferon response

Antiviral defense mechanisms, like the already mentioned DDR, are not only limited to the nucleus but start already in the cytoplasm upon entry of the virus. The innate immune response and especially the type I interferon signaling represents a fast

reaction of the cell against incoming pathogens. In the context of a KSHV infection, this cellular pathway was previously described to mainly play a role during *de novo* KSHV infection and upon induction of the lytic replication cycle.

The first step of this response involves the recognition of pathogen-associated molecular patterns (PAMPs) from the incoming virus. These patterns include on the one hand viral glycoproteins which are directly detected at the cell surface or on the other hand viral DNA or RNA which is recognized after the entrance of the virus into the cell. In order to detect these PAMPs, the host cell expresses a huge variety of pattern recognition receptors (PRRs). The best studied receptors are the Toll-like receptors (TLRs) which can be found according to their PAMP recognition on the host cell membrane or throughout the cytoplasm in different organelles (reviewed in Kawai & Akira, 2011). Beside the TLRs several other host factors exist which are involved in the sensing of pathogens. Upon *de novo* KSHV infection and also during lytic reactivation, different PRRs were shown to be activated. Not only TLRs but also cGAS and IFI16 as cytosolic DNA sensors, as well as RIG-I as a sensor of viral RNA were described to be involved in the recognition of the virus (West and Damania 2008; Ma et al. 2015; Zhang et al. 2018). Interestingly, IFI16 besides being a cytosolic sensor, was found to be one of the few PRRs which might enable the recognition of viral DNA in the nucleus (Kerur et al., 2011). The recognition of PAMPs leads to further signaling and results in the activation of the interferon regulatory transcription factors (IRFs) as well as NF- κ B. These transcription factors translocate to the nucleus where they bind the type I interferon (IFN) promoters, including mainly IFN- α and IFN- β , to induce their expression. IFNs are finally secreted and can either have autocrine or paracrine effects. They bind on the cell surface to the heterodimeric IFN- α receptor (IFNAR) which is composed of IFNAR1/2 subunits (Kim et al., 1997). The binding activates the receptor-associated kinases Janus kinase 1 (JAK1) and tyrosine kinase 2 (TYK2). This, in turn, leads to the phosphorylation of signal transducer and activator of transcription 1 (STAT1) and STAT2. The STAT proteins then dimerize and bind IRF9 which results in the interferon-stimulated gene factor 3 (ISGF3) complex. This complex when translocated to the nucleus can bind to interferon-responsive elements (ISREs) within numerous promoter regions and thereby transactivate interferon-responsive genes, like MX1, OAS2, and ISG15. These gene products establish an antiviral program which aims to restrict spreading of the pathogen (reviewed in McNab et al., 2015).

However, KSHV has evolved several strategies to subvert the type I interferon response. One of them involves the expression of several viral factors with counteracting functions at different steps of the host signaling cascade. Among these factors are predominantly lytic proteins, including for example the viral interferon-regulatory factors (vIRFs) (Fuld et al., 2006; Joo et al., 2007; Li et al., 1998; Wies et al., 2008) as well as ORF45 and ORF50 (Yu et al., 2005; Zhu et al., 2002). The previously identified short period of lytic viral gene expression upon *de novo* infection might therefore play an important role for inhibition of the type I interferon response (Krishnan et al., 2004; Purushothaman et al., 2015).

Another strategy involves the entry of KSHV into the latent infection state which is characterized by restricted viral gene expression and licensed DNA replication thereby allowing the virus to hide from the cellular immune response (reviewed in Broussard and Damania 2020).

1.2.3 Genome organization

One characteristic feature of herpesviruses is their large dsDNA genome which encodes for a large variety of genes. After its discovery in 1994, it took not long until initially partial sequences from KS lesions and subsequently the whole KSHV sequence was elucidated from BC-1, a PEL-derived tumor cell line (Russo et al., 1996). This revealed that the KSHV genome has a size of around 165-170 kb consisting of a long unique region (LUR) and a terminal repeat (TR) region. Both regions not only show considerable differences with regard to the length but also concerning the GC content. The LUR with a length of around 140 kb accounts for the major part of the genome and has a GC content of 54,5 %. In contrast, the TR region is only about 35-40 kb in size but has a GC content of 85 %. Further investigation of the TRs revealed, that a single copy is 801 bp long and that every genome harbors around 35-40 repeats (Lagunoff & Ganem, 1997). Interestingly, it was shown that the terminal repeats together with the latency-associated nuclear antigen (LANA, ORF73) are crucial for the persistence and the replication of the KSHV genome (Ballestas et al., 1999; Ballestas & Kaye, 2001; Grundhoff & Ganem, 2003; Hu et al., 2002; Verma, Choudhuri, et al., 2007). However, more recent investigations indicate the existence of alternative replication initiation sites within the KSHV genome which might function independent of LANA (Verma et al., 2011; Verma, Lan, et al., 2007). While the origin of latent KSHV replication (ori-P) was assigned to the TR region, the origin of lytic DNA

replication was identified within the LUR. Two duplicated copies, called ori-Lyt(L) and ori-Lyt(R) exist which are located between K4.2 and K5 and between K12 and ORF71, respectively (AuCoin et al., 2002; Lin et al., 2003).

First attempts of KSHV sequence analyses identified 81 open reading frames (ORFs) (Russo et al., 1996), which correspond well with more recent KSHV gene annotations. Additional studies complemented this annotation with some small ORFs, the viral miRNAs as well as additional lncRNAs (Cai et al., 2005; Chandriani et al., 2010; Grundhoff et al., 2006). Currently 87 ORFs are known to be encoded by KSHV. Their nomenclature derives from homologous proteins of the closely related herpesvirus saimiri (HVS) while the 15 genes unique to KSHV are marked by the letter “K” (also see Figure 3).

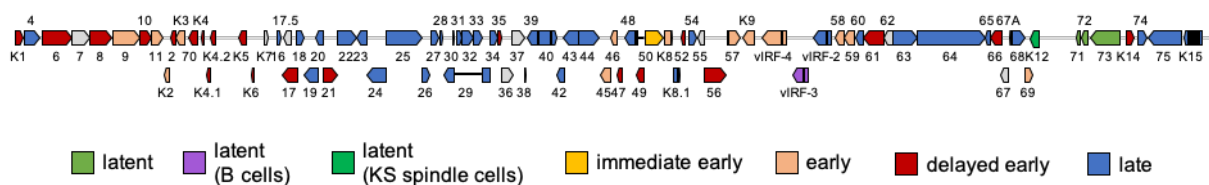


Figure 3: Schematic overview of the linear KSHV genome: An overview of the KSHV genome in the linear form is shown. The open reading frames (ORFs) are indicated as arrows. The color code gives information about the temporal expression of the genes (modified from (Arvin et al., 2007)).

With the advances of high-throughput sequencing methodologies in the recent years more and more potential coding but also non-coding transcripts were identified which might originate from alternative transcriptional start sites (TSS) or alternative splicing events (Arias et al., 2014). This leads to an even higher coding capacity of the KSHV genome than originally expected, further increasing the complexity of herpesviruses.

1.2.4 Biphasic lifecycle

KSHV shares the characteristic feature of having a biphasic lifecycle with other members of the herpesvirus family. The first part of the lifecycle, termed viral latency, aims to achieve lifelong persistence within the host without the production of viral progeny. After entrance of the host cell, the naked linear viral genome is injected into the nucleus and it was shown in several *in vitro* systems, that the virus by default enters the latent state. This is achieved by rapid circularization of the genome and by silencing large parts of the viral transcripts. Only a small subset of genes, including K12, v-FLIP (ORF71), v-Cyclin (ORF72), LANA (ORF73) and a group of viral microRNAs (miRNAs) is expressed during this phase of infection (Dittmer et al., 1998). Especially LANA,

which is able to tether the viral genome to the host chromosomes during cell division, fulfills crucial roles regarding virus persistence (Ballestas et al., 1999). This protein is also involved in the recruitment of the host replication machinery in order to enable latent viral DNA replication (Grundhoff & Ganem, 2003; Hu et al., 2002; Verma, Choudhuri, et al., 2007).

However, upon certain environmental or physiological stimuli, like hypoxia (Davis et al. 2001) or oxidative stress (Ye et al., 2011), the latent phase is reversible and lytic reactivation takes over with the aim of viral progeny production. This second phase of infection is marked and initiated by the expression of the replication and transcription activator (RTA, ORF50) (Lukac et al., 1998). This results in the expression of all the lytic viral genes in a temporal manner, leading to extensive viral DNA replication in so called replication centers. The replicated viral genome is encapsidated, surrounded by the tegument and finally enveloped during the release of the virus through the host membrane.

1.2.4.1 Latent infection

During latency the KSHV genome persists as a non-integrated, multi-copy, circularized episome within the nucleus with most of the genes being transcriptionally silenced (Renne et al. 1996). Expression of only a limited number of genes can be observed which include LANA, v-FLIP, v-Cyclin, Kaposin and the viral miRNAs (Cai et al., 2005; Dittmer et al., 1998; Gottwein et al., 2006; Staskus et al., 1997). Another protein expressed during latency but exclusively in PEL cells and MCD is vIRF3 encoded by K10.5 (Fakhari & Dittmer, 2002; Wies et al., 2008). While LANA, v-FLIP, and v-Cyclin are expressed from one constitutively active promoter LT_c, the three Kaposin members and most probably also the viral miRNAs make use of the LT_d promoter which is located downstream of LANA (Dittmer et al., 1998; Pearce et al., 2005). All mentioned proteins fulfill distinct functions in order to maintain the latent infection state but in part also provide mechanisms to drive the host cell towards transformation. LANA is probably one of the most important proteins when it comes to the establishment and maintenance of latency. This protein with a size of 1162 aa was shown to bind with its C terminal part to three specific LANA binding sites (LBS1-3) within the terminal repeats (Garber et al., 2002; Hellert et al., 2015; Kelley-Clarke et al., 2007). With its N terminus LANA can bind specifically to histones H2A and H2B on the host chromatin (Barbera et al., 2006). Simultaneous binding of the viral genome and host chromatin

allows proper segregation of the KSHV genomes to the daughter cells during cell division (Ballestas et al., 1999). Not only the involvement during the tethering mechanism but also the recruitment of the host replication machinery to the viral genome makes LANA a protein with crucial functions during the latent infection state. TR-bound LANA recruits several components of the pre-replication machinery but also replication licensing components in an orchestrated manner to the ori-P. These proteins include the origin recognition complex (ORC), cell division cycle 6 (CDC6) as well as several members of the minichromosome maintenance proteins (MCM) (Stedman et al., 2004; Verma et al., 2006) which results in one round of replication per cell cycle. Beside these functions, LANA was additionally described to interact with lytic viral proteins as well as host factors to keep the virus in a quiescent state. With regard to interactions with viral proteins, it was shown that LANA can not only interfere with the function of RTA, the immediate early protein during lytic reactivation, but it also inhibits its expression through binding to its promoter region (Lan et al. 2004). Kap1 was identified as a host interaction partner of LANA that might be recruited to the viral genome and downregulate expression of lytic viral genes (Sun et al. 2014). In recent years it became evident that KSHV might also use host epigenetic modifying enzymes in order to repress viral lytic transcripts. Posttranslational modifications can be found at several positions of the histone proteins. Depending on the modification this can have activating but also repressive outcome for gene expression. With evolving Chromatin-Immunoprecipitation (ChIP) methods it became possible to investigate the epigenetic landscape of KSHV (Figure 4).

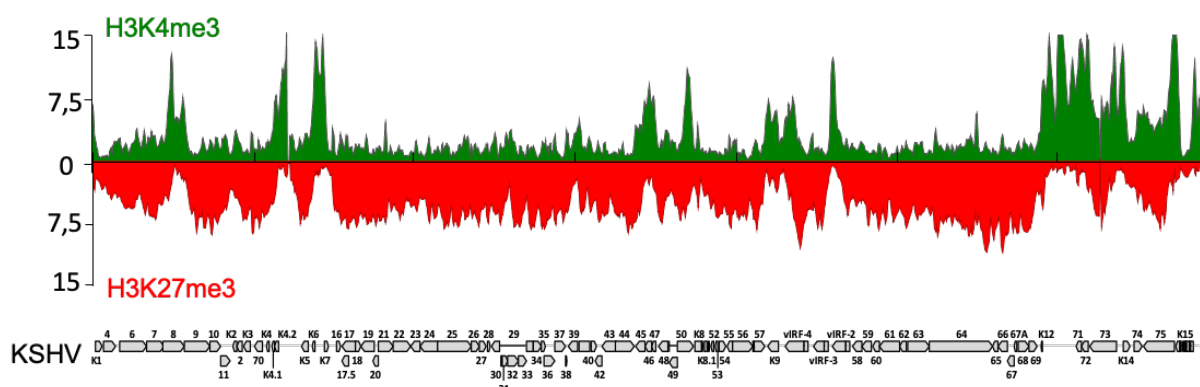


Figure 4: Epigenetic landscape of the KSHV genome: ChIP on microarray analysis from KSHV infected SLK cells 72 hpi reveals distinct patterns of the histone marks H3K4me3 (shown in green) and H3K27me3 (shown in red) (modified from (Günther et al., 2014)).

This revealed that the KSHV genome is decorated with activating as well as repressive marks rapidly after *de novo* infection and that these marks stay stable also in long-term

latently infected cells (Günther et al., 2014; Günther & Grundhoff, 2010; Toth et al., 2010). The activating histone mark H3K4me3 is predominantly enriched in regions where latently expressed genes are encoded. Interestingly, also in regions of lytic viral genes, for example in the locus of vIRF3, distinct peaks for H3K4me3 were identified without driving expression of stable transcripts. While most of the genome is covered with the repressive histone modification H3K27me3, the locus of ORF50 (RTA) represents one region where activating as well as repressive histone modifications can be found. This combination is referred to as bivalent chromatin, a state which keeps genes transcriptionally repressed but poised for rapid activation. These findings are in agreement with the concept of the herpesvirus lifecycle which includes on the one hand repression of large parts of the viral genome, but on the other hand also provides the possibility of a fast reaction to certain stimuli and reactivation of the whole gene cassette.

Another very interesting aspect concerning latency establishment, maintenance, and regulation of KSHV gene expression in general involves chromatin conformation and DNA looping. Cellular factors which are highly associated with DNA looping are the DNA binding protein CTCF and cohesin. While CTCF and cohesin mediated long range DNA interactions on the KSHV genome were shown to play a role in latent gene expression and genome maintenance, more recent studies imply that they also play important roles during the temporal gene expression upon viral reactivation (Campbell et al., 2018; Kang et al., 2011; Stedman et al., 2008).

1.2.4.2 Lytic reactivation

While the latent infection is marked by the limited expression of viral genes and licensed DNA replication, lytic reactivation implies the expression of most or all of the viral genes and extensive viral DNA replication. This part of the viral lifecycle fulfills the role of progeny production in order to achieve dissemination as well as transmission. Additionally, there is increasing evidence that lytic reactivation might also play a role in KSHV associated tumorigenesis.

Lytic reactivation is induced by different physiological or environmental conditions. These include stimuli like hypoxia (Davis et al. 2001), oxidative stress (Ye et al., 2011), but also co-infections with other viruses were shown to lead to a switch in the viral lifecycle (Varthakavi et al., 2002). In B cells, plasma cell differentiation and the expression of XBP-1s, a transcription factor activated by endoplasmic reticulum (ER)

stress, can induce KSHV reactivation (Wilson et al., 2007). *In vitro*, KSHV lytic reactivation can also be induced by certain chemicals. 12-O-tetradecanoyl-phorbol-13-acetate (TPA) as an activator of the MAPK/ERK pathway and the histone deacetylase (HDAC) inhibitor sodium butyrate were shown to be potent chemicals which can lead to lytic replication (Cohen et al., 2006; Miller et al., 1997). All of these stimuli lead to the expression of the viral lytic genes in a temporal fashion. According to their expression kinetics these genes can be classified into different groups (Figure 3) (Sun et al. 1999). The first genes which are expressed after induction of the lytic cycle are termed immediate early genes. Early and delayed early genes are the next groups which are induced. These three mentioned groups have in common that their expression does not depend on lytic DNA replication. Contrarily, the group of the late genes is dependent on lytic DNA replication and *de novo* protein synthesis. Predominantly structural proteins like the capsid proteins or the viral glycoproteins belong to this class. RTA encoded by ORF50 is one of the first genes expressed upon lytic reactivation. It was shown that the expression of this gene is necessary but also sufficient for KSHV reactivation (Sun et al. 1998; Lukac et al. 1998). The protein binds to RTA responsive elements (RRE) within the viral genome which results among others in the induction of K8. RTA can act independently but in most of the cases RTA uses a cellular co-activator. RBP-J κ was identified as important cellular factor which cooperates with RTA and supports the induction of responsive genes (Liang et al., 2002; Papp et al., 2018; Wang & Yuan, 2007). Epigenetic modifying enzymes, which were already described to play a role during latency, might also play a role during lytic reactivation. The long non-coding RNA (lncRNA) PAN, which is highly transcribed during lytic reactivation was shown to interact with host epigenetic modifiers like UTX, JMJD3, and MLL2 (Rossetto & Pari, 2012). While UTX and JMJD3 are lysine demethylases implicated in the demethylation of the repressive mark H3K27me3, MLL2 is an enzyme which catalyzes methylation of H3K4. This could result in the conversion from a repressed genome towards an activating surrounding and thus further supports lytic gene expression. The observation that overexpression of JMJD3 in BCBL-1 cells led to a global reduction of H3K27me3 and increased KSHV lytic reactivation further supports this notion (Günther & Grundhoff, 2010).

Beside the binding of RTA to promoters of lytic viral genes, the protein also cooperates with K8 at the ori-Lyt to recruit the pre-replication complex (Lin et al., 2003; S. E. Wang et al., 2003; Y. Wang et al., 2004). In contrast to the latent state where the host

replication machinery is recruited, lytic replication is mediated by viral proteins including a polymerase (ORF9), a polymerase processivity factor (ORF59), a single stranded binding protein (ORF6), a helicase (ORF44), a primase (ORF56), and a primase-associated factor (ORF40/41) (Wu et al. 2001). More recent studies revealed that beside these essential viral lytic genes, also host factors, like topoisomerases, are recruited to ori-Lyt and that they have supportive functions during replication (Y. Wang et al., 2008). Lytic replication is also distinct to latent DNA replication regarding the rate of amplification. While DNA amplification during latency is restricted to one cycle per cell division, lytic replication can result in the 100- to 1000- fold amplification of the viral genome. This is thought to be mediated by a rolling-circle mechanism in replication compartments within the nucleus which generates DNA concatemers that have to be cleaved prior to packaging. Encapsidated viral particles are transported to the cytoplasm and finally gain their envelope during the transport out of the cell.

1.2.5 Cell tropism

γ - herpesviruses are generally classified as lymphotropic viruses because they typically reside in B cells, like it is the case for KSHV and EBV, or in T cells. However, since transmission is thought to occur predominantly via salivary routes, *de novo* infection might take place in any other local cell type, like epithelial or endothelial cells. As the virus was not only detected in B cells but also in endothelial cells, monocytes, keratinocytes as well as epithelial cells *in vivo*, KSHV is expected to have a relatively broad cell tropism (Boshoff et al., 1995; Cesarman et al., 1995; Monini et al., 1999). With regard to KSHV associated tumors there seems to be a narrow cell range as only B cells and endothelial cells are thought to be involved in this process.

The cell tropism highly increases *in vitro* as KSHV was shown to infect a wide variety of cell types such as endothelial as well as epithelial cells, keratinocytes, fibroblasts and macrophages. KSHV can even infect different cell types from organisms like hamsters, mouse and rat in cell culture systems (Bechtel et al. 2003). Infection of these cells predominantly results in the latent infection state. However, lytic reactivation can be induced in most of the cells by the treatment with certain chemicals. Remarkably, one of the few cells which can hardly be infected in *in vitro* systems are B cells although they are known to be the latent reservoir *in vivo* and can give rise to KSHV associated lymphomas. As B cells express only low levels of heparan sulfate, the cell surface proteins for initial KSHV attachment, genetically modified B cells might be one of the

few possibilities to get low level infection *in vitro* (Jarousse et al., 2008). Another approach to obtain low level infection in cell culture is to use activated B cells as they show increased expression of DC-SIGN, one of the entry receptors of KSHV (Rappocciolo et al., 2008).

1.2.6 KSHV induced tumorigenesis

Initially identified in AIDS-associated KS lesions, KSHV was rapidly assigned as the etiological agent of this tumor (Chang et al., 1994; Whitby et al., 1995). It took not long until the virus was also linked to the B cell malignancies PEL and MCD (Cesarman et al., 1995; Soulier et al., 1995). The fact that predominantly latent viral gene products are detected in KS and B cell malignancies led to the assumption that latency might be the driving force towards tumorigenesis. In line with this, many studies describe diverse roles of KSHV latent gene products with regard to transformation. LANA, for example, was shown to interfere with the function of several tumor suppressors as well as oncogenes. The viral protein inhibits the transcriptional activity of the tumor suppressor p53 leading to reduced induction of apoptosis (Friborg et al., 1999). Radkov et al. studied the interaction of LANA with the retinoblastoma-E2F pathway and additionally showed that co-expression of LANA and the oncogene H-ras led to transformation in primary rat cells (Radkov et al., 2000). Additionally, LANA stabilizes c-Myc in several PEL cell lines by inhibition of the glycogen synthase kinase-3 β (GSK-3 β) (Bubman et al., 2007; Liu et al., 2007). Another latent gene product shown to have pro-tumorigenic functions is v-FLIP. Several studies indicate that this protein activates the NF- κ B pathway by phosphorylation of I κ B α which leads to the characteristic endothelial spindle cell form also observed in KS lesions (Liu et al. 2002; Grossmann et al. 2006). Furthermore, v-FLIP induces the expression of cytokines like IL-6 and cell surface adhesion proteins conferring a pro-inflammatory phenotype which is also a characteristic feature of KSHV associated tumors (An et al., 2003; Ballon et al., 2015). v-Cyclin, the viral homologue of the cellular cyclin D2, can modulate the host cell cycle by increasing the G1/S transition through constitutive activation of Cdk6 (Godden-Kent et al., 1997). Moreover, KSHV encodes a cluster of twelve precursor miRNAs which, in their mature form, can fulfill multiple functions including regulation of the host cell cycle, the immune response, and viral induced angiogenesis (Cai et al. 2005; Grundhoff, Sullivan, and Ganem 2006; Gottwein and Cullen 2010; Li et al. 2016). Interestingly, several studies describe viral miRNAs which can mimic their cellular

counterparts. This was for example shown for the viral miR-K12-11 which shows similarities to the human miR-155 concerning the sequence composition as well as the target genes (Dahlke et al., 2012; Gottwein et al., 2007).

The fact that latent KSHV infection does not lead to transformation *in vitro* and the notion that lytic viral transcripts can be detected in KS lesions as well as in PEL cell lines provided evidence that lytic replication might also play a role during tumorigenesis. As the KSHV lytic cycle is fatal for the host cells, it is thought that paracrine effects might influence latently infected cells instead. However, several studies also describe lytic gene products with a direct association to tumorigenesis. K15 for example was shown to increase the angiogenic potential as well as the invasiveness of infected cells (Bala et al., 2012; Gramolelli et al., 2015). A positive effect on angiogenesis was also described for v-IL6 (Aoki et al., 1999). This lytic protein, when expressed in mice, generated a MCD-like phenotype (Maier et al., 2004). Moreover, a pro-tumorigenic phenotype was observed upon overexpression of K1 and in transgenic mice when it was introduced into the mouse homologue MHV-68 (Douglas et al., 2004; Li et al., 2016).

In summary, multiple studies revealed that KSHV latent as well as lytic proteins can affect several cellular processes like cell cycle, apoptosis, and angiogenesis highlighting the transforming potential of the virus. Some viral proteins were even shown to transform cells *in vitro*. However, these observations originate predominantly from overexpression experiments in artificial cell culture systems and in part also by co-expression of cellular oncogenes. This highlights that there is an urgent need for *in vitro* but also *in vivo* KSHV transformation models.

1.3 KSHV associated malignancies

1.3.1 Seroprevalence and epidemiology

In contrast to other herpesviruses which infect the majority of healthy individuals, KSHV seroprevalence shows a distinct geographical pattern (Figure 5). While KSHV is highly endemic in sub-Saharan Africa with seroprevalence rates reaching over 50%, the virus is rather infrequent in Northern Europe, Asia and the United States. In the Mediterranean region the virus is moderately common with seroprevalence ranging from below 10-30% (Gao et al., 1996; Lennette et al., 1996; Simpson et al., 1996). With increasing seroprevalence rates also the incidence of Kaposi's sarcoma is rising. While rare in most areas of the world, KS displays one of the most common cancers

in several countries in Southern and Eastern Africa (Bray et al., 2018). Transmission of the virus is also thought to be at least partly dependent on the geographical region. KSHV, like other herpesviruses, is predominantly transmitted horizontally via saliva (Koelle et al., 1997; Pauk et al., 2000).

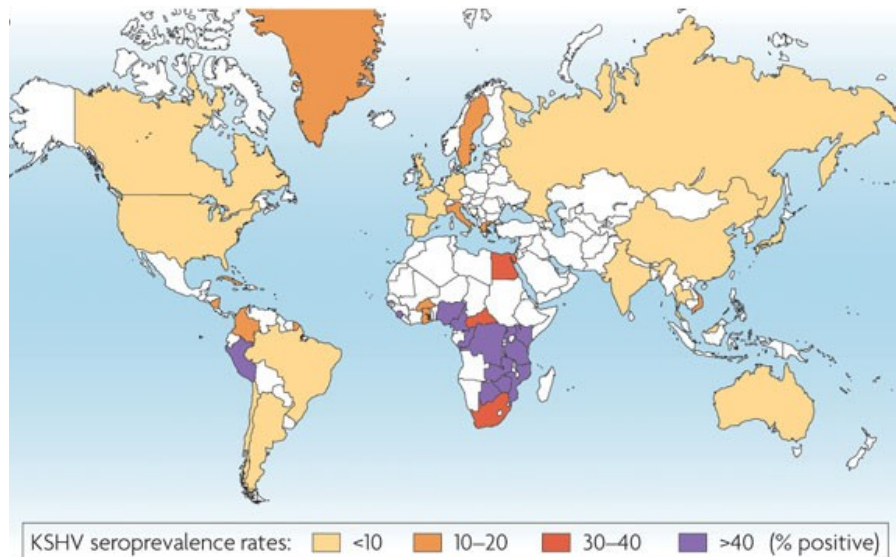


Figure 5: KSHV seroprevalence: Several studies were summarized to give KSHV seroprevalence rates for most of the countries. While the seroprevalence in sub-Saharan Africa reaches over 50%, KSHV is rather infrequent in Northern Europe, Asia and the United States. The Mediterranean area has an intermediate seroprevalence ranging from 10-30% (Mesri et al., 2010).

Especially in endemic areas, where the virus was shown to spread within families, infection seems to occur early in childhood (Dedicoat et al., 2004). There is also the possibility of sexual transmission between adults displaying a more important role in non-endemic areas (Kedes et al., 1996). Saliva seems here also to be the main route as well, as studies reporting the detection of KSHV in semen are contradictory (Diamond et al., 1997; Howard et al., 1997). Additionally, there is some evidence that KSHV transmission might rarely occur during blood transfusion (Blackbourn et al., 1997; Dollard et al., 2005) and organ transplantation (Francès et al., 2009; Regamey et al., 1998).

1.3.2 Primary Effusion Lymphoma

One of the KSHV-associated malignancies is Primary Effusion Lymphoma (PEL) a tumor of B cell origin (Cesarman et al., 1995). Proliferating cells of this monoclonal neoplasm are often present as effusions in body cavities and do not form solid tumors. The presence of immunoglobulin rearrangements and hypermutations indicate that PEL might represent post germinal center B cells (Matolcsy et al., 1998). Furthermore,

tumor cells were shown to have a plasma cell expression profile which is consistent with the expression of the marker CD138 (Jenner et al., 2003; Klein et al., 2003). PEL often occurs in immunocompromised patients and the median survival rate of around 6 months indicates poor prognosis (Boulanger et al., 2005).

In PEL cells, KSHV is present predominantly in the latent state with expression of LANA, v-FLIP, v-Cyclin, the viral miRNAs and v-IRF3. In 1-3% of the cells lytic replication can be observed. Several PELs have been isolated and can be passaged in cell culture systems. siRNA-mediated knock down (KD) of v-IRF3 and v-FLIP in these cell lines induces apoptosis, indicating that tumors are highly dependent on the expression of these genes (Guasparri et al., 2004; Wies et al., 2008). In accordance with the function of v-FLIP to constitutively activate the NF- κ B pathway, inhibitors against this pathway were also able to induce apoptosis in PEL cells (Keller et al., 2000). In addition to NF- κ B as a host dependency factor, Manzano et al. identified in an elegant CRISPR/Cas9-based screen IRF4, MDM2, CCND2, and MCL1 as additional host factors which are crucial for PEL survival (Manzano et al., 2018).

Another very interesting aspect about PEL is the co-occurrence of EBV in most of the cases (Cesarman et al., 1995). Although the mechanisms are not fully understood, there is experimental evidence that EBV might have at least supporting functions during the development of PEL. When Trivedi et al. infected EBV-negative PEL cell lines with recombinant EBV, they found increased tumorigenicity in SCID mice (Trivedi et al., 2004). Similar results were obtained in a humanized mouse model with co-infection of KSHV and EBV. Tumors growing from co-infected mice had a gene expression profile characteristic for PELs (McHugh et al., 2017). In both cases the tumorigenic potential of co-infected populations was increased in comparison to single infected controls. However, the fact that the tumors are highly dependent on KSHV gene expression and the presence of EBV negative PELs highlight that KSHV is the driving force in the context of this tumor.

1.3.3 Multicentric Castleman's Disease

Multicentric Castleman's Disease (MCD) is a rare polyclonal lymphoproliferative disorder which can occur in two forms. On the one hand there is the hyaline vascular type and on the other hand the plasmablastic variant exists which is highly associated with KSHV (Soulier et al., 1995). In contrast to PEL, where expression is predominantly restricted to viral latent genes, KSHV shows a more relaxed gene expression pattern

in MCD (Katano et al., 2000; Parravicini et al., 2000). Among the expressed proteins which were detected in immunohistochemistry of MCD samples, was v-IL6. This viral factor was shown to promote B cell growth and angiogenesis, two characteristic features of MCD (Aoki et al., 1999). Additionally, v-IL6 is able to activate its human counterpart and together with IL10 these factors can be correlated with the severity of the disease (Mori et al., 2000; Oksenhendler et al., 2000; Polizzotto et al., 2013).

1.3.4 Kaposi's sarcoma

While Kaposi's sarcoma (KS) was initially described as a rare skin tumor predominantly affecting elderly people, the incidence of KS was rising rapidly with the beginning of the AIDS pandemic in 1981 and it is one of the most common cancers in many subequatorial African countries (Bray et al., 2018; Kaposi, 1872). KS can be divided into four epidemiological forms (Gallo, 1998). The classic form of KS can be predominantly found in elderly people and is probably the one which was originally described. The endemic KS is mainly restricted to certain countries in Central and Eastern Africa and affects men as well as females, but notably also children with disseminated lymphadenopathy. KS which develops in immunosuppressed transplant recipients is termed as the iatrogenic form. The epidemic or AIDS-KS is the form where KSHV was first identified in and with which the virus is also highly associated (Chang et al., 1994; Whitby et al., 1995). The malignancy is thought to be of multiclonal origin due to the presence of several cell types including vascular and lymphatic endothelial cells, macrophages, lymphocytes, and plasma cells (Gill et al., 1998). Characteristic features of KS are the spindle shaped cells which are thought to be of endothelial origin and confer the replicating potential. The identity of these spindle cells is still highly debated as surface markers from different cell types can be detected (Jussila et al. 1998; Hong et al. 2004; Wang et al. 2004). Furthermore, the lesions are highly vascularized and inflammatory infiltrates are already present during early KS development.

The presence of KSHV within the tumors and the interplay of viral factors with the host reflects very well the characteristics of KS. Wang and Damania for example revealed that KSHV infection leads to a growth advantage of endothelial cells compared to uninfected cells (Wang and Damania 2008). Furthermore, the spindle cell shape was shown to be at least partly induced by the NF- κ B activation of v-FLIP (Alkharsah et al., 2011; Ballon et al., 2015; Grossmann et al., 2006). Several KSHV factors were

additionally shown to increase angiogenesis as well as invasiveness and migration of endothelial cells (Bala et al., 2012; Cheng et al., 2011; Gramolelli et al., 2015; Haas et al., 2013). Finally, KSHV infection induces the secretion of several cytokines like VEGF, IL-6, and IL-8, conferring a pro-angiogenic and pro-inflammatory micro-environment (Wang et al. 2004). Although KSHV was shown to be predominantly latent within the spindle cells, there is also a minor cell population where lytic transcripts are detectable (Dupin et al., 1999; Katano et al., 2000; Staskus et al., 1997). Lytic replication might be an important factor regarding re-infection within the tumor. This is evidenced by the fact that not all of the cells within a lesion are KSHV positive and moreover, endothelial cells tend to lose the virus *in vitro* (Grundhoff & Ganem, 2004a). Despite all these functions, KSHV infection of endothelial cells *in vitro* does not lead to the full transformation of cells. Additionally, attempts to isolate KS spindle cells from patients and to culture them *in vitro* were up until now only successful in the presence of several cytokines and growth factors. These observations imply that KSHV is necessary but not sufficient for KS to develop and that transformation highly relies on cofactors. One such cofactor is HIV1 as the incidence of developing KS increases from 1 in 100,000 in the general population to 1 in 20 in HIV1-infected individuals (Gallo, 1998). As the iatrogenic form also develops in immunocompromised patients, there is much evidence, that immunosuppression is one of crucial co-factors during KS development (reviewed in Mesri, Cesarman, and Boshoff 2010; Schulz and Cesarman 2015).

1.4 Epigenetic Modifications

1.4.1 DNA methylation

The term epigenetics describes the phenomenon of phenotypic inheritable changes that cannot be attributed to alterations in the DNA sequence. On the molecular level this term refers to mechanisms that are either directly associated with the DNA, including DNA methylation or it affects posttranslational modifications of DNA associated histones. DNA methylation is defined by the enzymatic conversion of cytosine to 5-methylcytosine. In eukaryotes, DNA methylation can occur in different genomic contexts, including for example CpA methylation which was detected in human embryonic stem cells or differentiated neurons (Guo et al., 2014; Ramsahoye et al., 2000). However, the most studied form of DNA methylation in mammals occurs in the context of CpG dinucleotides and information in this chapter are referring to this

form of methylation. The deposition of this modification is catalyzed by three conserved DNA-methyltransferases (DNMTs) which add a methyl group to the fifth carbon atom of the cytosine molecule. While DNMT3A and DNMT3B are *de novo* methyltransferases (Okano et al., 1999), DNMT1 is crucial for maintaining the DNA methylation pattern after DNA replication (Bestor et al., 1988) (Figure 6). The function of DNMT1 is nicely recapitulated by its preference for hemimethylated DNA as a substrate (Fatemi et al., 2001; Hermann et al., 2004) and the localization of the protein to the replication foci (Leonhardt et al., 1992).

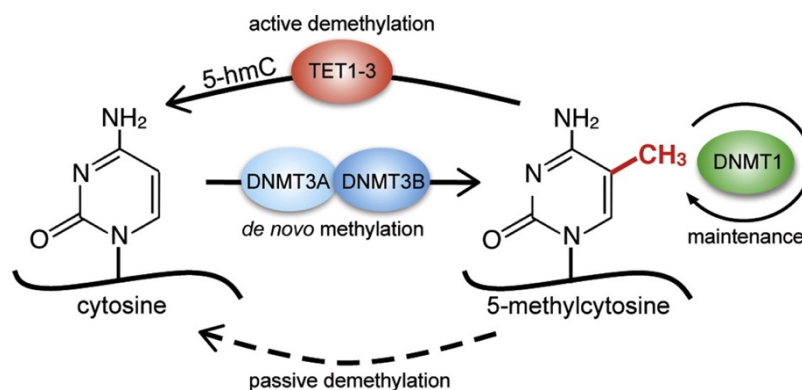


Figure 6: DNA methylation and its key players: Methylation of the fifth carbon atom of the cytosine base is enzymatically catalyzed by DNA-methyltransferases (DNMTs). While *de novo* DNA methylation is deposited by DNMT3A and DNMT3B, DNMT1 acts during replication in order to maintain the methylation pattern. While passive demethylation is observed, TET1-3 proteins are capable to actively remove these marks. This process involves the conversion of 5-methylcytosine to 5-hydroxymethylcytosine, 5-formylcytosine, and 5-carboxylcytosine. These products are finally removed through DNA repair mechanisms (Ambrosi et al., 2017).

Although DNA methylation is thought to be a stable epigenetic modification, at least two major processes are known to mediate demethylation. One of them prerequisites the lack of DNMT1 activity and rather constitutes a passive form of demethylation. As DNA methylation is diluted with every round of replication, this mark can be completely removed from a locus within just two rounds of cell divisions in the absence of DNMT1 activity. The second process includes the enzymatic activity of specific cellular factors and is therefore considered as the active form of demethylation. The Ten-Eleven Translocation (TET) proteins were shown to convert 5-methylcytosine to its oxidized derivatives 5-hydroxymethylcytosine, 5-formylcytosine, and finally to 5-carboxylcytosine (Ito et al., 2011; Tahiliani et al., 2009). These forms can then either be excised by cellular DNA repair mechanisms or removed during cell division (He et al. 2011). Three different TET family members are known and their expression during different developmental stages suggests that each of them might have discrete functions (Hackett et al., 2013; Shen et al., 2014). This is underlined by the assumption

that the different TET family members show preferential affinity for specific 5-methylcytosine derivatives (Hu et al. 2015).

The presence of CpG methylation in promoter regions is highly associated with long-term transcriptional repression. Depending on the organism and cell type, around 60-80 % of the CpG sites are found to be methylated in mammalian genomes. When it comes to CpG islands which are characterized by very high CpG concentrations, the relations are reversed (Bird, 1980). Only about 10-20% of CpG islands show high levels of DNA methylation. These methylated CpG islands are often located in promoter regions of imprinted genes or control the expression of tissue specific genes. The majority of the regions, however, is located in promoters of actively transcribed genes and there, DNA methylation is actively avoided. RNA polymerase II occupancy (Takeshima et al., 2009), transcription factor binding (Krebs et al., 2014) as well as the activating histone modification H3K4me3 (Balasubramanian et al., 2012) are thought to be involved in preventing these regions from DNA methylation.

Beside the classical and widely accepted anti-correlative relation between CpG methylation and gene expression, several publications also describe other or rather more detailed and locus specific functions of DNA methylation patterns. These functions include DNA methylation in gene bodies which might be associated with increased gene expression (Ball et al., 2009; Lister et al., 2009; Rauch et al., 2009). However, this observation seems to be at least partly context dependent as it is not a general feature which is found genome-wide or in different cell types (Lou et al., 2014). DNA methylation is highly connected to several developmental but also cellular processes including the repression of gamete-specific genes (Borgel et al., 2010) or genomic imprinting (Kaneda et al., 2004). Furthermore, this modification is involved in X chromosome inactivation (Beard et al., 1995) but also in silencing of endogenous transposable elements to maintain genome stability (Walsh et al., 1998). Recently, a fourth DNA methyltransferase was identified in mice, which was described to specifically silence retrotransposons during the male germ cell development. This enzyme was named DNMT3C and it was found to be a duplication of the previously introduced DNMT3B (Barau et al., 2016).

In addition to these crucial roles during development and differentiation, misregulation in DNA methylation processes can also lead to severe outcomes. One of the probably best investigated form of misregulation occurs during tumorigenesis and involves a global hypomethylation. Besides global loss of DNA methylation another often

observed process during cancer development and also in fully established tumors is the hypermethylation of CpG islands (Esteller et al. 2001; also reviewed in Pfeifer 2018).

1.4.2 Histone modifications

The up until now valid model that compaction of genomic DNA is achieved by entwining the DNA around an octamer of histone proteins dates back to the 1970s (Kornberg, 1974; Kornberg & Thomas, 1974). This octameric complex is composed of two copies of each histone core protein, called H2A, H2B, H3, and H4. The DNA which is wrapped around the histone complex has a consistent length of 146-147 bp. This compaction state is referred as nucleosome and represents the smallest unit of the chromatin organization. Several nucleosomes can also be connected by the linker histone H1 which then forms a fiber structure and leads to even higher compaction of the DNA.

The finding that histone proteins can undergo posttranslational modifications initiated a complex and far-reaching research field (Phillips, 1963). To date, a huge variety of histone modifications have been identified which predominantly occur at the protruding tails of the histone proteins and affect mainly methylation, acetylation, phosphorylation, and ubiquitination of distinct amino acids. Their function in influencing chromatin compaction and thereby also gene expression has a strong impact on almost all developmental and cellular processes. While some histone modifications seem to be context-dependent and rather variable as they are induced by certain stimuli, a subset of very stable histone marks exist throughout different cell types and organisms and are characteristic features for distinct genomic loci. These stable histone marks which are also re-established after cell division are considered, like DNA methylation, as epigenetic modifications.

Generally, histone modifications can be divided into two major groups according to their mode of chromatin remodeling and gene regulation. On the one hand, histone modifications like H3K4me3, H3K9ac or H3K14ac are predominantly associated with euchromatin and can be found in promoter regions of actively transcribed genes (Karmodiya et al., 2012; Santos-Rosa et al., 2002). Another histone modification which is associated with transcriptionally permissive chromatin is H3K27ac. This histone mark can also be detected at promoters but especially high levels are found in active enhancer regions where it is combined with H3K4me1 (Wang et al. 2008; Creighton et al. 2010). Additionally, bioinformatic predictions of super-enhancers, which represent a group of locally enriched enhancers with higher potential to transactivate

target genes than classical enhancers, can be based on the presence of H3K27ac (Whyte et al., 2013).

On the other hand, repressive histone modifications exist which are located in heterochromatic regions and can be assigned to gene repression. The most studied histone marks with regard to these properties are H3K27me3, which is a hallmark of facultative heterochromatin (Bernstein et al. 2006), as well as H3K9me3 as the histone mark of constitutive heterochromatin. The fact that histone modifications of either group can be present at the same amino acid, like acetylation of lysine 9 at histone 3 as an activating mark or trimethylation as a repressive histone modification highlights the complexity and variability observed within genomic loci. Another layer of complexity is added by the fact that activating as well as repressive marks can be located within one distinct region. This phenomenon was first described to occur in embryonic stem cells and includes the simultaneous presence of H3K4me3 and H3K27me3 (Bernstein et al. 2006). This so-called bivalent chromatin confers a poised state in which the associated gene is transcriptionally silenced but can be activated very quickly upon certain stimuli.

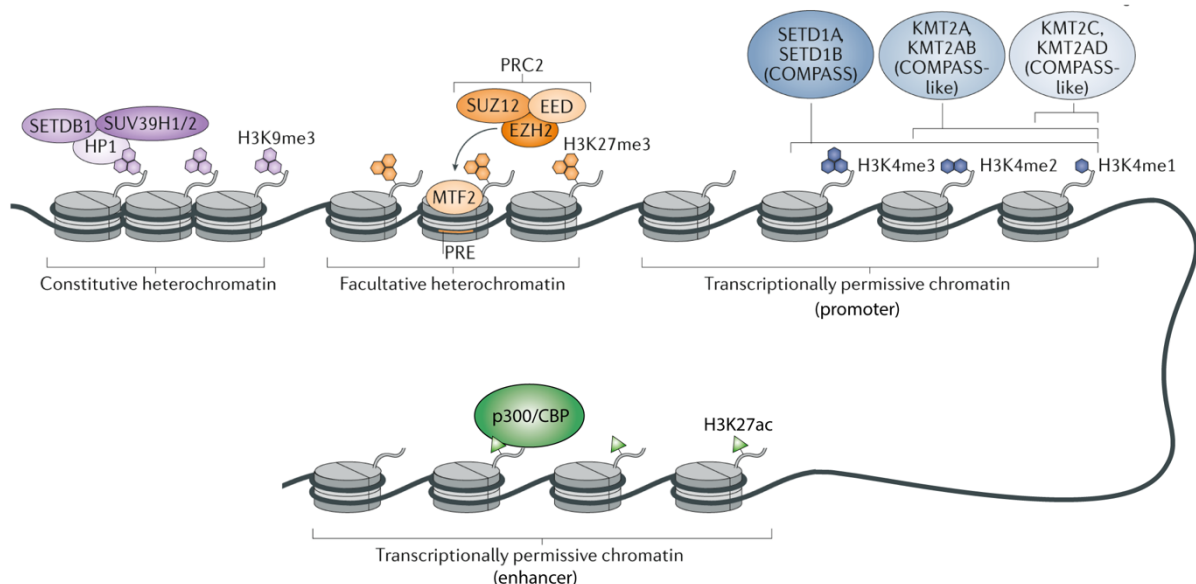


Figure 7: Histone modifications and their writer proteins/complexes: Compaction of genomic DNA is achieved by entwining the DNA around histone proteins and building up chromatin fibers. Posttranslational modifications of the protruding tails of the histones have effects on the chromatin compaction and therefore indirectly also on gene expression. The activating histone mark H3K4me3 which can be found predominantly in promoter regions is established by the Set1/COMPASS complex. Deposition of the enhancer specific mark H3K27ac is mediated by the cooperative function of p300 and CBP. The PRC2 complex, which is among others composed of the catalytic subunit EZH2 as well as of the important cofactors SUZ12 and EED, is responsible for the establishment of H3K27me3. While DNA motifs are known in *Drosophila* to recruit this complex, MTF2 might be an important recruiting factor in mammals. The histone modification H3K9me3 which is a hallmark of constitutive heterochromatin is established mainly by SETDB1 and SUV39H1. The mark is recognized by the chromodomain of HP-1 (modified from (Skvortsova et al., 2018)).

Complexity is even more increased with regard to the set of proteins which is associated with the posttranslational histone modifications. Almost every mark is known to have its own reader, writer, and eraser proteins (Figure 7).

The deposition of methyl groups to lysine residues of the histone proteins is a process which is generally catalyzed by lysine methyltransferases (KMTs). In the special context of H3K4me3 the Set1/COMPASS (complex of Set associated proteins) complex is responsible for the formation of this histone modification (T. Miller et al., 2001; Milne et al., 2002). In mammals, six related proteins of the enzymatically active Set1 were identified with partly overlapping but distinct functions with regard to H3K4me3 formation. Set1A and Set1B are the major lysine methyltransferases and known to be responsible for the genome wide deposition of H3K4me3 (Lee et al., 2007; Miller et al., 2001). MLL1 (KMT2A) and MLL2 (KMT2B) were identified to have a more restricted target gene repertoire. While MLL1 was described to only target a small subset of target genes including some of the HOX genes (Wang et al. 2009), MLL2 seems to be specific for the regulation of bivalent chromatin (Hu et al. 2013). Furthermore, MLL3 (KMT2C) and MLL4 (KMT2D) were shown to be specifically responsible for the deposition of H3K4me1 at enhancer regions (Herz et al. 2012; Hu et al. 2013; Lee et al. 2013). H3K4me3 can also be reversed by specific lysine demethylases (KDMs). LSD1 as well as LSD2 belong to this family and were shown to specifically demethylate H3K4me2 and H3K4me1 (Fang et al., 2010; Shi et al., 2004). The identification of JARID1 added a demethylase which can additionally to H3K4me2 erase specifically H3K4me3 (Christensen et al., 2007).

Acetylation of histone proteins is mediated by specific histone acetyltransferases (HATs). Similar to KMTs, specific acetyltransferases for distinct histone modifications exist. In the context of H3K27ac, CBP and p300 often act cooperatively to catalyze the formation of this epigenetic mark (Jin et al., 2011; Tie et al., 2009). Deacetylation of histones can be achieved by a wide range of up until now 18 identified histone deacetylases (HDACs) which can be subdivided into four groups (reviewed in Park and Kim 2020).

Trimethylation of H3K27 is mediated by the Polycomb Repressive Complex 2 (PRC2) which includes among others the catalytic subunit EZH2 (Czermin et al., 2002; Kuzmichev et al., 2002) as well as the important cofactors SUZ12 and EED (Birve et al., 2001; Margueron et al., 2009; Pasini et al., 2004). H3K27me3 is furthermore recognized by a chromodomain of PRC1 and the recruitment of this complex leads to

H2AK119ubi which is associated with a further repression of genomic loci (Fischle et al., 2003). The deposition of this histone mark is specifically catalyzed by RING1A/B which harbor a Ring finger domain. This domain was previously shown to be also a characteristic feature of E3 ubiquitin ligases (de Napoles et al., 2004; Fang et al., 2004). While in *Drosophila melanogaster*, specific DNA elements (PREs) were identified to recruit the PRC2 complex, the recruitment mechanism in mammals is still not completely understood (Simon et al., 1993). Very recent findings suggest that MTF2 might be one factor which binds to chromatin and is important for PRC2 recruitment at least in mouse embryonic stem cells (Perino et al., 2018). Erasure of H3K27me3 is again dependent on the catalytic activity of certain lysine demethylases. Especially UTX and JMJD3 were described to play a role in this process (Agger et al., 2007; Lan et al., 2007).

Finally, H3K9me3 as the modification of constitutive heterochromatin can also be established by several enzymes, but especially SUV39H1/2 as well as SETDB1 are important factors with regard to this histone mark (Rea et al., 2000; Schultz et al., 2002). This histone modification is recognized mainly by the chromodomain of HP-1, which recruits further histone modifying enzymes to increase heterochromatin formation (Bannister et al., 2001; Lachner et al., 2001). Demethylation of H3K9 is mediated again by different KDMs and interestingly LSD1 which was previously described to be important for H3K4 demethylation was also shown to act on H3K9me3 but in a very context dependent manner (Metzger et al., 2005).

1.4.3 KSHV and the interplay with host epigenetic pathways

KSHV gene regulation was previously shown to be highly dependent on histone modifications (Günther & Grundhoff, 2010; Toth et al., 2010). During the latent infection state large parts of the KSHV genome are repressed by H3K27me3 in order to inhibit lytic gene expression. However, upon certain stimuli this gene repression has to be reversible to enable induction of the lytic replication cycle. This is nicely reflected by the deposition of bivalent chromatin in the ORF50 (RTA) promoter which allows for the rapid initiation of lytic viral gene expression. This indicates that the virus highly relies on host epigenetic pathways during both infection states. Indeed, several studies describe a connection between KSHV and epigenetic pathways which affect the viral epigenome. There is also evidence that these interactions might have at least partly an influence on host epigenetic states.

As DNA methylation on the viral genome only arises after long-term infection, this epigenetic modification seems to play just a secondary role with regard to viral gene repression during latency (Günther & Grundhoff, 2010). Nevertheless, several studies describe interactions of KSHV latent and lytic gene products with DNMTs and highlight their functional outcome. LANA as one of the viral latent gene products was shown to interact with DNMT3A which results in increased DNA methylation levels at the host promoters of CCND2 and CDH13 (Shamay et al., 2006). In the same line, LANA downregulates TGF- β signaling by increasing the DNA methylation in the promoter region of the TGF- β type II receptor (Di Bartolo et al., 2008). Additionally, viral miR-K12-4-5p indirectly upregulates DNMT levels by targeting RBL2 (Lu et al., 2010). Among the lytic proteins v-IRF1 as well as v-IL6 are able to upregulate DNMT1 leading not only to increased DNA methylation of the miR-218 promoter but also to a global increase in DNA methylation levels (Li et al. 2019; Wu et al. 2014). All these mentioned studies share the observation that KSHV leads to either global hypermethylation or increased DNA methylation of certain genomic regions. Until now only a few genome-wide studies were conducted. One of them aimed to identify KSHV mediated host methylome patterns in *de novo* infected BJAB cells (an EBV-negative Burkitt's lymphoma cell line). 450K BeadChip analysis was performed to detect DNA methylation changes at a single CpG dinucleotide resolution between infected and non-infected cells. These data were correlated to RNA-seq from the same samples to investigate consequential transcriptional deregulation (Journo et al., 2018).

While data on DNA methylation is limited, multiple studies are dealing with interactions of KSHV encoded proteins and host chromatin modifying factors which might influence both, the viral and the host genome. As LANA was previously shown to bind to viral and host chromatin (Barbera et al., 2006), most of the studies concentrate on this viral factor. The viral protein can bind to several host factors which are associated with de-/methylation of H3K9, including KDM3A, SUV39H1, and HP-1 (Kim et al., 2013; Lim et al., 2003; Sakakibara et al., 2004). Furthermore, the H3K4 methyltransferase SET1 was identified as an interaction partner of LANA and correlative ChIP-seq analysis revealed that the viral protein associates preferentially to H3K4me3 positive loci on the host genome (Hu et al. 2014). Another study describes the interaction of LANA and BUB1, which results in the inhibition of H2AT120 phosphorylation. The absence of the phosphorylation leads to the dislocation of Sgo1, a protein involved in proper segregation of sister chromatids during mitosis, and induction of aneuploidy (Lang et

al., 2018). Additionally, several BET family members were shown to interact with LANA, including BRD2, BRD3, and BRD4 (Chen et al., 2017; Ottinger et al., 2006). Several studies also concentrate on the connection between viral proteins and the PRC2 complex which mediates the deposition of H3K27me3. While one of these studies describe direct interaction of LANA with PRC2 (Toth et al., 2016), other data imply that PRC2 recruitment to the viral genome is not dependent on LANA functions but rather requires viral cis-acting sequence features in form of unmethylated CpGs (Günther et al., 2019). Another aspect supporting the notion of a rather indirect PRC2 recruitment involves the finding that re-localization of the PML nuclear body component Sp100 occurs upon KSHV infection (Günther et al., 2014). Single components of the PRC2 complex were also shown to be affected by viral proteins. EZH2 for example is upregulated in a NF- κ B dependent manner by LANA and v-FLIP (He et al., 2012). JARID2 was additionally identified as a target of the viral miR-K12-11 (Dahlke et al., 2012).

Beside latent proteins, factors of the viral lytic cycle are also connected to host epigenetic pathways. The long non-coding PAN RNA interacts with MLL2, as well as with UTX and JMJD3 which was shown to have an effect on viral gene expression (Rossetto and Pari 2012). Furthermore, this viral factor was shown to interact with components of the PRC2 complex and to affect several cellular pathways by binding to host as well as viral chromatin (Rossetto et al. 2013). Additionally, v-IRF3 mediated reduction of HDAC5 phosphorylation was shown to play a role during virus induced angiogenesis (Lee et al., 2018).

While multiple studies describe interactions of viral proteins with host epigenetic factors and their role on the viral life cycle, little is known about the effect of such interactions with regard to the host. Information about host genomic regions that undergo epigenetic changes during KSHV infection is very limited. Although several ChIP-seq datasets for histone modifications in infected cells are available, only very few of them focus on a genome-wide analysis. The performance of such experiments would not only add important information about KSHV affected host pathways but could also lead to further insights about virus-mediated tumorigenesis.

2 Aim of the study

Since its discovery, the γ -herpesvirus KSHV has been associated to Kaposi's sarcoma, a tumor of endothelial origin, and the B cell malignancies Primary Effusion Lymphoma and Multicentric Castleman's Disease. The strong evidence from multiple molecular and epidemiological studies that KSHV is causally linked to these diseases, led to the classification of the virus to the human carcinogens. However, important questions about virus induced tumorigenesis remain unanswered. The fact that KSHV, in contrast to other human tumor viruses, does not seem to encode a single viral factor which is able to transform human cells *in vitro*, leaves the question about the exact cellular processes resulting in virus induced transformation. As KSHV mediated tumorigenesis is thought to be the result of a long-term infection, multiple or even combinatorial steps might be necessary to achieve cellular transformation. Such a scenario would include sustained viral gene expression but also the acquisition of heritable changes within a cell. This opens up the possibility that epigenetic changes might be involved in KSHV mediated pathogenesis. In fact, epigenetics have already been shown to play major roles during the KSHV lifecycle where viral gene expression highly depends on epigenetic modifications. Recent findings also support the assumption that KSHV might have an influence on host epigenetic patterns, but a detailed genome-wide investigation is missing. Therefore, this study addresses the question whether KSHV infection leads to changes of the host epigenome with immediately associated transcriptional responses. MeDIP-seq and nChIP-seq for the global investigation of host epigenetic short-and long-term consequences as well as RNA-seq to study transcriptomic deregulations were performed with the help of an *in vitro* KSHV infection model in endothelial cells. Furthermore, the heritability of potential epigenetic changes was addressed which would be of particular interest in a scenario where a viral infection is cleared by the cell. The results give further insights into KSHV deregulated cellular pathways and thereby provide new aspects important for virus mediated tumorigenesis.

3 Material and Methods

3.1 Material

3.1.1 Chemicals, commercial systems and expendable materials

If not stated elsewhere chemicals and expendable materials from the following manufacturers were used in this study: 10x Genomics, Abcam, Advanced Biotechnologies, Active Motif, Agilent, ATCC, BD Biosciences, BioLegend, Biotek, Bioo Scientific, Braun, Cell Signaling, Corning, Diagenode, Electron Microscopy Sciences, Eppendorf, GE Healthcare, Gibco, Greiner, Invitrogen, Invivogen, Kimtech, Life Technologies, LTF Labortechnik, Merck, New England Biolabs, Promocell, Quantabio, R&D Systems, Roth, Sarstedt, Sigma-Aldrich, Thermo Fisher Scientific, Upstate/Millipore, Vector Laboratories, VWR International and Zymo Research.

3.1.2 Instruments and equipment

Instruments and equipment of the following companies were used in this study: 10x Genomics, Agilent, BD Biosciences, Biometra, Diagenode, Eppendorf, Heraeus, Illumina, Nikon, Qiagen, Sorvall, Tecan, Thermo Fisher Scientific.

3.1.3 Software and online resources

The following tools and applications were used for data analysis and visualization: Photoshop 21.2.1 and Illustrator 24.2.3 (Adobe Inc.), Excel 16.42, Word 16.42, and PowerPoint 16.42 (Microsoft), Prism 8.4.3 (Graph Pad Software), CLC Main Workbench 7.9.1 (Qiagen), NIS Elements 4.51.01 (Nikon), Fiji 1.53c and the tool Angiogenesis Analyzer (Carpentier, 2012), Magellan™ (Tecan), R Studio 1.3.959, Bowtie 1.2.3 (Langmead et al., 2009), IGV 2.7.0 (Thorvaldsdóttir et al., 2013), DAVID Bioinformatics Resources 6.8 (Huang et al., 2007), STAR 2.6.0c (Dobin et al., 2013), Cell Ranger 2.2.0 (10x Genomics), diffReps 1.55.6 (Shen et al., 2013), MACS 2.1.2 (Yong Zhang et al., 2008), bedtools 2.27.1 (Quinlan & Hall, 2010), featureCounts 2.0.0 (Liao et al., 2014), EaSeq 1.11 (Lerdrup et al., 2016), Rotor-Gene Q Software 2.3.1 (Qiagen), FACS Diva 8.0.1 and FlowJo™ 10.7 (BD Biosciences), and BioDoc Analyzer 2.67.0.6 (Biometra).

3.1.4 Constructs

The following plasmids and KSHV containing bacmids were used in this study:

Table 1: Plasmids and KSHV containing bacmid

construct name	vector	insert	explanation
Lenti VSV env R861	phCMV	VSV env	plasmid for the production of infectious lentivirus containing supernatants
Lenti gag-pol	phCMV	gag-pol	plasmid for the production of infectious lentivirus containing supernatants
Lenti rev	phCMV	rev	plasmid for the production of infectious lentivirus containing supernatants
LeGo-G-2A-Hygro	LeGo-G	2A-hygromycin	used as infection and selection control for the Bac16 infection in TIME cells
pCR2.1	pCR2.1	-	internal control for MeDIP-seq
Bac16	Bac16	-	used for infection experiments in TIME cells (Brulois et al., 2012)

3.1.5 Oligonucleotides

Oligonucleotides were purchased from Eurofins Genomics (Ebersberg). The primers used in this study are listed in table 2:

Table 2: Oligonucleotides

primer name	sequence	usage	ref
ISG15 fwd	TGGACAAATGCGACGAACC	qRT-PCR	(L. Dai et al., 2016)
ISG15 rev	CCCGCTCACTTGCTGCTT	qRT-PCR	(L. Dai et al., 2016)
MX1 fwd	CAGACTCCGACACGAGTTCC	qRT-PCR	
MX1 rev	GCAGCTCTCTACCACGATACTG	qRT-PCR	
OAS2 fwd	GTGGCCATAGGTGGCTCC	qRT-PCR	
OAS2 rev	TCGAGGATGTCACGTTGGC	qRT-PCR	
TNC fwd	CACCACACGCTTGGATGCC	qRT-PCR	
TNC rev	CTCAATGCCATCGATCTCAGC	qRT-PCR	
PGK1 fwd	GCTCAACAACATGGAGATTGGCAC	qRT-PCR	
PGK1 rev	CAGGCAAGGTAATCTTCACACC	qRT-PCR	
HOXC10 fwd	TTGCTTTCTCAATGCTGGTG	qPCR	
HOXC10 rev	TCGCCATTTTAGGCTTTTTG	qPCR	
C1ORF43 fwd	AGTGGGTGGAGAATGCAGAC	qPCR	

C1ORF43 rev	GAGATTACCCCACCCCATTTC	qPCR
pCR2.1 151 fwd	TAGAAAGCCAGTCCGCAGAA	qPCR
pCR2.1 151 rev	CTGTCCATAAAACCGCCCAG	qPCR
pCR2.1 153 fwd	AAGTCGTGTCTTACCGGGTT	qPCR
pCR2.1 153 rev	GGCGCTTTCTCATAGCTCAC	qPCR
HOXC12 long fwd	AAAGCTTCCCCTGCAAAGA	qPCR
HOXC12 long rev	AAATCTGGGGGCGAACTACT	qPCR
ZNF268 fwd	AATGCATTTCCACACTGCAA	qPCR
ZNF268 rev	AAAGAGGTTGCTGCCAAGAC	qPCR
GAPDH fwd	TGTGTCCCTCAATATGGTCCTGTC	qPCR
GAPDH rev	ATGGTGGTGAAGACGCCAGT	qPCR
GFP fwd	CTGCTGCCCGACAACCA	qPCR
GFP rev	GAACTCCAGCAGGACCATGTG	qPCR

3.1.6 Antibodies

The following antibodies were used in this study (Table 3 and 4):

Table 3: Primary antibodies

target	description	application	company
H3K4me3	anti-trimethyl-histone H3 (Lys4) antibody, clone MC315, rabbit monoclonal	nChIP	Merck Millipore
H3K27ac	anti-histone H3 (acetyl K27) antibody, rabbit polyclonal	nChIP	abcam
H3K27me3	anti-methyl-histone H3 (Lys27) (C36B11), rabbit monoclonal	nChIP	Cell Signaling
H3K9me3	anti-histone H3K9me3 antibody, rabbit polyclonal	nChIP	Active Motif
5-methylcytosine	anti-5-methylcytosine antibody, mouse monoclonal	MeDIP	Diagenode
ISG15	anti-human ISG15/UCRP APC-conjugated antibody, rat monoclonal	FACS	R&D Systems
TNC	recombinant anti-Tenascin C antibody (EPR4219), rabbit monoclonal	IFA	abcam
k-ORF73	anti-KSHV ORF73 (LANA) antibody, rabbit polyclonal	IFA	
k-ORF59	anti-KSHV ORF59 antibody, mouse monoclonal	IFA, FACS	Advanced Biotechnologies

Table 4: Secondary antibodies

target	description	application	supplier/reference
rabbit IgG	goat anti-rabbit IgG (H+L) cross adsorbed Alexa Fluor 488-conjugated secondary antibody, polyclonal	IFA, FACS	Invitrogen/A11008
rabbit IgG	goat anti-rabbit IgG (H+L) cross adsorbed Alexa Fluor 555-conjugated secondary antibody, polyclonal	IFA	Invitrogen/A21428
mouse IgG	goat anti-mouse IgG (H+L) cross adsorbed Alexa Fluor 555-conjugated secondary antibody, polyclonal	IFA	Invitrogen/A21422
mouse IgG	goat anti-mouse IgG (H+L) cross adsorbed Alexa Fluor 405-conjugated secondary antibody, polyclonal	FACS	Invitrogen/A31553
mouse IgG	goat anti-mouse IgG (H+L) cross adsorbed Alexa Fluor 647-conjugated secondary antibody, polyclonal	IFA	Invitrogen/A21236

3.2 Methods of prokaryotic cell culture

3.2.1 Bacteria

The chemically competent *Escherichia coli* strain DH5 α was used for standard cloning approaches. GS1783 was used to perform *en passant* mutagenesis and to amplify bacterial artificial chromosome (BAC) constructs (Tischer, Smith, and Osterrieder 2010).

Table 5: *Escherichia coli* strains and their genotypes

strain	genotype
<i>E. coli</i> DH5 α	F ⁻ ϕ 80/lacZ Δ M15 Δ (lacZYA-argF)U169 recA1 endA1 hsdR17(r κ ⁻ , m κ ⁺) phoA supE44 λ ⁻ thi-1 gyrA96 relA1
<i>E. coli</i> GS1783	DH10B λ cl857 Δ (cro-bioA)<>araC-P _{BAD} I-sceI

3.2.2 Media and culture of bacteria

Bacteria were grown as liquid culture in LB medium (Roth, Luria/Miller, composition: 10 g/l tryptone, 5g/l yeast extract, 10g/l NaCl) or as single colonies on Lysogeny Broth

(LB) agar plates (Roth, Luria/Miller, composition: 10 g/l tryptone, 5g/l yeast extract, 10g/l NaCl, 15g/l agar-agar) at 37°C for standard plasmids or at 30°C for lentiviral/BAC constructs. Both, LB agar as well as LB medium, were autoclaved and the appropriate antibiotics for selection were added prior to usage (100 µg/ml ampicillin, 30 µg/ml kanamycin, 12.5 µg/ml chloramphenicol).

3.2.3 Preparation of chemically competent *E. coli*

The rubidium chloride method was used to generate chemically competent DH5 α . In a first step a small amount of an already frozen aliquot was streaked on a LB agar plate and incubated over night at 37 °C. A single colony was then inoculated to 5 ml sterilized LB medium and again incubated over night at 37 °C. The culture was diluted 1:100 in LB+ medium and incubated at 37 °C under agitation. Photometric measurements were regularly performed to track the growth curve of the bacteria. As soon as the culture reached an OD₆₀₀ of 0.3 – 0.5 it was incubated on ice for 15 min. After centrifugation (6000 x g, 5min, 4 °C) the supernatant was removed, and the cell pellet was resuspended in 150 ml Transformation Buffer I (see Table 6 for buffer compositions).

Table 6: Composition of buffers for the preparation of chemically competent *E. coli*

component	concentration
LB+ medium	
LB medium	500 ml
MgSO ₄	8 mM
KCl	10 mM
Transformation Buffer I	
RbCl ₂	100 mM
KAc	30 mM
CaCl ₂	10 mM
MnCl ₂ (x4H ₂ O)	50 mM
glycerol	15% (v/v)
acetic acid	to pH 5.8
Transformation Buffer II	
RbCl ₂	10 mM
MOPS	10 mM
CaCl ₂	75 mM
glycerol	15% (v/v)

The bacteria were incubated on ice for 90 min before the cells were again pelleted by centrifugation. Subsequently, the pellet was resuspended in Transformation Buffer II and 200 µl aliquots were flash-frozen in liquid nitrogen. One of the aliquots was used to perform a transformation with a control plasmid to calculate the transformation efficiency of the bacteria. The rest of the samples were stored at -80 °C.

3.2.4 Preparation of electro-competent *E. coli*

For the generation of electro-competent *Escherichia coli* GS1783 a small amount of an already frozen stock was inoculated to 10 ml LB medium. The culture was incubated over night at 30°C under constant agitation. The culture was diluted in 200 ml LB medium and again incubated at 30 °C until it reached an OD₆₀₀ of 0.5 – 0.6. Bacteria were subsequently heated to 42 °C in a waterbath for 15 min to induce the Red recombination system. This was followed by an incubation of the culture on ice for 20 min. Centrifugation (6000 x g, 10 min, 4 °C) was performed to pellet the bacteria. The pellet was washed twice in sterilized H₂O. The first washing step was performed in 200 ml H₂O, for the second washing step 100 ml H₂O were used. Bacteria were then resuspended in 2 ml 10% glycerol and stored as 100 µl aliquots in pre-cooled 1.5 ml tubes at -80°C. One of the aliquots was used to perform a transformation with a control plasmid to calculate the transformation efficiency.

3.2.5 Transformation of chemically competent *E. coli*

For the transformation of chemically competent DH5α one aliquot of bacteria was slowly thawed on ice. 50 µl of the cells were mixed with up to 100 ng plasmid DNA or 5 µl of the ligation product. The mixture was incubated on ice for 20 min to allow the attachment of the DNA to the bacterial surface. Samples were then incubated at 42 °C in the water bath for 90 sec and subsequently cooled down on ice for approximately 5 min. 900 µl LB medium was added to the bacteria and the samples were incubated at 37 °C for one hour. Bacteria were then plated on a LB agar plate with the appropriate antibiotics and incubated over night at 37 °C for standard plasmids or at 30 °C for lentiviral constructs.

3.2.6 Transformation of electro-competent *E. coli*

Electroporation was performed to transform large constructs, for example bacterial artificial chromosomes (BAC), into bacteria. Prior to transformation electro-competent

GS1783 were slowly thawed on ice in a 2 mm electroporation cuvette (Eurogentec). 100 μ l bacteria were mixed with 10 μ l of the ligation product or with up to 200 ng BAC DNA and incubated for 10 min on ice within the electroporation cuvette. Electroporation was performed with the Gene Pulser Xcell Electroporation System (Bio-Rad) using the following settings: 2.5 kV, 200 Ω , and 25 μ F. Optimal time constants should range between 3.5 and 4.5 msec. Subsequently, 900 μ l LB medium was added and pre-cultures were incubated at 30°C for 1 h. Cells were pelleted by centrifugation (300 x g, 3 min at RT). Bacteria were resuspended in 100 μ l LB medium and plated on a LB agar plate with the appropriate antibiotics (Table 7). The plates were incubated for two days at 30 °C depending on the growth of the bacteria.

Table 7: Antibiotic concentrations for the selection of prokaryotic cells (*E.coli*)

antibiotic	concentration
ampicillin	100 μ g/ml
kanamycin	50 μ g/ml
chloramphenicol	12.5 μ g/ml

3.3 Methods of eukaryotic cell culture and cell biology

3.3.1 Culture of eukaryotic cell lines

The eukaryotic cell lines used in this study are listed in Table 8.

Table 8: Cell lines

Name	Description	Company/Reference
TIME	human dermal microvascular endothelial cells immortalized with hTERT, adherent	ATCC (CRL-4025)
iSLK	human endothelial cell line derived from a Kaposi's sarcoma tumor with doxycycline inducible expression of k-RTA , adherent	(Myoung & Ganem, 2011)
BCBL-1	human KSHV-positive Primary Effusion Lymphoma derived cell line, suspension	DSMZ (Rolf Renne et al., 1996)
lenti-X™ 293T	subclone of the transformed human embryonic kidney cell line HEK 293, adherent	Clontech (Cat No. 632180)

Generally, all cells were cultured in polystyrene cell culture approved flasks or dishes and incubated at 37 °C, 5% CO₂ and a relative humidity of 95%. iSLK and lenti-X™ 293T cells were cultured in Dulbecco's Modified Eagle's Medium (DMEM, Gibco)

supplemented with 10% fetal bovine serum (FBS, Biochrom), 1% Penicillin/Streptomycin (Thermo Fisher Scientific) and 1% sodium pyruvate (Thermo Fisher Scientific). BCBL-1 cells were grown in RPMI-1640 medium supplemented with 10% FBS. Telomerase-immortalized microvascular endothelial (TIME) cells were kept in Vascular Basal Medium (ATCC) supplemented with the Microvascular Endothelial Cell Growth Kit – VEGF (ATCC). TIME cells were additionally treated with 12.5 µg/ml blasticidine (Invivogen) to select for telomerase-expressing cells. The composition of the media for the endothelial cells is described in table 9.

Table 9: Concentration of culture medium components for TIME cells

component	concentration
rh VEGF	5 ng/ml
rh EGF	5 ng/ml
rh FGF basic	5 ng/ml
rh IGF-1	15 ng/ml
L-glutamine	10 mM
heparin sulfate	0.75 U/ml
hydrocortisone	1 µg/ml
ascorbic acid	50 µg/ml
fetal bovine serum (FBS)	5 %

Adherent cells were passaged every three to four days. The media was aspirated, and cells were washed in 1-2 ml Trypsin/EDTA (concentration of Trypsin was dependent on the cell line). 2 ml Trypsin/EDTA were added and cells were incubated at 37°C for up to 5 min until cells detached from the culture vessel. The reaction was stopped by the addition of FCS containing buffer (e.g. complete medium or 2% FBS in PBS). Cells were pelleted, resuspended in fresh media and cell numbers were determined with a hemocytometer. The appropriate cell number was seeded in a new culture vessel and fresh media was added.

Suspension cells were diluted 1:5 every three to four days. Regularly, cells were pelleted by centrifugation (300 x g, 3 min) to remove all of the depleted media. The cell pellet was resuspended in fresh RPMI-1640 with all supplements to achieve a density of $\sim 1 \times 10^5$ cell/ml.

3.3.2 Long-term storage and initiation of cell cultures

Cells which reached $\sim 80\%$ confluency were trypsinized and pelleted by centrifugation (3 min at 300 x g). The pellet was resuspended in FBS containing 10% DMSO to reach

a cell density of 1×10^6 cells/ml. Cells were aliquoted in cryotubes and cooled down at a cooling rate of -1 °C/min in a freezing container until they reached a temperature of -80 °C. The aliquots were then either stored at -80 °C for short time frames or frozen in liquid nitrogen which allows the long-term storage of eukaryotic cultures. For the initiation of frozen cells one aliquot was thawed at 37 °C and directly resuspended in 9 ml of the appropriate cell culture medium. Cells were pelleted by centrifugation (3 min at $300 \times g$) to remove residual DMSO. The pellet was resuspended in 10 ml fresh culture medium. Cells were seeded in a T-75 culture flask and incubated at 37 °C and 5% CO_2 .

3.3.3 Transient transfection

For the transient transfection of plasmid DNA into eukaryotic cells the lipid-based transfection reagent Lipofectamine 2000 (Invitrogen) was used. The electrostatic interaction of positively charged head groups of the lipids with the phosphate groups of the nucleic acid reduces repulsive forces between the plasma membrane and the DNA thereby facilitating its import into the cell. After the entrance of the transfection complex the DNA diffuses through the cytoplasm and enters the nucleus where gene transcription takes place.

Depending on the experimental setup transfection of DNA was predominantly performed in 24-well plates. 24 h prior to transfection $\sim 2 \times 10^4$ cells were seeded per well of a 24-well plate. Based on the size, cells were seeded to be 70-90% confluent at the time point of transfection. The next day, the DNA-transfection mix was prepared by mixing 2 μl Lipofectamine 2000 reagent with 23 μl Opti-MEM in a 1,5 ml tube and 250 ng DNA in 25 μl Opti-MEM in a second 1,5 ml tube. The diluted DNA was added to the Lipofectamine 2000 reagent and the transfection mix was incubated for 5 min at room temperature. After incubation the DNA-lipid complex was added dropwise to the cells. The media was changed after 8h if sensitive cell lines or primary cells were transfected.

3.3.4 Production of lentiviral particles

Lentiviral particles were produced in lenti-X™ 293T, a cell line which shows high transfection rates and high expression of lentiviral proteins.

One day prior to transfection 5×10^6 lenti-X™ 293T cells were seeded into a 10 cm dish. Cells were transfected using polyethylenimine (PEI). For this, 10 μg of the lentiviral

construct was mixed with the packaging plasmids (10 µg phCMV-gag-pol, 5 µg phCMV-rev, 2 µg phCMV-VSV-G env) in 1 ml Opti-MEM (Gibco). 270 µl PEI was added to the transfection mix and the solution was incubated for 30 min at RT. During this incubation time the DNA-PEI complexes were formed. The media of the lenti-X™ 293T cells was discarded and replaced by 6 ml Opti-MEM. After the incubation time the transfection mix was added dropwise to the cells. 4-6h post transfection media was changed to 7 ml complete DMEM. 48 h and 72 h after transfection the supernatant was harvested, filtered through a 0.22 µm PES-membrane (Merck Millipore), and frozen as 2ml aliquots at -80 °C.

3.3.5 Transduction of cells with lentiviral particles

For the generation of cells with stable gene expression, the in 3.3.4 produced lentiviral particles were used to transduce eukaryotic cells.

1x10⁴ – 5x10⁴ cells were seeded per well of a 24 well plate. Lentiviral supernatants were directly added during the process of cell seeding. The volume was dependent on the titer of the supernatant which was determined after lentivirus production. If the titer was not known, different concentrations were tested. During the transduction 8 µg/ml polybrene (Sigma-Aldrich) were added. 8h post transduction the supernatant was discarded, and cells were incubated in fresh media. Two days post transduction, cells were either FACS sorted to obtain positive populations or treated with antibiotics to select for construct-containing cells (see Table 10 for antibiotics concentrations for different cell lines).

Table 10: Concentration of antibiotics for selection of regularly used eukaryotic cell lines

antibiotic	concentration for TIME cells	concentration for iSLK cells
hygromycin B	500 µg/ml	1 mg/ml
blastidicin	12.5 µg/ml	5 µg/ml
puromycin	0.5 µg/ml	1 µg/ml
gentamycin	500 µg/ml	1 mg/ml
zeocin	100 µg/ml	400 µg/ml

3.3.6 Preparation of infectious KSHV stocks

The preparation of infectious KSHV supernatants was performed as previously described (Grundhoff & Ganem, 2004a) with minor changes. Briefly, BCBL-1 cells were seeded into T-175 flasks with a density of 4×10^5 cells/ml. The cells were induced by the addition of 0.3 mM sodium butyrate (Sigma-Aldrich) and 20 ng/ml 12-O-Tetradecanoylphorbol-13-acetate (TPA, Sigma-Aldrich). While sodium butyrate functions as a histone deacetylase (HDAC) inhibitor (Candido et al., 1978), TPA is an activator of the protein kinase C (PKC) (Castagna et al., 1982) and known to induce reactive oxygen species (ROS) (Datta et al., 2000). Combinatorial treatment with both reagents leads to the lytic reactivation of KSHV in BCBL-1 cells. Four days after treatment cells were pelleted by centrifugation at $300 \times g$ for 10 min and the supernatant was filtered through a $0.45 \mu\text{m}$ PVDF-membrane (Fisher Scientific) Centrifugation at $21,000 \times g$ for 2h at 4°C in order to concentrate the virus supernatant. The pellet was resuspended in 1:100 of the starting volume in EBM-2 medium. Virus stocks were stored as 1 ml aliquots at -80°C . Infectivity was tested by performing an immunofluorescence of infected cells against ORF73 (LANA).

3.3.7 Preparation of infectious Bac16 stocks

For the preparation of infectious Bac16 supernatants the BAC construct had first to be transfected into iSLK cells (kind gift from Armin Ensser, University of Erlangen). These cells harbor a construct allowing the doxycycline-inducible expression of RTA which highly facilitates virus production in these cells (Myoung & Ganem, 2011). Transfection of these cells with the Bac16-construct was performed as described in 3.3.3. Two days post transfection cells were treated with $1200 \mu\text{g/ml}$ hygromycin to select for Bac16-containing cells until a 100% positive population was obtained. Prior to virus production iSLK-Bac16 cells were seeded into 15 cm dishes to reach $\sim 70\%$ confluency at the time point of induction. Hygromycin selection was interrupted during the process of virus production. One day later lytic reactivation of Bac16 in these cells was induced by the treatment with 0.3 mM sodium butyrate (Sigma-Aldrich) and $1 \mu\text{g/ml}$ doxycycline. Four days post induction the supernatant was harvested. For this, the medium was filtered through a $0.45 \mu\text{m}$ PVDF-membrane (Fisher Scientific) and subsequently centrifuged at $21,000 \times g$ for 2h at 4°C . The pellet was resuspended in EBM-2. The volume in which the pellet was resuspended corresponded to 1:100 of the original culture volume. The virus containing supernatant was stored as 1 ml aliquots at -80°C .

Infectivity was tested by FACS of GFP-positive cells after infection of cells with different dilutions of virus supernatant.

3.3.8 *De novo* KSHV infection

De novo KSHV/Bac16 infection was predominantly carried out in 24 well plates. One day prior to infection $2-5 \times 10^4$ cells were seeded per well of a 24 well plate. The cell number was dependent on the size of the cells. At the time point of infection cells should have reached a confluency of around 50% - 70%. The cell culture media was removed, and cells were washed once with 200 μ l EBM-2. The virus supernatant was diluted 1:3 to 1:10 in 300 μ l EBM-2 per well. The dilution was dependent on the infectivity of the virus stock. 8 μ g/ml polybrene (Sigma-Aldrich) was added as it was previously described to increase the efficiency of retroviral transductions and viral infections *in vitro* (H. E. Davis et al., 2002). Cells were incubated at 37 °C and 5% CO₂ for 2h. After incubation the virus supernatant was discarded and 500 μ l of the appropriate culture medium was added to the cells. In order to determine the ratio of infected cells LANA staining was performed 48h post infection.

3.3.9 Cell proliferation assay

Cell proliferation was measured by the usage of the MTT assay. This colorimetric assay is based on the reduction of the yellow tetrazolium salt 3-(4,5-dimethylthiazol-2-yl)-2,5-diphenyltetrazolium bromide to the purple crystalline product formazan by cellular NAD(P)H dependent oxidoreductases. The assay takes the cellular metabolic activity as a sign for cell viability and proliferation. Prior to the measurement, 5×10^3 cells were plated per well of a 96 well plate. Proliferation was measured every 24 h by adding 10 μ l of the MTT solution to the cells. Cells were incubated for 4 h at 37 °C and 5% CO₂. After the incubation time, media was aspirated and 100 μ l Solvent Solution (isopropyl alcohol + 0.04% hydrochloric acid) was added to dissolve the purple crystalline formazan structures. Photometric measurement was performed at an absorbance of 570 nm using the TECAN plate reader (Safire 2). 630 nm was used as a reference and measurements were performed in triplicates.

3.4 DNA techniques

3.4.1 Isolation of plasmid and bacmid DNA from bacteria

For up to 5 ml bacteria cultures the Plasmid Miniprep Kit I Classic Line (Peqlab) was used to isolate plasmid DNA as described in the manufacturer's instructions. For the isolation of small amounts of bacmid DNA, bacteria were first centrifuged at 6,000 x g for 10 min and then resuspended in 300 µl Resuspension Buffer. 300 µl Lysis Buffer was added and samples were inverted 3 to 5 times. After incubation at RT for 5 min, 300 µl Neutralization Buffer was added and samples were again mixed by inverting the tubes (buffer composition is depicted in Table 11).

Table 11: Components of buffers for bacmid DNA extraction from prokaryotic cells

component	concentration
Resuspension Buffer	
TRIS-HCl pH 8.0	50 mM
EDTA	10 mM
RNase A	100 µg/ml
adjust to pH 8 with HCl	
Lysis Buffer	
NaOH	200 mM
SDS	1% (w/v)
Neutralization Buffer	
Potassium acetate	2.8 M
adjust to pH 5.1 with acetic acid	

Centrifugation at 17,900 x g for 15 min was performed and the supernatant was transferred to a clean 2 ml tube. 750 µl isopropyl alcohol (0.8 volumes) were added and samples were centrifuged for 30 min at 17,900 x g and 4 °C. The supernatant was discarded, and the pellet was washed once in 300 µl 70% ethanol. After centrifugation the pellet was air dried and DNA was resuspended in 50 µl dH₂O. For bacmid preparations pipetting steps were minimized. If necessary, pipetting was performed very carefully and slowly to minimize shearing of the DNA.

Large amounts of plasmid DNA from up to 200 ml of bacteria were isolated by the Plasmid Plus Midi/Maxi Kit (Qiagen) according to the manufacturer's instructions. Bacmid DNA of up to 1 l cultures was isolated with the help of the NucleoBond Xtra Maxi Kit (Macherey-Nagel).

DNA concentrations were determined at the NanoDrop 1000 spectrophotometer. Samples were stored at 4°C for short timeframes. For long-term-storage the DNA was kept at -20 °C.

3.4.2 Extraction of genomic DNA from eukaryotic cells

Extraction of genomic DNA (gDNA) from eukaryotic cells was on the one hand performed prior to MeDIP analyses and allowed on the other hand for the quantification of viral copy numbers relative to host genome copies.

Cells were treated with trypsin/EDTA to achieve detachment from the culture vessel. The cell suspension was then pelleted by centrifugation at 300 x g for 5 min. Cells were washed once in PBS and after another centrifugation step, the pellet was resuspended in 400 µl gDNA Isolation Buffer supplemented with 100 µg/µl RNase A (Sigma-Aldrich) and 100 µg/µl Proteinase K (VWR) (table 12).

Table 12: gDNA Isolation Buffer

component	concentration
Tris HCl (pH 8)	10 mM
NaCl	100 mM
EDTA	25 mM
SDS	0.5 % (w/v)

RNA was degraded at 37 °C for 1 h in a thermo-shaker which was followed by protein digestion overnight at 55 °C. gDNA was isolated by Phenol/Chloroform extraction in 5PRIME Phase Lock Tubes (Quantabio). For this, samples were pipetted on top of the gel and 400 µl Phenol/Chloroform/Isoamyl alcohol (25:24:1, Roth) was added. The samples were vortexed and then centrifuged for 4 min at 18.000 x g and 4 °C. This step was repeated once again with Phenol/Chloroform/Isoamyl alcohol and once with Chloroform. The aqueous phase on top of the gel was transferred to a new 1.5 ml tube and DNA was precipitated by adding 1055 µl of 100 % ethanol, 24 µl of 5 M NaCl, and 3 µl of Glycogen (5 mg/ml, Thermo Fisher Scientific). After incubating the samples at -80 °C for a minimum of 1 h, centrifugation at 20.000 x g for 20 min was performed to pellet the precipitated DNA. The pellet was washed once in 500 µl 70 % ethanol. Finally, the DNA was air dried and then dissolved in DEPC treated H₂O.

3.4.3 Digestion of plasmid and bacmid DNA with restriction enzymes

Digestion of plasmid/bacmid DNA was performed to either control correct constructs extracted from prokaryotic cells or to obtain sequences of interest for sub-cloning approaches. For either approach the following components were mixed in a 1.5 ml tube and incubated for 30 min to 1h at 37 °C:

Table 13: Pipetting scheme for a restriction enzyme digestion of plasmid/bacmid DNA

component	volume
10x FastDigest Green buffer	2 μ l
plasmid/bacmid DNA	0.5-2 μ g
restriction enzyme (Life Technologies)	0.5 μ l
dH ₂ O	ad 20 μ l

For control digestions 0.5 μ g of DNA was used, whereas digestions for cloning required the digestion of up to 2 μ g DNA. Digested DNA was loaded on an agarose gel and investigated by gel electrophoresis.

3.4.4 Agarose gel electrophoresis

Agarose gel electrophoresis allows for the separation of DNA fragments according to their size in an electric field. This method was used to visualize PCR products, enzymatic restrictions of plasmids or bacmid, shearing efficiencies of DNA prior to MeDIP, and MNase digestion of chromatin prior to nChIP. Depending on the expected band sizes, the amount of agarose was adjusted while for standard applications 1 % agarose gels were poured. For pouring a 1 % agarose gel, 1g of agarose was diluted in 100 ml TAE buffer (400 mM Tris-acetate, 20 mM EDTA, pH 8.5). The solution was boiled in a microwave until the agarose was completely dissolved. 0.5 μ g/ml of the DNA intercalating dye ethidium bromide was added, and the gel was cast into a gel tray with a comb. During polymerization of the gel the samples were prepared by adding 6x Loading Buffer (Thermo Fisher Scientific). The gel was then transferred to an electrophoresis chamber and covered completely with TAE buffer. The samples as well as the GeneRuler™ Ladder Mix (Thermo Fisher Scientific) were pipetted into the pockets of the gel. A constant voltage of 5-10 V/cm was applied until the DNA fragments were completely separated. Analytical gels were visualized under UV light with a gel documentation system of Biometra and the BioDoc Analyzer software. For preparative gels a UV-transilluminator with a longer wavelength (365 nm) was used to

minimize DNA damage. Specific bands were excised from the gel and purified with the Zymoclean Gel Recovery Kit (Zymo Research).

3.4.5 Purification of DNA fragments and plasmid DNA from gels

PCR products and/or digested plasmids were either directly recovered by the usage of the DNA Clean & Concentrator Kit (Zymo Research) or excised from an agarose gel and purified using the Zymoclean Gel Recovery Kit (Zymo Research). Both kits were used as recommended by the manufacturer's instructions.

3.4.6 Ligation of DNA fragments

For the ligation of a DNA fragment into linearized vector T4 DNA Ligase (Thermo Fisher Scientific) was used. The reaction was prepared as described in table 14 and then incubated overnight at 4 °C.

Table 14: Reaction for the ligation of DNA fragments into linearized vector DNA

component	volume
vector DNA	50-100 ng
insert	3:1 – 5:1 molar ratio over vector
10x T4 DNA Ligase buffer	1 µl
T4 DNA Ligase	1 µl
DEPC treated H ₂ O	ad 10 µl

3.4.7 Gibson assembly

Gibson assembly was performed as an alternative to the standard cloning procedure as it allows for the isothermal assembly of several overlapping DNA fragments in one single reaction. This method which was previously described by Gibson et al. is based on the combined action of a 5' exonuclease, a DNA polymerase, and a DNA ligase. The 5' exonuclease generates single stranded DNA overhangs of the different molecules. These overhangs are annealing due to their complementarity and potential gaps are filled by the enzymatic activity of the DNA polymerase. Finally, the DNA ligase creates a diester bond between the 5' phosphate and the 3' hydroxyl termini of the DNA fragments (Gibson et al., 2009).

Briefly, the plasmid was digested with a restriction enzyme to generate linearized DNA fragments. The inserts were PCR amplified with specific primers to generate overhangs to the insertion site of the plasmid. Vector and insert DNA was purified and DNA concentrations were measured at the spectrophotometer. Vector, insert, and the

2x Gibson Assembly Master Mix (New England Biolabs) were mixed according to the manufacturer's instructions and incubated for up to 1h at 50 °C. The Gibson assembly product was then directly transformed into competent bacteria.

3.4.8 Amplification of DNA by Polymerase Chain Reaction (PCR)

The amplification of a specific DNA fragment by Polymerase Chain Reaction (PCR) was first described by Mullis et al. in 1986 (Mullis et al. 1986). This method allows the exponential amplification of a certain DNA fragment. The area of amplification is specified by flanking primers which serve as starting points for the DNA polymerase. A standard PCR reaction is composed of the following ingredients:

Table 15: Components of a standard PCR reaction

component	volume
DNA	2-10 ng
10x DreamTaq Buffer (Invitrogen)	5 µl
dNTPs (10mM each)	2 µl
primer fwd/rev	1 µl
DreamTaq (5 U/µl, Invitrogen)	0.5 µl
DEPC treated H ₂ O	ad 50 µl

Depending on the purpose of the PCR, different DNA polymerases were used. Colony-PCR for the screening of potential clones or amplification of short fragments were carried out with the Dream Taq polymerase (Invitrogen). Amplicons which were used for subsequent cloning approaches were produced by a Pfu polymerase (New England Biolabs or Agilent) with proof reading activity. The PCR reaction was then incubated in a thermocycler (Eppendorf) under the following conditions:

Table 16: Standard PCR program

1)	95 °C	5 min	initial denaturation	
2)	95 °C	30 sec	denaturation	
3)	T _m	30 sec	annealing	30 cycles
4)	72 °C	1 min/kb	elongation	
5)	72 °C	2 min	final elongation	
6)	4 °C	∞		

The annealing temperature for primer binding to the DNA should ideally range between 55-70 °C but is highly dependent on the sequence composition of the primers.

Additionally, elongation time could also be customized to the length of the PCR product.

3.4.9 Quantitative Real-time PCR

Quantitative Real-time PCR (qPCR) is based on the same principle as a standard PCR approach with the difference that during each round of amplification a DNA quantification step is included. For this step SYBR green is used, a fluorescent dye which upon excitation only emits fluorescence when bound to double stranded DNA. Due to this fact, the detected fluorescence signal is directly proportional to the total DNA amount within the sample. This results in a very sensitive method which can be used for absolute as well as relative quantification of a certain DNA template. In order to monitor the specificity of the PCR, a melting curve can be included which gives information about the PCR product and the presence of potential primer dimers. This melting curve is added at the end of a run by increasing the temperature from 70 – 95 °C in 0.5 °C steps. Specific products should have the same melting temperature across all the samples at which the fluorescence signal is rapidly declining while side products or primer dimers give additional signals at different temperatures. Furthermore, standard curves were performed in order to determine the PCR efficiency and to guarantee specificity of each primer pair. Serial dilutions of plasmid or genomic DNA were used in presence of the specific primers. Only if the PCR efficiency was between 0.8 and 1.1, and the PCR product was highly specific, the primer pair was used for the experiment.

In this study, qPCR was used to determine viral copy numbers relative to the host DNA, to quantify relative transcript levels of certain genes, and to validate ChIP and MeDIP experiments. Generally, 2x SensiMix SYBR HiRox Mastermix (Bioline) was used in the qPCR reaction, as depicted in Table 17.

Table 17: Components of a qPCR reaction

component	volume
2x SensiMix SYBR HiRox Mastermix (Bioline)	5 µl
Primer Mix (fwd + rev, 10 µM each)	0.6 µl
template	1.5 µl
DEPC treated H ₂ O	ad 10 µl

A standard qPCR program (Table 18) was used for all samples and primer sets in the RotorGene 6000 Light Cycler (Qiagen).

Table 18: Standard qPCR program

1)	95 °C	7 min	initial denaturation	
2)	95 °C	10 sec	denaturation	
3)	57 °C	40 sec	annealing	50 cycles
4)	72 °C	10 sec	elongation	
5)	70 - 95 °C		melt	

The appropriate controls including no template control as well as Reverse Transcriptase lacking samples for cDNA, were performed for every run. Standard curves were performed prior to the experiment and used during data analysis.

3.4.10 Determination of nucleic acid concentrations

Nucleic acid concentrations were either measured photometrically by using the NanoDrop 1000 (Peqlab) or with the Qubit® Fluorometer (Invitrogen). NanoDrop makes use of the property of nucleic acids to absorb light at a wavelength of 260 nm. As proteins rather absorb light at 280 nm, the ratio of the two wavelengths A260/A280 is a good indicator for the purity of the sample. In contrast, Qubit® is based on fluorescent dyes which can specifically bind to DNA or RNA. As these dyes are highly specific and do not bind to other contaminants within the sample, this assay is thought to be 1,000fold more sensitive than the photometric approach. However, this assay does not give any information about the purity or integrity of the nucleic acids.

3.4.11 Sanger-sequencing of DNA and sequence analysis

Sanger-sequencing of PCR products or plasmid DNA was performed by Eurofins Genomics (Ebersberg). Preparation of the samples was performed as described in the company's instructions. Sequencing results were analyzed with CLC Main Workbench 7 by Qiagen.

3.5 RNA techniques

3.5.1 Extraction of total RNA from eukaryotic cells

Extraction of total RNA from eukaryotic cells was performed with RNA Bee (amsbio, CS-501B), a monophasic solution containing phenol and quinidine thiocyanate. Depending on the availability up to 5×10^6 cells were pelleted by centrifugation for 5 min at 300 x g. The supernatant was removed, and cells were homogenized and lysed in

500 μ l RNA Bee. 100 μ l Chloroform was added and the samples were vortexed for 20 sec. After incubation on ice for 10 min samples were centrifuged at 12.000 x g to separate the aqueous and organic phase. The organic phase containing RNA was carefully pipetted into a new RNase-free tube. 250 μ l isopropyl alcohol was added and samples were incubated at room temperature for 10 min. RNA was pelleted by centrifugation at 20.000 x g for 5 min. Supernatant was discarded and RNA was washed with 500 μ l 75% ethanol. Subsequent to the centrifugation of the samples at 20.000 x g for 5 min the supernatant was removed, and the pellet was air dried for approximately 5 min. The pellet was resuspended in 10 – 50 μ l DEPC treated H₂O depending on the size of the pellet. RNA concentration was measured before RNA was further processed to cDNA or library construction for RNA-sequencing was performed.

3.5.2 cDNA synthesis from total RNA

cDNA was generated of up to 1 μ g total RNA depending on the amount of available material. DNase I treatment was performed prior to reverse transcription to remove residual DNA within the samples. For this reaction RNA was resuspended in 17 μ l of DEPC treated H₂O and 2 μ l DNase I buffer and 1 μ l DNase I were added. The reaction was performed for 15 min at room temperature. 1 μ l of 25 mM EDTA was added and the samples were incubated at 65 °C for 10 min to stop the reaction. 2 μ l of 10mM dNTPs and 2 μ l of 250 mM random hexamer primer were added to the samples. After incubation at 65 °C for 5 min, samples were kept on ice for 1 min. From each sample half of the volume was transferred to a new 0.1 ml tube and served as a negative control for the Reverse Transcriptase reaction (noRT control). The Reverse Transcriptase Mix (Table 19) was prepared and 7 μ l was added to each sample. For the noRT control the reverse transcriptase was substituted by DEPC treated H₂O.

Table 19: Composition of the Reverse Transcriptase Mix

component	volume
5x First Strand buffer	4 μ l
0.1 M DTT	1 μ l
RNaseOut	0.2 μ l
Superscript III	0.2 μ l
DEPC treated H ₂ O	1,6 μ l

Samples were incubated at 25 °C for 5 min and this was followed by an incubation at 55 °C for 60 min. The reverse transcriptase was heat-inactivated at 70 °C for 10 min. RNase H digestion was performed for 20 min at 37 °C to degrade the RNA strand of RNA-DNA hybrids that occur during reverse transcription. cDNA was diluted 1:5 in DEPC treated H₂O and was either directly used in a qRT-PCR or could be stored at -20 °C.

3.6 Microscopy-related methods

3.6.1 Tube formation assay

One possibility to study the angiogenic potential of different compounds or stimuli in endothelial cells is the Tube Formation Assay. Seeding the cells on extracellular matrix protein-rich Matrigel™ (Corning) leads to the formation of capillary-like structures which can be visualized by microscopy and also allows for a quantitative analysis.

50 µl Matrigel™ (Corning) was pipetted into one well of a 96 well plate without introducing air bubbles. The plate was incubated at 37 °C for 30 min to allow the gel to solidify. In the meantime, cells were detached from the culture vessel and pelleted by centrifugation for 5 min at 300 x g. The cell pellet was resuspended in 4 ml of the appropriate culture media and cells were counted in a hemocytometer. Cells were then diluted to achieve a density of 7×10^4 cells per 200 µl. 60 µl of the cell suspension was then added per well on top of the solidified Matrigel™. The cells were incubated at 37 °C and 5 % CO₂ for 12 h and then tube formation was assessed by light microscopy. Pictures of four different positions per well were taken and then further analyzed with the Angiogenesis Analyzer tool (Carpentier, 2012) for Fiji.

3.6.2 Immunofluorescence analysis

Immunofluorescence analysis was performed in TIME cells to confirm Bac16 infection by ORF73 staining. Additionally, ORF59 staining was performed to screen for lytic reactivation of the virus in these cells. Host factors like TNC and ISG15 were also investigated by immunofluorescence analysis to confirm increased expression observed in RNA-sequencing also on the protein level.

One day prior to staining, 2×10^4 cells were seeded in 24 well plates on a coverslip. As soon as the cells attached to the slides the media was aspirated and 200 µl of 4 % paraformaldehyde was added for fixation. After 10 min paraformaldehyde was substituted by 200 µl of Permeabilization Buffer (1 % Triton-X-100 (v/v), 0.1 % sodium

citrate (v/v) in PBS). Subsequently, cells were incubated in 200 µl of Blocking Solution (1 % Triton-X-100 (v/v), 0.5 % Tween 20 (v/v), 3 % BSA (w/v) in PBS to block unspecific binding sites within the cell. The primary antibody of interest was diluted in the Blocking Solution and added to the cells. After an incubation time of 2h at RT the antibody dilution was removed, and cells were washed three times in PBS. Cells were then incubated with a secondary fluorophore-tagged antibody for 1h at RT in the dark. This was again followed by three washing steps. Finally, the slides were embedded in Vectashield® DAPI containing mounting media (Vector Laboratories) on glass slides. Imaging of the immunofluorescence was performed at a confocal fluorescence microscope (Nikon Eclipse Ti-E stand with Yokogawa CSU-W1 Spinning Disk, Andor 888 camera, 100x NA 1.49 objective) .

3.7 FACS analysis

3.7.1 Titration of infectious (lenti-)viral particles

FACS-based titration of (lenti-)viral particles was possible if viruses were encoding a fluorescence protein. For this purpose, 2×10^4 cells were seeded per well of a 24 well plate. The next day cells were either transduced or infected as previously described in 3.3.5 or 3.3.8, respectively. Different dilutions of the virus supernatant were used for the titration assay. Two to three days after transduction/infection, cells were detached from the culture vessel and transferred to a 15 ml tube. Cells were pelleted by centrifugation at 300 x g for 5 min. Cells were washed two times in 2% FBS in PBS and then fixed in 100 µl 4 % paraformaldehyde. After 10 min of fixation, 300 µl PBS was added and the cell solution was transferred to tubes which are suitable for FACS. Cells were analyzed at the FACS LSR Fortessa (BD Biosciences) with settings adjusted to the experimental design.

3.7.2 Staining of intracellular molecules

Intracellular staining of ISG15 as a representative protein of the Type I IFN response was performed to evaluate the results obtained from the scRNA-seq experiment. For this purpose, 5×10^6 infected or control cells were harvested and pelleted by centrifugation at 300 x g for 5 min. The cells were resuspended in 100 µl 4% paraformaldehyde and incubated at RT for 10 min. Cells were again centrifuged at 300 x g for 5 min and then 100 µl of Permeabilization Buffer (1 % Triton-X-100 (v/v), 0.1 % sodium citrate (v/v) in PBS) was added. After another incubation time of 10 min

Permeabilization Buffer was exchanged by 100 μ l Blocking Solution (1 % Triton-X-100 (v/v), 0.5 % Tween 20 (v/v), 3 % BSA (w/v) in PBS. The cells were incubated for 30 min in this buffer to block unspecific binding sites. Cells were again pelleted by centrifugation and then the Blocking Solution containing the diluted antibody was added. After incubation for 2h in the dark cells were washed three times in PBS. As the antibody was already labeled with APC, no secondary antibody was needed. Cell suspensions were transferred to FACS suitable tubes and analyzed at the FACS LSR Fortessa (BD Biosciences) with the appropriate settings.

3.7.3 Annexin V apoptosis assay

Induction of apoptosis was measured by the Annexin V apoptosis detection kit (Biolegend). This FACS based assay stains for phosphatidylserine which is, due to structural changes of the cell membrane during apoptosis, translocated to the outer membrane. Annexin V is able to bind to these molecules on the cell surface when apoptosis is induced, but not in viable cells.

This assay was performed to investigate the induction of apoptosis in infected and control cells after a certain stimulus. One day prior to the treatment with the apoptosis-inducing stimulus, 2×10^5 cells were plated in a 10 cm dish. The next day cells were treated with 1 μ M staurosporine (abcam) to induce apoptosis. Staurosporine is an unspecific protein kinase inhibitor which is thought to act on the enzymes' ATP binding sites (Meggio et al., 1995). 12 h post treatment, the cells were detached from the culture vessel and pelleted by centrifugation at 300 x g for 5 min. Cells were washed two times in 2% FBS in PBS and then resuspended in 100 μ l Binding Buffer. 5 μ l Pacific Blue labeled Annexin V and 10 μ l Propidium Iodide were added to each sample. Cells were incubated for 10 min in the dark. Subsequently, 300 μ l Binding Buffer was added and analysis was performed at the FACS LSR Fortessa (BD Biosciences) with the appropriate settings for the experiment.

3.8 Native Chromatin Immunoprecipitation (nChIP)

While standard crosslinking chromatin immunoprecipitation methods require high cell numbers as starting material, native Chromatin Immunoprecipitation (nChIP) is applicable for samples with limited input material. The nChIP protocol was performed as previously described (Brind'Amour et al., 2015) with only minor modifications.

Cells were detached from the culture plate and resuspended in 10 ml of the appropriate medium. The number of cells needed for the experiment was transferred into a 1.5 ml tube and pelleted by centrifugation at 300 x g and 5 min. Cells were washed once in cold PBS supplemented with 1x Protease inhibitor cocktail (Roche), 1 mM Pefabloc® SC-Protease Inhibitor (Roth), and 5 mM sodium butyrate. The samples were again centrifuged to pellet the cells and this pellet was subsequently flash-frozen in liquid nitrogen and could be directly processed or stored at -80°C. In general, up to 2x10⁵ cells were used per antibody pull-down and 1/4 of this cell number served as an input control.

As soon as the protocol was resumed the cell pellets were resuspended in 50 µl Nuclear Isolation Buffer (Table 20) supplemented with 1x Protease inhibitor cocktail (Roche), 1 mM Pefabloc® SC-Protease Inhibitor (Roth), and 5 mM sodium butyrate.

Table 20: Nuclear Isolation Buffer

component	concentration
Hepes-KOH	50 mM
NaCl	140 mM
glycerol	10 % (v/v)
NP40	0.5 % (v/v)
Triton-X-100	0.25 % (v/v)

Samples were mixed by pipetting up and down 15-20 times and then placed back on ice. MNase master mix (Table 21) and 1:10 MNase dilution (200 U/µl) were prepared. 10 µl MNase master mix was added to each sample.

Table 21: MNase master mix

component	volume
10x MNase buffer (NEB)	6 µl
100 mM DTT	0.88 µl
DEPC treated H ₂ O	2.52 µl
1:10 MNase (NEB)	0.6 µl

Samples were incubated at 37°C for 12 min before 1/10 of the reaction volume of 100 mM EDTA was added to stop the MNase reaction. Subsequently, 1/10 of the reaction volume of 1 % Triton-X-100/1% deoxycholate solution was added and the samples were incubated on ice for 15 min. After vortexing the samples for approximately 30 sec Complete Immunoprecipitation Buffer (Table 22) supplemented with 1x Protease inhibitor cocktail (Roche), 1 mM Pefabloc® SC-Protease Inhibitor (Roth), and 5 mM

sodium butyrate were added to the digested chromatin. The volume depended on the available cell number and the antibodies that were used for the experiment. Generally, immunoprecipitation was performed in a total volume of 400 μ l and the chromatin fraction should not exceed 25 %.

Table 22: Complete Immunoprecipitation Buffer

component	concentration
Tris-HCl pH 8.0	20 mM
EDTA	2 mM
NaCl	150 mM
Triton-X-100	0.1 % (v/v)

The chromatin was incubated at 4°C for 1 h in a rotator. Samples were again vortexed for 30 sec and an input control was collected. The input was supplemented with $1/10$ volume of 10 % SDS, filled to 100 μ l with EB buffer (Qiagen) and stored at -20°C until DNA was extracted.

During the incubation steps of the chromatin preparation protein A/G magnetic beads (Dynabeads, Life Technologies) were pre-washed three times in Complete Immunoprecipitation Buffer. After the last washing steps the beads were resuspended in the volume needed for the experiment. This again depended on the number of samples and the antibodies that were handled. For the preparation of the antibody-beads complexes 10 μ l of the magnetic beads and 1 μ g of antibody were diluted in 400 μ l Complete Immunoprecipitation Buffer. For pre-clearing of the chromatin 10-50 μ l magnetic beads were added to each chromatin sample. Both, the antibody-beads complexes and the pre-clearing samples were incubated in a rotator at 4°C for 5 h. After the incubation antibody-beads complexes were placed on a magnetic rack and the supernatant was removed. Subsequently, the pre-cleared chromatin was also placed on the magnetic rack and the supernatant was transferred to the antibody-beads complexes. The samples were filled with Complete Immunoprecipitation Buffer to a volume of 400 μ l and then incubated in the rotator at 4°C overnight. Samples were placed on the magnetic rack and supernatant was discarded to remove unbound chromatin. Next, the beads were washed two times in 200 μ l Low Salt Buffer supplemented with 1x Protease inhibitor cocktail (Roche), 1 mM Pefabloc® SC-Protease Inhibitor (Roth), and 5 mM sodium butyrate and two times in 200 μ l High Salt Buffer supplemented with 1x Protease inhibitor cocktail (Roche), 1 mM Pefabloc® SC-Protease Inhibitor (Roth), and 5 mM sodium butyrate (Table 23).

Table 23: nChIP washing buffers

component	concentration
Low Salt Buffer	
TRIS-HCl pH 8.0	20 mM
EDTA	2 mM
NaCl	150 mM
Triton-X-100	1 % (v/v)
SDS	0.1 (w/v)
High Salt Buffer	
TRIS-HCl pH 8.0	20 mM
EDTA	2 mM
NaCl	500 mM
Triton-X-100	1 % (v/v)
SDS	0.1 % (w/v)

After the last washing step samples were transferred into new 1.5 ml tubes. After the removal of the supernatant, samples were centrifuged to spin down all the residual washing buffer. With a gel loading tip, the rest of the High Salt Buffer was removed, and beads were resuspended in 30 µl Elution Buffer (Table 24).

Table 24: Elution Buffer

component	concentration
TRIS-HCl pH 8.0	50 mM
EDTA	10 mM
SDS	1 % (w/v)

After the incubation for 1-1.5 h at 65°C the samples were again placed on the magnetic rack and the supernatant was transferred into a Phase Lock Tube (Quantabio). Beads were washed in 70 µl Elution Buffer and the supernatant was added to the Phase Lock Tubes. DNA preparation of the ChIP samples as well as of the input controls was performed as previously described (see chapter 3.4.2).

3.9 Methylated DNA Immunoprecipitation (MeDIP)

For the investigation of DNA methylation on a genome wide level Methylated DNA Immunoprecipitation was performed as previously described (Weber et al., 2005) and combined with high-throughput sequencing.

MeDIP requires the extraction of genomic DNA from eukaryotic cells, which was performed as described in 3.4.2. The DNA concentration was determined at the

NanoDrop 1000 spectrophotometer. DNA was diluted to 100 ng/μl with TE Buffer in a total volume of 100 μl in 0.65 ml Bioruptor Pico Microtubes (Diagenode). Fragmentation of the DNA was performed in a Bioruptor™ (Diagenode) for twelve cycles to achieve an average fragment size of 100-500 bp. 400 ng of *in vitro* methylated pCR2.1 plasmid was added to each sample as normalization and quantification control. The samples were then adjusted to a total volume of 500 μl with TE Buffer. Incubation at 98°C for 10 min in a water bath led to the denaturation of the DNA. This was followed by an incubation on ice for another 10 min. All the following steps were performed on ice to keep DNA single stranded. 50 μl of the fragmented DNA was transferred to a 1.5 ml tube and served as an input control. The MeDIP samples were refilled to 500 μl with 50 μl of 10x MeDIP buffer (Table 25).

Table 25: Composition of the 10x MeDIP buffer

component	concentration
sodium phosphate pH 7	100 mM
NaCl	1.4 M
Triton-X-100	0.5% (v/v)

2.5 μg anti-5-methylcytosine antibody (Diagenode) was added and samples were incubated on a rotator for 2h at 4 °C. During this incubation time, Dynabeads M-280 Sheep anti-Mouse IgG (Invitrogen) were washed two times in 1x MeDIP Buffer. The beads were resuspended in 950 μl 1x MeDIP Buffer and 50 μl of 20mg/ml BSA was added. The beads were incubated on a rotator for 1h at 4 °C to reduce unspecific binding sites. After the incubation, beads were again washed once and then resuspended in the appropriate volume needed for the experiment. 50 μl of the beads were added to the antibody-DNA complexes and the samples were incubated on a rotator for 2h at 4 °C. Samples were washed five times in 200 μl TE Buffer. After the washing steps, the samples as well as the input were resuspended in 200 μl TE Buffer, 1.3 μl RNase A (Sigma-Aldrich) was added, and they were incubated at 37 °C for 30 min in a thermo-shaker. Next, 200 μl Elution Buffer (Table 24), 7 μl 300 mM CaCl₂, and 4 μl Proteinase K (VWR) were added followed by an incubation at 55 °C for 30 min. DNA was again isolated as described in section 3.4.2. Gel electrophoresis of 10 μl of the input material was performed as a quality control for the DNA fragmentation. qPCR for positive and negative controls was performed to ensure functionality of the method.

3.10 High-Throughput sequencing

3.10.1 RNA-sequencing

Total RNA was isolated from KSHV-infected and control cells using RNA Bee as previously described. Prior to the library preparation the RNA quality was examined on a Bioanalyzer with the RNA Nano Kit (Agilent). Samples with an RNA Integrity Number (RIN) of 7 or higher were further processed. In a first step poly-adenylated RNA was enriched by the usage of the NEBNext Poly(A) Magnetic Isolation Module (New England Biolabs). This was then followed by the library preparation for strand specific RNA sequencing using the NEXTFlex™ Rapid Directional qRNA-Seq Kit (Bio Scientific) according to the manufacturer's instructions. Library quality was assessed on a Bioanalyzer with the High Sensitivity DNA Kit (Agilent). Single-read sequencing with a read length of 75 bp was performed on a NextSeq 500 platform aiming at a sequencing depth of 20-30 mio reads.

3.10.2 Single-Cell RNA-sequencing

Single-Cell RNA-sequencing was performed from Bac16 infected TIME cells to get further insights into the observed delayed Type I interferon response. For this, the infected TIME cells were detached from the culture vessel and centrifuged for 5 min at 300 x g. The cell pellet was resuspended in 10 ml complete culture media and cells were counted using a hemocytometer. A total of 2×10^5 cells were resuspended in 10 ml media. Cells were washed two times in 2 % FBS in PBS which also included a stepwise decrease of the volume. Each washing step included a centrifugation at 300 x g for 4 min. The cell pellet was resuspended with a wide-bore pipette tip to minimize shear forces. After the second washing step cells were resuspended in a volume of 200 μ l 2 % FBS in PBS to obtain a dilution of 1000 cells/ μ l. Duplets and debris was removed by filtering the cells through a cell strainer and cell number was again determined with a hemocytometer. Cells were immediately kept on ice until they were partitioned into Gel Bead-In-Emulsions (GEM) using the Chromium Single Cell 3' Reagent Kit v2 and the Chromium Controller (10x Genomics). The steps included in this kit are GEM generation and Barcoding, Post GEM-RT Cleanup, cDNA amplification, and library construction. A schematic representation of the workflow is depicted in Figure 8.

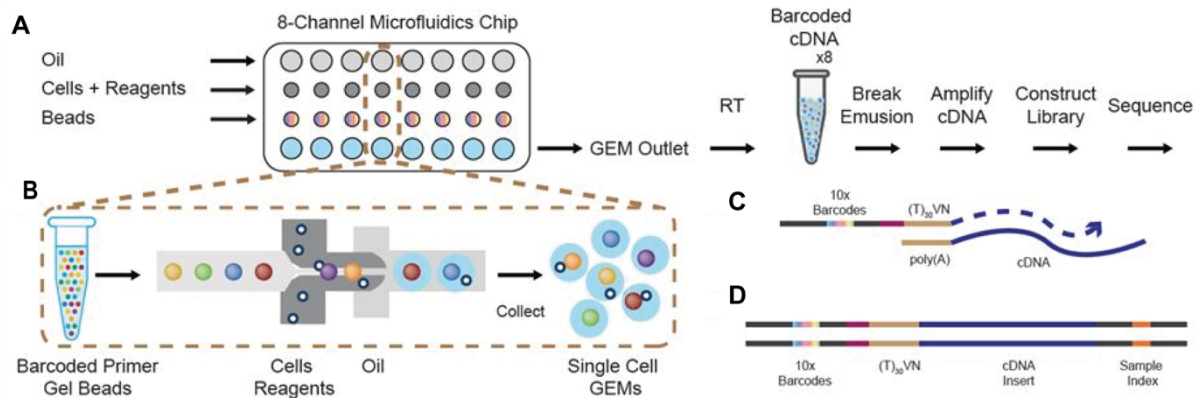


Figure 8: scRNA-sequencing workflow: (A) Schematic representation of the scRNA-seq workflow with the GemCode technology. Cells were mixed with the reagents in one well of the microfluidics chip and then combined with the gel beads from another well to form Gel In-Bead Emulsions (GEMs). This is followed by the reverse transcription which takes place inside each GEM. cDNA from each cell is pooled for amplification and library construction. (B) Zoom-in into the GEM generation within the microfluidic chip. Gel beads containing the primers and barcoded oligonucleotides are mixed with the cells before they get encased by the oil solution. (C) Oligonucleotides within the gel beads contain an Illumina adapter, 10x barcodes, unique molecular identifiers (UMIs) as well as oligo dTs. The latter allows for the reverse transcription of polyadenylated RNA. (D) The final library consists of molecules which can be sequenced on an Illumina sequencer for short reads (modified from Zheng et al. 2017).

All steps were exactly performed as described in the manufacturer's instructions. After library preparation, concentration was measured at the Qubit (Invitrogen). Mean size and quality of the library were assessed on a Bioanalyzer (Agilent) using the High Sensitivity DNA Kit (Agilent). Sequencing was performed on a NextSeq 500 with a read length of 75 bp and an intended sequencing depth of 20-30 million reads.

3.10.3 ChIP-sequencing

ChIP samples generated as described in chapter 3.7 were further processed for high-throughput sequencing. Library preparation of the samples was performed with the Nextflex® ChIP-Seq Library Prep Kit (Bioo Scientific) according to the manufacturer's instructions. Mean library size and quality were examined on a Bioanalyzer using the High Sensitivity DNA Kit (Agilent). Libraries were sequenced on a NextSeq 500 with an intended sequencing depth of 20-30 million reads.

3.10.4 MeDIP-sequencing

Sequencing libraries were generated from MeDIP samples which were produced as described in chapter 3.8. The DNA SMART™ ChIP-Seq Kit (Takara Clontech) was used for library preparation. The quality and the mean size of the library was controlled on a Bioanalyzer with the High Sensitivity DNA Kit (Agilent). Single-read sequencing with a read length of 75 bp was performed on a NextSeq 500 with an intended sequencing depth of 20-30 million reads.

3.11 Bioinformatic analysis

3.11.1 Analysis of RNA-sequencing

Bioinformatic analyses were generally performed on a RECT™ Workstation WS-2232B with a Linux operating system. Mapping of RNA sequencing data was performed by STAR 2.6.0c (Dobin et al., 2013) using hg38 and bac16 (KSHV) as reference genomes. Differential gene expression was analyzed with the R package DeSeq2 (Love et al., 2014). Genes with significant differential expression were identified by a log₂ fold change of > 1 or < -1 and an adjusted p-value of < 0.05. Plots were generated in R Studio 1.3.959 using ggplot2 3.3.2 or pheatmap 1.0.12. For the pathway analysis of significantly up- or downregulated genes DAVID 6.8 (Huang et al., 2007) was used.

scRNA sequencing data was analyzed with the Cell Ranger application 2.2.0 (10x Genomics) which allows for the alignment of reads, filtering steps and the counting of cellular barcodes as well as unique molecular identifiers (UMI) to generate feature-barcode matrices. Clustering, identification of marker genes within these clusters and pathway analysis was performed with the R tool Seurat 3.0 (Butler et al., 2018; Stuart et al., 2019).

3.11.2 Analysis of ChIP-sequencing

Mapping of ChIP-sequencing data was performed by Bowtie 1.2.3 (Langmead et al., 2009) with the standard settings using the -m 1 option to exclude reads which can be aligned to multiple positions of the reference. Hg38 for the human genome and bac16 for KSHV were used as references. Regions on the human genome with differential epigenetic profiles were identified by the usage of diffReps 1.55.6 (Shen et al., 2013). Here, the options for the analyzed window sizes were adjusted according to the peak size of the respective histone modification. Further analysis and data visualization was carried out in EaSeq 1.11 (Lerdrup et al., 2016).

3.11.3 Analysis of MeDIP-sequencing

Mapping of MeDIP-sequencing data was performed by Bowtie 1.2.3 (Langmead et al., 2009) with the standard settings. The -m 1 option was used to exclude reads which can be aligned to multiple positions of the reference. Hg38 for the human genome and bac16 for KSHV were used as references. As the first three nucleotides of every read derived from library preparation, they were trimmed prior to mapping. Differential

methyated regions were investigated using two different approaches. On the one hand, differential regions were identified globally by the usage of diffReps 1.55.6 (Shen et al., 2013). On the other hand, a more targeted approach was used including annotated CpG islands loaded from the UCSC browser. For this purpose, DNA methylation levels in the annotated CpG islands were counted with featureCounts 2.0.0 (Liao et al., 2014) and were then subjected to a DeSeq2 analysis. Further analysis and data visualization was carried out in EaSeq 1.11 (Lerdrup et al., 2016).

3.11.4 Coverage Plots of viral genomes

IGVTools (Thorvaldsdóttir et al., 2013) was used to generate coverage plots of the transcriptional or epigenetic profiles of the KSHV genomes. The viral genome was divided in 100 bp sections and the coverage in these sections was analyzed with the 'count' function. For the RNA-sequencing datasets forward and reverse reads were analyzed separately whereas reads of ChIP-sequencing as well as MeDIP-sequencing were analyzed without strand specificity. The obtained datasets were used to generate coverage plots in Microsoft Excel (script generated by Adam Grundhoff, unpublished).

3.12 Statistical analyses

Statistical analyses were performed in GraphPad Prism 8.4.3. Depending on the experimental setup, one-way ANOVA or two-way ANOVA was used to determine the statistical significance of multiple comparisons. An explanation of the exact statistical test used to analyze the datasets can be found in each figure legend.

4 Results

4.1 Latent KSHV infection model in endothelial cells

4.1.1 Experimental design to investigate transient and stable consequences of a KSHV infection

Previous findings revealed that the KSHV genome is decorated with epigenetic modifications upon *de novo* infection to regulate viral gene expression (Günther & Grundhoff, 2010; Toth et al., 2010). Additionally, more recent data showed that viral factors are able to interact with host epigenetic modifiers (Hu et al., 2014). These interactions might not only affect the epigenetic landscape of the viral genome but could also lead to altered patterns in certain host genomic loci. In fact, some data showed that certain host regions revealed differential epigenetic patterns upon KSHV infection (Di Bartolo et al., 2008; Shamay et al., 2006). However, a long-term and genome-wide analysis of KSHV induced host transcriptional changes as well as epigenetic alterations in a relevant *in vitro* system is still missing.

In order to investigate short- as well as long-term consequences of a latent KSHV infection, an *in vitro* infection model was established which allows for the cultivation of infected cells over long time periods (Figure 9A). While *in vitro* infected cells are generally able to maintain KSHV genomes, they still tend to lose viral copies over time for a yet unknown reason. Therefore, long-term infection experiments highly rely on mutant viruses which either express fluorescent markers or antibiotic resistance genes for selection. The bacterial artificial chromosome (BAC) of KSHV, called Bac16, represents a well suited system as it encodes for GFP as well as hygromycin (Figure 9B). This construct was used to infect telomerase-immortalized microvascular endothelial cells (TIME cells). TIME cells provide a well-established model system for KSHV infection in endothelial cells. In contrast to multiple other tumor cell lines, these cells lack the consecutive expression of a viral oncogene in order to provide constant cell growth. Instead, inhibition of growth arrest in these cells is achieved by the expression of hTERT. Furthermore, it is a diploid cell line with a modal chromosome number of 46 and only low rates of polyploidy. These characteristics allow for the investigation of long-term effects while still resembling a primary cell type. Even more importantly, potential findings in these cells could provide new aspects for virus mediated tumorigenesis, especially with regard to KS, as the characteristic spindle cells of this tumor are thought to be of endothelial origin.

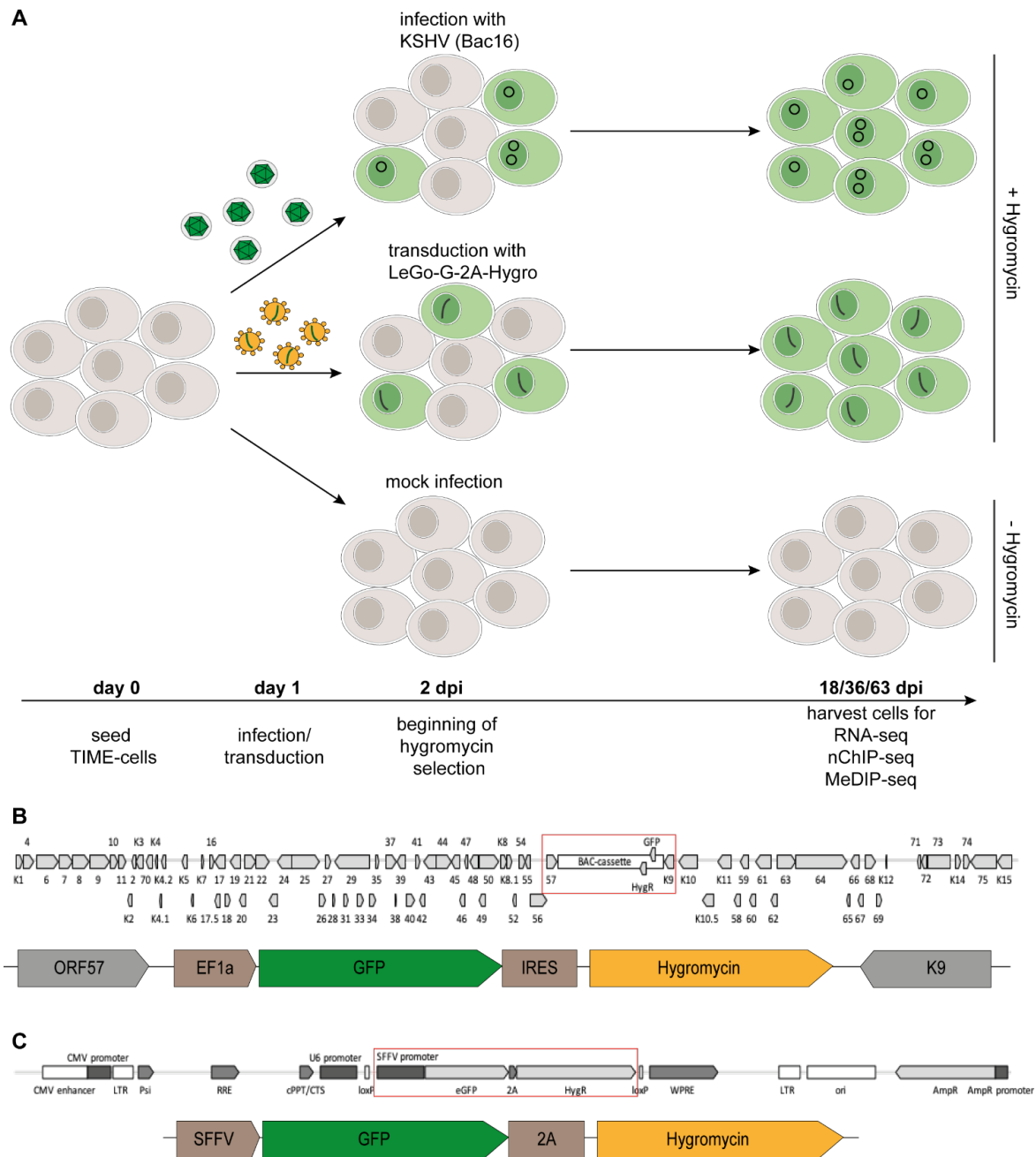


Figure 9: Experimental setup and schematic overview of the constructs: (A) Experimental setup to investigate host epigenetic changes and associated transcriptional alterations upon KSHV infection. TIME cells were either infected with Bac16, transduced with a lentiviral construct, or mock infected. Two days after infection hygromycin selection (200 $\mu\text{g}/\text{ml}$) was started for infected as well as transduced cells. 18, 36, and 63 dpi cells were harvested to perform RNA-seq, nChIP-seq, and MeDIP-seq. (B) Schematic overview of Bac16. The bacmid of KSHV encodes for all of the viral proteins. Additionally, a BAC cassette is inserted downstream of ORF57 which encodes among others for hygromycin and GFP. (C) Schematic overview of LeGo-G-2A-Hygro construct. This lentiviral construct also encodes for GFP and hygromycin. TIME cells transduced with this construct served beside the mock infected cells as an additional negative control.

After *de novo* infection of TIME cells with viral particles of Bac16, cells were grown two more days before hygromycin selection was started. The cells were kept under selection during the whole course of infection. However, only low concentrations of hygromycin were added to the culture media (200 $\mu\text{g}/\text{ml}$) to reduce the selection

pressure but still keep the population KSHV positive. Additionally, a control for the hygromycin selection and the consecutive GFP expression was included by transducing TIME cells with the lentiviral construct LeGo-G-2A-Hygro (Figure 9C). Mock infected cells served as a second negative control. All these populations were cultured in parallel until at three different time points, 18, 36, and 63 dpi, cells were harvested to perform MeDIP-seq, nChIP-seq as well as RNA-seq. While RNA-seq allowed for the investigation of transcriptional alterations after KSHV infection, MeDIP-seq as well as nChIP-seq enabled the identification of virus-induced epigenetic changes. The three time points made it possible to track either transient changes only occurring at a single time point or more stable patterns which are altered over the entire course of infection.

4.1.2 TIME cells are latently infected with KSHV

Prior to the investigation of host transcriptional alterations, the KSHV infection state in TIME cells was controlled at all three time points. RNA-seq data was mapped to the Bac16 reference genome to get an overview about the viral gene expression in infected cells (Figure 10).

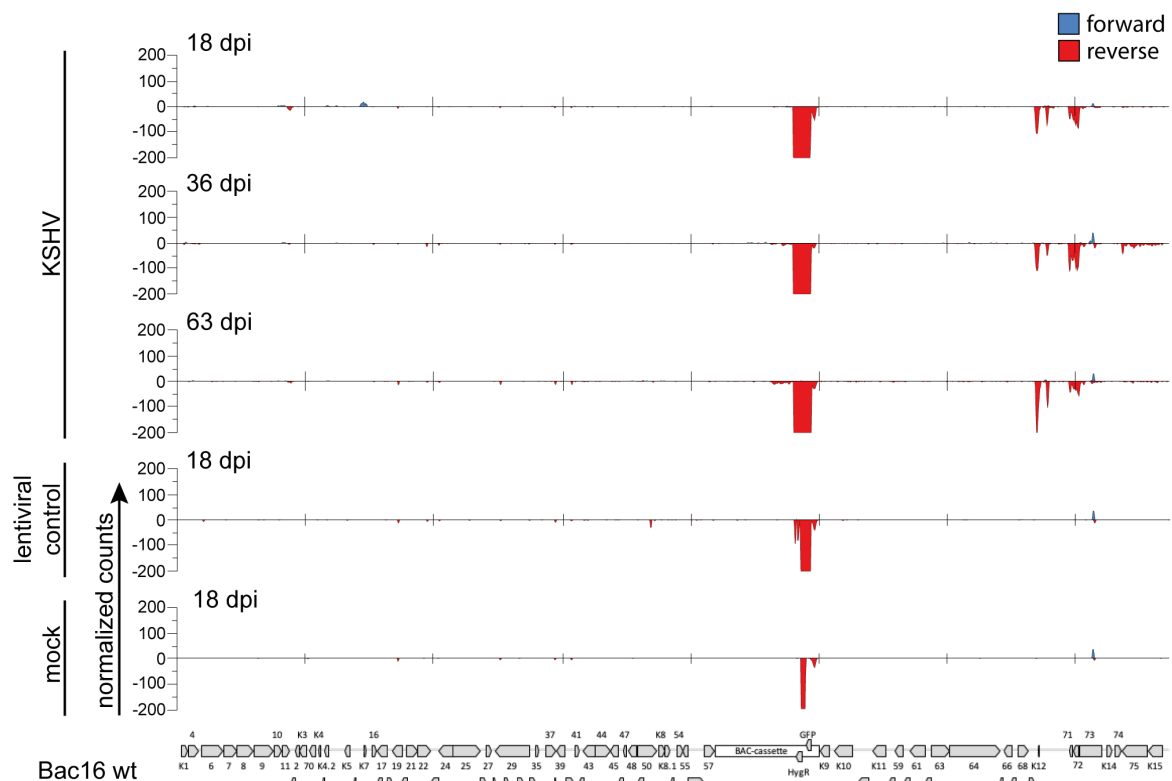


Figure 10: KSHV transcriptional profile in TIME cells: Raw sequencing data was mapped to the Bac16 reference genome. Reads were then counted in 100 bp windows by discriminating between forward (blue) and reverse (red) reads. Coverage plots for all three time points are depicted in the case of Bac16 infected samples. For lentiviral control and mock only one representative coverage plot for day 18 p.i. is depicted.

This revealed that highest signal was detectable in the BAC cassette where GFP and hygromycin are encoded. A signal in this region was also observed for both negative controls. In the case of the lentiviral control this is due to the fact that these cells also express GFP and hygromycin introduced via lentiviral transduction. The signal for the mock control can be explained by the presence of the human EF1 α promoter within the BAC cassette. More importantly, further signals were only detected in the region where KSHV specific genes are encoded. They were present at all three time points and only in the KSHV infected cells. Interestingly, peaks were restricted to one specific region of the viral genome ranging from K12 to ORF73 which represents the region where viral latent genes are encoded. These data indicate that KSHV is predominantly in the latent infection state.

These findings were evaluated on protein level by performing immunofluorescence for LANA as a latent viral protein. Additionally, co-staining of ORF59 was performed which served as a marker for KSHV lytic reactivation (Figure 11).

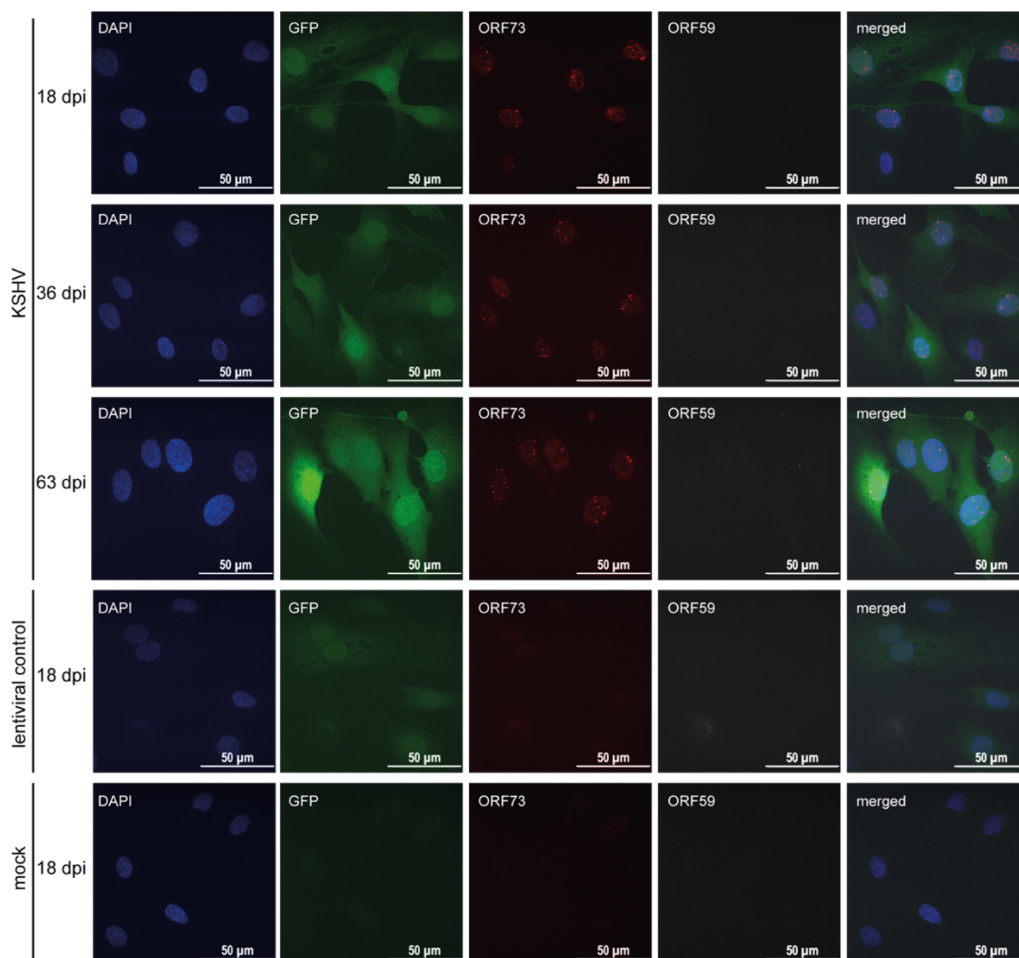


Figure 11: Immunofluorescence of LANA and ORF59: Staining of LANA as a latent protein (ORF73, red) and GFP expression served as infection controls. ORF59 staining (grey) was performed to identify KSHV lytic replication in infected cells. Nuclear DNA was stained with DAPI. Maximum intensity projections for all three time points are depicted in the case of Bac16 infected samples. For lentiviral control and mock only one representative image for day 18 p.i. is depicted.

Staining of LANA resulted in the characteristic dot structures throughout the nucleus and signal was only detected in KSHV infected samples at all three investigated time points. Additionally, LANA signal and GFP expression correlated, which justifies the usage of GFP expression as a marker for infected cells. GFP expression was also observed in the lentiviral control, as expected, but signal was lower compared to the KSHV infected cells. Similar to the RNA-seq data, there was no indication for KSHV lytic replication as ORF59 staining did not reveal any positive signal in infected endothelial cells. In summary, *in vitro* infection of TIME cells resulted in a stable latent infection.

4.2 Transient and stable transcriptional alterations upon latent KSHV infection

4.2.1 Prolonged type I interferon response in KSHV infected cells

The established *in vitro* infection system in endothelial cells was used to identify transient as well as stable transcriptome deregulations during long-term latent KSHV infection. Therefore, RNA-seq was performed from four biological replicates (except for KSHV infected cells 63 dpi with n=3) and for the analysis KSHV infected cells were compared to either of the controls from the same time point. Genes were considered as significantly deregulated if their log₂ foldchange was > 1 or < -1 and the p-value was on the same time < 0.01. In Figure 12, results of the comparison between KSHV infected cells and the lentiviral control are depicted.

Each time point revealed a characteristic set of significantly deregulated genes. While the number of downregulated genes was quite constant during the time course, upregulated genes underwent some changes between 36 dpi and 63 dpi. The number declined dramatically from 54 and 53 upregulated genes at day 18 and day 36 p.i., respectively to only six upregulated genes at day 63 p.i. In general, KSHV infection had rather moderate effects on the host transcriptome with regard to the number of deregulated genes at these late time points. Nevertheless, pathway analysis revealed that the type I interferon response plays a major role at day 36 p.i. but not at any other time point. Members of the IFIT family, but also IRF7, STAT1 and ISG15 were among the deregulated genes which could be allocated to this pathway. Genes downregulated 18 or 63 dpi were assigned for example to the term extracellular matrix organization.

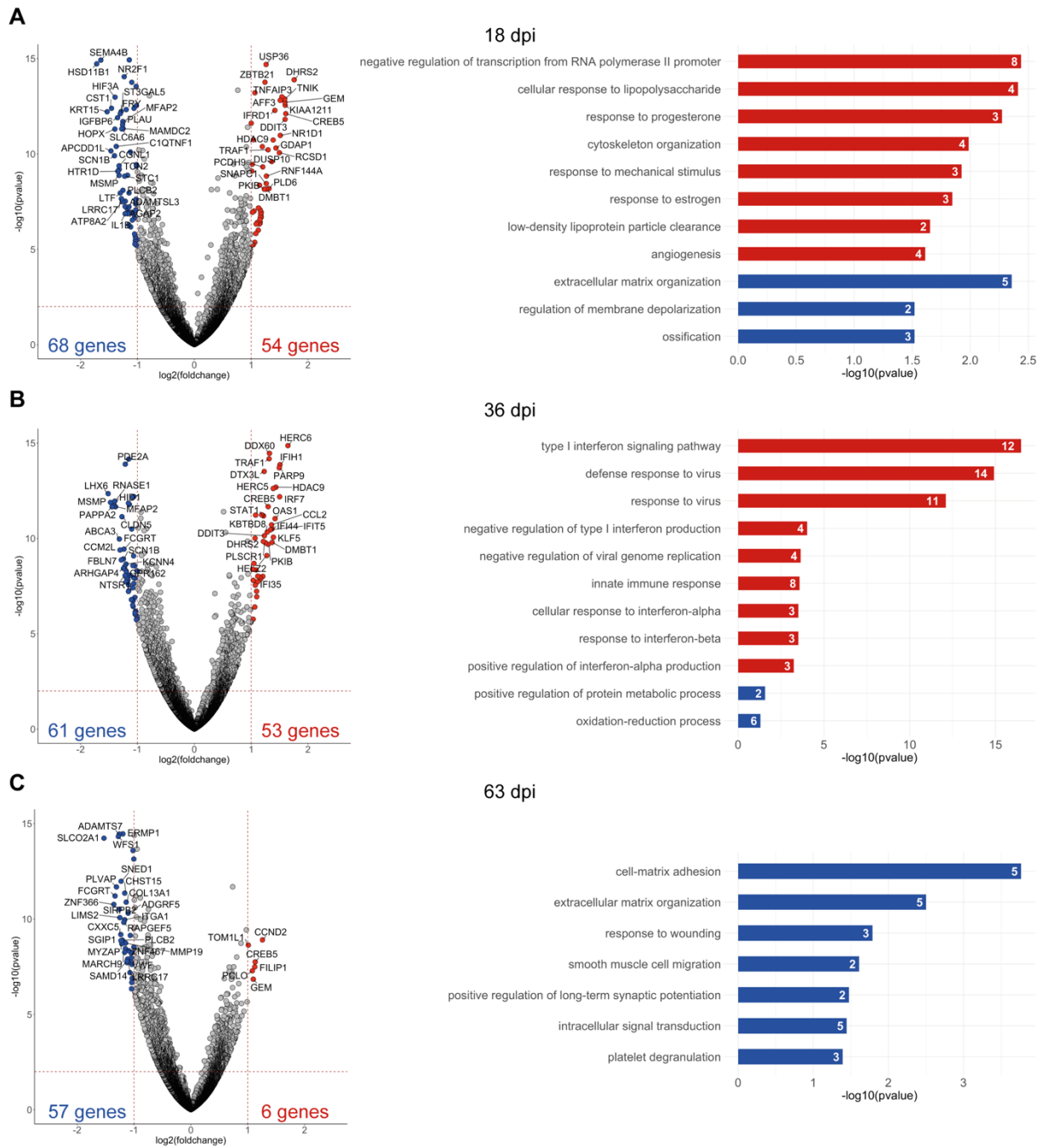


Figure 12: Transcriptional deregulation in KSHV infected cells: (A) KSHV induced transcriptional changes 18 dpi. The volcano plot summarizes the results from RNA-seq comparing KSHV infected and lentiviral transduced samples. Genes were considered significantly deregulated if $\log_2(\text{foldchange})$ was > 1 or < -1 and the p-value was < 0.01 which is also marked in the plot by red dashed lines. Numbers and dots representing significantly upregulated genes are depicted in red, while downregulation is marked by blue color. Significantly up- or downregulated genes were used to perform pathway analysis in DAVID. The top up- or down-regulated GO terms are depicted using the same color code as for the volcano plots. White numbers within the bars represent the number of genes, which can be allocated to this pathway. RNA-seq results for (B) 36 dpi and (C) 63 dpi were analyzed and depicted as described in (A) ($n=4$, except for KSHV, 63 dpi with $n=3$).

In order to get further insights into the transcriptional changes occurring upon KSHV infection, especially with regard to the time-dependent regulation of certain factors, all the genes which were significantly deregulated at least once during the time course were summarized in a heatmap (Figure 13A).

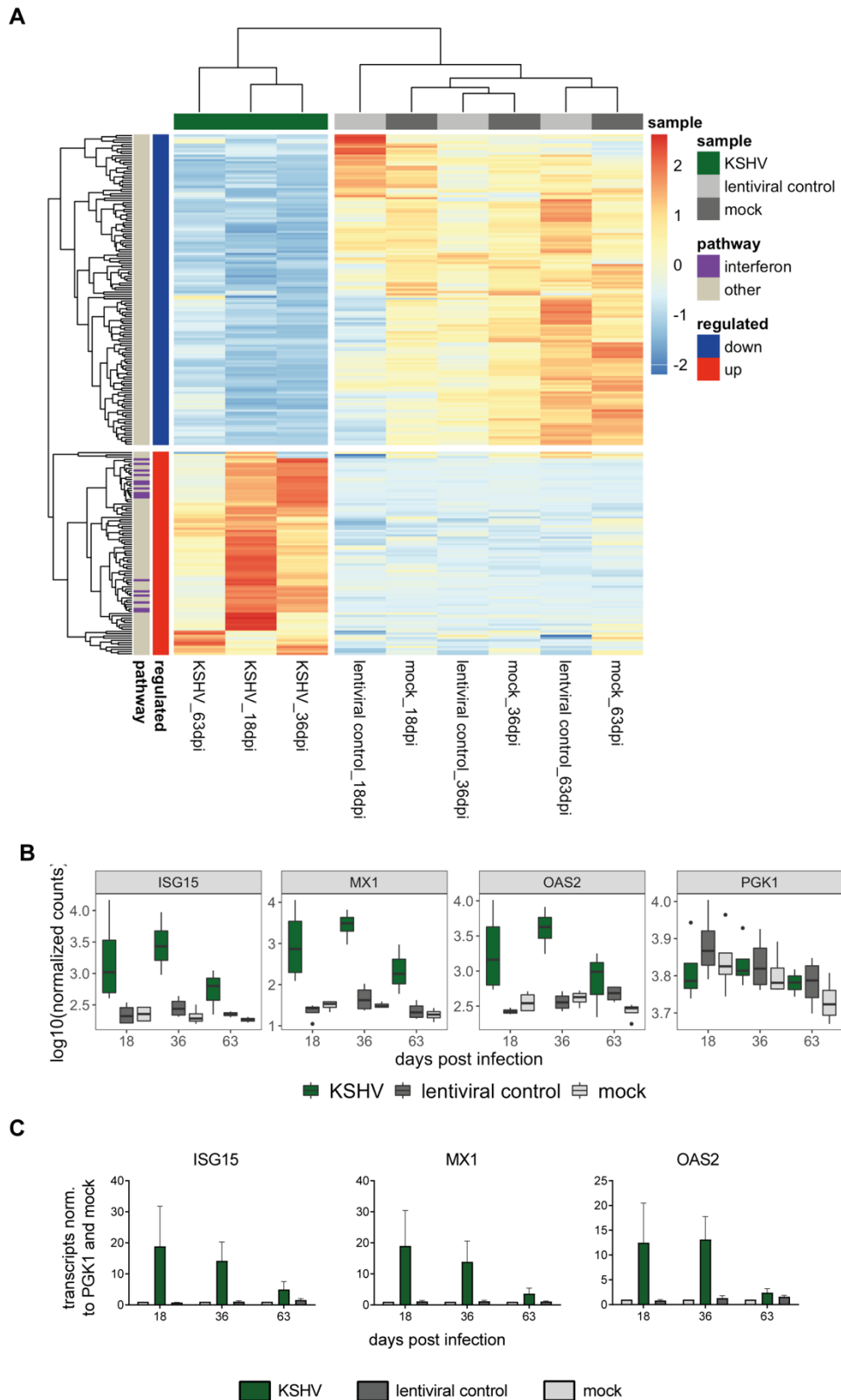


Figure 13: Time-dependent expression of interferon regulated genes: (A) Heatmap of significantly deregulated genes. All the genes which were significantly deregulated at least once during the time-course were summarized in a heatmap. z score calculation of normalized counts from each gene and sample was performed and is depicted in this heatmap. Hierarchical clustering was performed for the genes as well as for the samples. Genes were furthermore classified according to the pathway they can be assigned to and according to their mode of deregulation upon KSHV infection. (B) Normalized counts of specific interferon responsive genes. Normalized counts of ISG15, MX1, OAS2, and PGK1 from the RNA-seq experiment are shown for each condition over time. (C) qRT-PCR for interferon responsive genes. Transcript levels of ISG15, MX1, and OAS2 relative to PGK1 and mock were determined by qRT-PCR. Bars represent the mean with SEM. Statistical significance was assessed by two-way ANOVA (n=4, except for KSHV, 63 dpi with n=3).

Hierarchical clustering of the deregulated genes as well as of the samples was performed. This revealed that KSHV infected samples clustered distinct from both controls. With regard to the controls clustering was observed based on the time point rather than on the treatment. Clustering of the genes resulted in a clear discrimination between upregulated and downregulated genes. This was also nicely recapitulated by the classification of the genes according to their mode of deregulation. Genes were additionally classified based on their affiliation to the type I interferon response. This further highlighted that if deregulation was observed, genes which belong to this pathway are always upregulated upon KSHV infection. This heatmap gives also a temporal resolution of the deregulated genes. Upregulated genes at day 18 p.i. tend to be also upregulated at day 36 p.i. but rather not at day 63 p.i. The downregulated genes show the same expression pattern over the whole course of infection. Although downregulation of a gene might not be significant at all time points, there is still a trend into the same direction.

As endothelial cells were previously shown to be latently infected with KSHV over the whole course of infection (Figure 10 and 11), the prolonged type I interferon response observed at day 36 p.i. was rather unexpected. In order to get a more detailed view into the temporal gene expression patterns, normalized counts of individual interferon responsive genes, like ISG15, MX1, and OAS2 are depicted in Figure 13B. Furthermore, qRT-PCR for the same genes was performed, to further evaluate the RNA-seq data. Both methods supported the previous finding that expression of these genes was already increased at day 18 p.i. However, levels seem to be more variable within the different biological replicates at this time point. Additionally, this detailed view into at least some individual interferon responsive genes also revealed that a slight upregulation can still be observed at day 63 p.i. but to a far less extent when compared to the other time points.

In summary, the analysis of long-term transcriptional alterations upon KSHV infection revealed, despite moderate transcriptomic deregulation, a distinct interferon response for several weeks in strictly latent cultures.

4.2.2 Comparison of prolonged and *de novo* type I interferon responses

In order to get further insights into the exact temporal resolution of the type I interferon response, a time course experiment in Bac16 infected TIME cells was performed. Cells were harvested every three to four days to measure ISG15 transcript levels representatively for the type I interferon response by qRT-PCR (Figure 14A). Viral DNA

copy numbers were quantified in parallel by qPCR to investigate whether an increase in ISG15 levels resulted in simultaneous changes in KSHV copy numbers (Figure 14B).

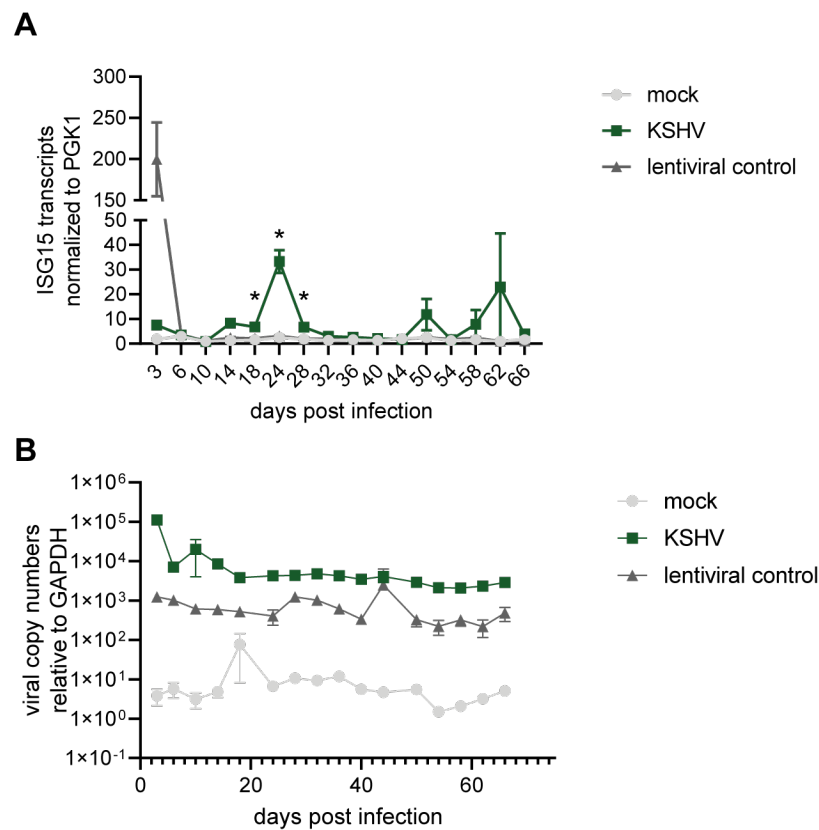


Figure 10: Temporal resolution of the interferon response upon KSHV infection: (A) Time course of ISG15 transcripts upon KSHV infection. RNA was isolated from KSHV infected and control cells at indicated time points post infection. Relative transcript levels for ISG15 were measured by qRT-PCR and then normalized to PGK1 (n=3). Statistical significance was assessed by Two-way ANOVA. Significance is indicated by asterisk if comparison between KSHV and each control revealed a p-value >0.05. (B) DNA was isolated from KSHV infected and control cells at indicated time points post infection. Relative viral copy numbers relative to GAPDH were determined by qPCR (n=3).

The time course started 3 dpi to include an immune response after *de novo* infection with KSHV. Previous infection experiments in TIME cells revealed that ISG15 transcripts are highest at that time point after *de novo* infection (Figure S1). Mock infected cells as well as LeGo-G-2A-Hygro transduced cells were cultured in parallel and served as controls. *De novo* KSHV infection in TIME cells led to an around 8-fold induction of ISG15 levels at day 3 p.i. compared to the mock control. However, transduction of the lentiviral construct led to an even 200-fold increase in ISG15 levels compared to mock infected cells. But in contrast to the KSHV infected cells, ISG15 levels did not rise at any other time point in the lentiviral control. ISG15 transcripts in mock cells stayed at constant low levels over the time course. While ISG15 transcripts decline after induction at day 3 p.i. in KSHV infected cells, numbers start again to rise 14 dpi until highest levels are reached at day 24 p.i. Between day 32 and 36 p.i. ISG15

transcript levels are again comparable to the mock and lentiviral control. This is a marked contrast to the RNA-seq data where type I interferon response was significantly upregulated at day 36 p.i. This implies that the observed responses seem to be partly flexible with regard to the temporal aspect. ISG15 transcripts again reached peaks at day 50 and 62 p.i., but levels are not that pronounced anymore and vary between replicates. Relative viral DNA normalized to the human GAPDH locus was additionally determined by qPCR to correlate changes in the type I interferon response to KSHV copy numbers. This revealed that KSHV copy numbers are highest 3 dpi. The numbers then rapidly decline until day 10 p.i. and are afterwards stable over the time course. As copy numbers were determined by a primer set specific for GFP, there was also a signal detectable for the lentiviral control. Mock infected cells only provided low background levels. In summary, these data suggest that the interferon response at late time points of infection is not a prolonged response originating from high levels after *de novo* KSHV infection but rather represents events of sporadically reoccurring responses. Furthermore, these sporadic events are more pronounced compared to the initial response observed upon *de novo* infection.

Due to the differences of early and late interferon responses regarding the strength of induction, RNA-seq of *de novo* infected cells at day 3 p.i. and day 10 p.i. was performed to further evaluate the findings from the time course experiment. (Figure 15). RNA-seq data was investigated with a focus on a subset of interferon responsive genes (Schoggins & Rice, 2011). Heatmaps were generated to provide comparisons between KSHV infected cells and mock infected cells or the lentiviral control, respectively (Figure 15 A + B). Comparisons were visualized in separate heatmaps to obtain better resolution for the individual genes because levels in the lentiviral control 3 dpi are by far higher as for the rest of the samples. In general, the data reflects very well the results obtained from the time course experiment. However, RNA-seq allowed for the investigation on a single gene resolution. This revealed that 3 dpi a specific subset of interferon responsive genes was upregulated which is neither observed in the lentiviral control at day 3 p.i. nor in the KSHV infected cells at day 18 and day 36 p.i. These genes are mainly CD74, SSBP3, and P2RY6. Additionally, some genes which are upregulated at late time points post infection also show a slight increase in expression during the early response.

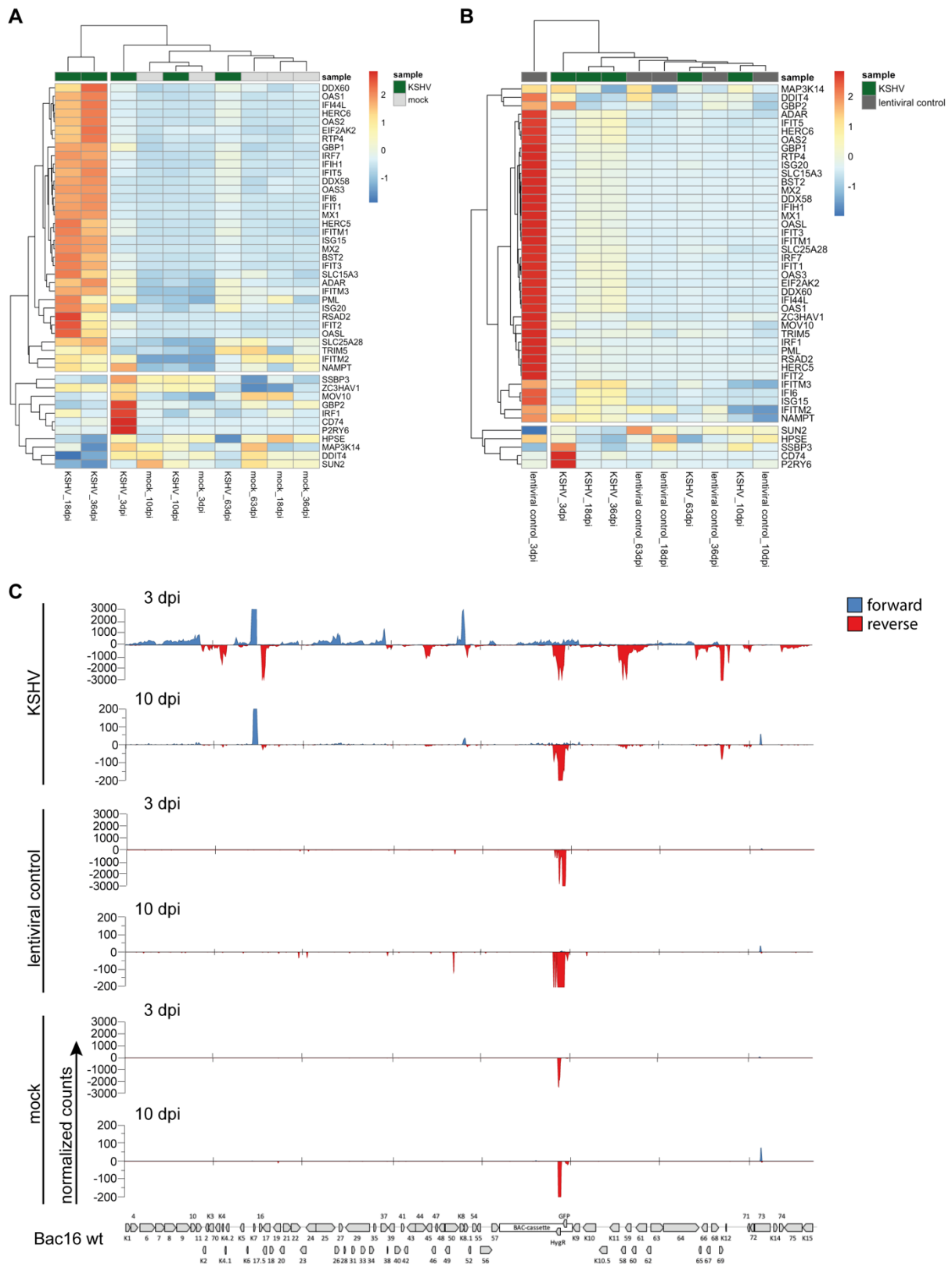


Figure 11: Interferon signatures and KSHV transcriptional profile after *de novo* infection: (A+B) Comparison of early and late interferon responses. Heatmaps of interferon responsive genes are depicted where z score calculation of normalized counts from each gene and sample was performed. Hierarchical clustering was performed for the genes as well as for the samples. (A) includes a comparison of KSHV infected cells and mock controls while (B) represents a comparison of KSHV infected cells and the lentiviral control. (C) KSHV transcriptional profile in TIME cells. Raw sequencing data was mapped to the Bac16 reference genome. Reads were then counted in 100 bp windows and by discriminating between forward (blue) and reverse (red) reads. Coverage plots from 3 dpi and 10 dpi are depicted for KSHV infected cells as well as for the controls.

One explanation for the observed differences in early and late type I interferon responses would be different transcriptional profiles of KSHV at the individual time points of infection. For this reason, the KSHV transcriptional profile was investigated at day 3 and 10 p.i. This revealed, that lytic viral transcripts can be detected 3 days after *de novo* infection which is in accordance with previous findings (Purushothaman et al., 2015) and indicates that lytic gene expression plays a role during very early stages of infection. However, the obtained coverage plot for KSHV at day 3 p.i. also suggests that only a subset of cells might represent this transcriptional pattern because signals are lower than in BCBL-1 cells which were treated with sodium butyrate and TPA to induce the KSHV lytic replication cycle (Figure S2). At day 10 p.i. KSHV expression profiles resemble that observed at late time points (Figure 10) with the exception of the K5 locus which exhibits high signals at that early time point. These observations lead to the hypothesis that KSHV lytic gene expression during *de novo* infection might be essential to downregulate host interferon responses. Indeed, KSHV encodes several viral interferon-regulatory factors which are able to repress interferon responsive genes (Fuld et al., 2006; Joo et al., 2007; Li et al., 1998; Wies et al., 2008). Additionally, other viral lytic factors like ORF45 or ORF50 were also described to inhibit the host interferon response (Yu et al., 2005; Zhu et al., 2002). Contrarily, at late time points when KSHV fully established latent infection, these factors are missing and cannot counteract host immune responses anymore which would explain the here observed high induction of interferon responsive genes at late time points of infection. As the above presented results only provided bulk information, the question remained whether the late type I interferon signature is a uniform response of all the cells, or whether it represents a strong response of a minority of spontaneously reactivating cells, which were not detected by simple immunofluorescence.

4.2.3 Single cells express high levels of interferon regulated genes

Previous experiments were incapable of identifying the cause of the detected late type I interferon response. Additionally, it was still unclear whether the type I interferon response represents a uniform bulk response, or whether only single cells are responsible for this observation. In order to address these questions single cell RNA sequencing (scRNA-seq) was performed from KSHV infected cells at day 25 p.i. (Figure 16). This enabled on the one hand the investigation of specific host transcriptional profiles and on the other hand allowed for the correlation of interferon

regulated genes with viral transcripts on a single cell level. Prior to these specific analyses, several steps were performed to ensure high quality and reliability of the data. Based on standard methods, non-single cells (doublets) and apoptotic cells were excluded from the analysis. This resulted in a total number of 3918 single cells which were further analyzed using the single cell analysis pipeline Seurat. Cells were subdivided into different clusters using Uniform Manifold Approximation and Projection for dimension reduction (UMAP) (Figure 16A).

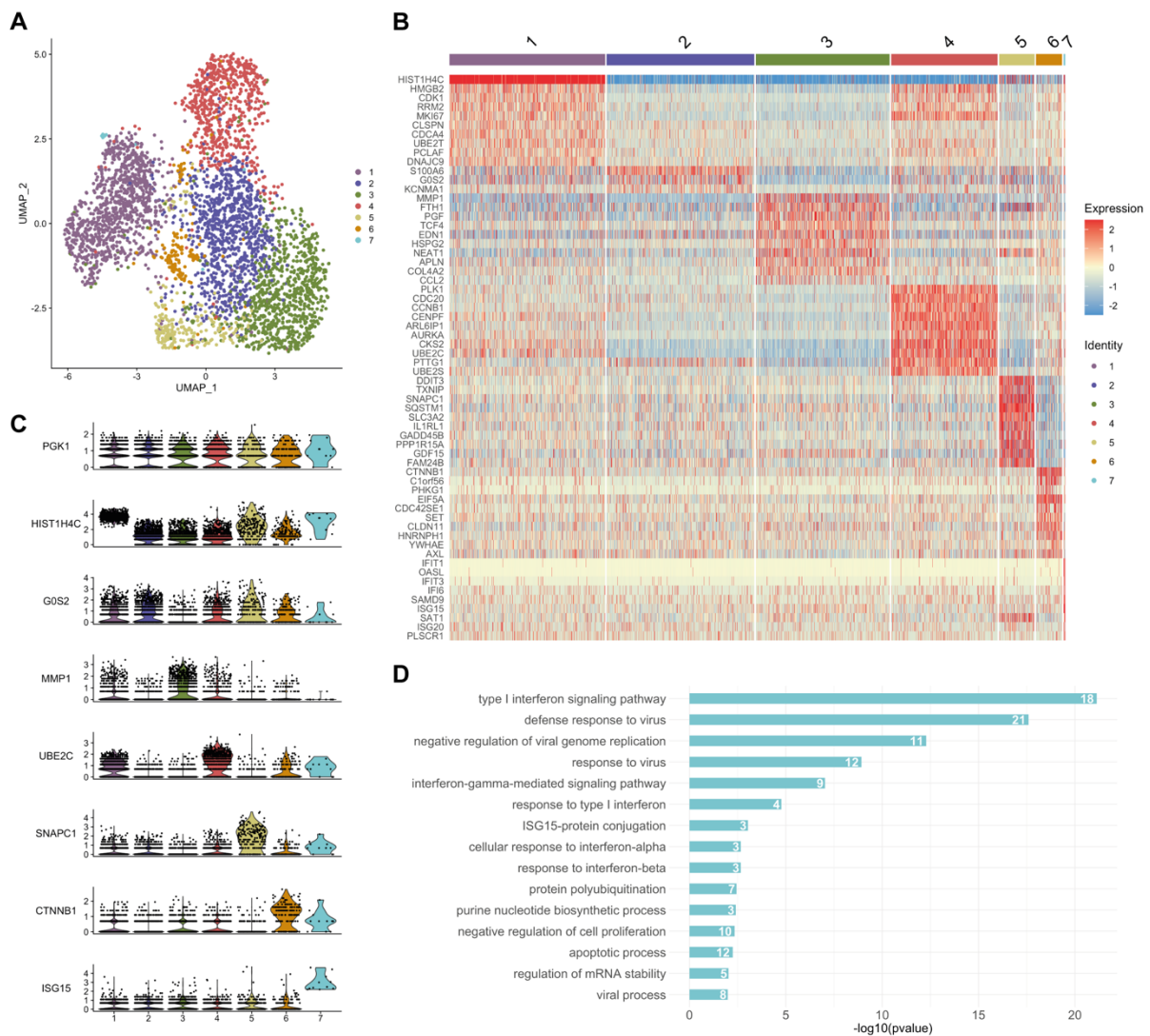
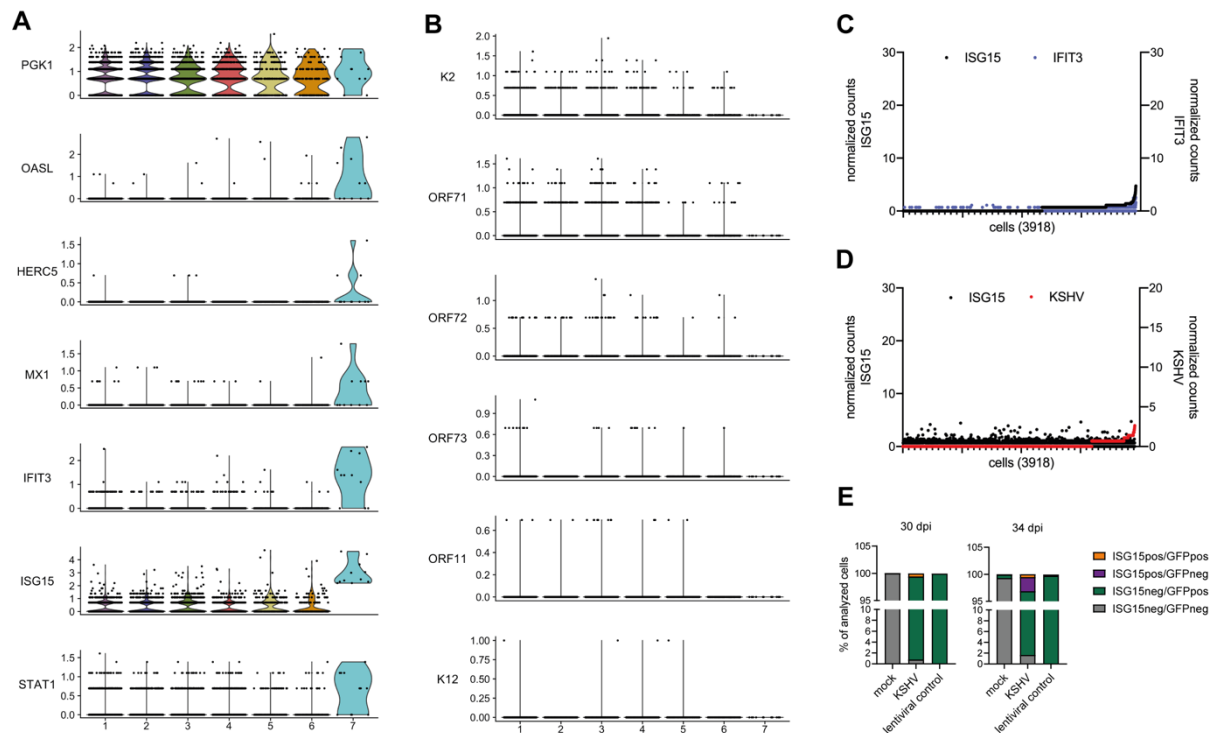


Figure 12: scRNA-seq of KSHV infected cells: (A) Clustering of single cells. scRNA-seq was performed by the usage of the 10x technology. The single cell analysis pipeline Seurat was used for data analysis. After removal of non-single cells and apoptotic cells, a total number of 3918 were further analyzed. Cells were clustered using UMAP (Uniform Manifold Approximation and Projection for dimension reduction). (B) Heatmap of top 10 marker genes per cluster. For every cluster marker genes were identified. The expression levels of the top 10 identified marker genes are visualized in a heatmap. Genes are sorted according to the cluster they belong to. (C) Violin plots of specific marker genes. One marker gene per cluster is visualized as violin plot, where every dot represents the expression of the gene within one cell. PGK1 served as a house keeping gene which is equally expressed in all clusters. (D) Pathway analysis of marker genes from cluster 7. The identified cluster specific marker genes were used to perform pathway analysis in DAVID. Pathways are sorted according to the highest $-\log_{10}(pvalue)$.

Seven distinct clusters were generated based on similar gene expression patterns of the individual cells. Specific marker genes were assigned which are highly expressed in cells of only one distinct cluster. The top 10 marker genes of each cluster are summarized in the heatmap of Figure 16B. Violin plots of one example gene from each cluster further revealed that expression of these marker genes is highly restricted especially in cluster 4 to 7 (Figure 16C). Pathway analysis of these genes furthermore enabled to classify these clusters into certain cellular programs including among others mitotic processes or transcriptional regulation in response to stress signals. Interestingly, pathway analysis of marker genes from cluster 7 which is comprised of only 11 single cells (see Table S1 for cell counts per cluster) resulted in almost the same GO terms which were already obtained from bulk sequencing at day 36 p.i. (Figure 16D). The most significant terms were type I interferon signaling pathway and defense response to virus.

This finding provided first evidence towards a scenario where only single cells might be responsible for the late type I interferon response upon KSHV infection. For this reason, further investigation of cluster 7 was performed to get a more detailed view especially regarding viral gene expression in these single cells (Figure 17). Expression of multiple interferon regulated genes, like OASL, MX1, ISG15, or STAT1 was assessed within the individual clusters. This revealed that all of these genes show highest expression in cluster 7. These data additionally demonstrated positive correlation between expression of individual interferon regulated genes within single cells (Figure 17A + C).

Interestingly, not a single viral transcript was detected for any of the representatively depicted viral genes in cluster 7 (Figure 17B). To investigate, whether cells of this cluster exhibited elevated levels of any transcript, we accumulated all viral counts and plotted the number of viral transcripts against the number of ISG15 counts per cell (Figure 17D). However, no correlation between the total viral transcripts and ISG15 expression was observed. As KSHV transcript levels were generally rather low also in the other clusters it cannot be fully excluded that detection of viral gene expression is insufficient at least in some of the cells with this method. However, previous results from bulk RNA-seq as well as from immunofluorescence staining already indicated that the majority of cells are latently infected with KSHV.



In summary, the data obtained from the scRNA-seq experiment indicate that single cells are responsible for the upregulated type I interferon response at late time points post infection. Furthermore, viral transcripts were completely absent in this small cell population which opens up the possibility that interferon regulated genes might play an important role for the silencing of viral gene expression. This, in turn, might have an influence on the latency maintenance of KSHV. In fact, recent findings indicate that the IFIT proteins are upregulated shortly after induction of the KSHV lytic cycle and are able to degrade viral mRNAs by direct binding (Li and Swaminathan 2019).

In order to confirm the findings from scRNA-seq, ISG15 staining of KSHV infected and control cells was performed at day 30 and 34 p.i. (Figure 17E). FACS analysis of ISG15-stained cells was performed and GFP expression was additionally measured to get information about the infection state of the cells. While mock infected cells did neither give a signal for GFP nor for ISG15, the cells of the lentiviral control were to almost 100 % GFP positive with no sign of ISG15 expression. In contrast to that, a low

percentage of KSHV infected cells revealed to be ISG15 positive with simultaneous expression of GFP at day 30 p.i. This subset of cells also exists 34 dpi, but another population arises which is ISG15 positive but at the same time GFP negative. These results not only hint towards a scenario where viral gene expression is reduced, but rather indicates that single cells might be able to clear a KSHV infection. However, further analyses are needed to confirm that the loss in GFP signal is also accompanied by a complete reduction of viral copy numbers.

4.3 Host DNA methylation patterns in KSHV infected cells

4.3.1 Quality control of methylated DNA immunoprecipitation sequencing

Previous data revealed that KSHV encoded factors can interact with host epigenetic modifiers, like DNA methyltransferases (Shamay et al., 2006). Furthermore, specific host genomic loci, including CCND2, CDH13 or TGFBR2, were described to undergo DNA methylation changes (Di Bartolo et al., 2008; Shamay et al., 2006). In order to investigate whether host DNA methylation changes occur genome-wide upon KSHV infection methylated DNA immunoprecipitation in combination with high-throughput sequencing was performed. Correlation with the already presented RNA-seq data furthermore enabled to elucidate whether potential epigenetic changes are associated with direct transcriptional deregulations.

Quality control steps to confirm functionality of MeDIP-seq were included at several stages of the experiment (Figure 18). One of these steps included the verification of proper shearing of the genomic DNA by running a small amount of the input material in an agarose gel (Figure 18A). Shearing of the DNA was sufficient when the average size of the DNA fragments was ranging between 100 and 500 bp. Fragmentation of genomic DNA is a crucial step during MeDIP-seq to provide good resolution of DNA methylation patterns in sequencing. The agarose gel electrophoresis of the input material confirmed sufficient fragmentation of the DNA. Another step of quality control was introduced prior to library preparation for sequencing. A small amount of the isolated DNA after immunoprecipitation was used to perform qPCR of host loci with a known DNA methylation state (Figure 18B). C1ORF43 on the one hand served as a negative control for DNA methylation, thus qPCR only provided low signals for this region. HOXC10 on the other hand represents a positive control. Additionally, an *in vitro* methylated plasmid (pCR2.1) was included as a spike-in control for the experiment and qPCR for this construct resulted in high signals. The comparison of

the GC content from input and precipitated samples also gives information about the functionality of the experiment after sequencing as DNA methylation occurs predominantly in the context of GC dinucleotides (Figure 18C). The percentage of GC in the precipitated samples was clearly increased compared to the input samples which provides evidence that methylated DNA was successfully enriched. For the analysis of host DNA methylation patterns upon KSHV infection CpG islands were of special interest because these regions often undergo dramatic changes during tumorigenesis (Costello et al., 2000; Weisenberger et al., 2006). Additionally, DNA methylation changes in CpG islands which are located in promoter regions often directly influence the transcriptional outcome of the associated gene (Song et al., 2005). Therefore, the identification of potential DNA methylation changes in these regions upon KSHV infection would directly provide a hint towards tumorigenesis and furthermore, correlation to transcriptional responses would also be facilitated.

Prior to the investigation of differential regions, individual host loci with known DNA methylation patterns were analyzed (Figure 18D). GGN as a testis-specific gene is depicted as an example of a methylated CpG island. Contrarily, the ubiquitously expressed gene ACTB is associated with an unmethylated CpG island. As methylated DNA in promoter regions is linked to gene repression and vice versa, the expression levels of these two genes were included from the previously performed RNA-seq data (Figure 18E). These data confirmed low expression levels for the highly methylated gene GGN. ACTB was highly expressed in TIME cells which was consistent with low DNA methylation levels in this locus. Before genome wide correlation between DNA methylation and gene expression was performed all of the annotated human CpG islands were grouped to general genomic features using ChIPseeker. This confirmed that CpG islands can be predominantly attributed to promoter regions. Around 60 % of these regions are located in proximal promoter regions. However, around 15 % of the regions can be found in distal intergenic regions which cannot be linked to specific gene expression. Nevertheless, a genome-wide analysis of host DNA methylation patterns within CpG islands was performed and associated gene expression levels were assigned. Heatmaps comprising an overview of the DNA methylation state of every CpG island were generated with the CpG islands sorted according to decreasing gene expression (Figure 18G). This revealed that low gene expression is associated with high DNA methylation and vice versa on a genome-wide level. This relation was observed in KSHV infected and control cells and for all the investigated time points.

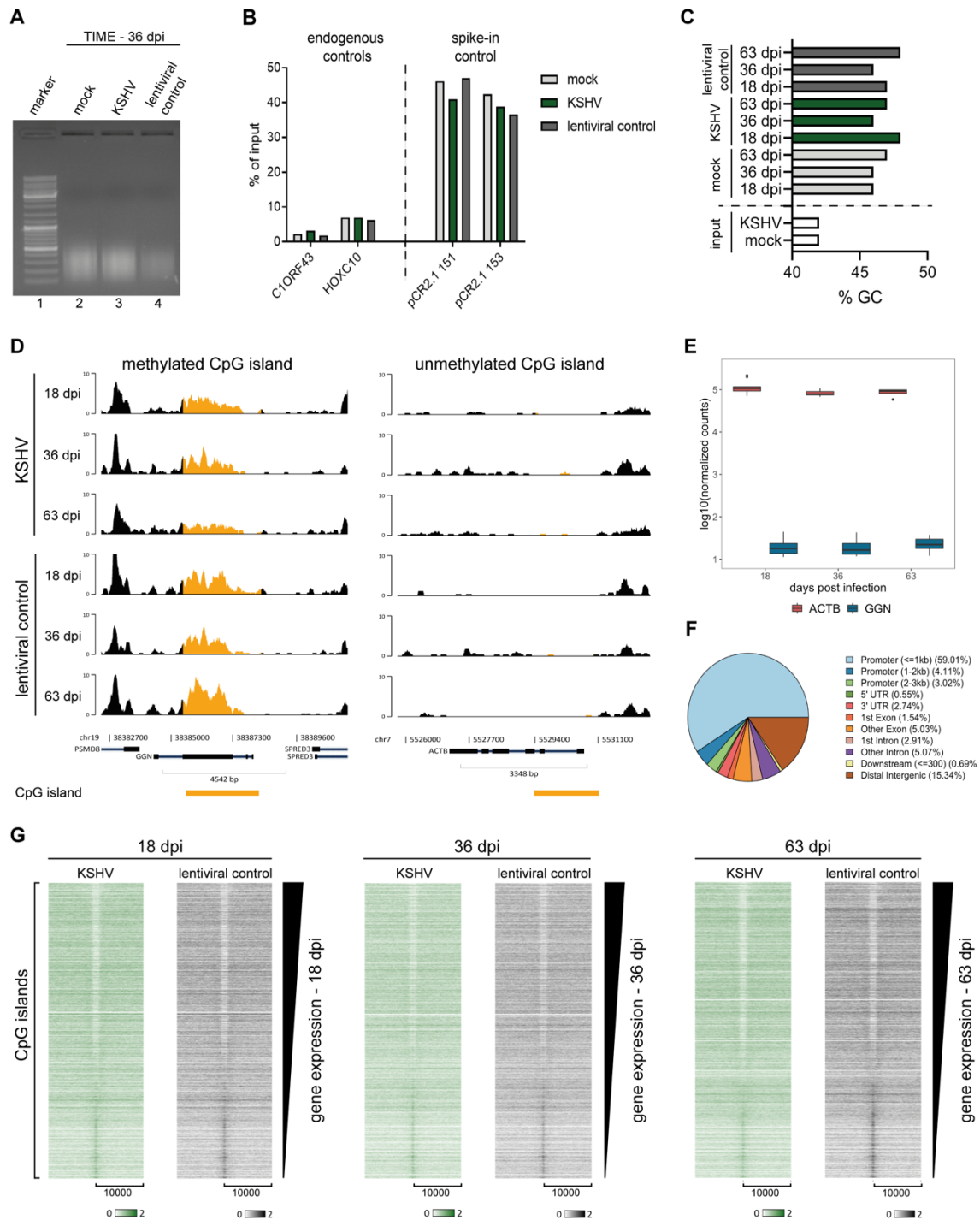


Figure 14: Quality control of MeDIP-seq: (A) Agarose gel for the shearing efficiency of input DNA. Shearing efficiency of the input DNA was confirmed by agarose gel electrophoresis and is representatively shown for infected and control cells at day 36 pi. (B) qPCR as one step of the quality control. qPCR was performed after isolation of precipitated DNA to control for the functionality of the method. C1ORF43 served as a host negative control for DNA methylation while HOXC10 represents a positive control. Additionally, an *in vitro* methylated plasmid (pCR2.1) was used as a spike-in and served as another positive control. (C) Comparison of GC content in input and immunoprecipitated samples. GC content of input samples and precipitated samples was compared after sequencing and is another step of quality control. (D) Examples for methylated and unmethylated CpG islands. One genomic loci with a methylated CpG island (GGN) and one example of an unmethylated CpG island (ACTB) are depicted. CpG islands are highlighted in orange. (E) Gene expression of GGN and ACTB. Gene expression patterns of these two loci are included from the RNA-seq dataset. (F) Genomic features of CpG islands. ChIPseeker was used to assign all of annotated human CpG islands to general genomic features. (G) Global analysis of CpG island methylation and associated gene expression. The DNA methylation state of every CpG island was determined in KSHV infected cells and the lentiviral control at each time point and are visualized in a heatmap. CpG islands were furthermore annotated to the closest gene and expression levels of the genes were attributed. CpG islands were then sorted according to decreasing gene expression levels which is highlighted as black triangle next to the heatmaps.

In summary, the different steps of quality control performed during the MeDIP-seq experiment ensured the functionality and reliability of this method to study host DNA methylation patterns.

4.3.2 KSHV infection does not induce global DNA methylation changes

Having ensured that MeDIP-seq serves as a reliable method to investigate genome-wide host DNA methylation patterns, further analyses of the obtained datasets were performed to investigate putative changes in KSHV infected endothelial cells (Figure 19). As already elucidated previously, CpG islands were considered as regions of special interest because their remodeling is often observed during tumorigenesis (Costello et al., 2000; Weisenberger et al., 2006).

The DNA methylation state of every CpG island was determined for KSHV infected cells as well as for the lentiviral control at each time point post infection. Differential DNA methylation patterns between these two subsets were then identified with the help of a DeSeq2 analysis (Figure 19A). As none of the regions passed the classical $\log_2(\text{foldchange})$ cutoff from RNA-seq analysis, every region with a $\log_2(\text{foldchange})$ of > 0.5 or < -0.5 was considered as differentially methylated. However, even with this lower cutoff only a very limited number of regions were identified which undergo DNA methylation changes upon KSHV infection. At day 36 p.i. only one single differential region was found to exhibit increased DNA methylation levels. In order to get further insights into the association with genomic features, ChIPseeker analysis of deregulated regions from day 18 and day 63 p.i. was performed (Figure 19B). At day 18 p.i. around 75 % of the CpG islands were attributed to distal intergenic regions or introns. Only 15 % of the regions with changes in DNA methylation were located in promoters. However, 50 % of the regions that underwent DNA methylation changes at day 63 p.i. could be assigned to proximal and distal promoters. As a large part of the deregulated regions at least at day 63 was located in promoter regions, a genome-wide correlation of the host transcriptome and the DNA methylation patterns from MeDIP-seq was performed (Figure 19C). CpG islands were annotated to the closest gene and $\log_2(\text{foldchanges})$ from RNA-seq were assigned for every time point. The DNA methylation status of every CpG island from KSHV infected cells was plotted against that of the lentiviral control (Figure 19C upper panel). RNA-seq data was included into this scatterplot by a color code (Figure 19C lower panel).

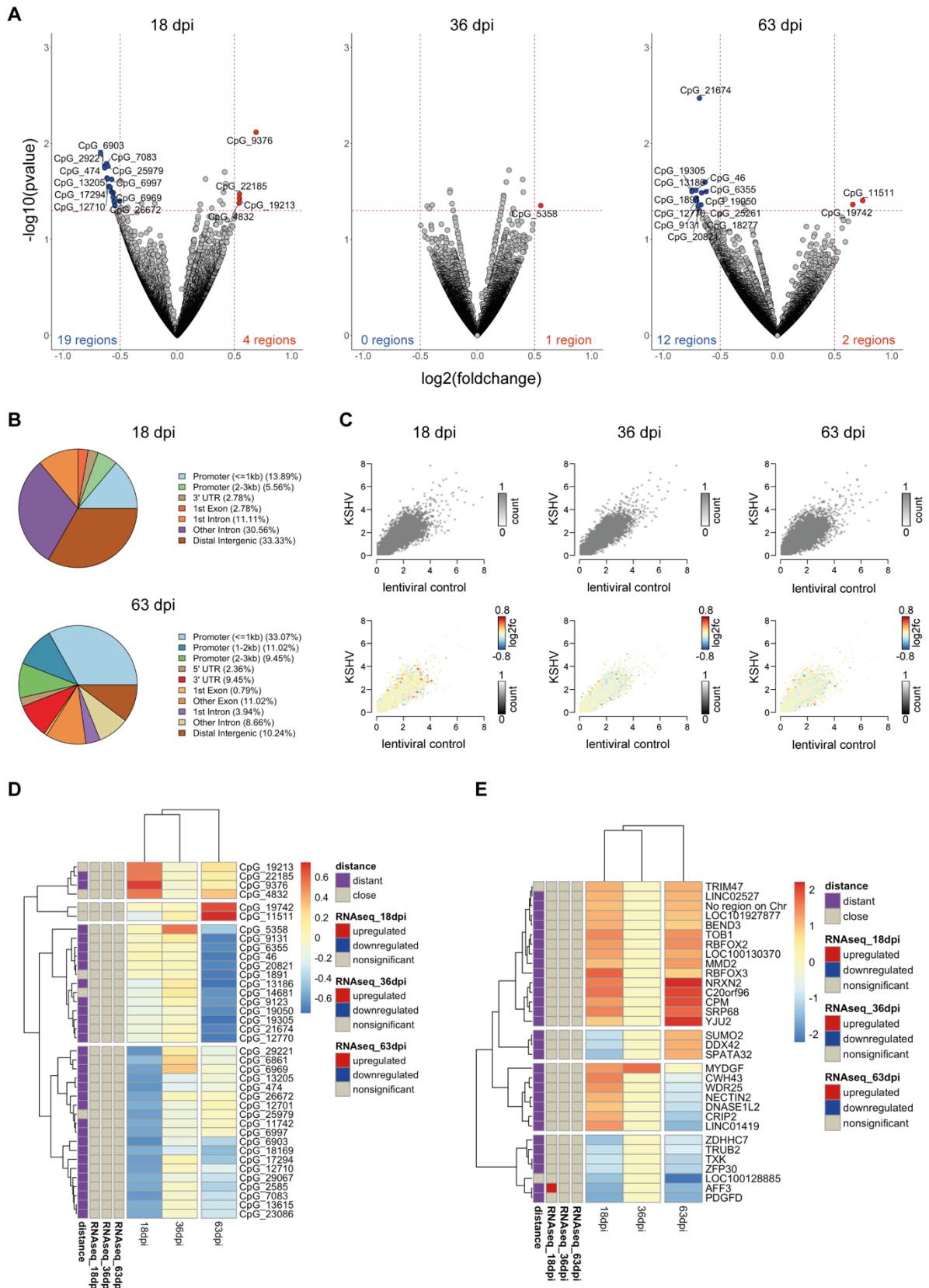


Figure 15: Identification of DNA methylation changes in KSHV infected cells: (A) Volcano plots of remodeled CpG islands. A DeSeq2 analysis was performed to identify DNA methylation changes in KSHV infected cells compared to the lentiviral control and results are visualized in volcano plots for every investigated time point. CpG islands were considered as significantly deregulated if $\log_2(\text{foldchange}) > 0.5$ or < -0.5 and the p-value was < 0.05 which is also marked in the plots by red dashed lines. Numbers and dots representing a significant increase in DNA methylation are depicted in red, while a decrease is marked by blue color. (B) Genomic features of remodeled CpG islands. ChIPseeker was used to assign CpG islands which underwent DNA methylation changes to general genomic features. (to be continued at the next page)

(C) Genome-wide correlation between DNA methylation and associated transcriptional responses. DNA methylation states of every CpG island in KSHV infected cells were plotted against the state of the lentiviral control (upper panel). $\log_2(\text{foldchanges})$ of annotated genes from the RNA-seq dataset were included by adding a color code (lower panel). (D) Temporal progression of DNA methylation changes in CpG islands. All the CpG islands which underwent significant changes in DNA methylation at least once during the time-course were summarized in a heatmap. $\log_2(\text{foldchanges})$ from each region and sample are depicted in this heatmap. Hierarchical clustering was performed for the regions as well as for the samples. CpG islands were furthermore classified according to their mode of associated transcriptional deregulation upon KSHV infection. Furthermore, the regions were classified based on the distance to the TSS (TSS < 3000 bp, close; TSS >3000 bp, distant) of the annotated gene. (E) Temporal progression of genome-wide DNA methylation changes. Heatmap was generated from overlapping regions which were identified at least at two investigated time points. All other aspects are consistent with (D) but this time a genome-wide analysis with diffReps was performed.

Regions with an increase upon KSHV infection and simultaneous downregulation of the annotated gene expression should be present as blue dots in the upper left quadrant of the plot. CpG islands with a decrease in DNA methylation and simultaneous upregulation of gene expression should be visible as red dots in the lower right quadrant of the plot. However, these patterns could not be observed at any of the investigated time points. As a global correlation between DNA methylation changes and transcriptional deregulations was not observed, the few identified remodeled CpG islands were investigated in more detail with regard to the temporal progression and potential associated gene expression changes (Figure 19D). A heatmap of the CpG islands which underwent DNA methylation changes at least at one of the time points was generated and $\log_2(\text{foldchanges})$ from every time point were included. This revealed that the observed changes were most likely restricted to one specific time point of infection. Furthermore, these regions were also classified according to associated gene expression changes. This revealed that none of the altered CpG islands were attributed to significant transcriptional deregulations. Further classification of the CpG islands regarding the distance to the annotated gene revealed that only 7 of the 38 investigated regions were assigned as close to the TSS.

Due to the fact that only minor changes in DNA methylation patterns were observed in CpG islands, a genome-wide analysis irrespective of any genomic feature was additionally performed with diffReps. Regions which were identified to be altered at least at two time points were summarized in a heatmap to obtain information about the timing of the observed changes and to correlate potential gene expression changes (Figure 19E). Consistent with the findings from the analysis of CpG islands the global investigation of DNA methylation changes led to the identification of only a few altered regions. Although overlapping regions which undergo DNA methylation changes between day 18 and day 63 p.i. exist, only a single region was attributed to a gene with direct associated transcriptional deregulation.

In summary, these data indicate that neither global DNA methylation patterns nor significant numbers of cellular loci are altered in endothelial cells upon KSHV infection.

4.4 Host chromatin changes upon KSHV infection

4.4.1 Quality control of native chromatin immunoprecipitation sequencing

Previous results revealed that host DNA methylation changes might if at all only play a minor role during latent KSHV infection of microvascular endothelial cells. Beside the investigation of DNA methylation, which rather represents a stable epigenetic modification involved in long-term transcriptional repression, alterations in host histone modification patterns induced by latent KSHV infection were analyzed.

In order to investigate changes in histone modifications of the host genome native chromatin immunoprecipitation in combination with high-throughput sequencing was performed (nChIP-seq). The transcriptionally activating marks H3K4me3 and H3K27ac as well as the repressive marks H3K27me3 and H3K9me3 were included into this study. Before global analyses were performed to investigate host chromatin changes induced by latent KSHV infection, multiple steps were included to ensure quality and reliability of the data (Figure 20). Similar to MeDIP-seq, fragmentation of the chromatin is a crucial step of the experiment. nChIP-seq which was performed as previously described (Brind'Amour et al., 2015) involves an enzymatic digestion of the chromatin by MNase. This endo-exonuclease cuts unspecifically in regions where DNA is not bound by proteins e.g. histones. In order to control for adequate and comparable MNase digestion of the chromatin samples, a low amount of the input material was loaded on an agarose gel (Figure 20A). The obtained pattern of the fragmented DNA corresponded to single or multiple nucleosome sizes as expected. Although also larger fragments were obtained of over 1000 bp, the major proportion of chromatin exhibited the single nucleosome size of around 150 bp. Furthermore, all samples revealed the same digestion pattern which ensured comparable treatment. Prior to next-generation sequencing of the samples, qPCR was performed to evaluate the efficiency of the nChIP procedure (Figure 20B). Host genomic loci of known epigenetic state were amplified by qPCR and served as either positive or negative control for the precipitation procedure. C1ORF43 served as a positive control for the two activating marks H3K4me3 as well as H3K27ac. HOXC12 long represents a positive control region for H3K27me3, the histone mark which is associated with facultative heterochromatin. A positive control for the constitutive heterochromatin mark H3K9me3 was the host locus

of ZNF268. All primers exhibited the expected enrichment pattern for the respective histone mark.

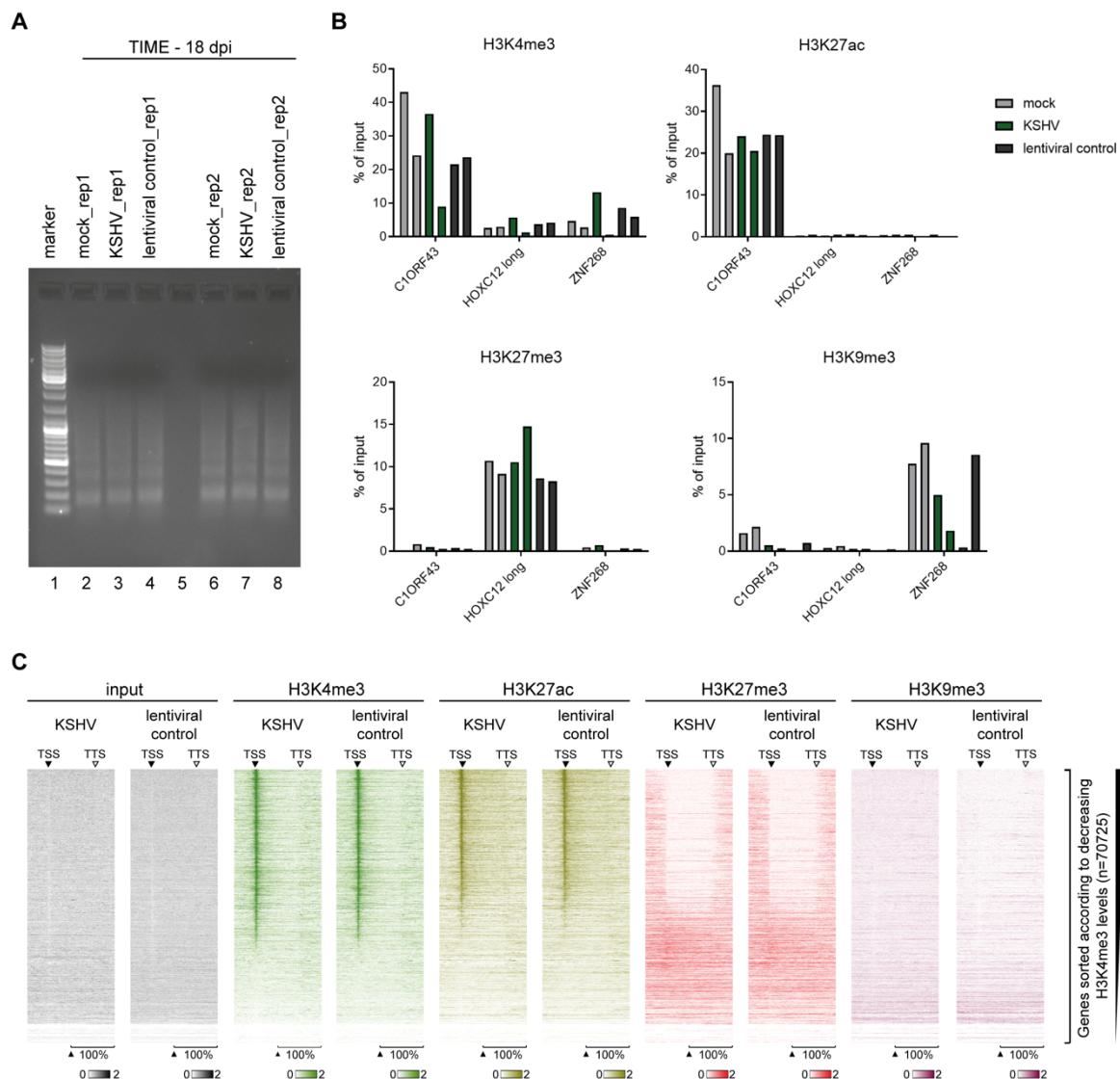


Figure 16: Quality control of nChIP-seq: Data for quality control steps of nChIP-seq are representatively shown of a single time point. (A) Agarose gel of MNase digested chromatin. Agarose gel electrophoresis was performed from the input chromatin material to ensure comparable and sufficient digestion of the samples. (B) qPCR as one step of the quality control. qPCR was performed after isolation of precipitated DNA to control for the functionality of the method. C1ORF43 served as a host positive control for the activating histone marks H3K4me3 and H3K27ac. HOXC12 long is a positive control for the repressive mark H3K27me3 and ZNF268 gives positive signal for H3K9me3. The positive controls for one of these marks served automatically as negative controls for all the other investigated histone marks. (C) Global analysis of histone modifications. Heatmaps were generated for input, H3K4me3, H3K27ac, H3K27me3, and H3K9me3 over all annotated genes from KSHV infected cells as well as for the lentiviral control. Relative gene lengths are depicted with 200 % of the genomic loci including transcriptional start site (TSS, marked by a filled triangle), gene body, and transcriptional termination site (TTS, marked by a non-filled triangle). Signals are sorted according to decreasing H3K4me3 levels.

After sequencing of the nChIP-seq libraries, the histone modification state of every gene was determined, and a genome-wide summary is depicted as heatmaps in Figure 20C. As relative gene lengths are depicted with 200 % of the genomic loci these heatmaps contain information about the epigenetic state of the TSS, the gene body,

and also the flanking regions of the gene loci. The activating marks H3K4me3 and H3K27ac were predominantly located at the transcriptional start site of a gene and appear as very distinct peaks. The repressive marks on the other hand exhibited high signals over the whole gene body. Additionally, if an activating histone modification was located at the TSS of a gene, they usually lacked repressive marks and vice versa. This confirmed the general anti-correlative occurrence of activating and repressive histone modifications.

Altogether, these data provide evidence for the successful and specific enrichment of respective histone modifications via nChIP but also for the reliability of the obtained datasets.

4.4.2 KSHV infection induces abundant epigenetic alterations on the host chromatin level

As several quality control steps were included into the experimental nChIP-seq procedure which ensured functionality of the method and provided evidence for the reliability of the datasets, analysis of host chromatin changes induced by latent KSHV infection was performed (Figure 21). In order to get a global overview, the histone modification state of every gene in KSHV infected cells was plotted against that of the lentiviral control. This was performed for every investigated histone modification and additionally for all the three time points. Results for the analysis of day 18 p.i. are representatively shown in Figure 21A. Significantly altered regions in KSHV infected cells compared to the lentiviral control were then identified with the tool diffReps by using a $\log_2(\text{foldchange})$ cutoff of > 1 or < -1 . In contrast to DNA methylation, several host loci were identified with differential histone modification patterns at day 18 p.i. (Figure 21B). The average signal of significantly differential regions with an increase or a decrease of the respective histone modification was plotted for KSHV infected cells, the lentiviral control, as well as for untreated cells. The latter population represents TIME cells which stayed completely untreated and served as a control for the initial state of the cells before infection or control treatments were performed. These data highlight that regions with an increase in the respective histone modification resulted in higher average signals of the KSHV infected cells compared to both controls. Exactly the opposite is true for the regions with a decrease in the respective histone modification. There the average signal is decreased in the KSHV infected

samples compared to the controls. For H3K9me3, no significant deregulations were observed.

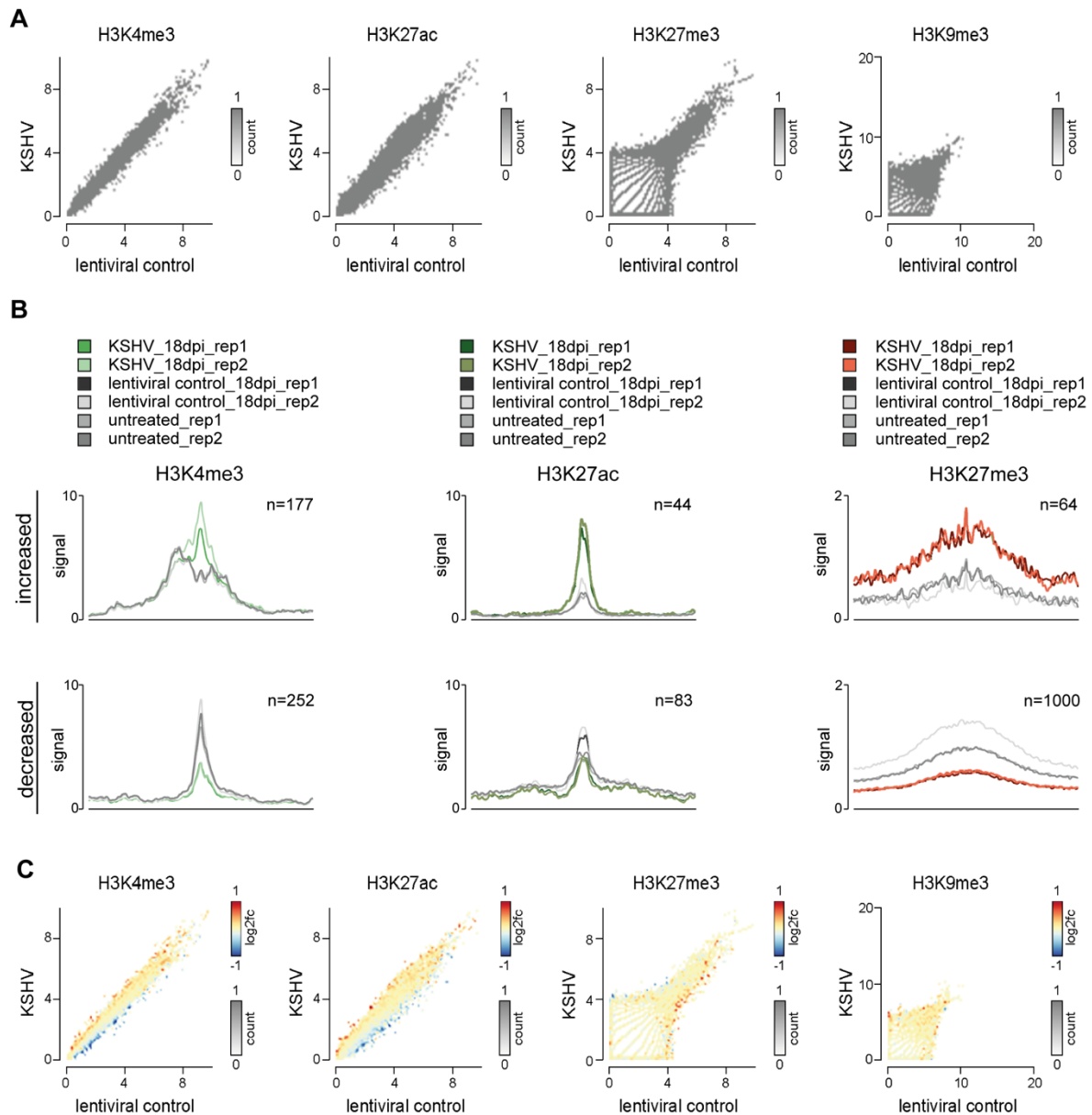


Figure 17: Identification of host loci with differential histone modification patterns: All data are representatively shown for day 18 p.i. (A) Identification of histone modification changes upon KSHV infection. The histone modification state of every gene was determined for the KSHV infected cells and compared to the states of the lentiviral control. (B) Latent KSHV infection leads to several remodeled host loci. Regions with a significant increase or decrease of the respective histone modification were identified by a $\log_2(\text{foldchange})$ cutoff of >1 or <-1 , respectively with the tool diffReps. The average signal of increased or decreased regions is plotted for the KSHV infected cells, the lentiviral control as well as for untreated cells. Numbers in the upper right corner represent the identified differential regions. (C) Genome wide correlation of histone modification changes and associated transcriptional responses. Same as in (A) but $\log_2(\text{foldchanges})$ from RNA-seq are included as color-code for every gene.

Next, we investigated whether a global correlation between histone modification changes and host transcriptional deregulations can be observed. For this purpose, histone modification states of infected and control cells were plotted exactly as described for Figure 21A, but this time $\log_2(\text{foldchanges})$ from RNA-seq were assigned

to every region by a color code (Figure 21C). This revealed that the observed alterations in histone modifications correlated well with the previously described transcriptional changes. Transcriptional activation can be observed together with increased activation marks and decreased repressive marks, whereas transcriptional suppression is accompanied by a decrease in activating histone marks and the formation of repressive chromatin .

Of particular interest was the chromatin state of interferon regulated genes, which were found to be altered on the transcriptional level throughout the course of long-term latent infection (Figure 22). Histone modification levels of a subset of interferon regulated genes were determined for KSHV infected samples and both controls at day 36 p.i.(Figure 22A).

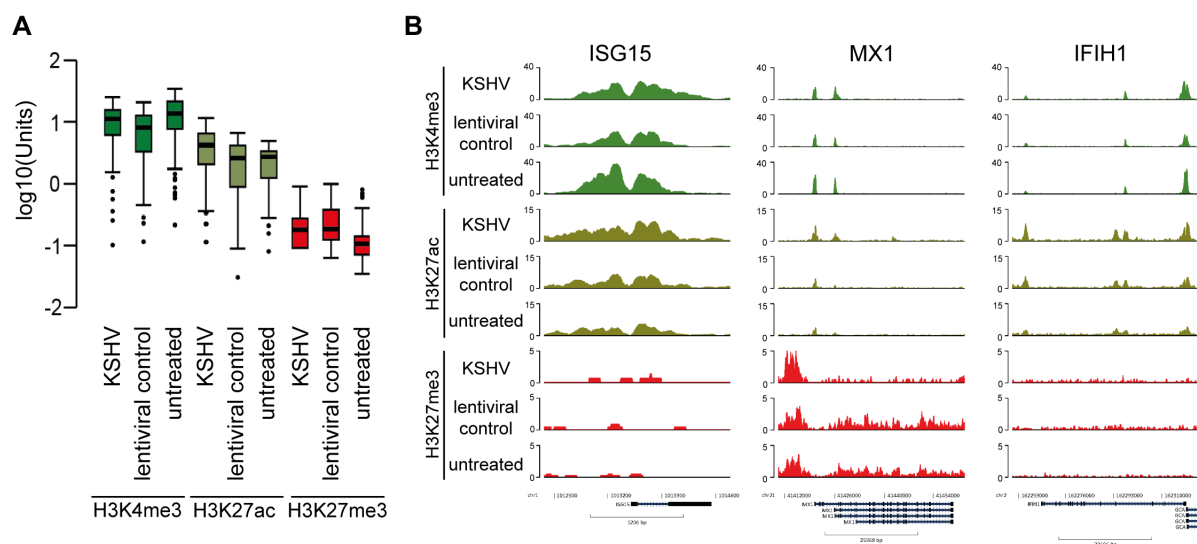


Figure 18: Histone modification states of interferon responsive genes: (A) Boxplot of chromatin state in a subset of interferon responsive genes. Histone modifications states of interferon regulated genes were determined for KSHV infected samples, lentiviral control, and untreated cells at day 36 p.i. and are summarized as boxplots. (B) Coverage plots of individual interferon regulated genes. ISG15, MX1 and IFIH1 genomic loci are depicted as exemplary regions of interferon regulated genes.

The histone modification levels of H3K4me3 and H3K27me3 were similar among the three different populations. A minor increase could be observed for H3K27ac levels in KSHV infected cells compared to the controls. The increase in H3K27ac can be partly recapitulated by a close-up view of individual genes (Figure 22B). While histone modification patterns of ISG15 are comparable between KSHV infected cells and controls, a slight increase in H3K27ac levels in KSHV infected cells can be observed for the MX1 and the IFIH1 loci. In the MX1 locus the slight increase in the activating mark is additionally accompanied by a decrease in H3K27me3 throughout the gene body, which is consistent with transcriptional activation. In all cases, high levels of

activating histone marks were also present in the lentiviral control and in the untreated cells. The high levels of activating marks in the untreated control led to the assumption that interferon regulated genes might be pre-activated to be rapidly induced upon viral infections or other stimuli. In summary, these data indicate that the transcriptional activation of interferon responsive genes in long-term latently infected cells does rely on a further increase of pre-existing activating histone modifications but might rather depend on the binding of transcriptional activators.

Similar to the investigation of DNA methylation changes, the temporal progression of histone modification changes was analyzed (Figure 23). For this purpose, every region which was at least once during the time course identified as significantly altered and was present at least at one more time point was included. $\text{Log}_2(\text{foldchanges})$ for all of these regions at every time point were included to visualize the temporal progression of histone modification changes. Hierarchical clustering of the regions as well as of the time points was performed and the transcriptional state of annotated genes was included from the RNA-seq datasets. Additionally, regions were grouped according to their distance to the TSS of the annotated gene. If the distance between the region and the TSS was above 3000 bp, it was considered distant. Regions within a distance of 3000 bp to the TSS of the annotated gene were classified as close.

Many regions were identified to be overlapping at least at two different time points for H3K4me3. Interestingly, the classification of the regions revealed, that the majority can be considered to be located in close proximity to the TSS of the annotated gene. This data is consistent with the classification of the same regions by ChIPseeker, which revealed that around 60 % of the regions can be found in proximal promoter regions (Figure 23D). Furthermore, gene expression changes were exclusively found in the regions which are close to the TSS. Interestingly, a large part of the regions was not attributed to significantly deregulated gene expression. The same heatmaps were also generated for H3K27ac as well as for H3K27me3 (Figure 23B + C, respectively). The number of overlapping regions for H3K27ac was not as pronounced as for H3K4me3. Nevertheless, several regions were identified that exhibited stable chromatin changes at all three time points. Classification of these loci according to the distance to the annotated gene as well as ChIPseeker results (Figure 23E) indicate that they are rather located in intronic or distal intergenic regions. Therefore, it is not unexpected, that significant transcriptional deregulation can only be observed for one annotated gene.

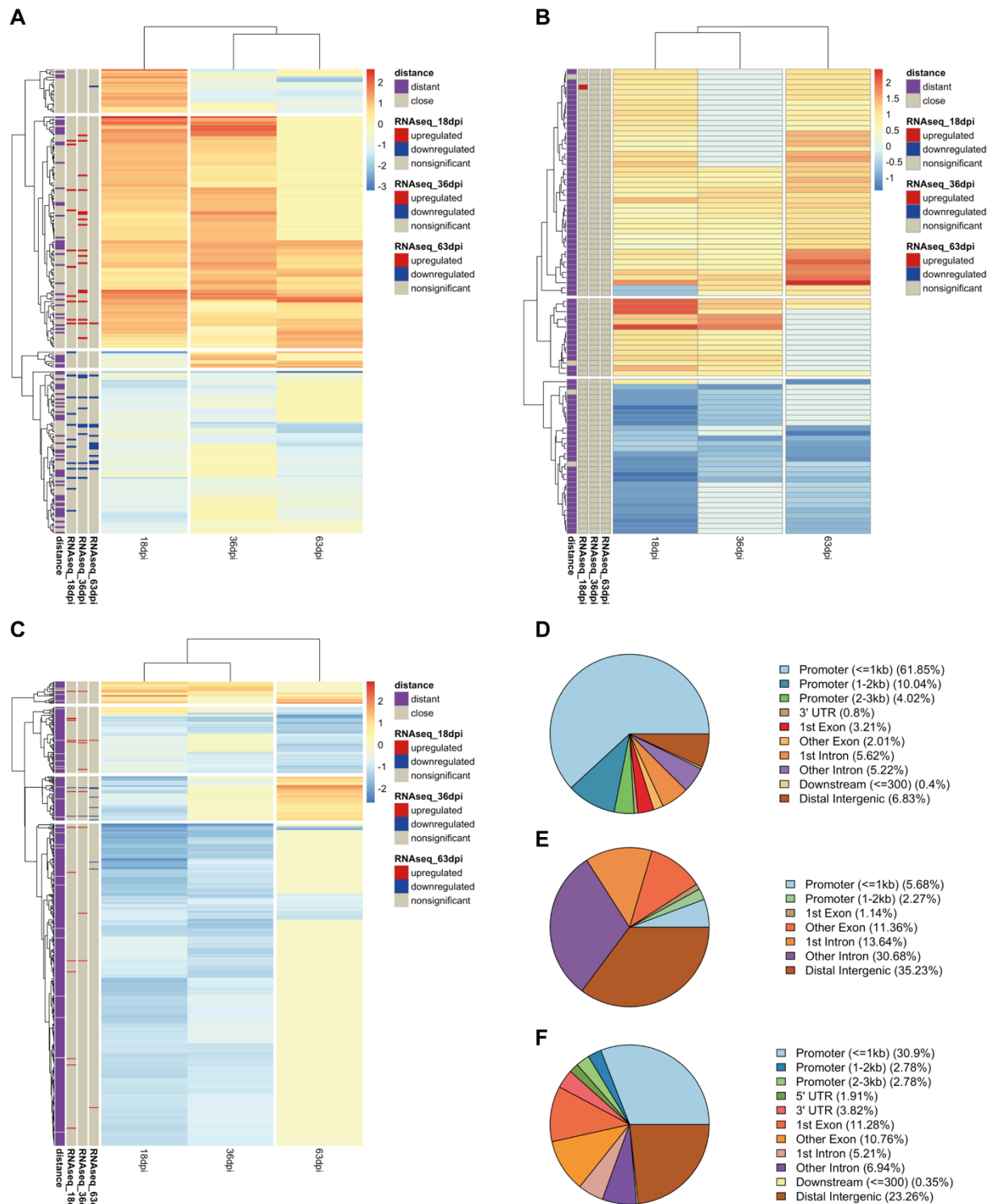


Figure 19: Temporal progression of host histone modification changes: (A-C) Temporal progression of histone modification changes. Heatmaps were generated from overlapping differential regions which were identified at least at two investigated time points for H3K4me3 (A), H3K27ac (B), and H3K27me3 (C). Hierarchical clustering was performed for the regions as well as for the samples. The regions were furthermore classified according to their mode of associated transcriptional deregulation upon KSHV infection. The regions were also classified based on the distance to the TSS of the annotated gene (TSS < 3000 bp, close; TSS >3000 bp, distant). (D-F) Classification of differential regions to genomic features. Overlapping regions for H3K4me3 (D), H3K27ac (E), and H3K27me3 (F) were classified to genomic features by performing an analysis with ChIPseeker.

Overlapping regions for H3K27me3 can be observed predominantly among the downregulated regions at day 18 and 36 p.i. (Figure 23C). However, like for the other

histone marks, a subset of stable histone modification changes at all three time points was detected. Classification of these regions by ChIPseeker demonstrated that around 30 % can be assigned to promoter regions, but almost the same percentage of regions is located in distal intergenic areas (Figure 23F). Significant transcriptional deregulations were only observed for some of the annotated genes.

In summary, the investigation of histone modification changes resulted in the identification of several regions with differential histone modification patterns upon KSHV infection. Although the analysis of host transcriptome data revealed a delayed type I interferon response, such an observation was not detected on the level of histone modifications. This was most likely due to the high level of pre-activation of the respective genes, which might not be further increased on the histone level. Furthermore, a more detailed investigation highlighted that at least a subset of the differential regions seems to stay stable over the whole course of infection. This detailed view also highlighted that, although a genome-wide correlation between histone modification changes and transcriptional deregulations exists, some of the remodeled regions seem not to undergo direct gene expression changes.

4.5 Identification of KSHV induced stable epigenetic changes

4.5.1 Loss of KSHV reconstitutes the initial transcriptomic profile

The investigation of transcriptomic as well as epigenetic changes upon KSHV infection revealed transient as well as stable alterations on the level of transcription and histone modifications. While a fraction of transcriptional changes could be directly linked to epigenetic alterations, several histone modification changes were independent of transcriptional deregulation. The latter one might be involved in chromatin alterations that result in different phenotypes only after stimulation of specific pathways. This also provides evidence that KSHV induced host epigenetic changes might be predisposed which could affect as a long-term consequence tumorigenesis. In order to investigate whether alterations on the level of histone modifications constitute stable epigenetic alterations or still depend on the ongoing latent infection, we compared KSHV infected cells with a population which resembles a cleared viral infection. Transient infection-dependent alterations might be reverted while stable ones would still exist. To this end, KSHV infected cells were subdivided at day 36 p.i. and cultivated in parallel (see Figure 24 for the experimental setup), omitting hygromycin selection in one of the populations to allow loss of KSHV episomes. This occurs over time in most cell culture systems

most likely due to inefficient tethering. The population was furthermore sorted after some weeks of cultivation according to GFP negative cells to obtain a homogenous KSHV negative cell population. These cells were further on referred as the cleared subset. At day 63 p.i. cells were harvested from these in parallel grown cultures and RNA-seq as well as nChIP-seq were performed to compare the transcriptional state as well as histone modification changes of the two populations.

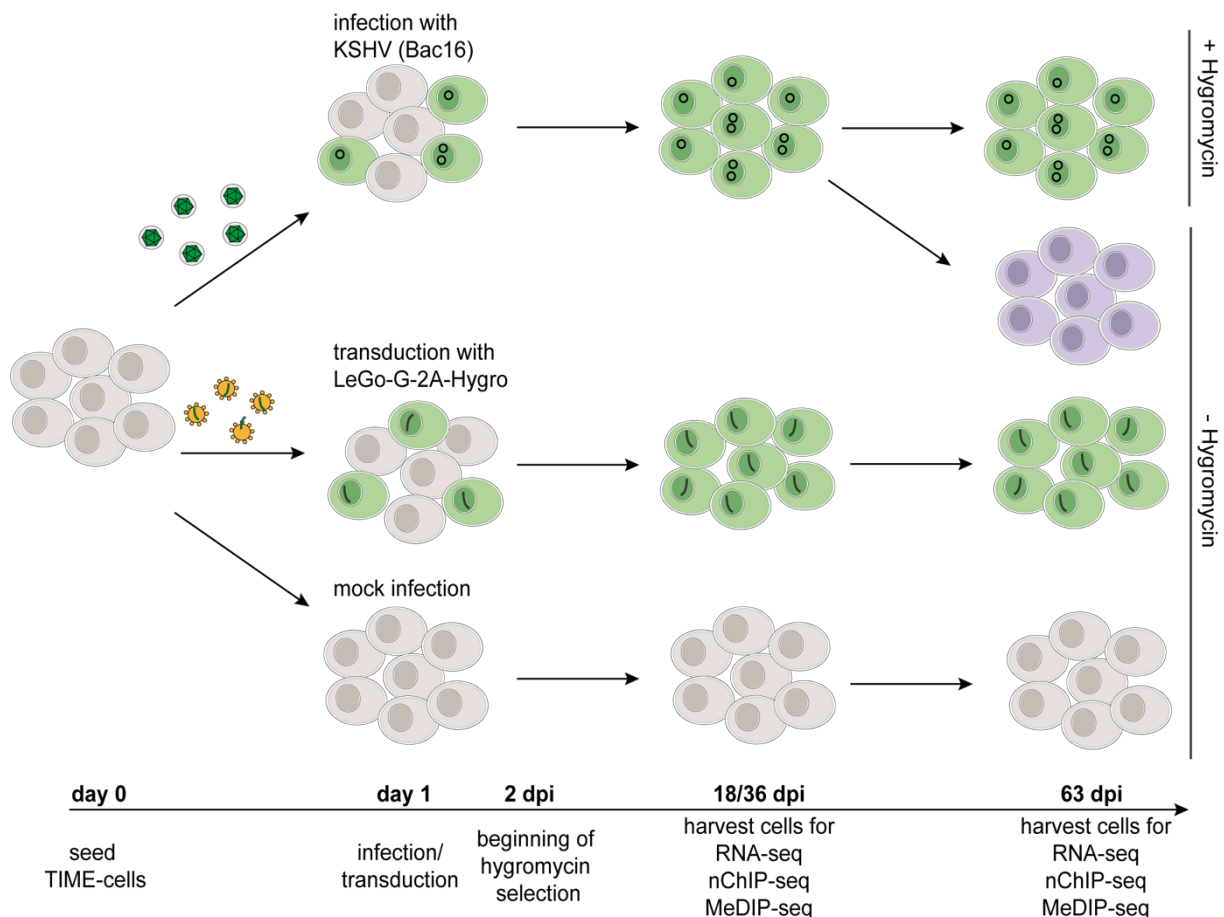


Figure 20: Experimental setup to investigate KSHV infected and cleared cells: Experimental setup to investigate host epigenetic changes in KSHV infected and cleared subsets. The experimental setup previously described is again recapitulated, which includes the infection/transduction of the cells and subsequent treatment with hygromycin to obtain 100 % positive populations. At day 36 p.i. KSHV infected cells were subdivided into two populations. One of them was cultivated as before and stayed KSHV positive due to the hygromycin treatment. The second population was cultivated without hygromycin. This led to the loss of viral copy numbers over time. In order to get a homogenous population GFP negative cells were additionally sorted. This population is further on referred as the cleared subset. At day 63 p.i. cells from in parallel growing cultures were harvested to perform RNA-seq as well as nChIP-seq.

Prior to host transcriptome analysis, coverage plots of the KSHV transcriptional profile from infected and cleared cells were compared to ensure that the cleared subset is devoid of any viral gene expression (Figure 25A). While KSHV infected cells, as already shown previously, had signals in the BAC cassette as well as in the latency control region, no signal for viral gene expression was detected in the cleared subset.

Only one sharp peak in the BAC cassette was visible which was previously also described to be detectable in the mock control.

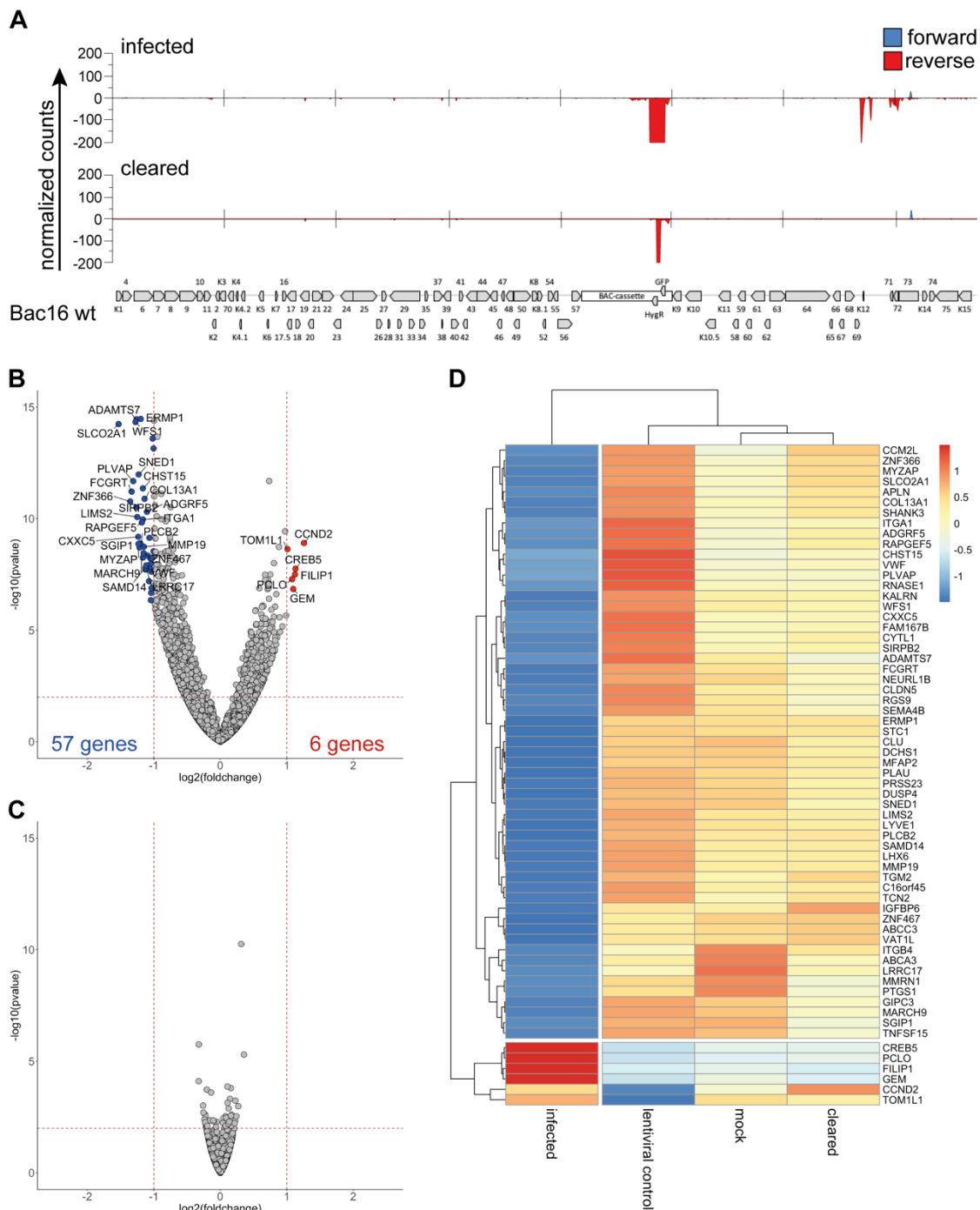


Figure 21: Transcriptional deregulations in infected and cleared cells: (A) KSHV transcriptional profile in infected and cleared cells. Raw sequencing data was mapped to the Bac16 reference genome and then reads were counted in 100 bp windows by discriminating between forward (blue) and reverse (red) reads. Coverage plots are depicted for KSHV infected cells as well as for the cleared subset. (B) KSHV induced transcriptional changes 63 dpi. The volcano plot summarizes the results from RNA-seq comparing KSHV infected and lentiviral transduced samples. Genes were considered significantly deregulated if $\log_2(\text{foldchange})$ was > 1 or < -1 and the p-value was < 0.01 which is also marked in the plot by red dashed lines. Numbers and dots representing significantly upregulated genes are depicted in red, while downregulation is marked by blue color (same as in Figure 12C, depicted again for the comparison with the cleared subset). (C) Transcriptional changes in the cleared subset. This figure was generated exactly as in (B) but for the cleared population. (D) Heatmap of significantly deregulated genes from the infected subset. The significantly deregulated genes identified in (B) were used as a basis for this heatmap. z-score calculation of normalized reads per gene and per treatment are depicted. Hierarchical clustering of genes and of samples was performed.

As described above, the host transcriptome analysis of KSHV infected cells resulted in the identification of moderate transcriptional deregulations, with 57 genes downregulated and 6 genes upregulated compared to the lentiviral control (Figure 25B). These data represent a recap of the previously shown transcriptome analysis from KSHV infected cells at day 63 p.i. (Figure 12C). In contrast, the cleared subset was indistinguishable from the uninfected or lentiviral control cells on the transcriptome level with no gene being significantly deregulated (Figure 25B). In order to get a more detailed view, the significantly deregulated genes observed in the infected subset were visualized in a heatmap (Figure 25C). Hierarchical clustering of the genes was performed which resulted in a clear discrimination of up- and downregulated genes in the infected subset compared to the lentiviral and the mock control. Hierarchical clustering of the samples additionally strengthened the observation that the cleared subset can be clearly attributed to the mock control and to a lesser extent also to the lentiviral control. This is due to the fact that expression patterns of the depicted genes are similar among these three samples and clearly distinguishable from the infected subset.

Overall, these findings led to the conclusion that a cleared viral infection results in a complete reconstitution of the initial transcriptional state.

4.5.2 A subset of KSHV-induced epigenetic changes remains stable after clearance

The clearance of the virus and the entire reversal of the cellular transcriptome generates a unique setting to investigate putative stable epigenetic alterations which became independent of the latent viral infection. Comparison of nChIP-seq data from KSHV infected and cleared cells was performed to obtain information about potential differential regions that are present in both co-cultivated populations (Figure 26). This revealed that, similar to the transcriptional deregulations, the majority of the significantly altered regions in the infected cells are reverted upon loss of KSHV (Figure 26A, marked by the dark green color in the pie charts). These alterations most likely depend on the presence of latent KSHV infection in the culture. Furthermore, regions exist, which are only present in the cleared population. (highlighted by the violet color in the pie charts). Interestingly, regions can be identified for every histone modification which are stably deregulated in infected as well as in cleared cells (highlighted in grey). They most likely represent epigenetic patterns which were altered upon infection but

became independent of the virus. The largest part of overlap can be observed for H3K27me3 where 25 % of the regions are detected in both subsets. Regarding the activating histone marks, around 5 % of altered regions in the infected and cleared subset are overlapping (see figure S2-S4 for a list of overlapping regions).

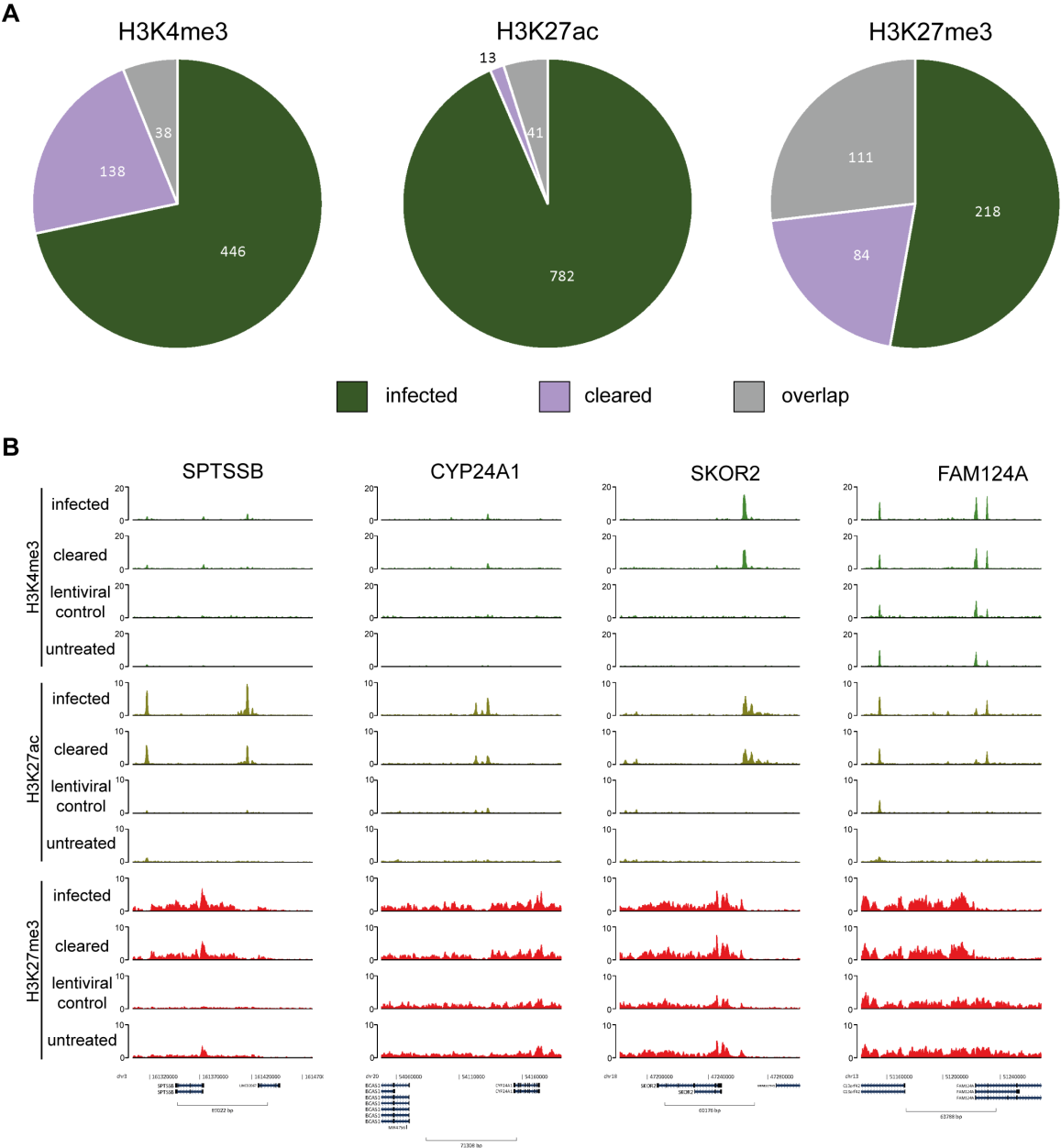


Figure 22: Comparison of histone modification changes in infected and cleared populations: (A) Overlapping differential regions in infected and cleared cells. A global nChIP-seq analysis of infected and cleared cells was performed using diffReps to identify histone modification changes in both populations compared to the lentiviral control. Overlapping regions between the two subsets were identified with bedtools intersect (a minimum overlap of 50 % was required). A pie chart including changes only occurring in infected cells, changes that can be solely attributed to the cleared population, and overlapping regions was generated for every investigated histone modification. (B) Examples for overlapping regions. Coverage plots of four exemplary regions with overlapping histone modification changes in infected and cleared cells are depicted. Coverage plots of the same regions for the lentiviral control and untreated cells serve as negative controls.

As this analysis only provided a general overview, coverage plots of exemplary regions with histone modification changes in the infected as well as the cleared subset were depicted (Figure 26B). These four regions, including SPTSSB, CYP24A1, SKOR2, and FAM124A were chosen, as they are among the genes, which show most pronounced changes in H3K27ac. This in-depth view into single host loci revealed that altered patterns in infected cells remain at almost same high levels in the cleared subset. While infected and cleared cells exhibit an increase in H3K27ac in the SKOR2 locus which is accompanied by increasing levels of H3K4me3, SPTSSB and CYP24A1 revealed to have increased levels in only one of the activating histone marks. High levels of H3K27ac in these two loci in infected and cleared cells together with low levels of H3K4me3 represent the typical histone modification pattern of enhancer regions. In the locus of FAM124A, the increase in H3K27ac can be observed in a region of already established H3K4me3. Interestingly, all these exemplary regions also exhibit increased H3K27me3 in the flanking regions of the H3K27ac peaks. This finding is most pronounced in the SPTSSB locus, but also visible for all the other regions. One exception represents the gene body of FAM124A, which has decreased H3K27me3 levels. Interestingly, among these four presented genes, FAM124A is the only gene with a slight transcriptional upregulation at day 63 p.i. in infected cells but not in the cleared subset.

In summary, these data provide evidence that a subset of specific KSHV-induced host epigenetic changes remains stable in cleared cells, indicating that they became at some point independent of the infection. As especially regions with an increase in H3K27ac were observed to be stable in the cleared subset, it is thought that KSHV induced changes might especially affect enhancer regions. However, increased H3K27me3 levels in the flanking regions of H3K27ac peaks might prevent the transcriptional activation of affected genes. This would, at least for some of the identified altered regions, provide an explanation for the absence of direct associated transcriptional deregulations in infected cells and more pronounced also in the cleared subset.

Altogether, these findings strengthen the hypothesis that the identified regions might constitute an epigenetic predisposition which potentially plays a role during virus-mediated tumorigenesis via mediating altered responses to certain stimuli.

4.6 Epigenetic predisposition alters the outcome of specific cellular pathways upon stimulation

4.6.1 Cells are not altered in their capability to induce apoptosis

The genome-wide investigation of host epigenetic changes upon KSHV infection in endothelial cells revealed that several regions exist which undergo stable remodeling. While DNA methylation seems to only play a minor role, multiple regions are affected with regard to histone modification changes. The comparison of long-term infected cells with a population that resembles a cleared viral infection furthermore demonstrated that a subset of overlapping differential regions exists which became independent of the infection. Moreover, directly associated transcriptional deregulations of annotated genes were absent in the cleared subset which provides evidence that these regions might constitute an epigenetic predisposition. The existence of epigenetic alterations without immediate effects on transcription allowed us to test the hypothesis that those changes express phenotypic differences only upon activation of specific pathways. For this purpose, cleared cells but also the infected population and the two negative control cells were challenged with different stimuli and responses were read out by functional assays.

Prior to stimulation of the cells, growth curves of the four cultures were conducted by MTT assays at five consecutive days (Figure 27A). Data was normalized to day 1 to correct for potential differences of varying initial cell counts. As until day 3, no differences in cell growth of the four different cultures were observed all subsequent experiments were performed in this time frame to avoid proliferation-induced bias.

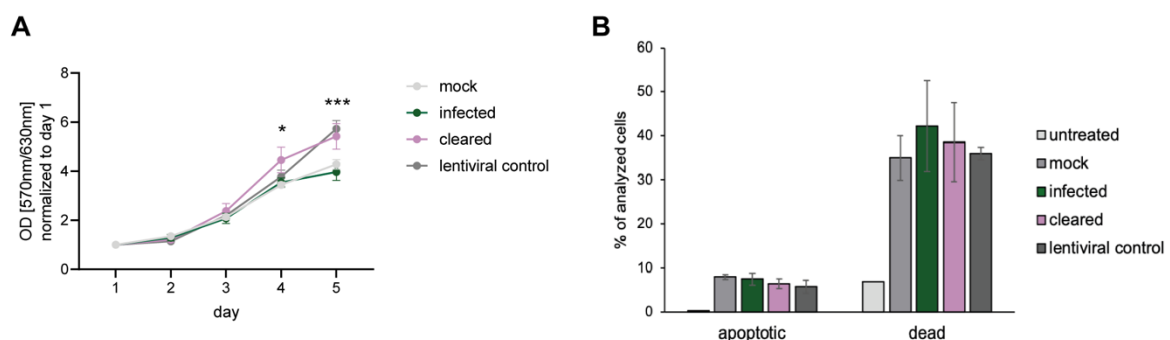


Figure 23: Growth curves and apoptotic responses of the different cell populations. (A) Proliferation rates of the different cell populations. Growth rates of the four different cell populations were measured by MTT assays at 5 consecutive days. Data was normalized to day 1 to correct for varying initial cell counts. Data of every time point represents the mean with SEM from $n = 4$. Statistical significance was assessed by two-way ANOVA. (B) Responses of the different subsets to apoptotic stimuli. The four different populations were treated with $1 \mu\text{M}$ staurosporine to induce apoptosis. The rate of cells which underwent apoptosis or were already dead was measured 12 h post induction by the Annexin V apoptosis assay with subsequent FACS analysis. TIME cells which were not treated with staurosporine but stained with Annexin V and PI to measure apoptotic/dead cells under normal culturing conditions were used as a control. Data represents the mean with SEM from $n = 4$.

Next, we investigated, whether the cells are altered in their capability to induce apoptosis. For this purpose, the four different populations were treated with 1 μ M staurosporine which is a protein kinase inhibitor and a well-known inducer of apoptosis. 12 hours post treatment cells were stained with fluorescence-labeled Annexin V and propidium iodide to stain for apoptotic and dead cells. TIME cells, which were not treated with staurosporine but stained with Annexin V and propidium iodide, were included to measure apoptotic/dead cells under normal culturing conditions. FACS staining of the different populations revealed, that induction of apoptosis was in general successful, as the percentage of apoptotic and dead cells in staurosporine treated cells was dramatically increased compared to the untreated cells (Figure 27B). However, induction of apoptosis by staurosporine did not result in any substantial differences between cleared, infected, and both control populations.

4.6.2 Increased angiogenic potential in infected and cleared subsets

One region which was found to exhibit an increase in the activating histone marks and a parallel decrease of H3K27me3 levels was annotated to tenascin C (TNC, table S2-S4). As the observed histone modification changes in this region predict potential transcriptional upregulation of the gene, expression levels of TNC were determined with the help of the previously introduced RNA-seq dataset as well as by qRT-PCR (Figure 28A + B). This revealed highest expression of this gene in KSHV infected cells at every time point of infection compared to both negative controls. Interestingly, the cleared subset, although not reaching levels of the infected cells, has still slightly increased expression compared to the negative controls. Next, we investigated whether higher mRNA transcripts are also accompanied by higher protein levels in infected cells. As the antibody for TNC did not give any signal in western blot, immunofluorescence with subsequent quantification of the signal was carried out instead (Figure 28C + D). Although the expression of TNC by immunofluorescence represents a slight punctate pattern throughout the whole area of a cell and is consistent with previously described patterns, protein levels were not elevated in KSHV infected cells compared to the negative controls at day 36 p.i.

Thus, it remains unclear, whether increased transcription directly influences protein expression, which was just not detectable via immunofluorescence, or whether TNC protein levels are regulated by other pathways, like proteasomal degradation.

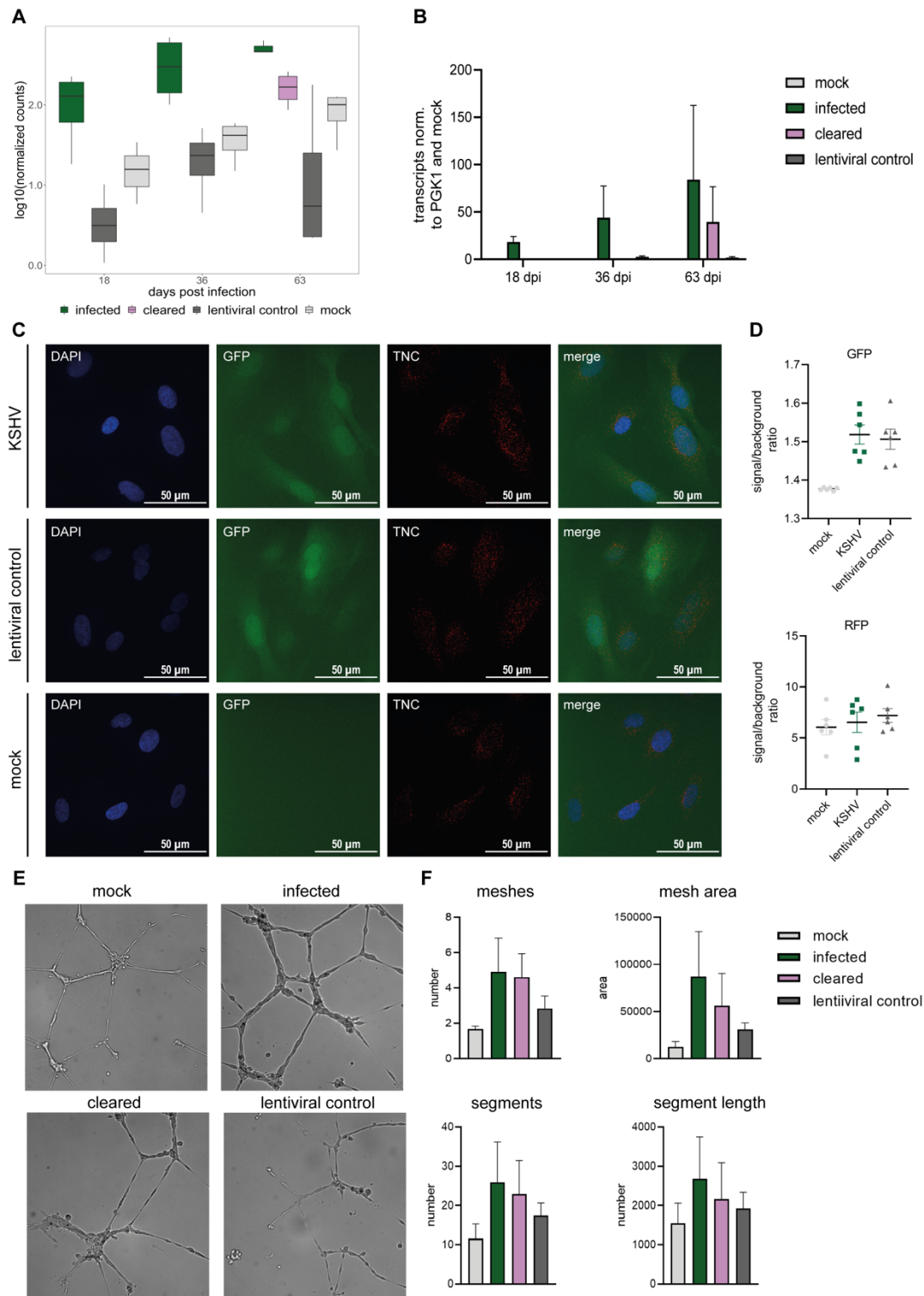


Figure 24: TNC expression and angiogenic potential in the different populations: (A) Normalized counts of TNC. Normalized counts of TNC from the RNA-seq dataset are depicted for each condition and every investigated time point. (B) qRT-PCR for TNC. Transcript levels of TNC relative to PGK1 and mock were determined by qRT-PCR. Bars represent the mean with SEM. Statistical significance was assessed by two-way ANOVA ($n=4$, except for KSHV, 63 dpi with $n=3$). (C) Immunofluorescence of TNC. Staining of TNC at day 36 p.i. was performed (red) and GFP expression served as infection control. Nuclear DNA was stained with DAPI. Images were taken at a confocal microscope and are depicted as maximum intensity projections. (D) Quantification of TNC levels. Immunofluorescence signals for TNC and GFP expression were quantified for every condition by calculating the signal to background ratio. (E) Angiogenic potential of the different cell populations. Tube formation assay was performed for KSHV infected and cleared cells as well as for both controls. Representative pictures are depicted. (F) Quantification of angiogenesis. The results obtained from the tube formation assay were quantified using the Fiji plugin Angiogenesis Analyzer. Different variables, like number of meshes, mesh area, number of segments and segment length were taken into account. Data represents the mean from $n = 2$ and SEM. One-way ANOVA was used to test for statistical significance.

High expression levels of TNC were previously described to influence angiogenesis in different cancer types (Borgia et al., 2010; Hill et al., 2011; Rupp et al., 2016). As altered histone modification patterns in the genomic locus of TNC were identified in infected and cleared cells compared to the controls, we hypothesized that growth of the different cell populations in a suitable milieu might result in different outcomes regarding the angiogenic potential of the cells. In order to test this hypothesis, cells were grown in Matrigel which confers an extracellular matrix environment and resembles 3D cell growth. As endothelial cells grow as tubular structures in this surrounding, it allows for the investigation of differential responses regarding angiogenesis.

A tube formation assay in this environment was performed which was followed by microscopic image acquisition (Figure 28E). Analysis of the microscopy images was performed by quantification of several variables, like mesh size or segment length, using the Fiji plugin Angiogenesis Analyzer (Figure 28F). This revealed, that KSHV infected cells, but also the cleared subset, tend to have an increased angiogenic potential compared to both negative controls.

4.6.3 Re-Infection with KSHV leads to more pronounced transcriptional responses in a subset of predisposed regions

As we found the type I interferon response to be upregulated in long-term latently infected endothelial cells, it was of particular interest whether induction of this pathway might lead to altered functional outcomes in the infected and cleared cells compared to the controls (Figure 29). For this purpose, KSHV infected cells, the cleared subset, and both negative controls were treated with 2'3'-cGAMP as well as poly(I:C) which are well known inducers of the type I interferon response (Figure 29A). 24 hours post treatment cells were harvested and qRT-PCR was performed to measure ISG15 transcripts as a read-out for the type I interferon response. Increasing concentrations of both reagents were used to monitor putative dose-dependent differences. Except for the lentiviral control, which exhibits higher responses to 2'3'-cGAMP and poly(I:C) treatment, similar increased expression levels of ISG15 were observed for the infected, cleared, and mock populations compared to untreated cells. These data indicate that induction of the type I interferon response does not result in altered responses of the infected or cleared cell populations.

Re-infection represents a conceivable scenario in the context of KSHV induced tumorigenesis. Therefore, we additionally tested whether re-infection of the different cell populations with KSHV might lead to an altered induction of the type I interferon response.

ISG15 transcript levels served again as a readout for the type I interferon response. Viral copy numbers were measured in parallel by qPCR to control for putative differences in infectability of the cells. These data revealed that the *de novo* infected mock cells respond in a dose dependent manner to increasing volumes of Bac16 supernatant. KSHV infected cells which were super-infected with Bac16 were partly responding to a second infection. Only the highest concentration of Bac16 supernatant resulted in low transcript levels of ISG15 in these cells. Interestingly, the cleared subset did not show any response to a secondary infection irrespective of the volume of virus supernatant. A reduced response was also observed in the lentiviral control, but this was not as pronounced as for the cleared population. The potential unresponsiveness to the type I interferon response measured by ISG15 transcript levels especially of the cleared subset was not due to a reduced infectability of these cells as viral copy numbers were comparable to the numbers of *de novo* infected mock cells. Higher copy numbers in the infected subset are most likely the result of the super-infection as viral copy numbers from the first and the second round of infection cannot be discriminated. Interestingly, the lentiviral control also revealed increased viral copy numbers which indicates that some lentiviral encoded factors might favor a KSHV infection.

The fact that only low levels of ISG15 transcripts were detected after re-infection of the cleared subset in comparison to the previously mock infected cells, raised the question whether this observation can be made for other interferon responsive genes. Therefore, RNA-seq from all different cell populations re-infected with 25 μ l of Bac16 supernatant was performed. A Principal Component Analysis (PCA) plot (Figure 29B) as well as a sample distance matrix (Figure 29C) were generated to get information about the overall similarity between individual samples. Both graphs revealed that *de novo* infected mock cells can be clearly distinguished from KSHV infected cells, the cleared subset but also from the lentiviral control. As differences concerning the interferon response were of particular interest, a heatmap including the expression levels of several interferon responsive genes of the super-infected cells, the re-infected cleared subset as well as the KSHV infected lentiviral control was generated (Figure 29D).

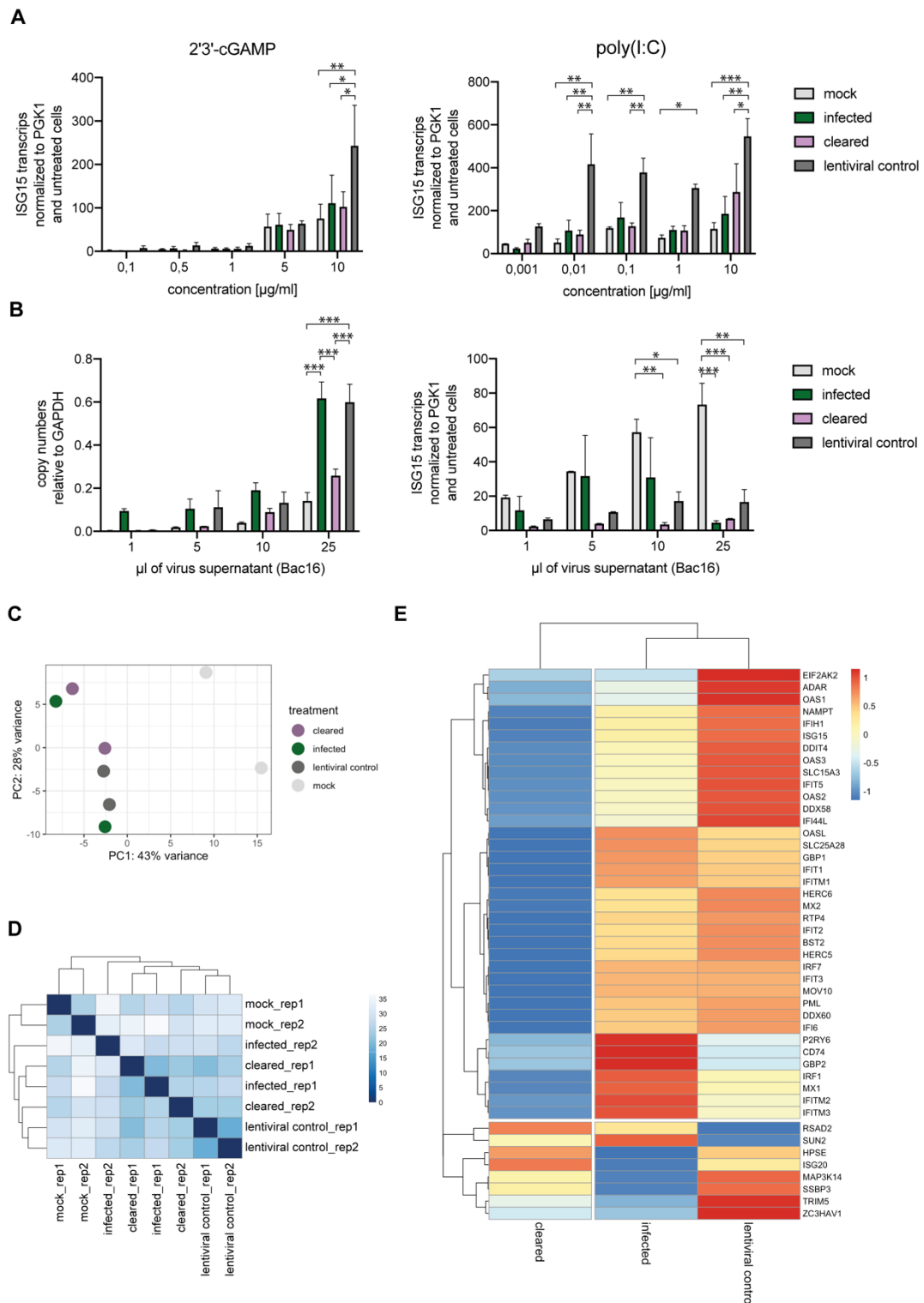


Figure 25: Re-infection of the cell populations with KSHV: (A) Treatment of the cells with different inducers of the type I interferon response. The different populations were treated with increasing concentrations of 2'3'-cGAMP or poly(I:C). 24 hours after treatment cells were harvested and ISG15 transcripts were determined by qRT-PCR. Data represents the mean with SEM from $n = 2$. Statistical significance was assessed by two-way ANOVA. (B) Interferon response after re-infection with KSHV. KSHV infected cells, the cleared cells as well as both negative controls were re-infected with different volumes of KSHV. Viral copy numbers as well as ISG15 transcripts were determined in parallel by qPCR or qRT-PCR, respectively. Data represents mean with SEM from $n = 2$. Two-way ANOVA was performed to test for statistical significance. (C-E) RNA-seq from re-infected cells. The samples infected with 25 μl of Bac16 supernatant were further processed for RNA-sequencing. (C) PCA plot and (D) distance matrix were generated to get information about the overall similarity of the samples. (E) Heatmap of interferon responsive genes after re-infection. z-score calculation of normalized reads per gene and per treatment are depicted. Hierarchical clustering of genes and of samples was performed.

Hierarchical clustering of genes as well as of the different treatments was performed. This revealed that, with some minor exceptions, almost all of the interferon responsive genes in the cleared subset are downregulated compared to the expression levels of infected cells and the lentiviral control. Although differences in deregulated genes after re-infection also exist between the infected population and the lentiviral control, these two subsets form one cluster and are clearly separated from the cleared population. The RNA-seq data from re-infected cells was additionally investigated with regard to previously identified regions which showed differential histone modification patterns. As changes in these regions were initially found to be not directly associated with transcriptional deregulations of annotated genes, it was of special interest whether a re-infection with KSHV would now lead to more pronounced responses (Figure 30). The investigation of these regions revealed that at least a subset of genes with previously described overlapping histone modification changes in infected and cleared cells showed a more pronounced transcriptional response to the re-infection (Figure 30B). The genes FRMD3, NTNG1, TNK1, and TNC are examples for a more pronounced increase in gene expression of the cleared population after re-infection. KIF16B represents one example for a more pronounced downregulation of gene expression in cleared cells compared to all other populations after re-infection.

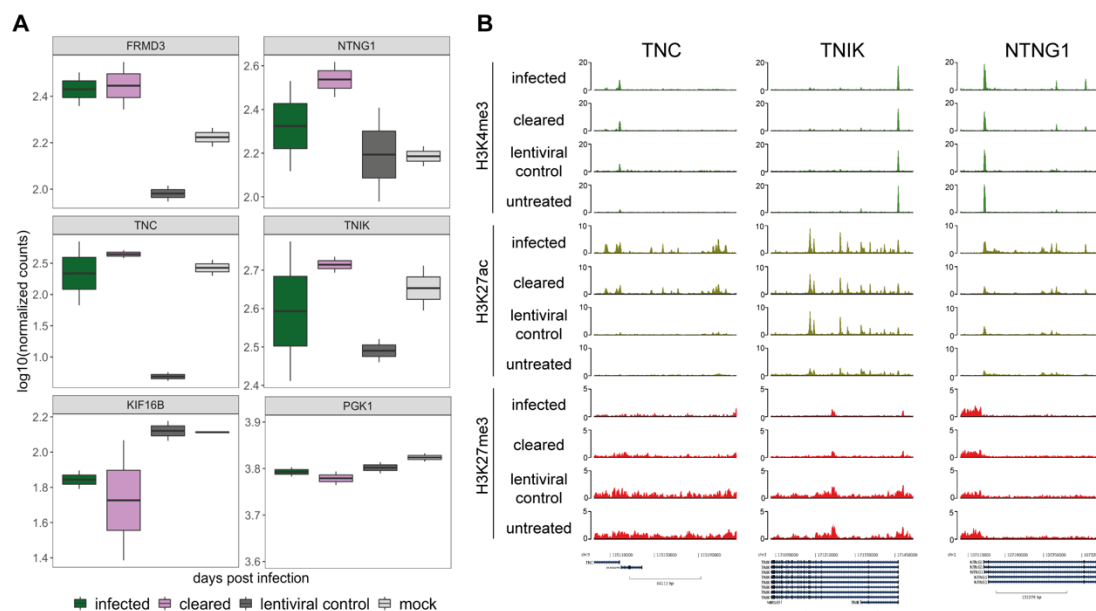


Figure 26: Transcriptional responses of predisposed regions after re-infection. (B) Expression levels of genes with epigenetic predisposition after re-infection with KSHV. RNA-seq from re-infected cells was performed and log₁₀(normalized counts) for a subset of genes are depicted in boxplots. Transcript levels of re-infected cleared cells, super-infected cells, as well as de novo infected mock and lentiviral control cells are shown for each gene. The genes were chosen as they were shown to undergo histone modification changes in the original infection scenario. (A) Examples of epigenetically predisposed regions. Coverage plots of three exemplary regions which showed histone modification changes in the infected as well as in the cleared subset are depicted. These data provide the histone modification states of H3K4me₃, H3K27ac, and H3K27me₃ in infected and cleared cells as well as in the two negative controls before re-infection.

More importantly, transcriptional deregulations after re-infection and the predisposed epigenetic patterns, previously identified in the original latent infection model, are consistent (Figure 30B). The genomic locus of TNC was identified with the help of the nChIP-seq data from infected and cleared cells as a potentially predisposed region with increased activating marks and a parallel decrease in the repressive histone mark H3K27me3. Interestingly, re-infection with KSHV led to the most pronounced increase in TNC expression in the cleared subset. In contrast, the genomic region where KIF16B is encoded, was in nChIP-seq of infected and cleared cells identified as a putative predisposed region, exhibiting a decrease in H3K4me3 (Figure S2). After re-infection this gene exhibited the most pronounced decrease in gene expression in the cleared subset.

In summary, the here presented global investigation of host epigenetic changes and transcriptional deregulations induced by latent KSHV infection led to the identification of several transient and stable histone modification changes. While most of the detected changes seem to be dependent on the infection, a subset of host chromatin changes was detected to become independent of the latent infection over time. This subset constitutes an epigenetic predisposition which results in altered responses upon certain stimuli. Altogether, these data provide evidence that changes of the host epigenome during KSHV infection might render the cell more susceptible to virus-mediated tumorigenesis.

5 Discussion

5.1 KSHV and the type I interferon response

5.1.1 Sporadic interferon signatures in strictly latent infected cells

The KSHV genome was previously shown to be decorated with histone modifications in order to repress lytic viral gene expression and enable latency establishment of the virus (Günther & Grundhoff, 2010; Toth et al., 2010). Furthermore, several viral proteins were identified to interact with host epigenetic modifying enzymes (Shamay et al. 2006; Rossetto and Pari 2012; Hu et al. 2014; Toth et al. 2016). This raises the possibility that not only the KSHV genome undergoes epigenetic remodeling, but also the host epigenome might be affected. In fact, some individual host regions were identified to undergo epigenetic changes upon KSHV infection (Di Bartolo et al., 2008; Shamay et al., 2006). However, genome-wide analyses of KSHV induced epigenetic changes and associated transcriptional deregulations are rare. The aim of this study was therefore to investigate short- as well as long-term epigenetic changes as well as transcriptional deregulations induced by KSHV with the help of an *in vitro* infection system in endothelial cells.

The transcriptome analysis revealed, beside mild transcriptional deregulations, a distinct type I interferon signature among the upregulated genes at day 36 p.i. in strictly latent cultures. A time course experiment furthermore unraveled that the interferon response at late time points of infection is not a prolonged response originating from high levels after *de novo* KSHV infection. It rather represents events of sporadically reoccurring responses. Comparison of early and late type I interferon responses additionally demonstrated that the late sporadic events are more pronounced than the initial response. The type I interferon response was so far only described in the context of *de novo* KSHV infection or upon lytic reactivation of the virus. Therefore, these late sporadic responses provide a new aspect regarding long-term consequences of a KSHV infection.

Although KSHV immediately enters the latent state after *de novo* infection in cell culture systems, several studies showed that expression of lytic viral genes can be observed during the first hours upon viral entry (Krishnan et al., 2004; Purushothaman et al., 2015). This is in line with previous findings, that predominantly lytic viral proteins counteract the type I interferon response. The most prominent examples represent the viral interferon-regulatory factors (vIRFs) which are able inhibit their cellular homologs

(Fuld et al., 2006; Joo et al., 2007; Li et al., 1998; Wies et al., 2008) Furthermore, ORF45 and ORF50 were also shown to downmodulate the type I interferon response at different stages (Yu et al., 2005; Zhu et al., 2002). Therefore, this early relaxed viral gene expression is thought to play an important role for counteracting the host immune response and to prevent the induction of apoptotic processes in infected cells. Investigation of the KSHV expression profile during early time points of infection in our study supports this hypothesis and is in accordance with previous findings. The KSHV transcriptional profile at day 3 p.i. revealed several lytic viral transcripts with highest peaks for the PAN RNA/K7/ORF17, K8, K11-ORF61, and K12. In the study of Purushothaman et al. 2015, exactly the same loci, except for K8, showed highest expression levels after 72h in KSHV infected telomerase immortalized vein endothelial cells (TIVE) as well as in PBMCs (Purushothaman et al., 2015). While K7 was previously shown to prevent infected cells from apoptosis (Wang et al. 2002), K11 as one of the four viral IRF homologs is able to counteract the type I interferon response by inhibiting cellular IRF3 as well as the ISGF3 complex (Fuld et al., 2006; Mutocheluh et al., 2011). The functions of these two exemplary genes nicely reflect the suspected relevance of early lytic gene expression during *de novo* KSHV infection. Our detailed comparison of early and delayed type I interferon responses with the respective viral transcriptional patterns, additionally provides more evidence for the previously proposed function of early lytic gene expression.

While we demonstrated that expression of lytic viral genes at day 3 p.i. is accompanied by rather mild transcript levels of interferon responsive genes, the type I interferon signature was remarkably high during late stages of infection when only latent viral genes were expressed. Subsequent scRNA-seq further unraveled that the late sporadic type I interferon response originates from single cells which do not express a single viral transcript. However, viral transcripts were generally at low levels in the scRNA-seq experiment although the whole population was infected with KSHV. Therefore, it cannot be fully excluded that this observation was made due to experimental drawbacks. The finding that single KSHV positive cells show expression of interferon responsive genes was previously described in another study where around 0.5% of Bac16 infected iSLK cells were IFIT3 positive according to immunofluorescence analyses (Li and Swaminathan 2019). The authors referred this observation to spontaneous lytic reactivation but did not perform any further investigation. However, this study still addressed an interesting role of the IFIT protein

family during KSHV infection which might be of functional relevance also for our study. They could show that the IFIT proteins are upregulated upon lytic reactivation of KSHV and that this results in decreased viral lytic gene expression and an overall reduction of viral progeny production. Comparable findings were also observed for other herpesviruses like hCMV where IFN- β could inhibit early lytic gene transcription (Dağ et al., 2014). Altogether, these data provide evidence that KSHV or herpesviruses in general make use of the type I interferon response to repress viral lytic gene expression and thereby maintain the latent infection state. However, neither our data nor previously published data were able to provide distinct mechanistic insights about the mode of activation of the interferon response. While most of the previous findings attributed the induction to lytic reactivation of KSHV, our study does not provide any evidence that lytic reactivation might be involved in the late type I interferon response. Based on our finding that only single cells produce sporadic high expression of interferon induced genes late during infection, we assume that this observation might be due to secondary effects of a KSHV infection. One possibility for this scenario represents the activation of endogenous retroviral elements (ERVs) which were previously shown by Dai et al. to be activated by KSHV latent gene products (Dai et al. 2018). Activation of these elements might be able to induce an interferon response in single cells. Future experiments are necessary to address this possible mechanism and to further unravel the role of the type I interferon response in this small subset of latently infected cells.

5.1.2 Unresponsiveness of cleared cells to a second infection

Beside the delayed type I interferon signature in single endothelial cells with a strictly latent KSHV profile another interesting finding was observed upon secondary infection with the virus. Cells with a cleared KSHV infection were challenged with a re-infection and effects on the type I interferon response were investigated. qRT-PCR as well as RNA-seq revealed that in cleared cells re-infected with KSHV only low transcript levels of interferon responsive genes were detected. As viral copy numbers were comparable to *de novo* infected TIME cells, the assumption that cleared cells might not be susceptible to virus infection anymore was not confirmed. Furthermore, our findings could not be ascribed to higher basal expression levels of interferon regulated genes in the cleared cells after primary infection. Thus, we assumed that cleared cells might be unresponsive to a secondary infection.

Data about secondary viral infections and their effect on the type I interferon response are rare and no such experiments have been performed for KSHV before. Alsharifi et al. investigated immune responses in mice after sequential viral infections. While primary infection with Semliki Forest virus led to a rapid type I interferon induction, a secondary infection with an unrelated virus did not induce an innate immune response. This observation was made in a timeframe of around 5 days while secondary infection after 9 days led again to normal type I interferon responses (Alsharifi et al., 2006). Another mouse study was also dealing with secondary infections and the type I interferon response in plasmacytoid dendritic cells (pDCs). Björck et al showed that DCs which had been exposed to HSV-1 *in vivo* for 24h were not able to react to a re-infection with the same virus anymore. Although this data seems to rather focus on a super-infection scenario, both studies draw the conclusion that this unresponsiveness is due to a reduced IFN production and may be caused by cellular exhaustion (Alsharifi et al., 2006; Björck, 2004).

Here we focused on long term effects, and thus re-infection experiments were performed more than two month after the initial infection with KSHV. RNA-seq data of long-term KSHV infected cells revealed prolonged type I interferon signatures following infection (Figure 12 + 13). In order to test whether these aberrant interferon signatures may result in general cellular exhaustion, cleared cells were treated with 2'3'-cGAMP or poly(I:C). These two agents are known to be strong inducers of the type I interferon response. In a general cellular exhaustion scenario, a dampened interferon response would be expected. However, upon treatment the cleared cell population exhibited increased expression of interferon responsive genes comparable to mock treated cells, suggesting that cleared cells do not suffer from general cellular exhaustion.

Intriguingly, as mentioned above re-infection of cleared cells with KSHV induced a dampened IFN response, while viral copy numbers were comparable to *de novo* infected cells. These data suggest that KSHV renders its host cells unresponsive to a second infection by a previously unrecognized molecular mechanism. Several studies suggest that an impaired type I interferon response either through mutations or because of primary infections favors the susceptibility to secondary infections (Dupuis et al. 2003; Wei et al. 2017). Thus, one crucial question for future studies is whether the presumed KSHV induced epigenetic reprogramming also facilitates infections by additional viruses that play an important role as co-factors in KSHV mediated tumorigenesis.

5.2 KSHV induced epigenetic changes

5.2.1 Host DNA methylation changes

The establishment of a long-term latent *in vitro* infection model in endothelial cells allowed not only for the investigation of transcriptomic deregulations but also for the study of host epigenetic changes induced by KSHV. As host epigenetic patterns of three different time points were assessed it enabled to differentiate between rather transient changes only occurring at a single time point and stable changes which were detectable over the whole course of infection. The fact that several previous studies described interactions between viral factors and DNMTs led to the hypothesis that this might have an effect on host DNA methylation patterns (Li et al., 2019; Lu et al., 2010; Shamay et al., 2006; Wu et al., 2014). Analysis of single loci like CDH13 and TGFBR11 which showed an increase in DNA methylation in LANA-expressing endothelial cells furthermore strengthened this hypothesis (Di Bartolo et al., 2008; Shamay et al., 2006). In order to get an overview about global DNA methylation changes upon KSHV infection, we performed MeDIP-seq in infected TIME cells as well as in control cells. Although functionality of the method and reliability of the datasets were ensured at several stages of the experiment, only a few transient but no stable DNA methylation changes during the course of infection were observed. Our findings are in contrast to previous analysis of single loci as well as to the few global datasets which are available. Global host DNA methylation changes have so far been investigated in the established PEL cell line BCBL-1 or in *de novo* infected BJAB cells (Journo et al., 2018). While differential analysis between KSHV positive BCBL-1 and virus-negative BJAB cells resulted in the identification of predominantly hypomethylated regions, investigation of *de novo* KSHV infected BJAB cells revealed only minor virus-induced DNA methylation changes. Additional data are available from a KSHV “hit and run” mouse model, where DNA methylation patterns of KSHV positive and KSHV negative tumors were compared (Naipauer et al., 2020). In their study, mouse bone-marrow endothelial-lineage cells (mECs) were transfected with a bacmid of KSHV. Transplantation of these cells into nude mice resulted in the formation of KSHV-infected tumors which show characteristics of KS. These tumors, when explanted and grown *in vitro* without antibiotics, led to the complete loss of KSHV copy numbers. These cells were shown to maintain their tumorigenic state and to be able to form KSHV negative tumors *in vivo*. Comparison of DNA methylation patterns in KSHV positive tumors with either

KSHV positive cells or KSHV negative tumors revealed that changes occurred during virus-dependent tumorigenesis as well as during episome loss. While in KSHV-dependent tumors changes affected most likely hypomethylation, host loci in KSHV negative tumors predominantly underwent hypermethylation. While both mentioned studies either investigated DNA methylation changes in already established tumor cell lines or during the progress of transformation, our data focused on a pre-tumorigenic state. Taken together, our analysis as well as recently published findings imply that DNA methylation changes might rather play a role at late stages of infection and gets especially important during virus-mediated transformation and in fully established tumors. The finding from both previously published data, that KSHV-positive tumors are rather marked by hypomethylated genomic loci is in accordance with general DNA methylation patterns observed in a wide range of cancers. Global decrease in CpG methylation is frequently observed in different cancer types and is thought to contribute to genomic instability (Chen et al. 1998; Rodriguez et al. 2006). One potential underlying mechanism with regard to genomic instability upon genome wide hypomethylation might involve the reactivation of transposable elements which are then able to integrate into various genomic loci. Another general observation from several tumors includes hypermethylation of specific CpG islands in promoter regions. The promoter of the Retinoblastoma (RB) tumor suppressor gene was the first described host region shown to exhibit high levels of DNA methylation in patients suffering from retinoblastoma (Greger et al., 1989). Another example represents the promoter region of H-cadherin (CDH13) which was reported to have high DNA methylation levels in Non-Small Cell Lung Carcinoma (Kim et al. 2005). This region was previously also shown by Shamay et al. 2006 to be affected in LANA-expressing cells as well as in the PEL cell line BCBL-1. Based on this, it can be assumed that KSHV-induced tumors might possess at least to some extent characteristic DNA methylation patterns, which have been described before for several cancer types. While BCBL-1 cells provide a powerful *in vitro* model to study host DNA methylation states in PEL, investigation in KS patient samples has not yet been performed. The fact, that the epigenetic landscape of the KSHV genome has been recently investigated in KS samples from patients opens up the possibility to extend this analysis also to the host (Sun et al. 2017). This would provide important information about the influence of DNA methylation states in an authentic tumor environment and could further validate the findings from *in vitro* studies.

5.2.2 A subset of stable histone modification changes stays even after cleared infection

Apart from analysis of host DNA methylation patterns, ChIP-seq experiments were performed to investigate host chromatin states upon KSHV infection. The parallel investigation of two controls (lentiviral control and untreated cells) allowed for the identification of host chromatin changes induced upon infection with KSHV. On the one hand, the histone marks H3K4me3 and H3K27ac, which are associated with an open chromatin state and gene expression were investigated. Moreover, H3K27ac enabled to study potential changes in enhancer regions. On the other hand, the histone marks H3K27me3 and H3K9me3, which are found in heterochromatic regions and are generally accompanied by gene repression were included. Altogether, our data provided the first global and detailed investigation of host chromatin states in latently KSHV infected endothelial cells. In contrast to DNA methylation where no stable changes were observed upon KSHV infection, several host loci were identified to undergo host chromatin changes. Although most of the regions were rather transient, a subset of histone modification changes persisted over the whole course of infection. This finding is in line with previous data describing interaction of viral proteins with different cellular histone modifying enzymes. Predominantly the latent viral protein LANA was recently shown to interact with the core proteins of the H3K4 methyltransferase complex Set1/COMPASS (Hu et al. 2014). Furthermore, LANA associates with the PRC2 subunits EZH2, SUZ12, and EED (Toth et al., 2016). However, these findings were predominantly connected to implications on the viral genome rather than on the host. Only one global analysis of host histone modification changes in the context of KSHV was performed in PDGFRA positive mouse mesenchymal stem cells (MSC) (Naipauer et al., 2019). These cells were either cultivated in normal MSC media or in KS-like media which represents a pro-angiogenic environment. While cells cultivated under these pro-angiogenic conditions were able to form tumors *in vivo*, MSC cells under normal culturing conditions were not. Investigation of the viral chromatin landscape in MSC cells cultivated in KS-like media revealed a decrease in H3K27me3 which was consistent with a de-repressed viral lytic gene expression. Based on a subsequent analysis of host H3K4me3 and H3K27me3 states in these cells, they claimed that the cells cultured in KS media better tolerate viral lytic gene expression. The authors' argument is based on the finding that the most

repressed loci identified by an increase in H3K27me3 in MSC-KS cells can be attributed to the innate immune response. In contrast to our data, their analysis of H3K4me3 did not result in any obvious changes on host loci. However, these previously published data concentrated on differences due to environmental conditions rather than on KSHV induced host chromatin changes.

Another aspect which was investigated in our study involved the relationship of histone modification changes and the transcriptional state of the corresponding gene. While a genome-wide analysis revealed global correlation, a more in-depth analysis of single host genomic loci highlighted that histone modification changes exist, which are not associated with direct transcriptional deregulation of the annotated gene. The finding from these individually analyzed regions is in contrast to the general assumption that histone modification levels are correlated to gene expression (Yu et al. 2008; Karličić et al. 2010). This finding led to the assumption that these differential regions might represent a predisposed state. In order to further evaluate this hypothesis, histone modifications in a subset of cells with a cleared viral infection were compared to those identified in long-term infected cells. This clearance was achieved by cultivating the previously infected cells in the absence of antibiotics, which led to a stepwise loss of viral copy numbers due to an inefficient tethering mechanism of KSHV *in vitro*. The observation that KSHV inefficiently tethers its genome in cell culture systems was previously described for TIME cells and it was used in this study to imitate a clearance of the virus (Grundhoff and Ganem 2004). The cleared population, although transcriptionally reverted to the initial uninfected state, harbored histone modification changes, which were also present in the infected subset. This finding additionally supports the hypothesis of a predisposition and indicates that a subset of KSHV induced chromatin changes can become independent of the infection. Challenging these cells with different stimuli, like re-infection, led to a more transcriptional response of some predisposed genes in the cleared subset.

While data obtained from our study strengthen the hypothesis that KSHV induced histone modification changes represent an epigenetic predisposition, analyses in EBV infected cells provide evidence for a rather direct involvement of such changes with regard to tumorigenesis. This closely related herpesvirus is highly associated with different types of lymphomas as well as nasopharyngeal carcinomas of epithelial origin. In contrast to KSHV, this virus has the ability to immortalize and transform B cells *in vitro* (Hollyoake et al., 1995; Kilger et al., 1998). Investigation of cellular histone

modification changes in both, B cells as well as epithelial cells, revealed a functional relevance of such alterations with regard to transformation. Infection of resting B cells with EBV led to a global reduction of repressive histone marks like H3K27me3 and H3K9me3, which was associated to transcriptional activation. As EBV infection in B cells leads to the induction of cell proliferation, the authors also showed, that these changes could be attributed to the infection rather than to increased cellular growth (Hernando et al., 2014). Another recently published analysis in EBV infected epithelial cells revealed changes in host bivalent chromatin regions, which can be predominantly attributed to genes involved in the DNA damage repair. These changes involved a decrease in H3K4me3 and a parallel increase in H3K27me3, which could also be recapitulated on gene expression levels. Lower expression levels of these DNA damage repair genes resulted in an unresponsiveness upon induction of DNA damage with hydrogen peroxide. The data furthermore provide evidence that the EBV factor EBNA1, which fulfills similar functions as the KSHV encoded protein LANA, might play a role in the downregulation of these genes (Leong et al., 2019). However, the mechanistic understanding of the identified host chromatin changes and the functional role of viral factors is still not investigated sufficiently for both viruses. As data from EBV infected cells indicate that EBNA1 might play a role, it would be interesting to further investigate the role of the KSHV related protein LANA with regard to host chromatin changes.

5.2.3 Putative epigenetic pre-activation of interferon responsive genes

The finding from the transcriptome analysis that infection of endothelial cells with KSHV results in a prolonged type I interferon signature, raised the question whether this could also be recapitulated by the host chromatin state. Analysis of the histone modification state of several interferon responsive genes revealed that transcriptional induction of these genes does not primarily depend on host chromatin changes. Data obtained from scRNA-seq indicated that only single cells show high expression levels of interferon responsive genes. This raises the possibility that bulk analysis of histone marks, as conducted in our study, might not be able to illustrate potential changes occurring only in single cells. However, the observation that even untreated cells had high levels of the activating marks H3K4me3 and H3K27ac in the loci of interferon induced genes provided evidence for a potential pre-activation. This would allow the fast transcriptional activation of these genes in order to fight bacterial or viral infections. In fact, the chromatin remodeling SWI/SNF-like BAF complex was described to

maintain an open chromatin state and to ensure fast binding of transcriptional activators upon induction of the interferon cascade (Cui et al., 2004). Despite the pre-activation of these host genomic loci, a slight increase in H3K27ac upon induction of the type I interferon response was still detectable at least in a subset of interferon regulated genes. This finding is again in accordance with available data, which describes an interaction of transcriptional activators of interferon induced genes with the histone acetyltransferase complex p300/CBP ((Bhattacharya et al., 1996; Yoneyama et al., 1998). In summary, these findings provide a confirmation of the current knowledge regarding the chromatin state of interferon responsive genes and additionally strengthen the reliability of the here presented global histone modification datasets.

5.2.4 Stable histone modification changes might affect enhancers

Comparison of histone modification changes between long-term KSHV infected cells and the cleared subset led to the identification of regions which were present in both cell populations. Although H3K27me3 represents the histone modification with the highest number of overlapping regions, changes in H3K27ac are the most pronounced. In most of the overlapping regions an increase of this histone modification can be observed. Importantly, H3K27ac is associated with enhancer regions which are genomic features known to cooperate with promoters to regulate gene expression (Creighton et al., 2010). While it is thought that these transcriptional regulatory elements predominantly affect the closest promoter regions, there are also examples for long-range interactions (Rao et al., 2014; Sanyal et al., 2012). Beside the histone modification H3K27ac, active enhancers are also marked by H3K4me1 and the presence of transcription factors, p300, the RNA polymerase II as well as the Mediator complex. Although the exact mechanism is not fully understood, the enhancer is thought to interact with the promoter region of a target gene by looping, thereby increasing the local concentration of the before mentioned factors and resulting in enhanced gene expression (reviewed in Field and Adelman 2020). Enhancers which are in close proximity to each other can additionally build up large regulatory condensates which are termed super-enhancers. Although these large regions are mainly based on *in silico* predictions, there is evidence that their effect on gene expression is much more pronounced compared to classical enhancers (Whyte et al., 2013). Both, the classical enhancers as well as super-enhancers, play important roles with regard to developmental processes and are highly associated with key

determinants of cellular identity (Heintzman et al., 2009; Whyte et al., 2013). Therefore, changes in potential enhancer regions, as detected in the present study, might affect these aspects, potentially leading to a de-differentiation of the cells. Interestingly, a preliminary *in silico* prediction of super-enhancers based on global H3K27ac peaks in the long-term KSHV infected cells identified 1382 potential super-enhancers when compared to the lentiviral control (Figure 31). Annotation of the highest ranked regions revealed at least two genes (SEMA3D, EPHA5), which were previously described to be involved in neuronal and cardiovascular development (reviewed in Wilkinson 2001; Valdembri et al. 2016). Interestingly, recent data from PEL cell lines indicate that the KSHV factor vIRF-3 acts together with the cellular transcription factors IRF4 and BATF at super-enhancers to increase the tumorigenic transcriptional pattern in these cells (Manzano et al., 2020).

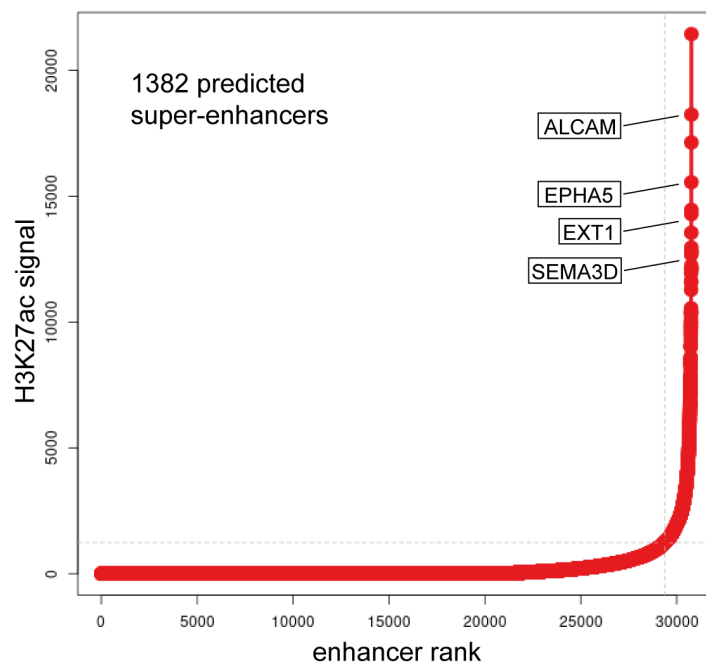


Figure 27: Super-enhancer prediction: The bioinformatic tool ROSE was used to perform an *in silico* prediction of super-enhancers in long-term KSHV infected cells compared to the lentiviral control. The H3K27ac signal of the enhancer regions in the KSHV infected cells is plotted against the rank of the enhancer. Enhancers, which appear above the inflection point are considered as super-enhancers.

A cooperation of viral and cellular factors would also be conceivable as a potential mechanism for the findings obtained in our present study. The fact that some differential regions are also observed in the cleared subset suggests that the cellular transcription factors might at some point be able to act independently of the viral protein.

However, the finding that a large part of the identified histone modification changes is not directly associated with transcriptional responses makes it difficult to assign a functional outcome. As the cleared subset even showed a complete reconstitution of the transcriptional state towards uninfected cells, it can be hypothesized that the chromatin changes detected in this study represent a predisposition. In the context of the enhancers, this would require a primed state, which does not result in a direct transcriptional response. Primed enhancers are currently thought to be bound by transcription factors and to have high H3K4me1 levels but no H3K27ac (reviewed by Calo and Wysocka 2013). This is in contrast to the observation that the here presented regions gain H3K27ac. Due to this discrepancy, a more detailed investigation of these potential enhancer regions would be important. On the one hand, ChIP experiments could unravel whether RNA polymerase II or the Mediator complex are associated to these regions. Furthermore, the identification of H3K4me1 in these genomic loci would strengthen the hypothesis that the observed remodeling affects authentic, cellular enhancers. As the correlation of enhancer regions to transcriptional deregulation might be complicated due to potential long-range interactions with promoters, chromosome conformation capture approaches could help to identify target genes of the enhancer regions. Furthermore, a CRISPR-targeting approach (enCRISPRa) to modulate the enhancer activity would lead to a more detailed characterization of the remodeled regions (Li et al. 2020) and could unravel whether predisposition actually plays a role.

5.3 KSHV mediated tumorigenesis and the role of epigenetics

Although various aspects about KSHV mediated tumorigenesis were investigated in recent years, some important steps towards transformation are still elusive. Especially with regard to KS there are several open questions which could not be answered with the actually available *in vitro* and *in vivo* systems. While PEL cell lines provide an elegant cell culture system to study KSHV induced tumorigenesis arising from B cells, establishment of an *in vitro* KS system was so far not successful. Furthermore, infection of endothelial cells, which are currently thought to be the cells of origin for KS, has not resulted in the transformation and outgrowth of KS-like tumors until now. This is probably due to the fact, that KSHV, in contrast to other human tumor viruses, does not encode for a classical viral oncogene. This raises the possibility that additionally to sustained viral gene expression, cellular reprogramming might be of importance with regard to KSHV-mediated tumorigenesis. As previous findings described several

interactions between viral encoded factors and host epigenetic modifying enzymes, it can be hypothesized that remodeling of the host epigenome might play a role in this process (Hu et al., 2014; Shamay et al., 2006; Toth et al., 2016). Data obtained from our genome-wide analysis of host epigenetic changes induced after *de novo* KSHV infection of TIME cells and associated transcriptional responses provide evidence that these changes have indeed an important function. While DNA methylation pattern, in contrast to other studies, were not altered after KSHV infection of endothelial cells, several histone modification changes were detected in short-term as well as long-term infected cells. Investigation of histone modification changes in a cleared population revealed that a subset of the identified host regions stayed altered. This indicates that KSHV induced changes might become independent of the virus at some point. More importantly, the absence of associated transcriptional deregulations in the cleared subset implies that a predisposition mechanism might play a role. The finding that some of these predisposed regions responded more pronounced at the transcriptional level after treatment with different stimuli further strengthens this hypothesis and opens up the possibility that the predisposition is based on epigenetic transcriptional memory. This term describes the phenomenon that organisms can adopt to previously encountered environmental or stress situations and are able to react faster and probably also more pronounced upon re-occurrence of the stimulus. This mechanism, originally found in yeast, which was grown under galactosidase conditions, is also present in plants and humans (Acar et al., 2005; Ding et al., 2012; Light et al., 2013). Epigenetic transcriptional memory in humans was identified upon repeated IFN- γ treatment for several IFN-inducible genes (Light et al., 2013). Recent findings also suggest that these memory genes share some characteristic features, which might also be conserved between different organisms. The mechanism is thought to be initiated by context-dependent transcription factors, which recruit on the one hand the Set1/COMPASS complex to deposit high levels of H3K4me2/3 and on the other hand paused RNA polymerase II (D'Urso et al., 2016; Ding et al., 2012). Another important aspect of the epigenetic transcriptional memory seems to be the re-localization of these genomic loci to the nuclear periphery and the association with the nuclear pore subunit Nup98 (Light et al., 2013). Interestingly, KSHV ORF10 was previously shown to form a complex with the RNA export protein Rae1 and Nup98 to inhibit mRNA export from the nucleus (Gong et al., 2016). This provides evidence that KSHV factors are generally able to cooperate with proteins or complexes involved in the epigenetic

transcriptional memory. However, future experiments would have to unravel whether this mechanism might indeed play a role with regard to the here proposed virus mediated predisposition of certain host genomic loci.

In summary, these here presented findings of host histone modification changes and the assumption that epigenetic transcriptional memory might be involved, can be very well implemented in the actual model of KSHV induced tumorigenesis (Figure 32).

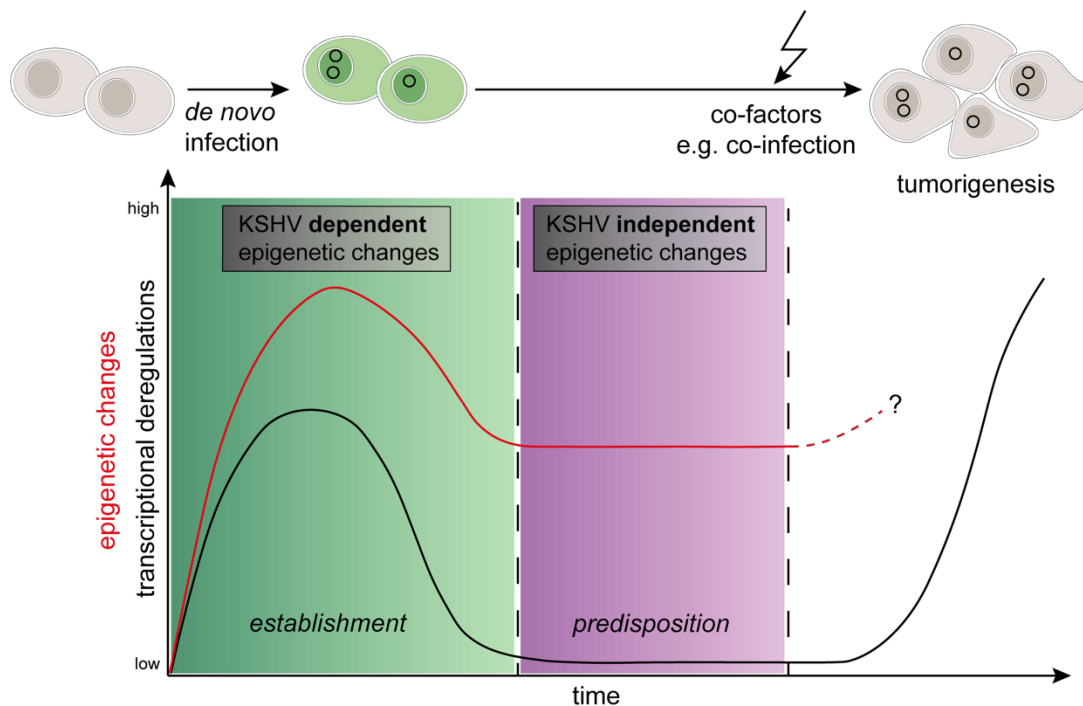


Figure 28: Proposed KSHV induced tumorigenesis model and the role of histone modifications: After *de novo* infection of endothelial cells with KSHV, the virus establishes latency and can maintain life-long in its host. In the early state of latent infection moderate transcriptional deregulations can be observed. While some of these deregulations can also be recapitulated on the host chromatin level, a set of cellular histone modification changes is established, which is not associated with transcriptional responses. With an ongoing infection and prolonged expression of KSHV latency genes, some of the epigenetic changes might even get independent of the infection. Together, the KSHV dependent and independent histone modification changes might represent a predisposition, which could be essential during the process of tumorigenesis. As KSHV does not encode for a classical viral oncogene, this model also includes a potential role of co-factors, like for example co-infection with other viruses. These co-factors might lead to more pronounced responses of genes which previously underwent KSHV induced chromatin changes thereby playing a secondary but important role during tumorigenesis.

Although there is increasing evidence that KSHV lytic replication might play a role in tumorigenesis via paracrine effects, it is still thought that latently infected endothelial cells give rise to KS. Upon *de novo* infection, KSHV is known, after a short time frame of a relaxed viral gene expression, to enter by default the latent infection state. During early stages of latent infection moderate host transcriptional changes occur, including among others, upregulation of type I interferon related genes. While some of these deregulations are reflected by alterations on the chromatin level, a subset of histone modification changes could not be attributed to significant transcriptional responses.

During this first phase of latent infection, it is thought that KSHV dependent cellular histone modification changes are established. With an ongoing infection or in the scenario of a cleared infection, transcriptional deregulations were either reduced or completely absent, respectively. In contrast to that, the host chromatin landscape remained altered implying the establishment of a subset of KSHV independent histone modifications. Thus, it can be hypothesized that cells in this later stage of infection enter a predisposition state, which is comprised of primed KSHV dependent and independent histone modifications. This predisposed state is very well in line with the assumption that KSHV mediated tumorigenesis is thought to depend on co-factors. Such co-factors, like environmental stimuli or co-infection with other viruses, might lead to more pronounced responses of the predisposed genes thereby playing a secondary but important function during KSHV mediated tumorigenesis.

The here presented model with its proposed rather indirect role of host histone modification changes during tumorigenesis is in contrast to the previously described tumorigenic potential of alterations in histone modification patterns. Changes in these patterns have been identified in several cancer types and they have been shown to directly correlate with transcriptional deregulations. In most of the cases it turned out that a mutation in one of the histone modifying enzymes was responsible for the altered landscape. The genomic region where MLL1 is encoded was shown to frequently undergo translocations in myeloid and lymphoid leukemias (Meyer et al., 2018). Furthermore, the lysine demethylase LSD1 was described to be upregulated in several cancer types, ranging from prostate carcinoma to neuroblastoma and is therefore considered as a classical oncogene (Lim et al., 2010; Schulte et al., 2009). Lastly, the PRC2 subunit EZH2 frequently undergoes mutations in its catalytic SET domain, which renders an altered substrate preference to the protein leading to increased H3K27me3 levels (Morin et al. 2010). Therefore, the here proposed functional role of histone modification changes in the context of KSHV mediated tumorigenesis seems not to follow the concept which is common in most cancer types.

5.4 Conclusion and Outlook

Despite over 20 years of research, many questions regarding KSHV mediated tumorigenesis remain unanswered. One of these questions includes the still unknown cell of origin of the proliferating KS spindle cells. Although it is thought that these cells are of endothelial origin, the finding that surface markers for other cell types can be

detected, implies that a de-differentiation step might be of importance during tumorigenesis. Furthermore, the fact that KSHV seems not to encode for a classical viral oncogene raises the question of how the exact molecular mechanisms towards tumorigenesis are mediated. As it is thought that long-term latently infected cells give rise to cancer and KSHV factors were shown to interact with host chromatin modifying enzymes, there is evidence that this interplay might have a function during the process of tumorigenesis.

The here presented investigation of long-term KSHV infected telomerase-immortalized microvascular endothelial cells highlight interesting new aspects about host chromatin changes induced by the virus. The analysis of host DNA methylation changes by MeDIP-seq, histone modification changes by nChIP-seq as well as associated transcriptional responses by RNA-seq gave detailed new insights into the genome-wide landscape of infected, pre-tumorigenic cells. While DNA methylation states were not altered upon infection, several host genomic loci were identified which undergo stable histone modification changes. The absence of associated transcriptional responses led to the assumption that these remodeled regions might represent a predisposed state. Interestingly, this proposed function seems not to follow the concept which is common in most cancer types where histone modification changes are directly correlated to gene expression changes.

Further studies are needed to finally increase the mechanistic understanding of the identified histone modification changes and to decipher the exact involvement of KSHV encoded factors. As LANA represents one of the genes which is expressed during latency and was shown to bind to host chromatin, it represents a prime candidate to investigate whether overexpression of this viral protein would lead to similar host chromatin patterns. Another important aspect involves the more detailed investigation of the here identified histone modification changes and their potential phenotypic manifestations after transcriptional induction. As potential enhancer regions were identified to undergo the most pronounced changes, it would be interesting to mediate their activation by previously established and refined CRISPR-based methods. Such methods allow for the targeted recruitment of transcription activators to the gene locus of interest. With this approach it would be possible to identify enhancer specific target genes which are probably regulated by long range interactions between enhancer and promoter. Furthermore, it would enable to directly link these identified remodeled regions to potential phenotypic outcomes.

In summary, this study provides important new insights regarding KSHV mediated cellular remodeling and potential implications in the tumorigenic progress. Although many aspects about the exact role of histone modification changes in the context of KS are still elusive, in a long-term perspective these data might provide an interesting starting-point for more targeted therapy options.

6 References

- Acar, M., Becskei, A., & van Oudenaarden, A. (2005). Enhancement of cellular memory by reducing stochastic transitions. *Nature*, *435*(7039), 228–232.
- Agger, K., Cloos, P. A. C., Christensen, J., Pasini, D., Rose, S., Rappsilber, J., Issaeva, I., Canaani, E., Salcini, A. E., & Helin, K. (2007). UTX and JMJD3 are histone H3K27 demethylases involved in HOX gene regulation and development. *Nature*, *449*(7163), 731–734.
- Akula, S. M., Naranatt, P. P., Walia, N.-S., Wang, F.-Z., Fegley, B., & Chandran, B. (2003). Kaposi's Sarcoma-Associated Herpesvirus (Human Herpesvirus 8) Infection of Human Fibroblast Cells Occurs through Endocytosis. *Journal of Virology*, *77*(14), 7978–7990.
- Akula, S. M., Pramod, N. P., Wang, F. Z., & Chandran, B. (2001). Human herpesvirus 8 envelope-associated glycoprotein B interacts with heparan sulfate-like moieties. *Virology*, *284*(2), 235–249.
- Akula, S. M., Pramod, N. P., Wang, F. Z., & Chandran, B. (2002). Integrin $\alpha 3\beta 1$ (CD 49c/29) is a cellular receptor for Kaposi's sarcoma-associated herpesvirus (KSHV/HHV-8) entry into the target cells. *Cell*, *108*(3), 407–419.
- Alkharsah, K. R., Singh, V. V., Bosco, R., Santag, S., Grundhoff, A., Konrad, A., Sturzl, M., Wirth, D., Dittrich-Breiholz, O., Kracht, M., & Schulz, T. F. (2011). Deletion of Kaposi's Sarcoma-Associated Herpesvirus FLICE Inhibitory Protein, vFLIP, from the Viral Genome Compromises the Activation of STAT1-Responsive Cellular Genes and Spindle Cell Formation in Endothelial Cells. *Journal of Virology*, *85*(19), 10375–10388.
- Alsharifi, M., Regner, M., Blanden, R., Lobigs, M., Lee, E., Koskinen, A., & Müllbacher, A. (2006). Exhaustion of Type I Interferon Response following an Acute Viral Infection. *The Journal of Immunology*, *177*(5), 3235–3241.
- Ambrosi, C., Manzo, M., & Baubec, T. (2017). Dynamics and Context-Dependent Roles of DNA Methylation. *Journal of Molecular Biology*, *429*(10), 1459–1475.
- An, J., Sun, Y., Sun, R., & Rettig, M. B. (2003). Kaposi's sarcoma-associated herpesvirus encoded vFLIP induces cellular IL-6 expression: The role of the NF- κ B and JNK/AP1 pathways. *Oncogene*, *22*(22), 3371–3385.
- Aoki, Y., Jaffe, E. S., Chang, Y., Jones, K., Teruya-Feldstein, J., Moore, P. S., & Tosato, G. (1999). Angiogenesis and Hematopoiesis Induced by Kaposi's Sarcoma-Associated Herpesvirus-Encoded Interleukin-6. *Blood*, *93*(12), 4034–4043.
- Arbuckle, J. H., Medveczky, M. M., Luka, J., Hadley, S. H., Luegmayer, A., Ablashi, D., Lund, T. C., Tolar, J., De Meirleir, K., Montoya, J. G., Komaroff, A. L., Ambros, P. F., & Medveczky, P. G. (2010). The latent human herpesvirus-6A genome specifically integrates in telomeres of human chromosomes in vivo and in vitro. *Proceedings of the National Academy of Sciences of the United States of America*, *107*(12), 5563–5568.
- Arias, C., Weisburd, B., Stern-Ginossar, N., Mercier, A., Madrid, A. S., Bellare, P., Holdorf, M., Weissman, J. S., & Ganem, D. (2014). KSHV 2.0: A Comprehensive Annotation of the Kaposi's Sarcoma-Associated Herpesvirus Genome Using Next-Generation Sequencing Reveals Novel Genomic and Functional Features. *PLoS Pathogens*, *10*(1).
- Arvin, A., Capadelli-Fiume, G., Mocarski, E., Moore, P. S., Roizman, B., Whitley, R., & Yamanishi, K. (2007). Human Herpesviruses - Biology, Therapy, and Immunoprophylaxis. *Cambridge University Press*.
- AuCoin, D. P., Colletti, K. S., Xu, Y., Cei, S. A., & Pari, G. S. (2002). Kaposi's Sarcoma-Associated Herpesvirus (Human Herpesvirus 8) Contains Two Functional Lytic Origins of DNA Replication. *Journal of Virology*, *76*(15), 7890–7896.
- Bala, K., Bosco, R., Gramolelli, S., Haas, D. A., Kati, S., Pietrek, M., Hävemeier, A., Yakushko, Y., Singh, V. V., Dittrich-Breiholz, O., Kracht, M., & Schulz, T. F. (2012). Kaposi's Sarcoma Herpesvirus K15 Protein Contributes to Virus-Induced Angiogenesis by Recruiting PLC γ 1 and Activating NFAT1-dependent RCAN1 Expression. *PLoS Pathogens*, *8*(9).
- Balasubramanian, D., Akhtar-Zaidi, B., Song, L., Bartels, C. F., Veigl, M., Beard, L., Myeroff, L., Guda, K., Lutterbaugh, J., Willis, J., Crawford, G. E., Markowitz, S. D., & Scacheri, P. C. (2012). H3K4me3 inversely correlates with DNA methylation at a large class of non-CpG-island-containing start sites. *Genome Medicine*, *4*(5), 1–11.
- Ball, M. P., Li, J. B., Gao, Y., Lee, J. H., Leproust, E. M., Park, I. H., Xie, B., Daley, G. Q., & Church, G. M. (2009). Targeted and genome-scale strategies reveal gene-body methylation signatures in human cells. *Nature Biotechnology*, *27*(4), 361–368.
- Ballestas, M. E., Chatis, P. A., & Kaye, K. M. (1999). Efficient persistence of extrachromosomal KSHV DNA mediated by latency-associated nuclear antigen. *Science*, *284*(5414), 641–644.
- Ballestas, M. E., & Kaye, K. M. (2001). Kaposi's Sarcoma-Associated Herpesvirus Latency-Associated

- Nuclear Antigen 1 Mediates Episome Persistence through cis-Acting Terminal Repeat (TR) Sequence and Specifically Binds TR DNA. *Journal of Virology*, 75(7), 3250–3258.
- Ballon, G., Akar, G., & Cesarman, E. (2015). Systemic Expression of Kaposi Sarcoma Herpesvirus (KSHV) Vflip in Endothelial Cells Leads to a Profound Proinflammatory Phenotype and Myeloid Lineage Remodeling In Vivo. *PLoS Pathogens*, 11(1), 1–20.
- Bannister, A. J., Zegerman, P., Partridge, J. F., Miska, E. A., Thomas, J. O., Allshire, R. C., & Kouzarides, T. (2001). Selective recognition of methylated lysine 9 on histone H3 by the HP1 chromo domain. *Nature*, 410(6824), 120–124.
- Barau, J., Teissandier, A., Zamudio, N., Roy, S., Nalesso, V., Hérault, Y., Guillou, F., & Bourc'his, D. (2016). The DNA methyltransferase DNMT3C protects male germ cells from transposon activity. *Science*, 354(6314), 909–912.
- Barbera, A. J., Chodaparambil, J. V., Kelley-Clarke, B., Joukov, V., Walter, J. C., Luger, K., & Kaye, K. M. (2006). The nucleosomal surface as a docking station for Kaposi's sarcoma herpesvirus LANA. *Science*, 311(5762), 856–861.
- Beard, C., Li, E., & Jaenisch, R. (1995). Loss of methylation activates Xist in somatic but not in embryonic cells. *Genes and Development*, 9(19), 2325–2334.
- Bechtel, J., Grundhoff, A., & Ganem, D. (2005). RNAs in the Virion of Kaposi's Sarcoma-Associated Herpesvirus. *Journal of Virology*, 79(16), 10138–10146.
- Bechtel, J. T., Liang, Y., Hvidding, J., & Ganem, D. (2003). Host Range of Kaposi's Sarcoma-Associated Herpesvirus in Cultured Cells. *Journal of Virology*, 77(11), 6474–6481.
- Bernstein, B. E., Mikkelsen, T. S., Xie, X., Kamal, M., Huebert, D. J., Cuff, J., Fry, B., Meissner, A., Wernig, M., Plath, K., Jaenisch, R., Wagschal, A., Feil, R., Schreiber, S. L., & Lander, E. S. (2006). A Bivalent Chromatin Structure Marks Key Developmental Genes in Embryonic Stem Cells. *Cell*, 125(2), 315–326.
- Bernstein, E., Duncan, E. M., Masui, O., Gil, J., Heard, E., & Allis, C. D. (2006). Mouse Polycomb Proteins Bind Differentially to Methylated Histone H3 and RNA and Are Enriched in Facultative Heterochromatin. *Molecular and Cellular Biology*, 26(7), 2560–2569.
- Bestor, T., Laudano, A., Mattaliano, R., & Ingram, V. (1988). Cloning and sequencing of a cDNA encoding DNA methyltransferase of mouse cells. The carboxyl-terminal domain of the mammalian enzymes is related to bacterial restriction methyltransferases. *Journal of Molecular Biology*, 203(4), 971–983.
- Bhattacharya, S., Eckner, R., Grossman, S., Oldread, E., Arany, Z., Andrea, A. D., & Livingston, D. M. (1996). p300 / CBP in signalling induced by interferon- α . *Letters to Nature*, 383(September), 344–347.
- Bird, A. P. (1980). DNA methylation and the frequency of CpG in animal DNA. *Nucleic Acids Research*, 8(7), 1499–1504.
- Birkmann, A., Mahr, K., Ensser, A., Yağuboğlu, S., Titgemeyer, F., Fleckenstein, B., & Neipel, F. (2001). Cell Surface Heparan Sulfate Is a Receptor for Human Herpesvirus 8 and Interacts with Envelope Glycoprotein K8.1. *Journal of Virology*, 75(23), 11583–11593.
- Birve, A., Sengupta, A. K., Beuchle, D., Larsson, J., Kennison, J. A., Rasmuson-Lestander, Å., & Müller, J. (2001). Su(z)12, a novel Drosophila Polycomb group gene that is conserved in vertebrates and plants. *Development*, 128(17), 3371–3379.
- Björck, P. (2004). Dendritic Cells Exposed to Herpes Simplex Virus In Vivo Do Not Produce IFN- α after Rechallenge with Virus In Vitro and Exhibit Decreased T Cell Alloreactivity. *The Journal of Immunology*, 172(9), 5396–5404.
- Blackbourn, D. J., Ambroziak, J., Lennette, E., Adams, M., Ramachandran, B., & Levy, J. A. (1997). Infectious human herpesvirus 8 in a healthy North American blood donor. *Lancet*, 349(9052), 609–611.
- Borgel, J., Guibert, S., Li, Y., Chiba, H., Schübeler, D., Sasaki, H., Forné, T., & Weber, M. (2010). Targets and dynamics of promoter DNA methylation during early mouse development. *Nature Genetics*, 42(12), 1093–1100.
- Borgia, B., Roesli, C., Fugmann, T., Schliemann, C., Cesca, M., Neri, D., & Giavazzi, R. (2010). A proteomic approach for the identification of vascular markers of liver metastasis. *Cancer Research*, 70(1), 309–318.
- Boshoff, C., Schulz, T. F., Kennedy, M. M., Graham, A. K., Fisher, C., Thomas, A., McGee, J. O., Weiss, R. A., & O'Leary, J. J. (1995). Kaposi's sarcoma-associated herpesvirus infects endothelial and spindle cells. 1(12), 1–5.
- Boulanger, E., Gérard, L., Gabarre, J., Molina, J. M., Rapp, C., Abino, J. F., Cadranet, J., Chevret, S., & Oksenhendler, E. (2005). Prognostic factors and outcome of human herpesvirus 8-associated primary effusion lymphoma in patients with AIDS. *Journal of Clinical Oncology*, 23(19), 4372–4380.
- Bray, F., Ferlay, J., Soerjomataram, I., Siegel, R. L., Torre, L. A., & Jemal, A. (2018). Global cancer

- statistics 2018: GLOBOCAN estimates of incidence and mortality worldwide for 36 cancers in 185 countries. *CA: A Cancer Journal for Clinicians*, 68(6), 394–424.
- Brind'Amour, J., Liu, S., Hudson, M., Chen, C., Karimi, M. M., & Lorincz, M. C. (2015). An ultra-low-input native ChIP-seq protocol for genome-wide profiling of rare cell populations. *Nature Communications*, 6, 1–8.
- Broussard, G., & Damania, B. (2020). KSHV: Immune Modulation and Immunotherapy. *Frontiers in Immunology*, 10(February).
- Brulois, K. F., Chang, H., Lee, A. S.-Y., Ensser, A., Wong, L.-Y., Toth, Z., Lee, S. H., Lee, H.-R., Myoung, J., Ganem, D., Oh, T.-K., Kim, J. F., Gao, S.-J., & Jung, J. U. (2012). Construction and Manipulation of a New Kaposi's Sarcoma-Associated Herpesvirus Bacterial Artificial Chromosome Clone. *Journal of Virology*, 86(18), 9708 LP – 9720.
- Bubman, D., Guasparri, I., & Cesarman, E. (2007). Deregulation of c-Myc in primary effusion lymphoma by Kaposi's sarcoma herpesvirus latency-associated nuclear antigen. *Oncogene*, 26(34), 4979–4986.
- Butler, A., Hoffman, P., Smibert, P., Papalexi, E., & Satija, R. (2018). Integrating single-cell transcriptomic data across different conditions, technologies, and species. *Nature Biotechnology*, 36(5), 411–420.
- Cai, X., Lu, S., Zhang, Z., Gonzalez, C. M., Damania, B., & Cullen, B. R. (2005). Kaposi's sarcoma-associated herpesvirus expresses an array of viral microRNAs in latently infected cells. *Proceedings of the National Academy of Sciences of the United States of America*, 102(15), 5570–5575.
- Calo, E., & Wysocka, J. (2013). Modification of Enhancer Chromatin: What, How, and Why? *Molecular Cell*, 49(5), 825–837.
- Campbell, M., Watanabe, T., Nakano, K., Davis, R. R., Lyu, Y., Tepper, C. G., Durbin-Johnson, B., Fujimuro, M., & Izumiya, Y. (2018). KSHV episomes reveal dynamic chromatin loop formation with domain-specific gene regulation. *Nature Communications*, 9(1).
- Candido, E. P. M., Reeves, R., & Davie, J. R. (1978). Sodium butyrate inhibits histone deacetylation in cultured cells. *Cell*, 14(1), 105–113.
- Carpentier, G. (2012). Angiogenesis Analyzer for ImageJ. *ImageJ News*.
- Castagna, M., Takai, Y., Kaibuchi, K., Sano, K., Ushio, K., & Nishizuka, Y. (1982). Direct Activation of Calcium-activated, Phospholipid-dependent Protein Kinase by Tumor-promoting Phorbol Esters. *Science*, 257(13), 7847–7851.
- Cesarman, E., Chang, Y., Moore, P. S., Said, J. W., & Knowles, D. M. (1995). Kaposi's sarcoma-associated herpesvirus-like DNA sequences in AIDS-related body-cavity-based lymphomas. *The New England Journal of Medicine*, 332(18), 1186–1191.
- Chandriani, S., Xu, Y., & Ganem, D. (2010). The Lytic Transcriptome of Kaposi's Sarcoma-Associated Herpesvirus Reveals Extensive Transcription of Noncoding Regions, Including Regions Antisense to Important Genes. *Journal of Virology*, 84(16), 7934–7942.
- Chang, Y., Cesarman, E., Pessin, M. S., Lee, F., Culpepper, J., Knowles, D. M., & Moore, P. S. (1994). Identification of herpesvirus-like DNA sequences in AIDS-associated Kaposi's sarcoma. *Science*, 266(5192), 1865–1869.
- Chen, H. S., De Leo, A., Wang, Z., Kerekovic, A., Hills, R., & Lieberman, P. M. (2017). BET-Inhibitors Disrupt Rad21-Dependent Conformational Control of KSHV Latency. *PLoS Pathogens*, 13(1), 1–22.
- Chen, R. Z., Pettersson, U., Beard, C., Jackson-Grusby, L., & Jaenisch, R. (1998). DNA hypomethylation leads to elevated mutation rates. *Nature*, 395(September), 89–93.
- Cheng, F., Pekkonen, P., Laurinavicius, S., Sugiyama, N., Henderson, S., Günther, T., Rantanen, V., Kaivanto, E., Aavikko, M., Sarek, G., Hautaniemi, S., Biberfeld, P., Aaltonen, L., Grundhoff, A., Boshoff, C., Alitalo, K., Lehti, K., & Ojala, P. M. (2011). KSHV-initiated notch activation leads to membrane-type-1 matrix metalloproteinase-dependent lymphatic endothelial-to-mesenchymal transition. *Cell Host and Microbe*, 10(6), 577–590.
- Christensen, J., Agger, K., Cloos, P. A. C., Pasini, D., Rose, S., Sennels, L., Rappsilber, J., Hansen, K. H., Salcini, A. E., & Helin, K. (2007). RBP2 Belongs to a Family of Demethylases, Specific for Tri- and Dimethylated Lysine 4 on Histone 3. *Cell*, 128(6), 1063–1076.
- Cohen, A., Brodie, C., & Sarid, R. (2006). An essential role of ERK signalling in TPA-induced reactivation of Kaposi's sarcoma-associated herpesvirus. *Journal of General Virology*, 87(4), 795–802.
- Costello, J. F., Frühwald, M. C., Smiraglia, D. J., Rush, L. J., Robertson, G. P., Gao, X., Wright, F. A., Feramisco, J. D., Peltomäki, P., Lang, J. C., Schuller, D. E., Yu, L., Bloomfield, C. D., Caligiuri, M. A., Yates, A., Nishikawa, R., Su Huang, H. J., Petrelli, N. J., Zhang, X., ... Plass, C. (2000). Aberrant CpG-island methylation has non-random and tumour-type-specific patterns. *Nature Genetics*, 24(2), 132–138.

- Creyghton, M. P., Cheng, A. W., Welstead, G. G., Kooistra, T., Carey, B. W., Steine, E. J., Hanna, J., Lodato, M. A., Frampton, G. M., Sharp, P. A., Boyer, L. A., Young, R. A., & Jaenisch, R. (2010). Histone H3K27ac separates active from poised enhancers and predicts developmental state. *Proceedings of the National Academy of Sciences of the United States of America*, *107*(50), 21931–21936.
- Cui, K., Tailor, P., Liu, H., Chen, X., Ozato, K., & Zhao, K. (2004). The Chromatin-Remodeling BAF Complex Mediates Cellular Antiviral Activities by Promoter Priming. *Molecular and Cellular Biology*, *24*(10), 4476–4486.
- Czermin, B., Melfi, R., McCabe, D., Seitz, V., Imhof, A., & Pirrotta, V. (2002). Drosophila enhancer of Zeste/ESC complexes have a histone H3 methyltransferase activity that marks chromosomal Polycomb sites. *Cell*, *111*(2), 185–196.
- D'Urso, A., Takahashi, Y. H., Xiong, B., Marone, J., Coukos, R., Randise-Hinchliff, C., Wang, J. P., Shilatifard, A., & Brickner, J. H. (2016). Set1/COMPASS and mediator are repurposed to promote epigenetic transcriptional memory. *ELife*, *5*(JUN2016), 1–29.
- Dağ, F., Dölken, L., Holzki, J., Drabig, A., Weingärtner, A., Schwerk, J., Lienenklaus, S., Conte, I., Geffers, R., Davenport, C., Rand, U., Köster, M., Weiß, S., Adler, B., Wirth, D., Messerle, M., Hauser, H., & Čičin-Šain, L. (2014). Reversible Silencing of Cytomegalovirus Genomes by Type I Interferon Governs Virus Latency. *PLoS Pathogens*, *10*(2).
- Dahlke, C., Maul, K., Christalla, T., Walz, N., Schult, P., Stocking, C., & Grundhoff, A. (2012). A microRNA Encoded by Kaposi Sarcoma-Associated Herpesvirus Promotes B-Cell Expansion In Vivo. *PLoS ONE*, *7*(11).
- Dai, L., Bai, L., Lin, Z., Qiao, J., Yang, L., Flemington, E. K., Zabaleta, J., & Qin, Z. (2016). Transcriptomic analysis of KSHV-infected primary oral fibroblasts: The role of interferon-induced genes in the latency of oncogenic virus. *Oncotarget*, *7*(30), 47052–47060.
- Dai, L., Del Valle, L., Miley, W., Whitby, D., Ochoa, A. C., Flemington, E. K., & Qin, Z. (2018). Transactivation of human endogenous retrovirus K (HERV-K) by KSHV promotes Kaposi's sarcoma development. *Oncogene*, *37*(33), 4534–4545.
- Dai, X., Gong, D., Wu, T.-T., Sun, R., & Zhou, Z. H. (2014). Organization of Capsid-Associated Tegument Components in Kaposi's Sarcoma-Associated Herpesvirus. *Journal of Virology*, *88*(21), 12694–12702.
- Datta, R., Yoshinaga, K., Kaneki, M., Pandey, P., & Kufe, D. (2000). Phorbol ester-induced generation of reactive oxygen species is protein kinase C β -dependent and required for SAPK activation. *Journal of Biological Chemistry*, *275*(52), 41000–41003.
- Davis, D. A., Rinderknecht, A. S., Paul Zoetewij, J., Aoki, Y., Read-Connole, E. L., Tosato, G., Blauvelt, A., & Yarchoan, R. (2001). Hypoxia induces lytic replication of Kaposi sarcoma-associated herpesvirus. *Blood*, *97*(10), 3244–3250.
- Davis, H. E., Morgan, J. R., & Yarmush, M. L. (2002). Polybrene increases retrovirus gene transfer efficiency by enhancing receptor-independent virus adsorption on target cell membranes. *Biophysical Chemistry*, *97*(2–3), 159–172.
- de Napoles, M., Mermoud, J. E., Wakao, R., Tang, Y. A., Endoh, M., Appanah, R., Nesterova, T. B., Silva, J., Otte, A. P., Vidal, M., Koseki, H., & Brockdorff, N. (2004). Polycomb group proteins ring1A/B link ubiquitylation of histone H2A to heritable gene silencing and X inactivation. *Developmental Cell*, *7*(5), 663–676.
- Dedicoat, M., Newton, R., Alkharsah, K. R., Sheldon, J., Szabados, I., Ndlovu, B., Page, T., Casabonne, D., Gilks, C. F., Cassol, S. A., Whitby, D., & Schulz, T. F. (2004). Mother-to-child transmission of human herpesvirus-8 in South Africa. *Journal of Infectious Diseases*, *190*(6), 1068–1075.
- Deng, Binbin; O'Connor, Christine M.; Kedes, Dean H.; Zhou, H. Z. (2008). Cryo-electron tomography of Kaposi's sarcoma-associated herpesvirus capsids reveals dynamic scaffolding structures essential to capsid assembly and maturation. *Journal of Structural Biology*, *161*(3), 419–427.
- Di Bartolo, D. L., Cannon, M., Liu, Y. F., Renne, R., Chadburn, A., Boshoff, C., & Cesarman, E. (2008). KSHV LANA inhibits TGF- β signaling through epigenetic silencing of the TGF- β type II receptor. *Blood*, *111*(9), 4731–4740.
- Diamond, C., Huang, M. L., Kedes, D. H., Speck, C., Rankin, G. W., Ganem, D., Coombs, R. W., Rose, T. M., Krieger, J. N., & Corey, L. (1997). Absence of detectable human herpesvirus 8 in the semen of human immunodeficiency virus - Infected men without Kaposi's Sarcoma. *Journal of Infectious Diseases*, *176*(3), 775–777.
- Ding, Y., Fromm, M., & Avramova, Z. (2012). Multiple exposures to drought “train” transcriptional responses in Arabidopsis. *Nature Communications*, *3*.
- Dittmer, D., Lagunoff, M., Renne, R., Staskus, K., Haase, A., & Ganem, D. (1998). A Cluster of Latently Expressed Genes in Kaposi's Sarcoma-Associated Herpesvirus. *Journal of Virology*, *72*(10), 8309–8315.

- Dobin, A., Davis, C. A., Schlesinger, F., Drenkow, J., Zaleski, C., Jha, S., Batut, P., Chaisson, M., & Gingeras, T. R. (2013). STAR: Ultrafast universal RNA-seq aligner. *Bioinformatics*, 29(1), 15–21.
- Dolan, A., Cunningham, C., Hector, R. D., Hassan-Walker, A. F., Lee, L., Addison, C., Dargan, D. J., McGeoch, D. J., Gatherer, D., Emery, V. C., Griffiths, P. D., Sinzger, C., McSharry, B. P., Wilkinson, G. W. G., & Davison, A. J. (2004). Genetic content of wild-type human cytomegalovirus. *Journal of General Virology*, 85(5), 1301–1312.
- Dollard, S. C., Nelson, K. E., Ness, P. M., Stambolis, V., Kuehnert, M. J., Pellett, P. E., & Cannon, M. J. (2005). Possible transmission of human herpesvirus-8 by blood transfusion in a historical United States cohort. *Transfusion*, 45(4), 500–503.
- Douglas, J., Dutia, B., Rhind, S., Stewart, J. P., & Talbot, S. J. (2004). Expression in a Recombinant Murid Herpesvirus 4 Reveals the In Vivo Transforming Potential of the K1 Open Reading Frame of Kaposi's Sarcoma-Associated Herpesvirus. *Journal of Virology*, 78(16), 8878–8884.
- Dupin, N., Fisher, C., Kellam, P., Ariad, S., Tulliez, M., Franck, N., Van Marck, E., Salmon, D., Gorin, I., Escande, J. P., Weiss, R. A., Alitalo, K., & Boshoff, C. (1999). Distribution of human herpesvirus-8 latently infected cells in Kaposi's sarcoma, multicentric Castlemans's disease, and primary effusion lymphoma. *Proceedings of the National Academy of Sciences of the United States of America*, 96(8), 4546–4551.
- Esteller, M., Corn, P. G., Baylin, S. B., & Herman, J. G. (2001). A gene hypermethylation profile of human cancer. *Cancer Research*, 61(8), 3225–3229.
- Fakhari, F. D., & Dittmer, D. P. (2002). Charting Latency Transcripts in Kaposi's Sarcoma-Associated Herpesvirus by Whole-Genome Real-Time Quantitative PCR. *Journal of Virology*, 76(12), 6213–6223.
- Fang, J., Chen, T., Chadwick, B., Li, E., & Zhang, Y. (2004). Ring1b-mediated H2A ubiquitination associates with inactive X chromosomes and is involved in initiation of X inactivation. *Journal of Biological Chemistry*, 279(51), 52812–52815.
- Fang, R., Barbera, A. J., Xu, Y., Rutenberg, M., Leonor, T., Bi, Q., Lan, F., Mei, P., Yuan, G. C., Lian, C., Peng, J., Cheng, D., Sui, G., Kaiser, U. B., Shi, Y., & Shi, Y. G. (2010). Human LSD2/KDM1b/AOF1 regulates gene transcription by modulating intragenic H3K4me2 Methylation. *Molecular Cell*, 39(2), 222–233.
- Farley, C. Austin; Banfield, William G; Kasnic Jr, George; Foster, W. S. (1972). Oyster Herpes-Type Virus. *Science*, 178(4062).
- Fatemi, M., Hermann, A., Pradhan, S., & Jeltsch, A. (2001). The activity of the murine DNA methyltransferase Dnmt1 is controlled by interaction of the catalytic domain with the N-terminal part of the enzyme leading to an allosteric activation of the enzyme after binding to methylated DNA. *Journal of Molecular Biology*, 309(5), 1189–1199.
- Field, A., & Adelman, K. (2020). Evaluating Enhancer Function and Transcription. *Annual Review of Biochemistry*, 89, 213–234.
- Fischle, W., Wang, Y., Jacobs, S. A., Kim, Y., Allis, C. D., & Khorasanizadeh, S. (2003). Molecular basis for the discrimination of repressive methyl-lysine marks in histone H3 by polycomb and HP1 chromodomains. *Genes and Development*, 17(15), 1870–1881.
- Francès, C., Marcelin, A. G., Legendre, C., Chevret, S., Dussaix, E., Lejeune, J., Euvrard, S., Bigorie, A., Schulz, T. F., Agbalika, F., & Lebbé, C. (2009). The impact of preexisting or acquired kaposi sarcoma herpesvirus infection in kidney transplant recipients on morbidity and survival. *American Journal of Transplantation*, 9(11), 2580–2586.
- Friborg, J., Kong, W. P., Hottlger, M. O., & Nabel, G. J. (1999). p53 Inhibition by the LANA protein of KSHV protects against cell death. *Nature*, 402(6764), 889–894.
- Fuld, S., Cunningham, C., Klucher, K., Davison, A. J., & Blackbourn, D. J. (2006). Inhibition of Interferon Signaling by the Kaposi's Sarcoma-Associated Herpesvirus Full-Length Viral Interferon Regulatory Factor 2 Protein. *Journal of Virology*, 80(6), 3092–3097.
- Gallo, R. C. (1998). The Enigmas of Kaposi's Sarcoma. *Science*, 282(5395), 1837–1839.
- Gao, S.-J., Kingsley, L., Li, M., Zheng, W., Parravicini, C., Ziegler, J., Newton, R., Rinaldo, C. R., Saah, A., Phair, J., Detels, R., Chang, Y., & Moore, P. S. (1996). KSHV antibodies among Americans, Italians and Ugandans with and without Kaposi's sarcoma. *Nature Medicine*, 2(8), 925–928.
- Garber, A. C., Hu, J., & Renne, R. (2002). Latency-associated nuclear antigen (LANA) cooperatively binds to two sites within the terminal repeat, and both sites contribute to the ability of LANA to suppress transcription and to facilitate DNA replication. *Journal of Biological Chemistry*, 277(30), 27401–27411.
- Garrigues, H. J., Rubinchikova, Y. E., DiPersio, C. M., & Rose, T. M. (2008). Integrin $\alpha\text{V}\beta\text{3}$ Binds to the RGD Motif of Glycoprotein B of Kaposi's Sarcoma-Associated Herpesvirus and Functions as an RGD-Dependent Entry Receptor. *Journal of Virology*, 82(3), 1570–1580.
- Gibson, D. G., Young, L., Chuang, R. Y., Venter, J. C., Hutchison, C. A., & Smith, H. O. (2009).

- Enzymatic assembly of DNA molecules up to several hundred kilobases. *Nature Methods*, 6(5), 343–345.
- Gill, P. S., Tsai, Y. C., Rao, A. P., Spruck, C. H., Zheng, T., Harrington, W. A., Cheung, T., Nathwani, B., & Jones, P. A. (1998). Evidence for multiclonality in multicentric Kaposi's sarcoma. *Proceedings of the National Academy of Sciences of the United States of America*, 95(14), 8257–8261.
- Godden-Kent, D., Talbot, S. J., Boshoff, C., Chang, Y., Moore, P., Weiss, R. A., & Mittnacht, S. (1997). The cyclin encoded by Kaposi's sarcoma-associated herpesvirus stimulates cdk6 to phosphorylate the retinoblastoma protein and histone H1. *Journal of Virology*, 71(6), 4193–4198.
- Gong, D., Kim, Y. H., Xiao, Y., Du, Y., Xie, Y., Lee, K. K., Feng, J., Farhat, N., Zhao, D., Shu, S., Dai, X., Chanda, S. K., Rana, T. M., Krogan, N. J., Sun, R., & Wu, T.-T. (2016). A herpesvirus protein selectively inhibits cellular mRNA nuclear export. *Cell Host Microbe*, 20(5), 642–653.
- Gottwein, E., Cai, X., & Cullen, B. R. (2006). Expression and function of microRNAs encoded by kaposi's sarcoma-associated herpesvirus. *Cold Spring Harbor Symposia on Quantitative Biology*, 71, 357–364.
- Gottwein, Eva, & Cullen, B. R. (2010). A Human Herpesvirus MicroRNA Inhibits p21 Expression and Attenuates p21-Mediated Cell Cycle Arrest. *Journal of Virology*, 84(10), 5229–5237.
- Gottwein, Eva, Mukherjee, N., Sachse, C., Frenzel, C., Majoros, W. H., Chi, J. T. A., Braich, R., Manoharan, M., Soutschek, J., Ohler, U., & Cullen, B. R. (2007). A viral microRNA functions as an orthologue of cellular miR-155. *Nature*, 450(7172), 1096–1099.
- Gramolelli, S., Weidner-Glunde, M., Aberer, B., Viejo-Borbolla, A., Bala, K., Rückert, J., Kremmer, E., & Schulz, T. F. (2015). Inhibiting the Recruitment of PLCy1 to Kaposi's Sarcoma Herpesvirus K15 Protein Reduces the Invasiveness and Angiogenesis of Infected Endothelial Cells. *PLoS Pathogens*, 11(8), 1–28.
- Greger, V., Passarge, E., Höpping, W., Messmer, E., & Horsthemke, B. (1989). Epigenetic changes may contribute to the formation and spontaneous regression of retinoblastoma. *Human Genetics*, 83(2), 155–158.
- Grossmann, C., Podgrabinska, S., Skobe, M., & Ganem, D. (2006). Activation of NF- κ B by the Latent vFLIP Gene of Kaposi's Sarcoma-Associated Herpesvirus Is Required for the Spindle Shape of Virus-Infected Endothelial Cells and Contributes to Their Proinflammatory Phenotype. *Journal of Virology*, 80(14), 7179–7185.
- Grundhoff, A., & Ganem, D. (2003). The Latency-Associated Nuclear Antigen of Kaposi's Sarcoma-Associated Herpesvirus Permits Replication of Terminal Repeat-Containing Plasmids. *Journal of Virology*, 77(7), 4470–4470.
- Grundhoff, A., & Ganem, D. (2004a). Inefficient establishment of KSHV latency suggests an additional role for continued lytic replication in Kaposi sarcoma pathogenesis. *Journal of Clinical Investigation*, 113(1), 124–136.
- Grundhoff, A., & Ganem, D. (2004b). Inefficient establishment of KSHV latency suggests an additional role for continued lytic replication in Kaposi sarcoma pathogenesis. *Journal of Clinical Investigation*, 113(1), 124–136.
- Grundhoff, A., Sullivan, C. S., & Ganem, D. (2006). A combined computational and microarray-based approach identifies novel microRNAs encoded by human gamma-herpesviruses. *Rna*, 12(5), 733–750.
- Guasparri, I., Keller, S. A., & Cesarman, E. (2004). KSHV vFLIP Is Essential for the Survival of Infected Lymphoma Cells. *Journal of Experimental Medicine*, 199(7), 993–1003.
- Günther, T., Fröhlich, J., Herrde, C., Ohno, S., Burkhardt, L., Adler, H., & Grundhoff, A. (2019). A comparative epigenome analysis of gammaherpesviruses suggests cis-acting sequence features as critical mediators of rapid polycomb recruitment. In *PLoS Pathogens* (Vol. 15, Issue 10).
- Günther, T., & Grundhoff, A. (2010). The epigenetic landscape of latent kaposi sarcoma-associated herpesvirus genomes. *PLoS Pathogens*, 6(6).
- Günther, T., Schreiner, S., Dobner, T., Tessmer, U., & Grundhoff, A. (2014). Influence of ND10 Components on Epigenetic Determinants of Early KSHV Latency Establishment. *PLoS Pathogens*, 10(7), e1004274.
- Guo, J. U., Su, Y., Shin, J. H., Shin, J., Li, H., Xie, B., Zhong, C., Hu, S., Le, T., Fan, G., Zhu, H., Chang, Q., Gao, Y., Ming, G. L., & Song, H. (2014). Distribution, recognition and regulation of non-CpG methylation in the adult mammalian brain. *Nature Neuroscience*, 17(2), 215–222.
- Haas, D. A., Bala, K., Büsche, G., Weidner-Glunde, M., Santag, S., Kati, S., Gramolelli, S., Damas, M., Dittrich-Breiholz, O., Kracht, M., Rückert, J., Varga, Z., Keri, G., & Schulz, T. F. (2013). The Inflammatory Kinase MAP4K4 Promotes Reactivation of Kaposi's Sarcoma Herpesvirus and Enhances the Invasiveness of Infected Endothelial Cells. *PLoS Pathogens*, 9(11).
- Hackett, J. A., Sengupta, R., Zyllicz, J. J., Murakami, K., Lee, C., Down, T. A., & Surani, M. A. (2013). Germline DNA Demethylation Dynamics and Imprint Erasure Through 5-Hydroxymethylcytosine.

- Science*, 339(January), 448–453.
- Hahn, A., Birkmann, A., Wies, E., Dorer, D., Mahr, K., Stürzl, M., Titgemeyer, F., & Neipel, F. (2009). Kaposi's Sarcoma-Associated Herpesvirus gH/gL: Glycoprotein Export and Interaction with Cellular Receptors. *Journal of Virology*, 83(1), 396–407.
- Hahn, A. S., Kaufmann, J. K., Wies, E., Naschberger, E., Panteleev-Ivlev, J., Schmidt, K., Holzer, A., Schmidt, M., Chen, J., König, S., Ensser, A., Myoung, J., Brockmeyer, N. H., Stürzl, M., Fleckenstein, B., & Neipel, F. (2012). The ephrin receptor tyrosine kinase A2 is a cellular receptor for Kaposi's sarcoma-associated herpesvirus. *Nature Medicine*, 18(6), 961–966.
- He, M., Zhang, W., Bakken, T., Schutten, M., Toth, Z., Jung, J. U., Gill, P., Cannon, M., & Gao, S.-J. (2012). Cancer angiogenesis induced by Kaposi's sarcoma-associated herpesvirus is mediated by EZH2. *Cancer Research*, 72(14), 3582–3592.
- He, Y.-F., Bin-Zhong, L., Zheng, L., Liu, P., Wang, Y., Tang, Q., Ding, J., Jia, Y., Chen, Z., Li, L., Sun, Y., Li, X., Dai, Q., Song, C.-X., Zhang, K., He, C., & Xu, G.-L. (2011). Tet-Mediated Formation of 5-Carboxylcytosine and Its Excision by TDG in Mammalian DNA. *Science*, 333(September), 1303–1308.
- Heintzman, N. D., Hon, G. C., Hawkins, R. D., Kheradpour, P., Stark, A., Harp, L. F., Ye, Z., Lee, L. K., Stuart, R. K., Ching, C. W., Ching, K. A., Antosiewicz-Bourget, J. E., Liu, H., Zhang, X., Green, R. D., Lobanenkov, V. V., Stewart, R., Thomson, J. A., Crawford, G. E., ... Ren, B. (2009). Histone modifications at human enhancers reflect global cell-type-specific gene expression. *Nature*, 459(7243), 108–112.
- Hellert, J., Weidner-Glunde, M., Krausze, J., Lünsdorf, H., Ritter, C., Schulz, T. F., & Lührs, T. (2015). The 3D structure of Kaposi sarcoma herpesvirus LANA C-terminal domain bound to DNA. *Proceedings of the National Academy of Sciences of the United States of America*, 112(21), 6694–6699.
- Hermann, A., Goyal, R., & Jeltsch, A. (2004). The Dnmt1 DNA-(cytosine-C5)-methyltransferase methylates DNA processively with high preference for hemimethylated target sites. *Journal of Biological Chemistry*, 279(46), 48350–48359.
- Hernando, H., Islam, A. B. M. M. K., Rodríguez-Ubreva, J., Forné, I., Ciudad, L., Imhof, A., Shannon-Lowe, C., & Ballestar, E. (2014). Epstein-Barr virus-mediated transformation of B cells induces global chromatin changes independent of the acquisition of proliferation. *Nucleic Acids Research*, 42(1), 249–263.
- Herz, H. M., Mohan, M., Garruss, A. S., Liang, K., Takahashi, Y. hei, Mickey, K., Voets, O., Verrijzer, C. P., & Shilatifard, A. (2012). Enhancer-associated H3K4 monomethylation by trithorax-related, the drosophila homolog of mammalian MLL3/MLL4. *Genes and Development*, 26(23), 2604–2620.
- Hill, J. J., Tremblay, T. L., Pen, A., Li, J., Robotham, A. C., Lenferink, A. E. G., Wang, E., O'connor-Mccourt, M., & Kelly, J. F. (2011). Identification of vascular breast tumor markers by laser capture microdissection and label-free LC-MS. *Journal of Proteome Research*, 10(5), 2479–2493.
- Hollyoake, M., Stühler, A., Farrell, P., Sinclair, A., & Gordon, J. (1995). The Normal Cell Cycle Activation Program Is Exploited during the Infection of Quiescent B Lymphocytes by Epstein-Barr Virus. *Cancer Research*, 55(21), 4784–4787.
- Hong, Y. K., Foreman, K., Shin, J. W., Hirakawa, S., Curry, C. L., Sage, D. R., Libermann, T., Dezube, B. J., Fingerhuth, J. D., & Detmar, M. (2004). Lymphatic reprogramming of blood vascular endothelium by Kaposi sarcoma-associated herpesvirus. *Nature Genetics*, 36(7), 683–685.
- Howard, M. R., Whitby, D., Bahadur, G., Suggett, F., Boshoff, C., Tenant-Flowers, M., Schulz, T. F., Kirk, S., Matthews, S., Weller, I. V.D., Tedder, R. S., & Weiss, R. A. (1997). Detection of human herpesvirus 8 DNA in semen from HIV-infected individuals but not healthy semen donors. *Aids*, 11(2), 15–19.
- Hu, D., Gao, X., Morgan, M. A., Herz, H.-M., Smith, E. R., & Shilatifard, A. (2013). The MLL3/MLL4 Branches of the COMPASS Family Function as Major Histone H3K4 Monomethylases at Enhancers. *Molecular and Cellular Biology*, 33(23), 4745–4754.
- Hu, Deqing, Garruss, A. S., Gao, X., Morgan, M. A., Cook, M., Smith, E. R., & Shilatifard, A. (2013). The Mll2 branch of the COMPASS family regulates bivalent promoters in mouse embryonic stem cells. *Nature Structural and Molecular Biology*, 20(9), 1093–1097.
- Hu, J., Garber, A. C., & Renne, R. (2002). The Latency-Associated Nuclear Antigen of Kaposi's Sarcoma-Associated Herpesvirus Supports Latent DNA Replication in Dividing Cells. *Journal of Virology*, 76(22), 11677–11687.
- Hu, J., Yang, Y., Turner, P. C., Jain, V., McIntyre, L. M., & Renne, R. (2014). LANA Binds to Multiple Active Viral and Cellular Promoters and Associates with the H3K4Methyltransferase hSET1 Complex. *PLoS Pathogens*, 10(7).
- Hu, L., Lu, J., Cheng, J., Rao, Q., Li, Z., Hou, H., Lou, Z., Zhang, L., Li, W., Gong, W., Liu, M., Sun, C.,

- Yin, X., Li, J., Tan, X., Wang, P., Wang, Y., Fang, D., Cui, Q., ... Xu, Y. (2015). Structural insight into substrate preference for TET-mediated oxidation. *Nature*, 527(7576), 118–122.
- Huang, D. W., Sherman, B. T., Tan, Q., Collins, J. R., Alvord, W. G., Roayaei, J., Stephens, R., Baseler, M. W., Lane, H. C., & Lempicki, R. A. (2007). The DAVID Gene Functional Classification Tool: A novel biological module-centric algorithm to functionally analyze large gene lists. *Genome Biology*, 8(9).
- Ito, S., Shen, L., Dai, Q., Wu, S. C., Collins, L. B., Swenberg, J. A., He, C., & Zhang, Y. (2011). Tet proteins can convert 5-methylcytosine to 5-formylcytosine and 5-carboxylcytosine. *Science*, 333(6047), 1300–1303.
- Jarousse, N., Chandran, B., & Coscoy, L. (2008). Lack of Heparan Sulfate Expression in B-Cell Lines: Implications for Kaposi's Sarcoma-Associated Herpesvirus and Murine Gammaherpesvirus 68 Infections. *Journal of Virology*, 82(24), 12591–12597.
- Jenner, R. G., Maillard, K., Cattini, N., Weiss, R. A., Boshoff, C., Wooster, R., & Kellam, P. (2003). Kaposi's sarcoma-associated herpesvirus-infected primary effusion lymphoma has a plasma cell gene expression profile. *Proceedings of the National Academy of Sciences of the United States of America*, 100(18), 10399–10404.
- Jin, Q., Yu, L. R., Wang, L., Zhang, Z., Kasper, L. H., Lee, J. E., Wang, C., Brindle, P. K., Dent, S. Y. R., & Ge, K. (2011). Distinct roles of GCN5/PCAF-mediated H3K9ac and CBP/p300-mediated H3K18/27ac in nuclear receptor transactivation. *EMBO Journal*, 30(2), 249–262.
- Joo, C. H., Shin, Y. C., Gack, M., Wu, L., Levy, D., & Jung, J. U. (2007). Inhibition of Interferon Regulatory Factor 7 (IRF7)-Mediated Interferon Signal Transduction by the Kaposi's Sarcoma-Associated Herpesvirus Viral IRF Homolog vIRF3. *Journal of Virology*, 81(15), 8282–8292.
- Journo, G., Tushinsky, C., Shterngas, A., Avital, N., Eran, Y., Karpuj, M. V., Frenkel-Morgenstern, M., & Shamay, M. (2018). Modulation of Cellular CpG DNA Methylation by Kaposi's Sarcoma-Associated Herpesvirus. *Journal of Virology*, 92(16), 1–19.
- Jussila, L., Valtola, R., Partanen, T. A., Salven, P., Heikkilä, P., Matikainen, M. T., Renkonen, R., Kaipainen, A., Detmar, M., Tschachler, E., Alitalo, R., & Alitalo, K. (1998). Lymphatic endothelium and Kaposi's sarcoma spindle cells detected by antibodies against the vascular endothelial growth factor receptor-3. *Cancer Research*, 58(8), 1599–1604.
- Kaleeba, Johnan A.R.; Berger, E. A. (2006). Kaposi's Sarcoma-Associated Herpesvirus Fusion-Entry Receptor: Cystine Transporter xCT. *Science*, 311(5769), 1921–1924.
- Kaneda, M., Okano, M., Hata, K., Sado, T., Tsujimoto, H., Li, E., & Sasaki, H. (2004). Essential role for de novo DNA methyltransferase Dnmt3a in paternal and maternal imprinting. *Nature*, 429(6994), 900–903.
- Kang, H., Wiedmer, A., Yuan, Y., Robertson, E., & Lieberman, P. M. (2011). Coordination of KSHV latent and lytic gene control by CTCF-cohesin mediated chromosome conformation. *PLoS Pathogens*, 7(8).
- Kaposi, M. (1872). Idiopathisches multiples Pigmentsarkom der Haut. *Arch. Dermatol. Syph.*
- Karlič, R., Chung, H. R., Lasserre, J., Vlahoviček, K., & Vingron, M. (2010). Histone modification levels are predictive for gene expression. *Proceedings of the National Academy of Sciences of the United States of America*, 107(7), 2926–2931.
- Karmodiya, K., Krebs, A. R., Oulad-Abdelghani, M., Kimura, H., & Tora, L. (2012). H3K9 and H3K14 acetylation co-occur at many gene regulatory elements, while H3K14ac marks a subset of inactive inducible promoters in mouse embryonic stem cells. *BMC Genomics*, 13(1).
- Karsten Tischer, B., Smith, G. A., & Osterrieder, N. (2010). En passant mutagenesis: A Two Markerless red recombination system. *Methods in Molecular Biology*.
- Katano, H., Sato, Y., Kurata, T., Mori, S., & Sata, T. (2000). Expression and localization of human herpesvirus 8-encoded proteins in primary effusion lymphoma, Kaposi's sarcoma, and multicentric Castleman's disease. *Virology*, 269(2), 335–344.
- Kawai, T., & Akira, S. (2011). Toll-like Receptors and Their Crosstalk with Other Innate Receptors in Infection and Immunity. *Immunity*, 34(5), 637–650.
- Kedes, D. H., Operskalski, E., Busch, M., Kohn, R., Flood, J., & Ganem, D. (1996). The seroepidemiology of human herpesvirus 8 (Kaposi's sarcoma-associated herpesvirus): Distribution of infection in KS risk groups and evidence for sexual transmission. *Nature Medicine*, 2(8), 918–924.
- Keller, S. A., Schattner, E. J., & Cesarman, E. (2000). Inhibition of NF- κ B induces apoptosis of KSHV-infected primary effusion lymphoma cells. *Blood*, 96(7), 2537–2542.
- Kelley-Clarke, B., Ballestas, M. E., Srinivasan, V., Barbera, A. J., Komatsu, T., Harris, T.-A., Kazanjian, M., & Kaye, K. M. (2007). Termination of Kaposi's Sarcoma-Associated Herpesvirus C-Terminal Latency-Associated Nuclear Antigen Residues Mediating Chromosome Association and DNA Binding. *Journal of Virology*, 81(8), 4348–4356.
- Kerur, N., Veettil, M. V., Sharma-Walia, N., Bottero, V., Sadagopan, S., Otageri, P., & Chandran, B.

- (2011). IFI16 acts as a nuclear pathogen sensor to induce the inflammasome in response to Kaposi sarcoma associated herpesvirus infection. *Cell Host Microbe*, 9(5), 363–375.
- Kilger, E., Kieser, A., Baumann, M., & Hammerschmidt, W. (1998). Epstein-Barr virus-mediated B-cell proliferation is dependent upon latent membrane protein 1, which simulates an activated CD40 receptor. *EMBO Journal*, 17(6), 1700–1709.
- Kim, J. S., Han, J., Shim, Y. M., Park, J., & Kim, D. H. (2005). Aberrant methylation of H-cadherin (CDH13) promoter is associated with tumor progression in primary nonsmall cell lung carcinoma. *Cancer*, 104(9), 1825–1833.
- Kim, K. Y., Huerta, S. B., Izumiya, C., Wang, D.-H., Martinez, A., Shevchenko, B., Kung, H.-J., Campbell, M., & Izumiya, Y. (2013). Kaposi's Sarcoma-Associated Herpesvirus (KSHV) Latency-Associated Nuclear Antigen Regulates the KSHV Epigenome by Association with the Histone Demethylase KDM3A. *Journal of Virology*, 87(12), 6782–6793.
- Kim, S. H., Cohen, B., Novick, D., & Rubinstein, M. (1997). Mammalian type I interferon receptors consists of two subunits: IFNaR1 and IFNaR2. *Gene*, 196(1–2), 279–286.
- Klein, U., Ghoghini, A., Gaidano, G., Chadburn, A., Cesarman, E., Dalla-Favera, R., & Carbone, A. (2003). Gene expression profile analysis of AIDS-related primary effusion lymphoma (PEL) suggests a plasmablastic derivation and identifies PEL-specific transcripts. *Blood*, 101(10), 4115–4121.
- Koelle, D. M., Huang, M. L., Chandran, B., Vieira, J., Piepkorn, M., & Corey, L. (1997). Frequent detection of Kaposi's sarcoma-associated herpesvirus (human herpesvirus 8) DNA in saliva of human immunodeficiency virus-infected men: Clinical and immunologic correlates. *Journal of Infectious Diseases*, 176(1), 94–102.
- Kornberg, R. D. (1974). Chromatin Structure : A Repeating Unit of Histones and DNA. *Science*, 184, 868–871.
- Kornberg, R. D., & Thomas, J. O. (1974). Chromatin Structure : Oligomers of the Histones. *Science*, 184, 865–868.
- Krebs, A. R., Dessus-Babus, S., Burger, L., & Schübeler, D. (2014). High-throughput engineering of a mammalian genome reveals building principles of methylation states at CG rich regions. *ELife*, 3, e04094.
- Krishnan, H. H., Naranatt, P. P., Smith, M. S., Zeng, L., Bloomer, C., & Chandran, B. (2004). Concurrent Expression of Latent and a Limited Number of Lytic Genes with Immune Modulation and Antiapoptotic Function by Kaposi's Sarcoma-Associated Herpesvirus Early during Infection of Primary Endothelial and Fibroblast Cells and Subsequent Decline of L. *Journal of Virology*, 78(7), 3601–3620.
- Kuzmichev, A., Nishioka, K., Erdjument-Bromage, H., Tempst, P., & Reinberg, D. (2002). Histone methyltransferase activity associated with a human multiprotein complex containing the enhancer of zeste protein. *Genes and Development*, 16(22), 2893–2905.
- Lachner, M., O'Carroll, D., Rea, S., Mechtler, K., & Jenuwein, T. (2001). Methylation of histone H3 lysine 9 creates a binding site for HP1 proteins. *Nature*, 410(6824), 116–120.
- Lagunoff, M., & Ganem, D. (1997). The structure and coding organization of the genomic termini of Kaposi's sarcoma-associated herpesvirus (human herpesvirus 8). *Virology*, 236(1), 147–154.
- Lan, F., Bayliss, P. E., Rinn, J. L., Whetstone, J. R., Wang, J. K., Chen, S., Iwase, S., Alpatov, R., Issaeva, I., Canaani, E., Roberts, T. M., Chang, H. Y., & Shi, Y. (2007). A histone H3 lysine 27 demethylase regulates animal posterior development. *Nature*, 449(7163), 689–694.
- Lan, K., Koppers, D. A., Verma, S. C., & Robertson, E. S. (2004). Kaposi's Sarcoma-Associated Herpesvirus-Encoded Latency-Associated Nuclear Antigen Inhibits Lytic Replication by Targeting Rta: a Potential Mechanism for Virus-Mediated Control of Latency. *Journal of Virology*, 78(12), 6585–6594.
- Lang, F., Sun, Z., Pei, Y., Singh, R. K., Jha, H. C., & Robertson, E. S. (2018). Shugoshin 1 is dislocated by KSHV-encoded LANA inducing aneuploidy. *PLoS Pathogens*, 14(9), 1–22.
- Langmead, B., Trapnell, C., Pop, M., & Salzberg, S. L. (2009). Ultrafast and memory-efficient alignment of short DNA sequences to the human genome. *Genome Biology*, 10(3).
- Lee, H. R., Li, F., Choi, U. Y., Yu, H. R., Aldrovandi, G. M., Feng, P., Gao, S. J., Hong, Y. K., & Jung, J. U. (2018). Deregulation of HDAC5 by viral interferon regulatory factor 3 plays an essential role in kaposi's sarcoma-associated herpesvirus-induced lymphangiogenesis. *MBio*, 9(1), 1–12.
- Lee, J. E., Wang, C., Xu, S., Cho, Y. W., Wang, L., Feng, X., Baldrige, A., Sartorelli, V., Zhuang, L., Peng, W., & Ge, K. (2013). H3K4 mono- And di-methyltransferase MLL4 is required for enhancer activation during cell differentiation. *ELife*, 2013(2), 1–25.
- Lee, J. H., Tate, C. M., You, J. S., & Skalik, D. G. (2007). Identification and characterization of the human Set1B histone H3-Lys 4 methyltransferase complex. *Journal of Biological Chemistry*, 282(18), 13419–13428.
- Lennette, E. T., Blackbourn, D. J., & Levy, J. A. (1996). Antibodies to human herpesvirus type 8 in the

- general population and in Kaposi's sarcoma patients. *Lancet*, 348(9031), 858–861.
- Leong, M. M. L., Cheung, A. K. L., Dai, W., Tsao, S. W., Tsang, C. M., Dawson, C. W., Ko, J. M. Y., & Lung, M. L. (2019). EBV infection is associated with histone bivalent switch modifications in squamous epithelial cells. *Proceedings of the National Academy of Sciences of the United States of America*, 116(28), 14144–14153.
- Leonhardt, H., Page, A. W., Weier, H. U., & Bestor, T. H. (1992). A targeting sequence directs DNA methyltransferase to sites of DNA replication in mammalian nuclei. *Cell*, 71(5), 865–873.
- Lerdrup, M., Johansen, J. V., Agrawal-Singh, S., & Hansen, K. (2016). An interactive environment for agile analysis and visualization of ChIP-sequencing data. *Nature Structural and Molecular Biology*, 23(4), 349–357.
- Li, D., & Swaminathan, S. (2019). Human IFIT proteins inhibit lytic replication of KSHV: A new feed-forward loop in the innate immune system. *PLoS Pathogens*, 15(2), 1–27.
- Li, K., Liu, Y., Cao, H., Zhang, Y., Gu, Z., Liu, X., Yu, A., Kaphle, P., Dickerson, K. E., Ni, M., & Xu, J. (2020). Interrogation of enhancer function by enhancer-targeting CRISPR epigenetic editing. *Nature Communications*, 11(1), 1–16.
- Li, M., Lee, H., Guo, J., Neipel, F., Fleckenstein, B., Ozato, K., & Jung, J. U. (1998). Kaposi's Sarcoma-Associated Herpesvirus Viral Interferon Regulatory Factor. *Journal of Virology*, 72(7), 5433–5440.
- Li, W., Jia, X., Shen, C., Zhang, M., Xu, J., Shang, Y., Zhu, K., Hu, M., Yan, Q., Qin, D., Lee, M. S., Zhu, J., Lu, H., Krueger, B. J., Renne, R., Gao, S. J., & Lu, C. (2016). A KSHV microRNA enhances viral latency and induces angiogenesis by targeting GRK2 to activate the CXCR2/AKT pathway. *Oncotarget*, 7(22), 32286–32305.
- Li, W., Wang, Q., Feng, Q., Wang, F., Yan, Q., Gao, S. J., & Lu, C. (2019). Oncogenic KSHV-encoded interferon regulatory factor upregulates HMGB2 and CMPK1 expression to promote cell invasion by disrupting a complex lncRNA-OIP5-AS1/miR-218-5p network. *PLoS Pathogens*, 15(1).
- Liang, Y., Chang, J., Lynch, S. J., Lukac, D. M., & Ganem, D. (2002). The lytic switch protein of KSHV activates gene expression via functional interaction with RBP-J κ (CSL), the target of the Notch signaling pathway. *Genes and Development*, 16(15), 1977–1989.
- Liao, Y., Smyth, G. K., & Shi, W. (2014). FeatureCounts: An efficient general purpose program for assigning sequence reads to genomic features. *Bioinformatics*, 30(7), 923–930.
- Lieberman, P. M. (2013). Keeping it quiet: Chromatin control of gammaherpesvirus latency. *Nature Reviews Microbiology*, 11(12), 863–875.
- Light, W. H., Freaney, J., Sood, V., Thompson, A., D'Urso, A., Horvath, C. M., & Brickner, J. H. (2013). A Conserved Role for Human Nup98 in Altering Chromatin Structure and Promoting Epigenetic Transcriptional Memory. *PLoS Biology*, 11(3).
- Lim, C., Lee, D., Seo, T., Choi, C., & Choe, J. (2003). Latency-associated nuclear antigen of Kaposi's sarcoma-associated herpesvirus functionally interacts with heterochromatin protein 1. *Journal of Biological Chemistry*, 278(9), 7397–7405.
- Lim, S., Janzer, A., Becker, A., Zimmer, A., Schüle, R., Buettner, R., & Kirfel, J. (2010). Lysine-specific demethylase 1 (LSD1) is highly expressed in ER-negative breast cancers and a biomarker predicting aggressive biology. *Carcinogenesis*, 31(3), 512–520.
- Lin, C. L., Li, H., Wang, Y., Zhu, F. X., Kudchodkar, S., & Yuan, Y. (2003). Kaposi's Sarcoma-Associated Herpesvirus Lytic Origin (ori-Lyt)-Dependent DNA Replication: Identification of the ori-Lyt and Association of K8 bZip Protein with the Origin. *Journal of Virology*, 77(10), 5578–5588.
- Lister, R., Pelizzola, M., Downen, R. H., Hawkins, R. D., Hon, G., Tonti-Filippini, J., Nery, J. R., Lee, L., Ye, Z., Ngo, Q. M., Edsall, L., Antosiewicz-Bourget, J., Stewart, R., Ruotti, V., Millar, A. H., Thomson, J. A., Ren, B., & Ecker, J. R. (2009). Human DNA methylomes at base resolution show widespread epigenomic differences. *Nature*, 462(7271), 315–322.
- Liu, J., Martin, H. J., Liao, G., & Hayward, S. D. (2007). The Kaposi's Sarcoma-Associated Herpesvirus LANA Protein Stabilizes and Activates c-Myc. *Journal of Virology*, 81(19), 10451–10459.
- Liu, L., Eby, M. T., Rathore, N., Sinha, S. K., Kumar, A., & Chaudhary, P. M. (2002). The human herpes virus 8-encoded viral FLICE inhibitory protein physically associates with and persistently activates the I κ B kinase complex. *Journal of Biological Chemistry*, 277(16), 13745–13751.
- Lou, S., Lee, H. M., Qin, H., Li, J. W., Gao, Z., Liu, X., Chan, L. L., Lam, V. K. L., So, W. Y., Wang, Y., Lok, S., Wang, J., Ma, R. C. W., Tsui, S. K. W., Chan, J. C. N., Chan, T. F., & Yip, K. Y. (2014). Whole-genome bisulfite sequencing of multiple individuals reveals complementary roles of promoter and gene body methylation in transcriptional regulation. *Genome Biology*, 15(7), 1–21.
- Love, M. I., Huber, W., & Anders, S. (2014). Moderated estimation of fold change and dispersion for RNA-seq data with DESeq2. *Genome Biology*, 15(12), 1–21.
- Lu, F., Stedman, W., Yousef, M., Renne, R., & Lieberman, P. M. (2010). Epigenetic Regulation of

- Kaposi's Sarcoma-Associated Herpesvirus Latency by Virus-Encoded MicroRNAs That Target Rta and the Cellular Rbl2-DNMT Pathway. *Journal of Virology*, 84(6), 2697–2706.
- Lukac, D. M., Renne, R., Kirshner, J. R., & Ganem, D. (1998). Reactivation of Kaposi's sarcoma-associated herpesvirus infection from latency by expression of the ORF 50 transactivator, a homolog of the EBV R protein. *Virology*, 252(2), 304–312.
- Ma, Z., Jacobs, S. R., West, J. A., Stopford, C., Zhang, Z., Davis, Z., Barber, G. N., Glaunsinger, B. A., Dittmer, D. P., & Damania, B. (2015). Modulation of the cGAS-STING DNA sensing pathway by gammaherpesviruses. *Proceedings of the National Academy of Sciences of the United States of America*, 112(31), E4306–E4315.
- Maier, B., Gluba, W., Bernier, B., Turner, T., Mohammad, K., Guise, T., Sutherland, A., Thorner, M., & Scrable, H. (2004). Modulation of mammalian life span by the short isoform of p53. *Genes & Development*, 18(3), 306–319.
- Manzano, M., Günther, T., Ju, H., Nicholas, J., Bartom, E. T., Grundhoff, A., & Gottwein, E. (2020). Kaposi's Sarcoma-Associated Herpesvirus Drives a Super-Enhancer-Mediated Survival Gene Expression Program in Primary Effusion Lymphoma. *MBio*, 11(4), 1–23.
- Manzano, M., Patil, A., Waldrop, A., Dave, S. S., Behdad, A., & Gottwein, E. (2018). Gene essentiality landscape and druggable oncogenic dependencies in herpesviral primary effusion lymphoma. *Nature Communications*, 9(1).
- Margueron, R., Justin, N., Ohno, K., Sharpe, M. L., Son, J., Drury, W. J., Voigt, P., Martin, S. R., Taylor, W. R., De Marco, V., Pirrotta, V., Reinberg, D., & Gambin, S. J. (2009). Role of the polycomb protein EED in the propagation of repressive histone marks. *Nature*, 461(7265), 762–767.
- Matolcsy, A., Nádor, R. G., Cesarman, E., & Knowles, D. M. (1998). Immunoglobulin V(H) gene mutational analysis suggests that primary effusion lymphomas derive from different stages of B cell maturation. *American Journal of Pathology*, 153(5), 1609–1614.
- Matsuzaki, K., Deng, G., Tanaka, H., Kakar, S., Miura, S., & Kim, Y. S. (2005). The relationship between global methylation level, loss of heterozygosity, and microsatellite instability in sporadic colorectal cancer. *Clinical Cancer Research*, 11(24), 8564–8569.
- McGeoch, D. J., Cook, S., Dolan, A., Jamieson, F. E., & Telford, E. A. R. (1995). Molecular phylogeny and evolutionary timescale for the family of mammalian herpesviruses. *Journal of Molecular Biology*, 247(3), 443–458.
- McHugh, D., Caduff, N., Barros, M. H. M., Rämer, P. C., Raykova, A., Murer, A., Landtwing, V., Quast, I., Styles, C. T., Spohn, M., Fowotade, A., Delecluse, H. J., Papoudou-Bai, A., Lee, Y. M., Kim, J. M., Middeldorp, J., Schulz, T. F., Cesarman, E., Zbinden, A., ... Münz, C. (2017). Persistent KSHV Infection Increases EBV-Associated Tumor Formation In Vivo via Enhanced EBV Lytic Gene Expression. *Cell Host and Microbe*, 22(1), 61-73.e7.
- McNab, F., Mayer-Barber, K., Sher, A., Wack, A., & O'Garra, A. (2015). Type I interferons in infectious disease. *Nature Reviews Immunology*, 15(2), 87–103.
- Meggio, F., Deana, A. D., Ruzzene, M., Brunati, A. M., Cesaro, L., Guerra, B., Meyer, T., Mett, H., Fabbro, D., Furet, P., Dobrowolska, G., & Pinna, L. A. (1995). Different Susceptibility of Protein Kinases to Staurosporine Inhibition: Kinetic Studies and Molecular Bases for the Resistance of Protein Kinase CK2. *European Journal of Biochemistry*, 234(1), 317–322.
- Mesri, E. A., Cesarman, E., & Boshoff, C. (2010). Kaposi's sarcoma and its associated herpesvirus. *Nature Reviews Cancer*, 10(10), 707–719.
- Metzger, E., Wissmann, M., Yin, N., Müller, J. M., Schneider, R., Peters, A. H. F. M., Günther, T., Buettner, R., & Schüle, R. (2005). LSD1 demethylates repressive histone marks to promote androgen-receptor-dependent transcription. *Nature*, 437(7057), 436–439.
- Meyer, C., Burmeister, T., Gröger, D., Tsaur, G., Fechina, L., Renneville, A., Sutton, R., Venn, N. C., Emerenciano, M., Pombo-De-Oliveira, M. S., Barbieri Blunck, C., Almeida Lopes, B., Zuna, J., Trka, J., Ballerini, P., Lapillonne, H., De Braekeleer, M., Cazzaniga, G., Corral Abascal, L., ... Marschalek, R. (2018). The MLL recombinome of acute leukemias in 2017. *Leukemia*, 32(2), 273–284.
- Miller, G., Heston, L., Grogan, E., Gradoville, L., Rigsby, M., Sun, R., Shedd, D., Kushnaryov, V. M., Grossberg, S., & Chang, Y. (1997). Selective switch between latency and lytic replication of Kaposi's sarcoma herpesvirus and Epstein-Barr virus in dually infected body cavity lymphoma cells. *Journal of Virology*, 71(1), 314–324.
- Miller, T., Krogan, N. J., Dover, J., Erdjument-Bromage, H., Tempst, P., Johnston, M., Greenblatt, J. F., & Shilatifard, A. (2001). COMPASS: A complex of proteins associated with a trithorax-related SET domain protein. *PNAS*, 98(23), 12902–12907.
- Milne, T. A., Briggs, S. D., Brock, H. W., Martin, M. E., Gibbs, D., Allis, C. D., & Hess, J. L. (2002). MLL Targets SET Domain Methyltransferase Activity to Hox Gene Promoters. *Molecular Cell*, 10(5), 1107–1117.

- Monini, P., Colombini, S., Stürzl, M., Goletti, D., Cafaro, A., Sgadari, C., Buttò, S., Franco, M., Leone, P., Fais, S., Leone, P., Melucci-Vigo, G., Chiozzini, C., Carlini, F., Ascherl, G., Cornali, E., Zietz, C., Ramazzotti, E., Ensoli, F., ... Ensoli, B. (1999). Reactivation and persistence of human herpesvirus-8 infection in B cells and monocytes by Th-1 cytokines increased in Kaposi's sarcoma. *Blood*, *93*(12), 4044–4058.
- Moore, P. S., Gao, S. J., Dominguez, G., Cesarman, E., Lungu, O., Knowles, D. M., Garber, R., Pellett, P. E., McGeoch, D. J., & Chang, Y. (1996). Primary characterization of a herpesvirus agent associated with Kaposi's sarcoma. *Journal of Virology*, *70*(1), 549–558.
- Mori, Y., Nishimoto, N., Ohno, M., Inagi, R., Dhepakson, P., Amou, K., Yoshizaki, K., & Yamanishi, K. (2000). Human herpesvirus 8-encoded interleukin-6 homologue (viral IL-6) induces endogenous human IL-6 secretion. *Journal of Medical Virology*, *61*(3), 332–335.
- Morin, R. D., Johnson, N. A., Severson, T. M., Mungall, A. J., An, J., Goya, R., Paul, J. E., Boyle, M., Woolcock, B. W., Kuchenbauer, F., Yap, D., Humphries, R. K., Griffith, O. L., Shah, S., Zhu, H., Kimbara, M., Shashkin, P., Charlot, J. F., Tcherpakov, M., ... Marra, M. A. (2010). Somatic mutations altering EZH2 (Tyr641) in follicular and diffuse large B-cell lymphomas of germinal-center origin. *Nature Genetics*, *42*(2), 181–185.
- Mullis K, Faloona F, Scharf S, Saiki R, Horn G, E. H. (1986). Specific Enzymatic Amplification of DNA In Vitro: The Polymerase Chain Reaction. *Cold Spring Harb Symp Quant Biol*, *51*, 263–273.
- Mutocheluh, M., Hindle, L., Aresté, C., Chanas, S. A., Butler, L. M., Lowry, K., Shah, K., Evans, D. J., & Blackbourn, D. J. (2011). Kaposi's sarcoma-associated herpesvirus viral interferon regulatory factor-2 inhibits type 1 interferon signalling by targeting interferon-stimulated gene factor-3. *Journal of General Virology*, *92*(10), 2394–2398.
- Myoung, J., & Ganem, D. (2011). Generation of a doxycycline-inducible KSHV producer cell line of endothelial origin: Maintenance of tight latency with efficient reactivation upon induction. *Journal of Virological Methods*, *174*(1–2), 12–21.
- Naipauer, J., Rosario, S., Gupta, S., Premer, C., Méndez-Solís, O., Schlesinger, M., Ponzinibbio, V., Jain, V., Gay, L., Renne, R., Chan, H. L., Morey, L., Salyakina, D., Abba, M., Williams, S., Hare, J. M., Goldschmidt-Clermont, P. J., & Mesri, E. A. (2019). PDGFRA defines the mesenchymal stem cell Kaposi's sarcoma progenitors by enabling KSHV oncogenesis in an angiogenic environment. In *PLoS Pathogens* (Vol. 15, Issue 12).
- Naipauer, J., Salyakina, D., Journo, G., Rosario, S., Williams, S., Abba, M., Shamay, M., & Mesri, E. A. (2020). High-throughput sequencing analysis of a “hit and run” cell and animal model of KSHV tumorigenesis. *PLoS Pathogens*, *16*(6), 1–26.
- Naranatt, P. P., Krishnan, H. H., Smith, M. S., & Chandran, B. (2005). Kaposi's Sarcoma-Associated Herpesvirus Modulates Microtubule Dynamics via RhoA-GTP-Diaphanous 2 Signaling and Utilizes the Dynein Motors To Deliver Its DNA to the Nucleus. *Journal of Virology*, *79*(2), 1191–1206.
- Nealon, K., Newcomb, W. W., Pray, T. R., Craik, C. S., Brown, J. C., & Kedes, D. H. (2001). Lytic Replication of Kaposi's Sarcoma-Associated Herpesvirus Results in the Formation of Multiple Capsid Species: Isolation and Molecular Characterization of A, B, and C Capsids from a Gammaherpesvirus. *Journal of Virology*, *75*(6), 2866–2878.
- Okano, M., Bell, D. W., Haber, D. A., & Li, E. (1999). DNA methyltransferases Dnmt3a and Dnmt3b are essential for de novo methylation and mammalian development. *Cell*, *99*(3), 247–257.
- Oksenhendler, E., Carcelain, G., Aoki, Y., Boulanger, E., Maillard, A., Clauvel, J. P., & Agbalika, F. (2000). High levels of human herpesvirus 8 viral load, human interleukin-6, interleukin-10, and C reactive protein correlate with exacerbation of multicentric Castleman disease in HIV-infected patients. *Blood*, *96*(6), 2069–2073.
- Ottinger, M., Christalla, T., Nathan, K., Brinkmann, M. M., Viejo-Borbolla, A., & Schulz, T. F. (2006). Kaposi's Sarcoma-Associated Herpesvirus LANA-1 Interacts with the Short Variant of BRD4 and Releases Cells from a BRD4- and BRD2/RING3-Induced G1 Cell Cycle Arrest. *Journal of Virology*, *80*(21), 10772–10786.
- Papp, B., Motlagh, N., Smindak, R. J., Jin Jang, S., Sharma, A., Alonso, J. D., & Toth, Z. (2018). Genome-Wide Identification of Direct RTA Targets Reveals Key Host Factors for Kaposi's Sarcoma-Associated Herpesvirus Lytic Reactivation. *Journal of Virology*, *93*(5), 1–22.
- Park, S. Y., & Kim, J. S. (2020). A short guide to histone deacetylases including recent progress on class II enzymes. *Experimental and Molecular Medicine*, *52*(2), 204–212.
- Parravicini, C., Chandran, B., Corbellino, M., Berti, E., Paulli, M., Moore, P. S., & Chang, Y. (2000). Differential Viral Protein Expression in Kaposi's Sarcoma-Associated Herpesvirus-Infected Diseases. *American Journal of Pathology*, *156*(3), 743–749.
- Pasini, D., Bracken, A. P., Jensen, M. R., Denchi, E. L., & Helin, K. (2004). Suz12 is essential for mouse development and for EZH2 histone methyltransferase activity. *EMBO Journal*, *23*(20), 4061–4071.

- Pauk, J., Huang, M.-L., Brodie, S. J., Wald, A., Koelle, D. M., Schacker, T., Celum, C., Selke, S., & Corey, L. (2000). Mucosal shedding of human herpesvirus 8. *New England Journal of Medicine*, 343(19), 1369–1377.
- Pearce, M., Matsumura, S., & Wilson, A. C. (2005). Transcripts Encoding K12, v-FLIP, v-Cyclin, and the MicroRNA Cluster of Kaposi's Sarcoma-Associated Herpesvirus Originate from a Common Promoter. *Journal of Virology*, 79(22), 14457–14464.
- Perino, M., Van Mierlo, G., Karemaker, I. D., Van Genesen, S., Vermeulen, M., Marks, H., Van Heeringen, S. J., & Veenstra, G. J. C. (2018). MTF2 recruits Polycomb Repressive Complex 2 by helical-shape-selective DNA binding. *Nature Genetics*, 50(7), 1002–1010.
- Pfeifer, G. P. (2018). Defining driver DNA methylation changes in human cancer. *International Journal of Molecular Sciences*, 19(4), 1–13.
- Phillips, D. M. P. (1963). The presence of Acetyl Groups in Histones. *Biochemical Journal*, 87, 258–263.
- Polizzotto, M. N., Uldrick, T. S., Wang, V., Aleman, K., Wyvill, K. M., Marshall, V., Pittaluga, S., O'Mahony, D., Whitby, D., Tosato, G., Steinberg, S. M., Little, R. F., & Yarchoan, R. (2013). Human and viral interleukin-6 and other cytokines in Kaposi sarcoma herpesvirus-associated multicentric Castlemans disease. *Blood*, 122(26), 4189–4198.
- Purushothaman, P., Thakker, S., & Verma, S. C. (2015). Transcriptome Analysis of Kaposi's Sarcoma-Associated Herpesvirus during De Novo Primary Infection of Human B and Endothelial Cells. *Journal of Virology*, 89(6), 3093–3111.
- Quinlan, A. R., & Hall, I. M. (2010). BEDTools: A flexible suite of utilities for comparing genomic features. *Bioinformatics*, 26(6), 841–842.
- Radkov, S. A., Kellam, P., & Boshoff, C. (2000). The latent nuclear antigen of Kaposi sarcoma-associated herpesvirus targets the retinoblastoma-E2F pathway and with the oncogene Hras transforms primary rat cells. *Nature Medicine*, 6(10), 1121–1127.
- Ramsahoye, B. H., Biniszkiwicz, D., Lyko, F., Clark, V., Bird, A. P., & Jaenisch, R. (2000). Non-CpG methylation is prevalent in embryonic stem cells and may be mediated by DNA methyltransferase 3a. *Proceedings of the National Academy of Sciences of the United States of America*, 97(10), 5237–5242.
- Rao, S. S. P., Huntley, M. H., Durand, N. C., Stamenova, E. K., Bochkov, I. D., Robinson, J. T., Sanborn, A. L., Machol, I., Omer, A. D., Lander, E. S., & Aiden, E. L. (2014). A 3D map of the human genome at kilobase resolution reveals principles of chromatin looping. *Cell*, 159(7), 1665–1680.
- Rappocciolo, G., Hensler, H. R., Jais, M., Reinhart, T. A., Pegu, A., Jenkins, F. J., & Rinaldo, C. R. (2008). Human Herpesvirus 8 Infects and Replicates in Primary Cultures of Activated B Lymphocytes through DC-SIGN. *Journal of Virology*, 82(10), 4793–4806.
- Rappocciolo, G., Jenkins, F. J., Hensler, H. R., Piazza, P., Jais, M., Borowski, L., Watkins, S. C., & Rinaldo, C. R. (2006). DC-SIGN Is a Receptor for Human Herpesvirus 8 on Dendritic Cells and Macrophages. *The Journal of Immunology*, 176(3), 1741–1749.
- Rauch, T. A., Wu, X., Zhong, X., Riggs, A. D., & Pfeifer, G. P. (2009). A human B cell methylome at 100-base pair resolution. *Proceedings of the National Academy of Sciences of the United States of America*, 106(3), 671–678.
- Rea, S., Eisenhaber, F., O'Carroll, D., Strahl, B. D., Sun, Z. W., Schmid, M., Opravil, S., Mechtler, K., Ponting, C. P., Allis, C. D., & Jenuwein, T. (2000). Regulation of chromatin structure by site-specific histone H3 methyltransferases. *Nature*, 406(6796), 593–599.
- Regamey, N., Tamm, M., Wernli, M., Wtischli, A., Thiel, G., Cathomas, G., & Erb, P. (1998). Transmission of Human Herpesvirus 8 infection from renal-transplant donors to recipients. *New England Journal of Medicine*, 339(19), 1358–1363.
- Renne, R., Lagunoff, M., Zhong, W., & Ganem, D. (1996). The size and conformation of Kaposi's sarcoma-associated herpesvirus (human herpesvirus 8) DNA in infected cells and virions. *Journal of Virology*, 70(11), 8151–8154.
- Renne, R., Zhong, W., Herndier, B., McGrath, M., Abbey, N., Kedes, D., & Ganem, D. (1996). Lytic growth of Kaposi's sarcoma-associated herpesvirus (human herpesvirus 8) in culture. *Nature Medicine*, 2(3), 342–346.
- Rodriguez, J., Frigola, J., Vendrell, E., Risques, R. A., Fraga, M. F., Morales, C., Moreno, V., Esteller, M., Capellà, G., Ribas, M., & Peinado, M. A. (2006). Chromosomal instability correlates with genome-wide DNA demethylation in human primary colorectal cancers. *Cancer Research*, 66(17), 8462–8468.
- Rossetto, C. C., Tarrant-Elorza, M., Verma, S., Purushothaman, P., & Pari, G. S. (2013). Regulation of Viral and Cellular Gene Expression by Kaposi's Sarcoma-Associated Herpesvirus Polyadenylated Nuclear RNA. *Journal of Virology*, 87(10), 5540–5553.
- Rossetto, C. C., & Pari, G. (2012). KSHV PAN RNA associates with demethylases UTX and

- JMJD3 to activate lytic replication through a physical interaction with the virus genome. *PLoS Pathogens*, 8(5).
- Roy, A., Dutta, D., Iqbal, J., Pisano, G., Gjyshi, O., Ansari, M. A., Kumar, B., & Chandran, B. (2016). Nuclear Innate Immune DNA Sensor IFI16 Is Degraded during Lytic Reactivation of Kaposi's Sarcoma-Associated Herpesvirus (KSHV): Role of IFI16 in Maintenance of KSHV Latency. *Journal of Virology*, 90(19), 8822–8841.
- Rupp, T., Langlois, B., Koczorowska, M. M., Radwanska, A., Sun, Z., Hussenet, T., Lefebvre, O., Murdamoothoo, D., Arnold, C., Klein, A., Biniossek, M. L., Hyenne, V., Naudin, E., Velazquez-Quesada, I., Schilling, O., Van Obberghen-Schilling, E., & Orend, G. (2016). Tenascin-C Orchestrates Glioblastoma Angiogenesis by Modulation of Pro- and Anti-angiogenic Signaling. *Cell Reports*, 17(10), 2607–2619.
- Russo, J. J., Bohenzky, R. A., Chien, M.-C., Chen, J., Yan, M., Maddalena, D., Parry, J. P., Peruzzi, D., Edelman, I. S., Chang, Y., & Moore, P. S. (1996). Nucleotide sequence of the Kaposi sarcoma-associated herpesvirus (HHV8). *Proceedings of the National Academy of Sciences*, 93(December), 14862–14867.
- Said, J. W., Chien, K., Tasaka, T., & Koeffler, H. P. (1997). Ultrastructural characterization of human herpesvirus 8 (Kaposi's sarcoma-associated herpesvirus) in Kaposi's sarcoma lesions: Electron microscopy permits distinction from cytomegalovirus (CMV). *Journal of Pathology*, 182(3), 273–281.
- Sakakibara, S., Ueda, K., Nishimura, K., Do, E., Ohsaki, E., Okuno, T., & Yamanishi, K. (2004). Accumulation of Heterochromatin Components on the Terminal Repeat Sequence of Kaposi's Sarcoma-Associated Herpesvirus Mediated by the Latency-Associated Nuclear Antigen. *Journal of Virology*, 78(14), 7299–7310.
- Santos-Rosa, H., Schneider, R., Bannister, A. J., Sherriff, J., Bernstein, B. E., Emre, N. C. T., Schreiber, S. L., Mellor, J., & Kouzarides, T. (2002). Active genes are tri-methylated at K4 of histone H3. *Nature*, 419(6905), 407–411.
- Sanyal, A., Lajoie, B. R., Jain, G., & Dekker, J. (2012). The long-range interaction landscape of gene promoters. *Nature*, 489(7414), 109–113.
- Sathish, N., & Yuan, Y. (2010). Functional characterization of Kaposi's sarcoma-associated herpesvirus small capsid protein by bacterial artificial chromosome-based mutagenesis. *Virology*, 407(2), 306–318.
- Schoggins, J. W., & Rice, C. M. (2011). Interferon-stimulated genes and their antiviral effector functions. *Current Opinion in Virology*, 1(6), 519–525.
- Schulte, J. H., Lim, S., Schramm, A., Friedrichs, N., Koster, J., Versteeg, R., Ora, I., Pajtler, K., Klein-Hitpass, L., Kuhfittig-Kulle, S., Metzger, E., Schüle, R., Eggert, A., Buettner, R., & Kirfel, J. (2009). Lysine-specific demethylase 1 is strongly expressed in poorly differentiated neuroblastoma: Implications for therapy. *Cancer Research*, 69(5), 2065–2071.
- Schultz, D. C., Ayyanathan, K., Negorev, D., Maul, G. G., & Rauscher, F. J. (2002). SETDB1: A novel KAP-1-associated histone H3, lysine 9-specific methyltransferase that contributes to HP1-mediated silencing of euchromatic genes by KRAB zinc-finger proteins. *Genes and Development*, 16(8), 919–932.
- Schulz, T. F., & Cesarman, E. (2015). Kaposi Sarcoma-associated Herpesvirus: Mechanisms of oncogenesis. *Current Opinion in Virology*, 14, 116–128.
- Shamay, M., Krithivas, A., Zhang, J., & Hayward, S. D. (2006). Recruitment of the de novo DNA methyltransferase Dnmt3a by Kaposi's sarcoma-associated herpesvirus LANA. *Proceedings of the National Academy of Sciences of the United States of America*, 103(39), 14554–14559.
- Shen, L., Inoue, A., He, J., Liu, Y., Lu, F., & Zhang, Y. (2014). Tet3 and DNA replication mediate demethylation of both the maternal and paternal genomes in mouse zygotes. *Cell Stem Cell*, 15(4), 459–471.
- Shen, L., Shao, N. Y., Liu, X., Maze, I., Feng, J., & Nestler, E. J. (2013). diffReps: Detecting Differential Chromatin Modification Sites from ChIP-seq Data with Biological Replicates. *PLoS ONE*, 8(6).
- Shi, Y., Lan, F., Matson, C., Mulligan, P., Whetstine, J. R., Cole, P. A., Casero, R. A., & Shi, Y. (2004). Histone demethylation mediated by the nuclear amine oxidase homolog LSD1. *Cell*, 119(7), 941–953.
- Simon, J., Chang, A., Bender, W., Shimell, M. J., & O'Connor, M. (1993). Elements of the Drosophila Bithorax Complex That Mediate Repression by Polycomb Group Products. *Developmental Biology*, 158, 131–144.
- Simpson, G. R., Schulz, T. F., Whitby, D., Cook, P. M., Boshoff, C., Rainbow, L., Howard, M. R., Gao, S. J., Bohenzky, R. A., Simmonds, P., Lee, C., De Ruiter, A., Hatzakis, A., Tedder, R. S., Weller, I. V. D., Weiss, R. A., & Moore, P. S. (1996). Prevalence of Kaposi's sarcoma associated herpesvirus infection measured by antibodies to recombinant capsid protein and latent

- immunofluorescence antigen. *Lancet*, 348(9035), 1133–1138.
- Singh, V. V., Dutta, D., Ansari, M. A., Dutta, S., Chandran, B., & Longnecker, R. (2014). Kaposi's Sarcoma-Associated Herpesvirus Induces the ATM and H2AX DNA Damage Response Early during De Novo Infection of Primary Endothelial Cells, Which Play Roles in Latency Establishment. *Journal of Virology*, 88(5), 2821–2834.
- Skvortsova, K., Iovino, N., & Bogdanović, O. (2018). Functions and mechanisms of epigenetic inheritance in animals. *Nature Reviews Molecular Cell Biology*, 19(12), 774–790.
- Song, F., Smith, J. F., Kimura, M. T., Morrow, A. D., Matsuyama, T., Nagase, H., & Held, W. A. (2005). Association of tissue-specific differentially methylated regions (TDMs) with differential gene expression. *Proceedings of the National Academy of Sciences of the United States of America*, 102(9), 3336–3341.
- Soulier, J., Grollet, L., Oksenhendler, E., Cacoub, P., Cazals-Hatem, D., Babinet, P., D'Agay, M. F., Clauvel, J. P., Raphael, M., Degos, L., & Sigaux, F. (1995). Kaposi's sarcoma-associated herpesvirus-like DNA sequences in multicentric Castlemann's disease. *Blood*, 86(4), 1276–1280.
- Staskus, K. A., Zhong, W., Gebhard, K., Herndier, B., Wang, H., Renne, R., Beneke, J., Pudney, J., Anderson, D. J., Ganem, D., & Haase, A. T. (1997). Kaposi's sarcoma-associated herpesvirus gene expression in endothelial (spindle) tumor cells. *Journal of Virology*, 71(1), 715–719.
- Stedman, W., Deng, Z., Lu, F., & Lieberman, P. M. (2004). ORC, MCM, and Histone Hyperacetylation at the Kaposi's Sarcoma-Associated Herpesvirus Latent Replication Origin. *Journal of Virology*, 78(22), 12566–12575.
- Stedman, W., Kang, H., Lin, S., Kissil, J. L., Bartolomei, M. S., & Lieberman, P. M. (2008). Cohesins localize with CTCF at the KSHV latency control region and at cellular c-myc and H19/Igf2 insulators. *EMBO Journal*, 27(4), 654–666.
- Stuart, T., Butler, A., Hoffman, P., Hafemeister, C., Papalexi, E., Mauck, W. M., Hao, Y., Stoeckius, M., Smibert, P., & Satija, R. (2019). Comprehensive Integration of Single-Cell Data. *Cell*, 177(7), 1888–1902.e21.
- Sun, R., Liang, D., Gao, Y., & Lan, K. (2014). Kaposi's Sarcoma-Associated Herpesvirus-Encoded LANA Interacts with Host KAP1 To Facilitate Establishment of Viral Latency. *Journal of Virology*, 88(13), 7331–7344.
- Sun, Ren, Lin, S.-F., Staskus, K., Gradoville, L., Grogan, E., Haase, A., & Miller, G. (1999). Kinetics of Kaposi's Sarcoma-Associated Herpesvirus Gene Expression. *Journal of Virology*, 73(3), 2232–2242.
- Sun, Ren, Lin, S. F., Gradoville, L., Yuan, Y., Zhu, F., & Miller, G. (1998). A viral gene that activates lytic cycle expression of Kaposi's sarcoma-associated herpesvirus. *Proceedings of the National Academy of Sciences of the United States of America*, 95(18), 10866–10871.
- Sun, Rui, Tan, X., Wang, X., Wang, X., Yang, L., Robertson, E. S., & Lan, K. (2017). Epigenetic Landscape of Kaposi's Sarcoma-Associated Herpesvirus Genome in Classic Kaposi's Sarcoma Tissues. *PLoS Pathogens*, 13(1), 1–21.
- Tahiliani, M., Koh, K. P., Shen, Y., Pastor, W. A., Bandukwala, H., Brudno, Y., Agarwal, S., Iyer, L. M., Liu, D. R., Aravind, L., & Rao, A. (2009). Conversion of 5-methylcytosine to 5-hydroxymethylcytosine in mammalian DNA by MLL partner TET1. *Science*, 324(5929), 930–935.
- Takekoshi, H., Yamashita, S., Shimazu, T., Niwa, T., & Ushijima, T. (2009). The presence of RNA polymerase II, active or stalled, predicts epigenetic fate of promoter CpG islands. *Genome Research*, 19(11), 1974–1982.
- Thorvaldsdóttir, H., Robinson, J. T., & Mesirov, J. P. (2013). Integrative Genomics Viewer (IGV): High-performance genomics data visualization and exploration. *Briefings in Bioinformatics*, 14(2), 178–192.
- Tie, F., Banerjee, R., Stratton, C. A., Prasad-Sinha, J., Stepanik, V., Zlobin, A., Diaz, M. O., Scacheri, P. C., & Harte, P. J. (2009). CBP-mediated acetylation of histone H3 lysine 27 antagonizes *Drosophila* Polycomb silencing. *Development*, 136(18), 3131–3141.
- Toth, Z., Maglinte, D. T., Lee, S. H., Lee, H. R., Wong, L. Y., Brulois, K. F., Lee, S., Buckley, J. D., Laird, P. W., Marquez, V. E., & Jung, J. U. (2010). Epigenetic analysis of KSHV latent and lytic genomes. *PLoS Pathogens*, 6(7), 1–17.
- Toth, Z., Papp, B., Brulois, K., Choi, Y. J., Gao, S.-J., & Jung, J. U. (2016). LANA-Mediated Recruitment of Host Polycomb Repressive Complexes onto the KSHV Genome during De Novo Infection. *PLoS Pathogens*, 12(9), e1005878.
- Trivedi, P., Takazawa, K., Zompetta, C., Cuomo, L., Anastasiadou, E., Carbone, A., Uccini, S., Belardelli, F., Takada, K., Frati, L., & Faggioni, A. (2004). Infection of HHV-8+ primary effusion lymphoma cells with a recombinant Epstein-Barr virus leads to restricted EBV latency, altered phenotype, and increased tumorigenicity without affecting TCL1 expression. *Blood*, 103(1), 313–316.
- Trus, B. L., Heymann, J. B., Nealon, K., Cheng, N., Newcomb, W. W., Brown, J. C., Kedes, D. H., &

- Steven, A. C. (2001). Capsid Structure of Kaposi's Sarcoma-Associated Herpesvirus, a Gammaherpesvirus, Compared to Those of an Alphaherpesvirus, Herpes Simplex Virus Type 1, and a Betaherpesvirus, Cytomegalovirus. *Journal of Virology*, 75(6), 2879–2890.
- Unal, A., Pray, T. R., Lagunoff, M., Pennington, M. W., Ganem, D., & Craik, C. S. (1997). The protease and the assembly protein of Kaposi's sarcoma-associated herpesvirus (human herpesvirus 8). *Journal of Virology*, 71(9), 7030–7038.
- Valdembri, D., Regano, D., Maione, F., Giraudo, E., & Serini, G. (2016). Class 3 semaphorins in cardiovascular development. *Cell Adhesion and Migration*, 10(6), 641–651.
- Varthakavi, V., Smith, R. M., Deng, H., Sun, R., & Spearman, P. (2002). Human immunodeficiency virus type-1 activates lytic cycle replication of Kaposi's sarcoma-associated herpesvirus through induction of KSHV Rta. *Virology*, 297(2), 270–280.
- Veettil, M. V., Sadagopan, S., Sharma-Walia, N., Wang, F.-Z., Raghu, H., Varga, L., & Chandran, B. (2008). Kaposi's Sarcoma-Associated Herpesvirus Forms a Multimolecular Complex of Integrins (α V β 5, α V β 3, and α 3 β 1) and CD98-xCT during Infection of Human Dermal Microvascular Endothelial Cells, and CD98-xCT Is Essential for the Postentry Stage of Infection. *Journal of Virology*, 82(24), 12126–12144.
- Verma, S. C., Choudhuri, T., Kaul, R., & Robertson, E. S. (2006). Latency-Associated Nuclear Antigen (LANA) of Kaposi's Sarcoma-Associated Herpesvirus Interacts with Origin Recognition Complexes at the LANA Binding Sequence within the Terminal Repeats. *Journal of Virology*, 80(5), 2243–2256.
- Verma, S. C., Choudhuri, T., & Robertson, E. S. (2007). The Minimal Replicator Element of the Kaposi's Sarcoma-Associated Herpesvirus Terminal Repeat Supports Replication in a Semiconservative and Cell-Cycle-Dependent Manner. *Journal of Virology*, 81(7), 3402–3413.
- Verma, S. C., Lan, K., Choudhuri, T., Cotter, M. A., & Robertson, E. S. (2007). An Autonomous Replicating Element within the KSHV Genome. *Cell Host and Microbe*, 2(2), 106–118.
- Verma, S. C., Lu, J., Cai, Q., Kosiyatrakul, S., McDowell, M. E., Schildkraut, C. L., & Robertson, E. S. (2011). Single molecule analysis of replicated DNA reveals the usage of multiple KSHV genome regions for latent replication. *PLoS Pathogens*, 7(11).
- Walsh, C. P., Chaillet, J. R., & Bestor, T. H. (1998). Transcription of IAP endogenous retroviruses is constrained by cytosine methylation [4]. *Nature Genetics*, 20(2), 116–117.
- Wang, H. W., Sharp, T. V., Koumi, A., Koentges, G., & Boshoff, C. (2002). Characterization of an anti-apoptotic glycoprotein encoded by Kaposi's sarcoma-associated herpesvirus which resembles a spliced variant of human survivin. *EMBO Journal*, 21(11), 2602–2615.
- Wang, H. W., Trotter, M. W. B., Lagos, D., Bourbouli, D., Henderson, S., Mäkinen, T., Elliman, S., Flanagan, A. M., Alitalo, K., & Boshoff, C. (2004). Kaposi sarcoma herpesvirus-induced cellular reprogramming contributes to the lymphatic endothelial gene expression in Kaposi sarcoma. *Nature Genetics*, 36(7), 687–693.
- Wang, L., & Damania, B. (2008). Kaposi's sarcoma-associated herpesvirus confers a survival advantage to endothelial cells. *Cancer Research*, 68(12), 4640–4648.
- Wang, P., Lin, C., Smith, E. R., Guo, H., Sanderson, B. W., Wu, M., Gogol, M., Alexander, T., Seidel, C., Wiedemann, L. M., Ge, K., Krumlauf, R., & Shilatifard, A. (2009). Global Analysis of H3K4 Methylation Defines MLL Family Member Targets and Points to a Role for MLL1-Mediated H3K4 Methylation in the Regulation of Transcriptional Initiation by RNA Polymerase II. *Molecular and Cellular Biology*, 29(22), 6074–6085.
- Wang, S. E., Wu, F. Y., Yu, Y., & Hayward, G. S. (2003). CCAAT/Enhancer-Binding Protein- α Is Induced during the Early Stages of Kaposi's Sarcoma-Associated Herpesvirus (KSHV) Lytic Cycle Reactivation and Together with the KSHV Replication and Transcription Activator (RTA) Cooperatively Stimulates the Viral RTA. *Journal of Virology*, 77(17), 9590–9612.
- Wang, Y., Li, H., Chan, M. Y., Zhu, F. X., Lukac, D. M., & Yuan, Y. (2004). Kaposi's Sarcoma-Associated Herpesvirus ori-Lyt-Dependent DNA Replication: cis-Acting Requirements for Replication and ori-Lyt-Associated RNA Transcription. *Journal of Virology*, 78(16), 8615–8629.
- Wang, Y., Li, H., Tang, Q., Maul, G. G., Yuan, Y., Ai, W. E. T., & Irol, J. V. (2008). Kaposi's Sarcoma-Associated Herpesvirus ori-Lyt-Dependent DNA Replication: Involvement of Host Cellular Factors. *Journal of Virology*, 82(6), 2867–2882.
- Wang, Y., & Yuan, Y. (2007). Essential role of RBP-Jk in activation of the K8 delayed-early promoter of Kaposi's sarcoma-associated herpesvirus by ORF50/RTA. *Virology*, 359(1), 19–27.
- Wang, Z., Zang, C., Rosenfeld, J. A., Schones, D. E., Barski, A., Cuddapah, S., Cui, K., Roh, T. Y., Peng, W., Zhang, M. Q., & Zhao, K. (2008). Combinatorial patterns of histone acetylations and methylations in the human genome. *Nature Genetics*, 40(7), 897–903.
- Weber, M., Davies, J. J., Wittig, D., Oakeley, E. J., Haase, M., Lam, W. L., & Schübeler, D. (2005). Chromosome-wide and promoter-specific analyses identify sites of differential DNA methylation in normal and transformed human cells. *Nature Genetics*, 37(8), 853–862.

- Weisenberger, D. J., Siegmund, K. D., Campan, M., Young, J., Long, T. I., Faasse, M. A., Kang, G. H., Widschwendter, M., Weener, D., Buchanan, D., Koh, H., Simms, L., Barker, M., Leggett, B., Levine, J., Kim, M., French, A. J., Thibodeau, S. N., Jass, J., ... Laird, P. W. (2006). CpG island methylator phenotype underlies sporadic microsatellite instability and is tightly associated with BRAF mutation in colorectal cancer. *Nature Genetics*, *38*(7), 787–793.
- West, J., & Damania, B. (2008). Upregulation of the TLR3 Pathway by Kaposi's Sarcoma-Associated Herpesvirus during Primary Infection. *Journal of Virology*, *82*(11), 5440–5449.
- Whitby, D., Boshoff, C., Hatzioannou, T., Weiss, R. A., Schulz, T. F., Howard, M. R., Brink, N. S., Tedder, R. S., Tenant-Flowers, M., Copas, A., Suggett, F. E. A., Aldam, D. M., Denton, A. S., Miller, R. F., & Weller, I. V.D. (1995). Detection of Kaposi sarcoma associated herpesvirus in peripheral blood of HIV-infected individuals and progression to Kaposi's sarcoma. *The Lancet*, *346*(8978), 799–802.
- Whyte, W. A., Orlando, D. A., Hnisz, D., Abraham, B. J., Lin, C. Y., Kagey, M. H., Rahl, P. B., Lee, T. I., & Young, R. A. (2013). Master transcription factors and mediator establish super-enhancers at key cell identity genes. *Cell*, *153*(2), 307–319.
- Wies, E., Mori, Y., Hahn, A., Kremmer, E., Stürzl, M., Fleckenstein, B., & Neipel, F. (2008). The viral interferon-regulatory factor-3 is required for the survival of KSHV-infected primary effusion lymphoma cells. *Blood*, *111*(1), 320–327.
- Wilkinson, D. G. (2001). Multiple roles of eph receptors and ephrins in neural development. *Nature Reviews Neuroscience*, *2*(3), 155–164.
- Wilson, S. J., Tsao, E. H., Webb, B. L. J., Ye, H., Dalton-Griffin, L., Tsantoulas, C., Gale, C. V., Du, M.-Q., Whitehouse, A., & Kellam, P. (2007). X Box Binding Protein XBP-1s Transactivates the Kaposi's Sarcoma-Associated Herpesvirus (KSHV) ORF50 Promoter, Linking Plasma Cell Differentiation to KSHV Reactivation from Latency. *Journal of Virology*, *81*(24), 13578–13586.
- Wu, F. Y., Ahn, J.-H., Alcendor, D. J., Jang, W.-J., Xiao, J., Hayward, S. D., & Hayward, G. S. (2001). Origin-Independent Assembly of Kaposi's Sarcoma-Associated Herpesvirus DNA Replication Compartments in Transient Cotransfection Assays and Association with the ORF-K8 Protein and Cellular PML. *Journal of Virology*, *75*(3), 1487–1506.
- Wu, J., Xu, Y., Mo, D., Huang, P., Sun, R., Huang, L., Pan, S., & Xu, J. (2014). Kaposi's Sarcoma-Associated Herpesvirus (KSHV) vIL-6 promotes cell proliferation and migration by upregulating DNMT1 via STAT3 activation. *PLoS ONE*, *9*(3), 2–7.
- Wu, L., Lo, P., Yu, X., Stoops, J. K., Forghani, B., & Zhou, Z. H. (2000). Three-Dimensional Structure of the Human Herpesvirus 8 Capsid. *Journal of Virology*, *74*(20), 9646–9654.
- Yap, D. B., Chu, J., Berg, T., Schapira, M., Cheng, S. W. G., Moradian, A., Morin, R. D., Mungall, A. J., Meissner, B., Boyle, M., Marquez, V. E., Marra, M. A., Gascoyne, R. D., Humphries, R. K., Arrowsmith, C. H., Morin, G. B., & Aparicio, S. A. J. R. (2011). Somatic mutations at EZH2 Y641 act dominantly through a mechanism of selectively altered PRC2 catalytic activity, to increase H3K27 trimethylation. *Blood*, *117*(8), 2451–2459.
- Ye, F., Zhou, F., Bedolla, R. G., Jones, T., Lei, X., Kang, T., Guadalupe, M., & Gao, S. J. (2011). Reactive oxygen species hydrogen peroxide mediates Kaposi's sarcoma-associated herpesvirus reactivation from latency. *PLoS Pathogens*, *7*(5).
- Yoneyama, M., Suhara, W., Fukuhara, Y., Fukuda, M., Nishida, E., & Fujita, T. (1998). Direct triggering of the type I interferon system by virus infection: Activation of a transcription factor complex containing IRF-3 and CBP/p300. *EMBO Journal*, *17*(4), 1087–1095.
- Yu, H., Zhu, S., Zhou, B., Xue, H., & Han, J. D. J. (2008). Inferring causal relationships among different histone modifications and gene expression (Genome Research (2008) 18, (1314-1324)). *Genome Research*, *18*(9), 1544.
- Yu, Y., Wang, S. E., & Hayward, G. S. (2005). The KSHV immediate-early transcription factor RTA encodes ubiquitin E3 ligase activity that targets IRF7 for proteasome-mediated degradation. *Immunity*, *22*(1), 59–70.
- Zhang, Yong, Liu, T., Meyer, C. A., Eeckhoute, J., Johnson, D. S., Bernstein, B. E., Nussbaum, C., Myers, R. M., Brown, M., Li, W., & Shirley, X. S. (2008). Model-based analysis of ChIP-Seq (MACS). *Genome Biology*, *9*(9).
- Zhang, Yugen, Dittmer, D. P., Mieczkowski, P. A., Host, K. M., Fusco, W. G., Duncan, J. A., & Damania, B. (2018). RIG-I Detects Kaposi's Sarcoma-Associated Herpesvirus Transcripts in a RNA Polymerase III-Independent Manner. *MBio*, *9*(4), 1–17.
- Zheng, G. X. Y., Terry, J. M., Belgrader, P., Ryvkin, P., Bent, Z. W., Wilson, R., Ziraldo, S. B., Wheeler, T. D., McDermott, G. P., Zhu, J., Gregory, M. T., Shuga, J., Montesclaros, L., Underwood, J. G., Masquelier, D. A., Nishimura, S. Y., Schnall-Levin, M., Wyatt, P. W., Hindson, C. M., ... Bielas, J. H. (2017). Massively parallel digital transcriptional profiling of single cells. *Nature Communications*, *8*.
- Zhu, F. X., Chong, J. M., Wu, L., & Yuan, Y. (2005). Virion Proteins of Kaposi's Sarcoma-Associated

Herpesvirus. *Journal of Virology*, 79(2), 800–811.

Zhu, F. X., King, S. M., Smith, E. J., Levy, D. E., & Yuan, Y. (2002). A Kaposi's sarcoma-associated herpesviral protein inhibits virus-mediated induction of type I interferon by blocking IRF-7 phosphorylation and nuclear accumulation. *Proceedings of the National Academy of Sciences of the United States of America*, 99(8), 5573–5578.

7 Supplementary Material

Table S 1: Number of cells per cluster from scRNA-seq

cluster	number of cells
1	1005
2	954
3	864
4	687
5	229
6	168
7	11
total	3918

Table S 2: Overlapping histone modification changes in infected and cleared cells for H3K4me3

Chr	Start	End	infected	cleared	Gene Name	Distance to TSS
chr1	107326901	107328600	2,6	1,39	NTNG1	179682,5
chr19	56566601	56568200	2,57	2,61	ZNF470	66,5
chr1	107272701	107274400	1,93	1,62	NTNG1	125482,5
chr1	75100301	75102000	1,7	1,58	LHX8	27282,5
chr11	28705401	28706400	1,68	1,07	MIR8068	228352,5
chr3	158107401	158108700	1,51	1,39	SHOX2	1887,5
chr10	119131001	119132600	1,34	1,4	FAM45A	27688,5
chr1	216530501	216532700	1,31	1,24	USH2A	108152,5
chr14	28768501	28770100	1,25	1,77	FOXG1	2514,5
chr2	162404601	162406100	1,22	1,22	GCA	60970,5
chr3	116857501	116859500	1,17	1,31	MIR4447	8133,5
chr9	115117101	115119000	1,16	1,15	TNC	106,5
chr17	6939301	6940500	1,13	1,14	ALOX12P2	46124,5
chr2	41425601	41427600	1,13	1,31	LINC01913	450953,5
chr5	161685701	161687700	1,13	1,26	GABRA6	980,5
chr13	51229701	51231500	1,11	1,03	FAM124A	8267,5
chr2	237599601	237600700	1,1	1,62	RAB17	9024,5
chr5	129619101	129620900	1,1	1,12	MINAR2	128189,5
chr12	122528201	122529200	1,06	1,13	KNTC1	1452,5
chr6	152317401	152318600	1,05	1,09	SYNE1-AS1	62528,5
chr2	102337501	102338700	1,03	1,38	IL1RL1	851,5
chr3	87642901	87644400	1,03	1,14	HTR1F	149115,5
chr3	127735301	127736300	-1,07	-1,15	ABTB1	62849,5
chr20	16574201	16576100	-1,29	-1,29	KIF16B	1716,5
chr18	55396101	55397100	-1,32	-1,42	TCF4	5376,5
chr15	81296501	81297500	-1,35	-1,07	IL16	88,5
chr2	98868201	98869300	-1,39	-1,25	KIAA1211L	67474,5
chr3	19701601	19703100	-1,42	-1,19	EFHB	231866,5
chrX	118115501	118117600	-1,42	-2	KLHL13	789,5
chr10	114631301	114633000	-1,5	-1,32	ABLIM1	246,5
chr6	105453001	105455700	-1,5	-1,99	PREP	51226,5
chr4	89893801	89899300	-1,79	-1,03	MMRN1	1697,5
chr1	66533401	66536500	-1,84	-1,28	SGIP1	1382,5
chr10	95756101	95757400	-1,87	-1,36	ENTPD1	588,5
chr7	54932601	54934200	-1,87	-1,07	EGFR	85615,5
chr5	174335701	174338300	-1,88	-2,16	LINC01411	647,5
chr2	147608901	147610500	-2,05	-1,55	ACVR2A	234815,5
chr3	129655901	129657000	-2,51	-1,59	TMCC1	32281,5

Table S 3: Overlapping histone modification changes in infected and cleared cells for H3K27ac

Chr	Start	End	infected	cleared	Gene Name	Distance to TSS
chr11	110832001	110834000	3,41	3,26	ARHGAP20	119811,5
chr12	18382501	18384400	2,33	2,13	PIK3C2G	121911,5
chr3	161315701	161317200	2,32	2,04	SPTSSB	55632,5
chr18	56402001	56404400	2,11	1,18	LOC642484	211938,5
chr21	26869401	26871100	1,86	1,63	ADAMTS1	24841,5
chr10	52664901	52666800	1,69	1,6	LOC105378305	89553,5
chr14	26776001	26777000	1,68	1,21	LINC02293	32846,5
chr9	83471001	83475000	1,55	1,12	FRMD3	5258,5
chr5	166370601	166372600	1,5	1,16	LINC01947	554769,5
chr6	121951401	121953300	1,47	1,24	HSF2	447199,5
chr1	94544201	94546200	1,36	1,07	MIR12133	1499,5
chr10	119131201	119132500	1,21	1,25	FAM45A	27738,5
chr1	233355801	233357400	1,18	1,09	MAP3K21	28877,5
chr3	24146101	24147400	1,13	1,01	LOC101927854	4572,5
chr14	102821601	102822600	1,02	1,02	TRAF3	44622,5
chr3	70737401	70739100	-1,07	-1,01	FOXP1	326672,5
chr5	127092101	127093300	-1,14	-1,12	C5orf63	19208,5
chr11	47905601	47906700	-1,16	-1,09	NUP160	57606,5
chr4	105059801	105061600	-1,18	-1,05	TET2	85173,5
chr3	8110401	8111900	-1,2	-1,04	LOC101927394	94843,5
chr16	80023001	80025100	-1,27	-1,26	LINC01229	228802,5
chr21	46060301	46061400	-1,27	-1,46	COL6A2	37267,5
chr5	133735001	133736200	-1,28	-1,51	FSTL4	123059,5
chr2	119454701	119456500	-1,35	-1,07	LOC107105282	20852,5
chr14	63199501	63201300	-1,43	-1,03	RHOJ	4041,5
chr13	94304501	94306200	-1,45	-1,12	GPC6-AS1	117359,5
chrX	118215201	118217100	-1,46	-1,44	KLHL13	98810,5
chr3	7455701	7457300	-1,51	-1,28	GRM7-AS1	78783,5
chr8	133025501	133027400	-1,52	-1,03	MIR7848	20130,5
chr7	51121301	51123100	-1,55	-1,18	COBL	194608,5
chr2	14234401	14236000	-1,56	-1,03	LINC00276	165757,5
chr13	24347901	24349600	-1,67	-1,13	LINC00566	17301,5
chr3	40744701	40746900	-1,73	-1,24	ZNF621	220841,5
chr3	7345401	7347800	-1,8	-1,59	GRM7-AS1	188683,5
chr18	25517201	25519200	-1,82	-1,3	ZNF521	165950,5
chr3	7382401	7383600	-1,87	-2,3	GRM7-AS1	152283,5
chr20	24364101	24365200	-1,93	-1,72	SYNDIG1	104547,5
chr8	133032101	133033700	-1,94	-1,44	MIR7848	13680,5
chr13	41492201	41493700	-2,08	-1,3	RGCC	35401,5
chr8	133053301	133054500	-2,36	-1,38	PTCSC1	1057,5
chr3	7306601	7308200	-2,6	-2,18	GRM7-AS1	227883,5

Table S 4: Overlapping histone modification changes in infected and cleared cells for H3K27me3

Chr	Start	End	infected	cleared	Gene	Distance to TSS
chr6	47002001	47032000	2,03	1,87	ADGRF1	25331,5
chr14	26862001	26880000	2,01	1,78	MIR4307HG	2131,5
chr8	29348001	29367000	1,85	1,32	DUSP4	8695,5
chr8	55373001	55391000	1,82	1,4	SBF1P1	73320,5
chr17	65105001	65123000	1,76	1,35	LOC100507002	13189,5
chr11	110885001	110898000	1,75	2,47	ARHGAP20	178311,5
chr3	124282001	124298000	1,71	1,42	MIR6083	84330,5
chr5	10469001	10482000	1,7	1,54	MIR6131	2535,5
chr5	141357001	141375000	1,55	1,55	PCDHGA6	8082,5
chr11	110682001	110741000	1,54	1,85	ARHGAP20	1688,5
chr9	114786001	114801000	1,53	1,42	TNFSF15	12538,5
chr10	30137001	30154000	1,3	1,16	JCAD	30006,5
chr1	162198001	162210000	1,26	1,47	MIR4654	46894,5
chr1	244090001	244108000	1,26	1,23	ZBTB18	45796,5
chr18	62462001	62482000	1,26	1,44	ZCCHC2	51023,5
chr9	114752001	114771000	1,26	1,35	TNFSF15	31029,5
chr8	130583001	130598000	1,24	1,33	ASAP1	146826,5
chr11	95076001	95089000	1,23	1,15	ENDOD1	7344,5
chr3	124190001	124220000	1,23	1,07	MIR5002	72072,5
chr9	126321001	126335000	1,23	1,07	MVB12B	1172,5
chr3	124533001	124547000	1,22	1,02	KALRN	44657,5
chr8	8656001	8672000	1,21	1,34	CLDN23	37935,5
chr17	65141001	65154000	1,2	1,28	RGS9	10131,5
chr10	6732001	6742000	1,19	1,33	LINP1	380,5
chr10	23318001	23332000	1,18	1,13	LOC105376453	18955,5
chr10	17437001	17465000	1,17	1,1	ST8SIA6	3594,5
chr6	114109001	114133000	1,12	1,09	HS3ST5	58123,5
chr18	73858001	73877000	1,11	1,16	FBXO15	280263,5
chr8	29780001	29802000	1,11	1,02	LOC101929470	37503,5
chr1	58552001	58564000	1,08	1,04	OMA1	11274,5
chr1	162233001	162249000	1,08	1,1	MIR4654	83894,5
chr15	38788001	38811000	1,08	1,18	RASGRP1	234686,5
chr7	30483001	30496000	1,08	1,05	NOD1	10634,5
chr8	115334001	115417000	1,08	1,01	TRPS1	292511,5
chr2	99790001	99804000	1,07	1,06	REV1	306944,5
chr14	101075001	101089000	1,06	1,21	MEG9	12090,5
chr1	115288001	115304000	1,02	1,11	NGF-AS1	12967,5
chr10	6675001	6717000	1,02	1,27	LINP1	41380,5
chr2	110178001	110190000	1,02	1,2	NPHP1	21061,5
chr8	10651001	10673000	1,02	1,08	C8orf74	10626,5
chr8	31612001	31652000	1,02	1,03	NRG1	7750,5
chr4	72291001	72304000	-1,04	-1,19	NPFFR2	258369,5
chr11	123843001	123857000	-1,06	-1,03	TMEM225	35641,5
chr10	33039001	33049000	-1,07	-1,19	IATPR	72806,5
chr4	186638001	186678000	-1,07	-1,05	FAT1	65855,5
chr7	121789001	121801000	-1,07	-1,58	PTPRZ1	78103,5
chr6	122019001	122047000	-1,08	-1,17	HSF2	366549,5
chr6	121874001	121884000	-1,09	-1,28	GJA1	443355,5
chr6	121999001	122016000	-1,1	-1,24	HSF2	392049,5
chr8	10414001	10424000	-1,11	-1,41	LINCRC-0001	55563,5
chr8	88606001	88620000	-1,11	-1,18	MMP16	285517,5
chr8	104018001	104030000	-1,11	-1,14	RIMS2	199333,5
chr11	95419001	95434000	-1,12	-1,17	SESN3	193959,5
chr4	155343001	155354000	-1,13	-1,19	LOC102724776	5714,5
chr12	92626001	92658000	-1,14	-1,07	C12orf74	60841,5
chr5	85329001	85345000	-1,14	-1,83	NBPF22P	945442,5

chr6	154040001	154081000	-1,15	-1,07	OPRM1	21090,5
chr2	182577001	182591000	-1,16	-1,41	PDE1A	61155,5
chr12	18646001	18668000	-1,17	-1,12	PLCZ1	80508,5
chr8	88388001	88399000	-1,17	-1,1	MMP16	66017,5
chr11	95374001	95384000	-1,18	-1,21	SESN3	146459,5
chr18	31490001	31507000	-1,18	-1,03	DSG2	324,5
chr2	182512001	182522000	-1,18	-1,19	PDE1A	5608,5
chr4	183898001	183914000	-1,18	-1,46	STOX2	694,5
chr7	121755001	121774000	-1,19	-1,54	PTPRZ1	108603,5
chr7	79553001	79570000	-1,2	-1,01	MAGI2-AS3	107541,5
chr7	121830001	121848000	-1,21	-1,69	PTPRZ1	34103,5
chr9	115208001	115225000	-1,25	-1,52	LOC101928748	78091,5
chr5	143474001	143489000	-1,29	-1,08	NR3C1	45988,5
chr7	112670001	112682000	-1,29	-1,15	LOC101928012	53620,5
chr4	111682001	111692000	-1,31	-1,16	FAM241A	458452,5
chr12	68937001	68962000	-1,33	-1,25	CPM	13739,5
chr3	81951001	81962000	-1,33	-1,17	LINC02008	29640,5
chr4	72318001	72362000	-1,33	-1,28	ADAMTS3	229220,5
chr6	154009001	154019000	-1,33	-1,8	OPRM1	3505,5
chr7	141237001	141253000	-1,38	-1,3	TMEM178B	170937,5
chr10	114623001	114642000	-1,41	-1,7	ABLIM1	18747,5
chr12	70137001	70215000	-1,41	-1,25	CNOT2	66992,5
chr6	8380001	8390000	-1,43	-1,45	SLC35B3	50544,5
chr7	121853001	121886000	-1,44	-1,35	PTPRZ1	3659,5
chr6	135725001	135743000	-1,45	-1,21	PDE7B	117699,5
chr9	115013001	115068000	-1,46	-1,1	TNC	77656,5
chr6	135770001	135793000	-1,47	-1,06	PDE7B	70199,5
chr13	73048001	73068000	-1,49	-1,02	KLF5	3025,5
chr15	51227001	51252000	-1,51	-1,04	CYP19A1	16288,5
chr7	121673001	121686000	-1,52	-1,68	PTPRZ1	193603,5
chr8	88648001	88658000	-1,55	-1,52	MMP16	325517,5
chr1	199653001	199666000	-1,57	-1,09	NR5A2	368100,5
chr4	72454001	72477000	-1,57	-1,4	ADAMTS3	103720,5
chr2	221825001	221835000	-1,59	-1,11	EPHA4	255798,5
chr3	7955001	7979000	-1,6	-1,73	LOC101927394	49306,5
chr4	44241001	44255000	-1,61	-1,44	KCTD8	200808,5
chr12	25502001	25517000	-1,68	-1,46	LMNTD1	43782,5
chr1	200103001	200131000	-1,7	-1,58	NR5A2	74176,5
chr6	127621001	127631000	-1,73	-1,51	C6orf58	48827,5
chr6	116474001	116494000	-1,75	-1,02	CALHM6	22626,5
chr11	126650001	126662000	-1,79	-1,06	LOC101929427	3223,5
chr4	72421001	72440000	-1,8	-1,48	ADAMTS3	138720,5
chr2	215944001	215963000	-1,85	-1,32	MREG	60050,5
chr8	88801001	88817000	-1,86	-2,01	MMP16	481517,5
chr12	92414001	92424000	-1,89	-1,62	CLLU1	2529,5
chr8	88729001	88775000	-1,94	-1,56	MMP16	424517,5
chr2	215975001	216001000	-1,96	-1,19	MREG	25550,5
chr7	121742001	121754000	-1,99	-1,54	PTPRZ1	125103,5
chr3	7988001	8008000	-2,06	-2,29	LOC101927394	18306,5
chr1	200151001	200181000	-2,08	-1,6	NR5A2	123176,5
chr8	88662001	88683000	-2,14	-1,72	MMP16	345017,5
chr8	88777001	88796000	-2,22	-2,15	MMP16	459017,5
chr3	171231001	171250000	-2,36	-1,23	MIR569	133741,5
chr4	167228001	167244000	-2,99	-3,22	SPOCK3	1574,5
chr9	83532001	83544000	-3,03	-1,87	FRMD3	432,5

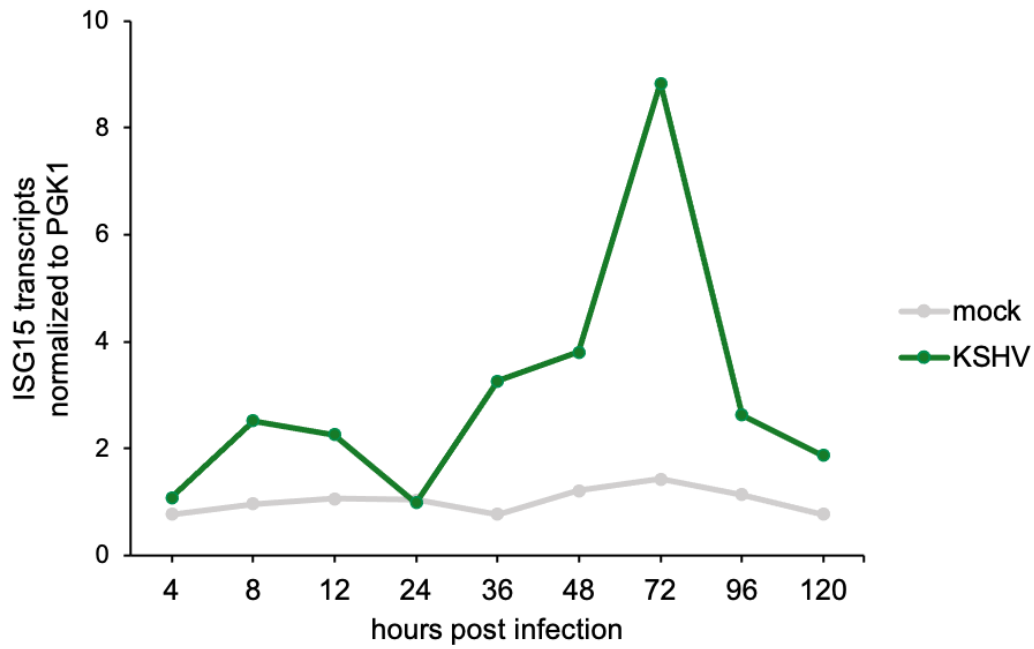


Figure S 1: *De novo* type I interferon response upon KSHV infection: (A) Time course of ISG15 transcripts upon KSHV infection. RNA was isolated from KSHV infected and mock infected cells at indicated time points post infection. Relative transcript levels for ISG15 were measured by qRT-PCR and then normalized to PGK1 (n=1).

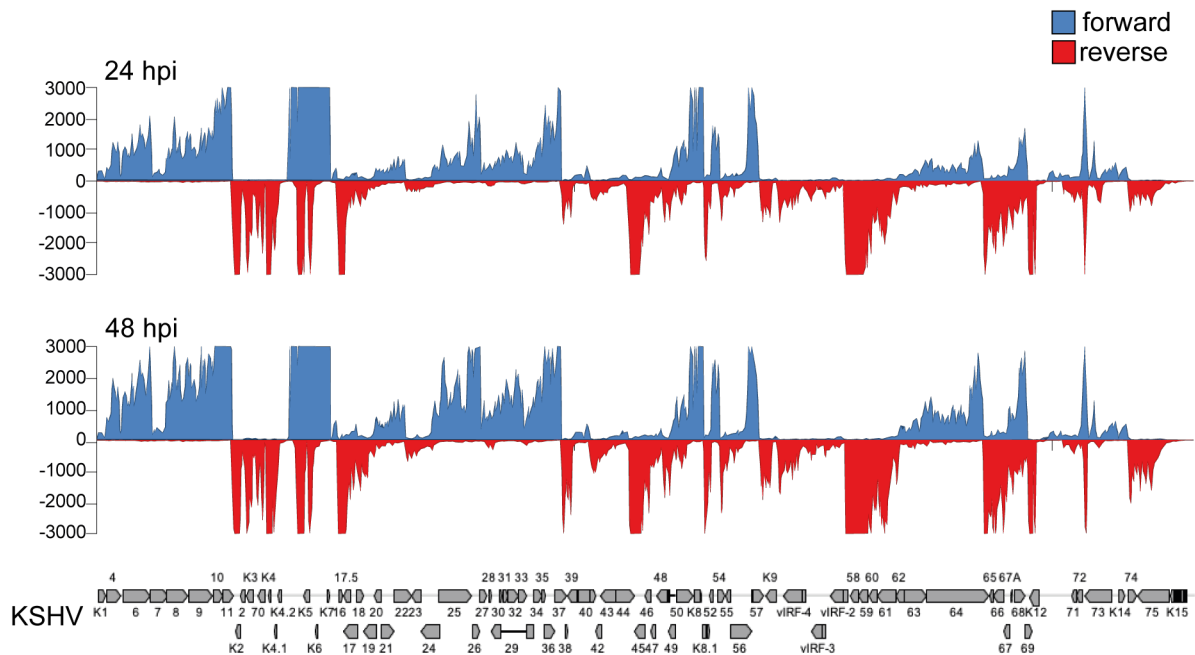


Figure S 2: BCBL1 transcriptional profile after lytic induction: BCBL-1 cells were treated with sodium butyrate and TPA to induce lytic replication of KSHV. Raw sequencing data was mapped to the KSHV reference genome and then reads were counted in 100 bp windows by discriminating between forward (blue) and reverse (red) reads. Coverage plots from 24 and 48 hpi after induction are depicted.

8 Indices

8.1 Figures

Figure 1: Phylogenetic tree of the herpesvirus family	1
Figure 2: KSHV virion and early steps of infection	4
Figure 3: Schematic overview of the linear KSHV genome	8
Figure 4: Epigenetic landscape of the KSHV genome	10
Figure 5: KSHV seroprevalence.....	16
Figure 6: DNA methylation and its key players	20
Figure 7: Histone modifications and their writer proteins/complexes	23
Figure 8: scRNA-sequencing workflow	57
Figure 9: Experimental setup and schematic overview of the constructs	61
Figure 10: Transcriptional deregulation in KSHV infected cells	65
Figure 11: Time-dependent expression of interferon regulated genes	66
Figure 12: KSHV transcriptional profile in TIME cells	62
Figure 13: Immunofluorescence of LANA and ORF59.....	63
Figure 14: Temporal resolution of the interferon response upon KSHV infection	68
Figure 15: Interferon signatures and KSHV transcriptional profile after de novo infection.....	70
Figure 16: scRNA-seq of KSHV infected cells	72
Figure 17: Correlation between interferon regulated genes and viral transcripts.....	74
Figure 18: Quality control of MeDIP-seq	77
Figure 19: Identification of DNA methylation changes in KSHV infected cells.....	79
Figure 20: Quality control of nChIP-seq	82
Figure 21: Identification of host loci with differential histone modification patterns.....	84
Figure 22: Histone modification states of interferon responsive genes.....	85
Figure 23: Temporal progression of host histone modification changes.....	87
Figure 24: Experimental setup to investigate KSHV infected and cleared cells:.....	89
Figure 25: Transcriptional deregulations in infected and cleared cells	90
Figure 26: Comparison of histone modification changes in infected and cleared populations	92
Figure 27: Growth curves and apoptotic responses of the different cell populations.....	94
Figure 28: TNC expression and angiogenic potential in the different populations	96
Figure 29: Re-infection of the cell populations with KSHV	99
Figure 30: Transcriptional responses of potentially predisposed regions after re-infection .	100
Figure 31: Super-enhancer prediction.....	112
Figure 32: Proposed KSHV induced tumorigenesis model and the role of histone modifications	115
Figure S 1: De novo type I interferon response upon KSHV infection	141
Figure S 2: BCBL1 transcriptional profile after lytic induction	141

8.2 Tables

Table 1: Plasmids and KSHV containing bacmid	30
Table 2: Oligonucleotides.....	30
Table 3: Primary antibodies	31
Table 4: Secondary antibodies.....	32
Table 5: Escherichia coli strains and their genotypes	32
Table 6: Composition of buffers for the preparation of chemically competent E. coli	33
Table 7: Antibiotic concentrations for the selection of prokaryotic cells (E.coli).....	35
Table 8: Cell lines.....	35
Table 9: Concentration of culture medium components for TIME cells.....	36
Table 10: Concentration of antibiotics for selection of regularly used eukaryotic cell lines....	38
Table 11: Components of buffers for bacmid DNA extraction from prokaryotic cells.....	41
Table 12: gDNA Isolation Buffer.....	42
Table 13: Pipetting scheme for a restriction enzyme digestion of plasmid/bacmid DNA	43
Table 14: Reaction for the ligation of DNA fragments into linearized vector DNA	44
Table 15: Components of a standard PCR reaction	45
Table 16: Standard PCR program.....	45
Table 17: Components of a qPCR reaction	46
Table 18: Standard qPCR program.....	47
Table 19: Composition of the Reverse Transcriptase Mix	48
Table 20: Nuclear Isolation Buffer	52
Table 21: MNase master mix	52
Table 22: Complete Immunoprecipitation Buffer	53
Table 23: nChIP washing buffers	54
Table 24: Elution Buffer.....	54
Table 25: Composition of the 10x MeDIP buffer	55
Table S 1: Number of cells per cluster from scRNA-seq.....	137
Table S 2: Overlapping histone modification changes in infected and cleared cells for H3K4me3	137
Table S 3: Overlapping histone modification changes in infected and cleared cells for H3K27ac	138
Table S 4: Overlapping histone modification changes in infected and cleared cells for H3K27me3	139

Abbreviations

aa	amino acid	HVS	Herpesvirus saimiri
AIDS	Acquired Immunodeficiency Syndrome	IFI16	Interferon Gamma Inducible Protein 16
BAC	Bacterial Artificial Chromosome	IFN	Interferon
bp	base pair	IL-6	Interleukin-6
BRD2	Bromodomain Containing 2	IRF3	Interferon Regulatory Factor 3
CBP	CREB Binding Protein	ISG15	Interferon Stimulated Gene 15
CDH13	Cadherin 13	JMJD3	Jumonji Domain-Containing Protein 3
CCND2	Cyclin D2	JAK2	Janus Kinase 2
CDC6	Cell Division Cycle 6	JARID2	Jumonji and AT-rich Interaction Domain Containing 2
cDNA	complementary DNA	kb	kilobase
ChIP	chromatin immunoprecipitation	KDM	Lysine Demethylase
CO ₂	carbon dioxide	KMT	Lysine Methyltransferase
CRISPR	Clustered Regularly Interspaced Short Palindromic Repeats	kV	kilovolt
CTCF	CCCTC-Binding Factor	KS	Kaposi's sarcoma
DDR	DNA damage repair	KSHV	Kaposi's sarcoma associated herpesvirus
DNA	deoxyribonucleic acid	l	liter
DNMT	DNA methyltransferase	LANA	latency associated nuclear antigen
DMSO	dimethyl sulfoxide	lncRNA	long non-coding RNA
dpi	days post infection	LSD1	Lysine Demethylase 1
EBV	Epstein-Barr Virus	LUR	long unique region
EBNA1	Epstein-Barr nuclear antigen 1	M	molar
EED	Embryonic Ectoderm Development	MCD	Multicentric Castleman's Disease
EZH2	Enhancer of Zeste 2	MCL1	Myeloid Cell Leukemia Sequence 1
FACS	fluorescence-activated cell sorting	MCM	Minichromosome Maintenance Proteins
FBS	fetal bovine serum	MCP	Major Capsid Protein
fwd	forward	MeDIP	methylated DNA immunoprecipitation
g	gram	MHV68	Murine Gammaherpesvirus 68
gB	glycoprotein B	min	minute
gDNA	genomic DNA	miRNA	micro RNA
GFP	green fluorescent protein	MLL2	Myeloid/Lymphoid or Mixed-Lineage Leukemia Protein 2
H ₂ O	water	MSC	mesenchymal stem cells
H3	histone 3	MTF2	Metal Response Element Binding Transcription Factor 2
HDAC	histone deacetylase	NF- κ B	Nuclear Factor Kappa B
HHV-6	Human Herpesvirus 6	nm	nanometer
HIV1	Human Immunodeficiency Virus 1	OD	optical density
HSV-1	Herpes Simples Virus 1	ORF	open reading frame
		PAMP	pathogen-associated molecular patterns

PCA	Principal Component Analysis
PCR	Polymerase Chain Reaction
pDC	plasmacytoid dendritic cells
PEL	Primary Effusion Lymphoma
PRC2	Polycomb Repressive Complex 2
PRR	Pattern Recognition Receptor
RB	Retinoblastoma
RBP-J κ	Recombination Signal Binding Protein for Immunoglobulin Kappa J
rev	reverse
RIN	RNA integrity number
RING1A	Ring Finger Protein 1A
RNA	ribonucleic acid
ROS	reactive oxygen species
RRE	RTA responsive element
RT	room temperature
RTA	Replication and Transcription Activator
scRNA- seq	single cell RNA sequencing
SEM	standard error of the mean
SETDB1	SET Domain Bifurcated Histone Lysine Methyltransferase 1
SUV39H1	Suppressor of Variegation 3-9 Homolog 1
SUZ12	Suppressor of Zeste 12 Protein Homolog
STAT1	Signal Transducer and Activator of Transcription 1
TGF- β	
TIME	telomerase immortalized microvascular endothelial cells
TLR	Toll-like Receptor
TPA	12-O-Tetradecanoylphorbol- 13-acetate
TR	Terminal Repeat
TSS	transcriptional start site
TYK2	Tyrosine Kinase 2
UTX	Ubiquitously Transcribed X Chromosome Tetratricopeptide Repeat Protein
VEGF	Vascular Endothelial Growth Factor A
v-FLIP	viral FLICE-like inhibitory protein
°C	degrees celsius
x g	times gravity

9 Publications, Oral Presentations, and Awards

Publications

Günther T, Fröhlich J, Herrde C, Ohno S, Burkhardt L, Adler H, Grundhoff A (2019)
A comparative epigenome analysis of gammaherpesviruses suggests cis-acting
sequence features as critical mediators of rapid polycomb recruitment. PLOS
Pathogens 15(10):e1007838

Fröhlich J, Grundhoff, A (2020) Epigenetic control in Kaposi's sarcoma-associated
herpesvirus infection and associated disease. Semin Immunopathol 42, 143–157

Oral Presentations

Fröhlich J, Günther T, Spohn M, Grundhoff A
Manipulation of Host Chromatin by Kaposi's Sarcoma-associated Herpesvirus
Jahrestagung der Gesellschaft für Virologie e.V. (GfV) 2019, Düsseldorf

Fröhlich J, Günther T, Spohn M, Herrde C, Indenbirken D, Grundhoff A
A Temporal Analysis of Host Chromatin Changes and Transcriptional Responses
Induced by Latent Kaposi's Sarcoma-associated Herpesvirus Infection
22nd International Workshop on Kaposi's Sarcoma Herpesvirus and Related Agents
2019, New York

Awards

Trainee Travel Award for Outstanding Achievement
22nd International Workshop on Kaposi's Sarcoma Herpesvirus and Related Agents
2019, New York

10 Acknowledgements

At the end of my thesis, I would like to take the opportunity and thank all the people who were involved in this study and made it possible.

First and foremost, I would like to thank Prof. Dr. Adam Grundhoff for giving me the possibility to perform this study in his research group. Without his ideas, criticism and support this work would not have been possible.

I would also like to thank Prof. Dr. Stefan Hoth who was willing to supervise and review this thesis.

All the current and former members of the Grundhoff lab contributed significantly to this work. A big thanks to all of you for your great help and a lot of fun in the lab. Special thanks goes to Thomas Günther, who helped me a lot with new ideas, critical reflections and trained me in the basic steps of bioinformatic data analysis. I would also like to thank him and Simon Weißmann for critical reading and correcting my thesis.

I would also like to express deepest gratitude to Heidi Meissner, Romina Vargas Ayala, Svenja Siebels, Emma Kraus, Martin Hamann, Daniel Pohlmann, Marion Ziegler, and Christine Block who helped me through hard times and always managed to cheer me up again. It was a pleasure to work with all of you.

Furthermore, I would like to especially mention the whole team of the sequencing platform – Daniela Indenbirken, Lia Burkhardt, Kerstin Reumann, and Christina Herrde – you were a big support. Thank you, for the preparation and sequencing of all my samples. I would also like to thank Sanamjeet Viridi, Alexis Robitaille, and Michael Spohn for their help when my bioinformatical knowledge was exceeded.

I also want to thank Nicole Fischer and all members of her group – Manja Czech-Sioli, Silvia Albertini, Denise Ohnezeit, Tabea Schlemeyer, Veronika Brinschwitz, Hannes Roggenkamp, and Claudia Schmidt – who participated in our weekly seminars and

joint retreats. Thank you for the fruitful discussions but also the funny moments we had together.

I would like to thank Timothy Soh for reading my thesis and correcting my English language.

Thank you, Tom for being at my side and supporting me through all the good and bad moments of my PhD. Without you, I would not have been able to finish this work.

Last but not least, I would like to thank my parents who have always been the greatest support. Your help and trust always encouraged me to pursue my ambitions.



HPI

Heinrich Pette Institute
Leibniz Institute for Experimental Virology

HPI • Martinstraße 52 • D-20251 Hamburg

Dr. Timothy Soh, Ph.D.

Research Department of
"Quantitative and Molecular Virology"

Phone: +49 (0) 40 480 51-270
timothy.soh@leibniz-hpi.de

Page 1 of 1

Hamburg, November 15, 2020

Fakultät für Mathematik, Informatik
und Naturwissenschaften
Fachbereich Biologie
Universität Hamburg
Ohnhorststraße 18
22609 Hamburg

I hereby declare as a native English speaker that I have checked the thesis entitled "**A Temporal Analysis of Host Chromatin Changes and Transcriptional Responses Induced by Latent Kaposi's Sarcoma-associated Herpesvirus Infection**" written by **Jacqueline Fröhlich** for grammatically correct English.

Kind regards,

12 Eidesstattliche Versicherung

Hiermit erkläre ich an Eides statt, dass ich die vorliegende Dissertationsschrift selbst verfasst und keine anderen als die angegebenen Quellen und Hilfsmittel verwendet habe.

Hamburg, November 2020

Jacqueline Fröhlich